ornl

ORNL/TM-12996

RECEIVED
FEB 27 1996
OSTI

OAK RIDGE NATIONAL LABORATORY

MARTIN MARIETTA

Analysis of the In-Vessel Control Rod Guide Tube and Subpile Room Shielding Design for the ANS Reactor

F. X. Gallmeier

August 1995

MASTER

Advanced Neutron Source

DISTRIBUTION OF THIS DOCUMENT IS UNLIMITED

MANAGED BY
MARTIN MARIETTA ENERGY SYSTEMS, INC.
FOR THE UNITED STATES
DEPARTMENT OF ENERGY

This report has been reproduced directly from the best available copy.

Available to DOE and DOE contractors from the Office of Scientific and Technical Information, P.O. Box 62, Oak Ridge, TN 37831; prices available from (615) 576-8401, FTS 626-8401.

Available to the public from the National Technical Information Service, U.S. Department of Commerce, 5285 Port Royal Rd., Springfield, VA 22161.

This report was prepared as an account of work sponsored by an agency of the United States Government. Neither the United States Government nor any agency thereof, nor any of their employees, makes any warranty, express or implied, or assumes any legal liability or responsibility for the accuracy, completeness, or usefulness of any information, apparatus, product, or process disclosed, or represents that its use would not infringe privately owned rights. Reference herein to any specific commercial product, process, or service by trade name, trademark, manufacturer, or otherwise, does not necessarily constitute or imply its endorsement, recommendation, or favoring by the United States Government or any agency thereof. The views and opinions of authors expressed herein do not necessarily state or reflect those of the United States Government or any agency thereof.

ORNL/TM-12996

Computational Physics and Engineering Division

ANALYSIS OF THE IN-VESSEL CONTROL ROD GUIDE TUBE AND SUBPILE ROOM SHIELDING DESIGN FOR THE ADVANCED NEUTRON SOURCE REACTOR

F. X. Gallmeier
J. A. Bucholz
W. W. Engle, Jr.
L. R. Williams

August 1995

Prepared by the
OAK RIDGE NATIONAL LABORATORY
Oak Ridge, Tennessee 37831
operated by
LOCKHEED MARTIN ENERGY SYSTEMS, INC.
for the
U.S. DEPARTMENT OF ENERGY
under Contract No. DE-AC05-84OR21400

DISTRIBUTION OF THIS DOCUMENT IS UNLIMITED

CONTENTS

Page

LIST OF TABLES v

LIST OF FIGURES ix

ACRONYMS xi

ABSTRACT xiii

1. INTRODUCTION 1

2. GEOMETRY DESCRIPTION 3

3. DATA SETS 17
   3.1 NEUTRON AND PHOTON CROSS SECTION 17
   3.2 QUADRATURE SET 17
   3.3 EXTERNAL BOUNDARY SOURCES 17
   3.4 KERMA FACTORS 24
   3.5 FLUX-TO-DOSE CONVERSION FACTORS 24
   3.6 FLUX-TO-DPA CONVERSION FACTORS 29

4. THE DORT ITERATION SCHEME 33

5. FLUX RESULTS AND DOSE RATES 35

6. DISPLACEMENTS PER ATOM AND HELIUM PRODUCTION IN THE STEEL COMPONENTS 41

7. HEATING IN THE SHIELD 45

8. DEPLETION AND ACTIVATION OF THE HAFNIUM SHIELD 47

9. CONCLUSION 53

10. REFERENCES 55

APPENDIX A. DETAILED FLUX AND DOSE RESULTS A-1

APPENDIX B. DISPLACEMENTS PER ATOM AND HELIUM-PRODUCTION DATA FOR CASES R400, R500, AND R550 . . . . . B-1

APPENDIX C. DETAILED HEATING RESULTS C-1

LIST OF TABLES

Table | Page

2.1 Description of the zones of model R500 in Fig. 2.2 6
2.2 Radial mesh boundaries 13
2.3 Axial mesh boundaries 14

3.1 Energy group boundaries of the 39 neutron and 44 gamma groups of the ANSL-V library 18
3.2 Nuclide number densities for the materials used in the DORT calculations 20
3.3 The fully symmetric S_{10} quadrature set with 70 discrete directions as used in the DORT calculations 23
3.4 Neutron kerma factors for boral and hafnium 26
3.5 Gamma kerma factors for boral and hafnium 27
3.6 Neutron and gamma flux-to-dose-rate conversion factors in the 39 neutron group and 44 gamma group structure of the ANSL-V library 28

8.1 Hafnium isotope concentration in the ten zones of the shield at beginning of reactor operation and after two full-power years. 49
8.2 Gamma sources in the ten zones of the hafnium shield from an irradiation time of two full-power years followed by a cooling time of one day after shutdown . . . 51

A.1 The broad group definition for the flux plots A-3
B.1 Helium production and DPA data in the PCSA/PCST at radius 270.0 mm in case R550 without shield B-10
B.2 Helium production and DPA data in the PCSA/PCST at radius 280.0 mm in case R550 without shield B-11
B.3 Helium production and DPA data in the PCSA/PCST at radius 286.5 mm in case R550 without shield B-12
B.4 Helium production and DPA data in the PCSA/PCST at radius 289.5 mm in case R550 without shield B-13
B.5 Helium production and DPA data in the PCSA/PCST at radius 294.5 mm in case R550 without shield B-14
B.6 Helium production and DPA data in the PCSA/PCST at radius 301.5 mm in case R550 without shield B-15
B.7 Helium production and DPA data in the flange at height −8.9 mm in case R550 without shield B-16
B.8 Helium production and DPA data in the flange at height −26.7 mm in case R550 without shield B-17
B.9 Helium production and DPA data in the flange at height −44.5 mm in case R550 without shield B-18
B.10 Helium production and DPA data in the flange at height −62.3 mm in case R550 without shield B-19

B.11 Helium production and DPA data in the flange at height –80.10 mm in case R550 without shield B-20
B.12 Helium production and DPA data in the PCSA/PCST at radius 270.0 mm for case R500 with restricted hafnium shield B-21
B.13 Helium production and DPA data in the PCSA/PCST at radius 280.0 mm for case R500 with restricted hafnium shield B-22
B.14 Helium production and DPA data in the PCSA/PCST at radius 286.5 mm for case R500 with restricted hafnium shield B-23
B.15 Helium production and DPA data in the PCSA/PCST at radius 289.5 mm for case R500 with restricted hafnium shield B-24
B.16 Helium production and DPA data in the PCSA/PCST at radius 294.5 mm for case R500 with restricted hafnium shield B-25
B.17 Helium production and DPA data in the PCSA/PCST at radius 301.5 mm for case R500 with restricted hafnium shield B-26
B.18 Helium production and DPA data in the flange at height –8.9 mm for case R500 with restricted hafnium shield B-27
B.19 Helium production and DPA data in the flange at height –26.7 mm for case R500 with restricted hafnium shield B-28
B.20 Helium production and DPA data in the flange at height –44.5 mm for case R500 with restricted hafnium shield B-29
B.21 Helium production and DPA data in the flange at height –62.3 mm for case R500 with restricted hafnium shield B-30
B.22 Helium production and DPA data in the flange at height –80.10 mm for case R500 with restricted hafnium shield B-31
B.23 Helium production and DPA data in the PCSA/PCST at radius 270.0 mm for case R400 with extended boral shield B-32
B.24 Helium production and DPA data in the PCSA/PCST at radius 280.0 mm for case R400 with extended boral shield B-33
B.25 Helium production and DPA data in the PCSA/PCST at radius 286.5 mm for case R400 with extended boral shield B-34
B.26 Helium production and DPA data in the PCSA/PCST at radius 289.5 mm for case R400 with extended boral shield B-35
B.27 Helium production and DPA data in the PCSA/PCST at radius 294.5 mm for case R400 with extended boral shield B-36
B.28 Helium production and DPA data in the PCSA/PCST at radius 301.5 mm for case R400 with extended boral shield B-37
B.29 Helium production and DPA data in the flange at height –8.9 mm for case R400 with extended boral shield B-38
B.30 Helium production and DPA data in the flange at height –26.7 mm for case R400 with extended boral shield B-39
B.31 Helium production and DPA data in the flange at height –44.5 mm for case R400 with extended boral shield B-40
B.32 Helium production and DPA data in the flange at height –62.3 mm for case R400 with extended boral shield B-41

B.33 Helium production and DPA data in the flange at height −80.10 mm for case R400 with extended boral shield B-42
C.1 Heating rate in the horizontal part of the shield for case R500 with restricted hafnium shield C-3
C.2 Heating rate in the inner vertical part of the shield for case R500 with restricted hafnium shield C-4
C.3 Heating rate in the outer vertical part of the shield for case R500 with restricted hafnium shield C-5
C.4 Heating rate in the horizontal part of the shield for case R450 with restricted boral shield C-6
C.5 Heating rate in the inner vertical part of the shield for case R450 with restricted boral shield C-7
C.6 Heating rate in the outer vertical part of the shield for case R450 with restricted boral shield C-8

LIST OF FIGURES

Figure		Page
2.1	The lower part of the ANS reflector vessel as modeled by Fig. 2.2.	4
2.2	DORT model R500. The description of the labeled zones is given in Table 2.1.	5
2.3	The fine mesh configuration of the upper part of the DORT model. The mesh boundaries are listed in Tables 2.1 and 2.2.	15
2.4	The fine mesh configuration of the lower part of the DORT model. The mesh boundaries are listed in Tables 2.1 and 2.2.	16
3.1	Post-processing of the ANSL-V cross section data into DORT-ready cross sections for the shielding task.	19
3.2	Plot of the neutron kerma factors for boral and hafnium.	25
3.3	Plot of the gamma kerma factors for boral and hafnium.	25
3.4	DPA level in stainless steel 316NG vs thermal fluence	31
3.5	Helium production in stainless steel 316NG vs fluence	31
6.1	Radially averaged DPA level in the PCSA vs height for cases R550, R500, and R400 after 40 years of reactor operation.	42
6.2	Radially averaged helium production in the PCSA vs height for cases R550, R500, and R400 after 40 years of reactor operation	42
6.3	DPA level in the flange near the reflector vessel vs radius for cases R550, R500, and R400 after 40 years of reactor operation	43
6.4	Helium production in the flange near the reflector vessel vs radius for cases R550, R500, and R400 after 40 years of reactor operation.	43
7.1	Heating rate in the vertical part of the shield vs height for the boral shield of case R450 and for the hafnium shield of case R500.	46
7.2	Heating rate in the horizontal part of the shield vs radius for the boral shield of case R450 and for the hafnium shield of case R500.	46
8.1	Definition of the ten zones of the L-shaped restricted hafnium shield for the depletion/activation analyses.	48
8.2	Gamma dose rates for the case R500 with the restricted hafnium shield one day after shutdown of reactor power.	52
A.1	Fast neutron flux in units for case R550 without shield.	A-4
A.2	Epithermal-1 neutron flux in units for case R550 without shield.	A-5
A.3	Epithermal-2 neutron flux in units for case R550 without shield.	A-6
A.4	Thermal neutron flux in units for case R550 without shield.	A-7
A.5	High-energy gamma flux in units for case R550 without shield.	A-8
A.6	Low-energy flux in units for case R550 without shield.	A-9
A.7	Neutron dose rate in units for case R550 without shield.	A-10
A.8	Gamma dose rate in units for case R550 without shield.	A-11
A.9	Fast neutron flux in units for case R400 with L-shaped boral shield.	A-12

A.10 Epithermal-1 neutron flux in units for case R400 with L-shaped boral shield. . . A-13
A.11 Epithermal-2 neutron flux in units for case R400 with L-shaped boral shield. . . A-14
A.12 Thermal neutron flux in units for case R400 with L-shaped boral shield. A-15
A.13 High-energy gamma flux in units for case R400 with L-shaped boral shield. . . . A-16
A.14 Low-energy flux in units for case R400 with L-shaped boral shield. A-17
A.15 Neutron dose rate in units for case R400 with L-shaped boral shield. A-18
A.16 Gamma dose rate in units for case R400 with L-shaped boral shield. A-19
A.17 Fast neutron flux in units for case R500 with restricted hafnium shield. A-20
A.18 Epithermal-1 neutron flux in units for case R500 with restricted hafnium shield. A-21
A.19 Epithermal-2 neutron flux in units for case R500 with restricted hafnium shield. A-22
A.20 Thermal neutron flux in units for case R500 with restricted hafnium shield. . . . A-23
A.21 High-energy gamma flux in units for case R500 with restricted hafnium shield. . A-24
A.22 Low-energy gamma flux in units for case R500 with restricted hafnium shield. . . A-25
A.23 Neutron dose rate in units for case R500 with restricted hafnium shield. A-26
A.24 Gamma dose rate in units for case R500 with restricted hafnium shield. A-27
B.1 DPA level in the PCSA vs height for case R550 without shield after 40 years of reactor operation. B-4
B.2 Helium production in the PCSA vs height for case R550 without shield after 40 years of reactor operation. B-4
B.3 DPA level in the flange near the reflector vessel vs radius for case R550 without shield after 40 years of reactor operation. B-5
B.4 Helium production in the flange near the reflector vessel vs radius for case R550 without shield after 40 years of reactor operation. B-5
B.5 DPA level in the PCSA vs height for case R500 with radially restricted hafnium shield after 40 years of reactor operation. B-6
B.6 Helium production in the PCSA vs height for case R500 with radially restricted hafnium shield after 40 years of reactor operation. B-6
B.7 DPA level in the flange near the reflector vessel vs radius for case R500 with radially restricted hafnium shield after 40 years of reactor operation. B-7
B.8 Helium production in the flange near the reflector vessel vs radius for case R500 with radially restricted hafnium shield after 40 years of reactor operation. B-7
B.9 DPA level in the PCSA vs height for case R400 with radially extended boral shield after 40 years of reactor operation. B-8
B.10 Helium production in the PCSA vs height for case R400 with radially extended boral shield after 40 years of reactor operation. B-8
B.11 DPA level in the flange near the reflector vessel vs radius for case R400 with radially extended boral shield after 40 years of reactor operation. B-9
B.12 Helium production in the flange near the reflector vessel vs radius for case R400 with radially extended boral shield after 40 years of reactor operation. B-9

ACRONYMS

2-D	two-dimensional
ANS	Advanced Neutron Source
ANSI	American National Standards Institute
CPBT	core pressure boundary tube
CPU	central processing unit
CRGT	control rod guide tube
DPA	displacements per atom
PCSA	primary coolant supply adapter
PCST	primary coolant supply tube

ABSTRACT

An extensive shielding analysis of the control rod guide tube (CRGT) and the subpile room was performed for the Advanced Neutron Source (ANS) reactor. A two-dimensional model for the CRGT and subpile room was developed, and the boundary source used in the model was taken from the *Initial Global 2-D Shielding Analysis of the ANS Core and Reflector* (J.A. Bucholz, ORNL/TM-12672, 1994). Coupled 39 neutron group and 44 gamma group calculations with the multigroup DORT discrete ordinates transport code were done using cross sections from the ANSL-V library including photoneutron production.

Different shield designs were investigated with a shield thickness of 10 to 15 mm. None of the shields affected the neutron dose rate and gamma dose rate at the top of the subpile room, which were $1 \cdot 10^5$ mrem/h and $1 \cdot 10^3$ mrem/h, respectively. An L-shaped cylindrical boral shield positioned around the core pressure boundary tube at the bottom of the reflector vessel with the horizontal part extended over the whole bottom of the reflector vessel reduced the maximal displacements per atom (DPA) level and helium production level in the primary coolant supply adapter and its flange after 40 years of reactor operation from 1 and 500 appm to $5 \cdot 10^{-3}$ and $2 \cdot 10^{-2}$ appm compared with the unshielded arrangement. Shields of boral and hafnium with the horizontal part of the shield restricted to a radius of 485 mm gave a maximal DPA of $5 \cdot 10^{-2}$ and a helium production of up to 20 appm. Heat loads of up to 70 $W \cdot cm^{-3}$ were calculated at the most exposed parts of the shield both for boral and hafnium shields.

A depletion/activation analysis of the hafnium shield showed that at the most exposed part of the shield, the naturally occuring isotope ^{177}Hf is 34% depleted at the end of two years of reactor operation. This high burnup is somewhat balanced by a subsequent buildup of ^{178}Hf, ^{179}Hf, and ^{180}Hf. In all other parts of the shield, the burnup is much smaller.

1. INTRODUCTION

In the Advanced Neutron Source (ANS) reactor,[1] the three hafnium control rods balance the reactivity of the system by axial movements in the center of the cylindrical core. To keep the upper part of the reflector vessel as free as possible for experimental facilities and for access when the reactor is refueled or the in-core experiments reconfigured, the control rod drives are located below the reflector vessel. As a consequence, the core pressure boundary tube (CPBT), which contains the fuel elements and the control rods and provides the flow of coolant, extends about 2 m below the reflector vessel to hold the control rod drive structures and enable control rod movements. This control rod guide tube (CRGT) is filled with D_2O and penetrates the H_2O and barytes concrete biological shield. For this reason it allows neutrons and photons to stream down into the subpile room below the reactor.

Concerns about high neutron and gamma dose rates in the subpile room led to the decision to perform a detailed shielding analysis of this region. Preliminary flux results indicated high thermal neutron fluxes at the flange and the primary coolant supply adapter (PCSA), which are steel components located at the bottom of the reflector vessel and which are used to connect the CPBT to the CRGT (see Figure 2.1). The high radiation damage levels in these components, which are expected to exceed any acceptable levels, were additional concerns of the design team. Hence the objective of this shielding task had to be extended and can be summarized as follows:

- It must be determined whether a shield inserted in the reflector vessel can protect the steel PCSA and the steel flange, which are susceptible to radiation damage.
- A shielding solution must be found that meets the design constraints of at least two years of lifetime and removability.
- The neutron and gamma dose rates during reactor operation and after shutdown must be obtained in the subpile room to get an idea of the level of the radiation dose rates that maintenance workers could be exposed to.

A two-dimensional (2-D) R-Z model was set up for the region 3.5 m below the reflector vessel with a radial extension of 0.9 m to perform neutron and photon transport calculations with the discrete ordinates code DORT.[2] Later, the model was extended axially about 0.9 m into the reflector vessel to be able to insert shields and to investigate their effect. The calculation has a high degree of complexity. Neutrons and gammas created in the reactor and its vicinity stream down the CRGT. With a certain probability, the neutrons are absorbed in structural material and generate more high-energy photons, which are themselves able to produce more neutrons in photo-disintegration reactions in heavy water. Thus, outer iterations over energy must be performed to account for all these effects and arrive at a converged solution.

This report contains a description of the geometry models developed for this study, which differ in the shielding design as the refinement of the design was resolved. It also contains a description of the cross sections, source terms, and various data sets prepared for the calculations and the evaluation of the heating and radiation damage in certain materials. Brief results are given for all the cases considered in order to document the ongoing work, whereas for the cases that are relevant for the final reactor design, broad group neutron and gamma fluxes are presented in addition to neutron and gamma dose rates, displacements per atom (DPA), and helium-production levels in the steel components, as well as the expected heating rates in the

shield. Depletion calculations for the shield material provide information about lifetime and activation of the shield and give the source terms for subsequent calculations of the dose rates generated by the decay gammas in the shield after reactor shutdown.

During the course of this study, the concept of the ANS reactor was fundamentally changed by replacing the two-element core design with a three-element core design, which necessitated changes in the radial dimensions of the fuel elements. These changes were necessary to ensure that the three-element design performs similarly to the two-element design in terms of cycle length and thermal neutron fluxes in the reflector but using fuel with 50% enriched uranium instead of 93% enriched uranium. These changes in the design concept were not taken into account directly; however, their effect on the shielding design is briefly discussed in the final chapter of this report.

2. GEOMETRY DESCRIPTION

Figure 2.1 shows the lower part of the reflector vessel and the region below it. The CPBT, fabricated of aluminum with an outer diameter of 506 mm, contains the fuel elements and the control rods. The cooling water flow enters the bottom of the reflector vessel via the PCSA. The top part of the PCSA extends below the reflector vessel and is connected to the CRGT by a flange. The CRGT holds the control rod drive structures and provides the primary coolant supply. The control rod drive motors are located at the bottom of the CRGT about 2 m below the bottom of the reflector vessel. The whole CRGT, which is filled with D_2O, penetrates the biological shield of H_2O and barytes concrete and is fixed by a bellows seal construction to the steel liner of the concrete floor.

The whole arrangement deviates from the cylindrical symmetry as follows:

- The control rod system consists of three rods moving vertically inside the fuel elements.
- Two primary coolant supply tubes (PCSTs) are connected to the CRGT.
- Some bolts and screws are neutronically of minor importance.
- At two locations, the bottom of the reflector vessel is penetrated by flanges connecting the reflector vessel coolant supply tubes.

A 2-D R-Z DORT model based on the arrangement just described has been developed. In this model, the overall axial and radial extensions had to be justified and the deviations from cylindrical symmetry had to be taken into consideration in a neutronically suitable manner:

- In the first model, the axial dimensions were chosen to range from the bottom of the reflector vessel, defined as origin, to 3.5 m below the reflector vessel to be able to calculate the activation of the structural elements and the dose rates in the subpile room. The need to place shield configurations in the reflector vessel required the extension of the model 0.89 m up into the reflector vessel.
- All components and areas of interest lie within a radius of 0.4 m. Because the neutrons and gammas mainly stream through the D_2O column (with a radius of about 250 mm provided by the CPBT and the CRGT) and because the neutron fluxes fall off with a steep gradient in the biological shield, it was deemed sufficient to restrict the model radially to 0.89 m.
- The reflector coolant supply tubes, which penetrate the bottom of the reflector vessel at a radius of 0.90 m, are not modeled because they are well shielded by the surrounding H_2O. Therefore, they have little influence on the flux levels in the components of interest and/or the dose rates in the subpile room. The nearest component is the flange, which is located 0.20 m from the reflector vessel coolant supply tube, a distance over which the thermal neutron flux drops by three orders of magnitude.

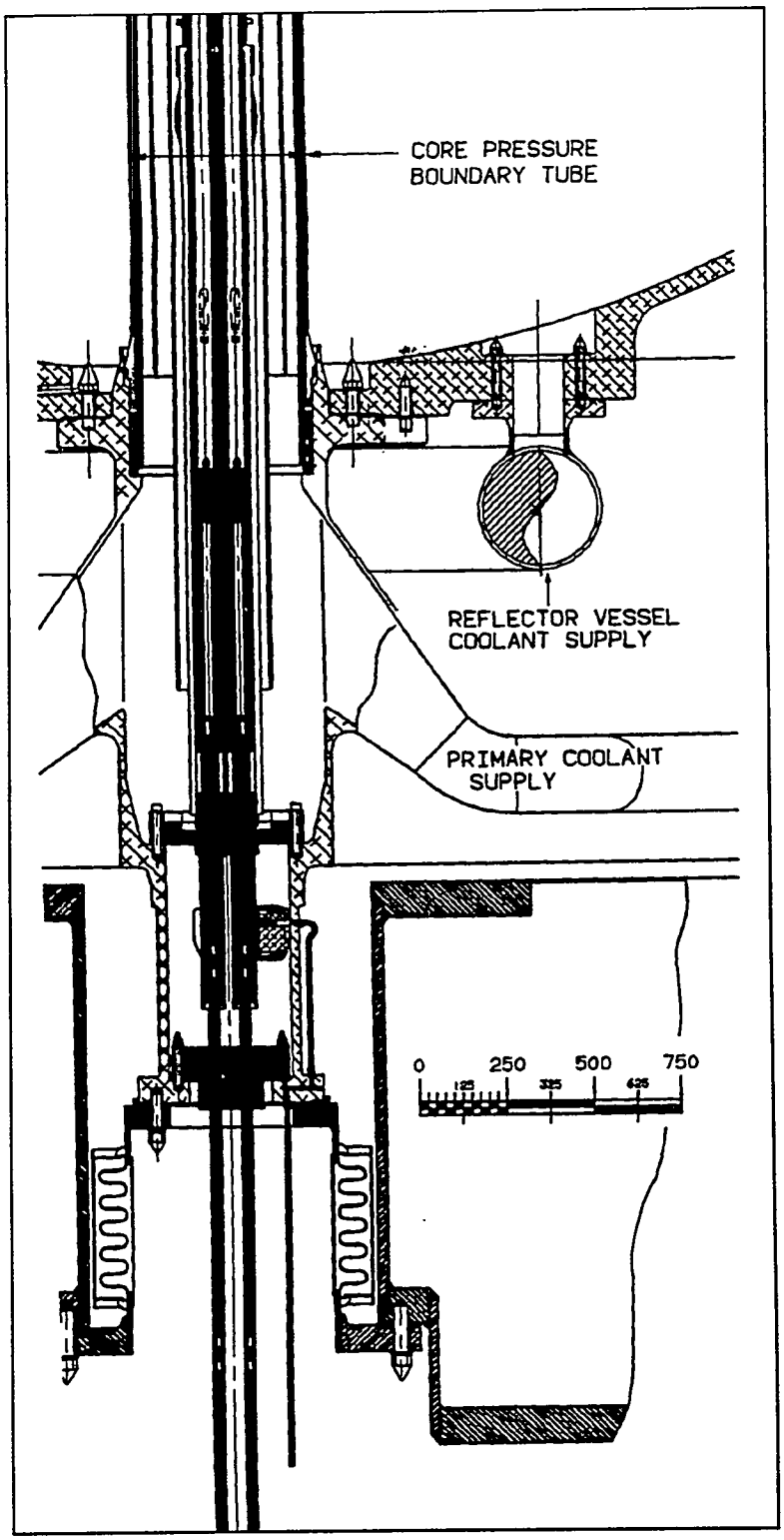

Fig. 2.1. The lower part of the ANS reflector vessel as modeled by Fig. 2.2.

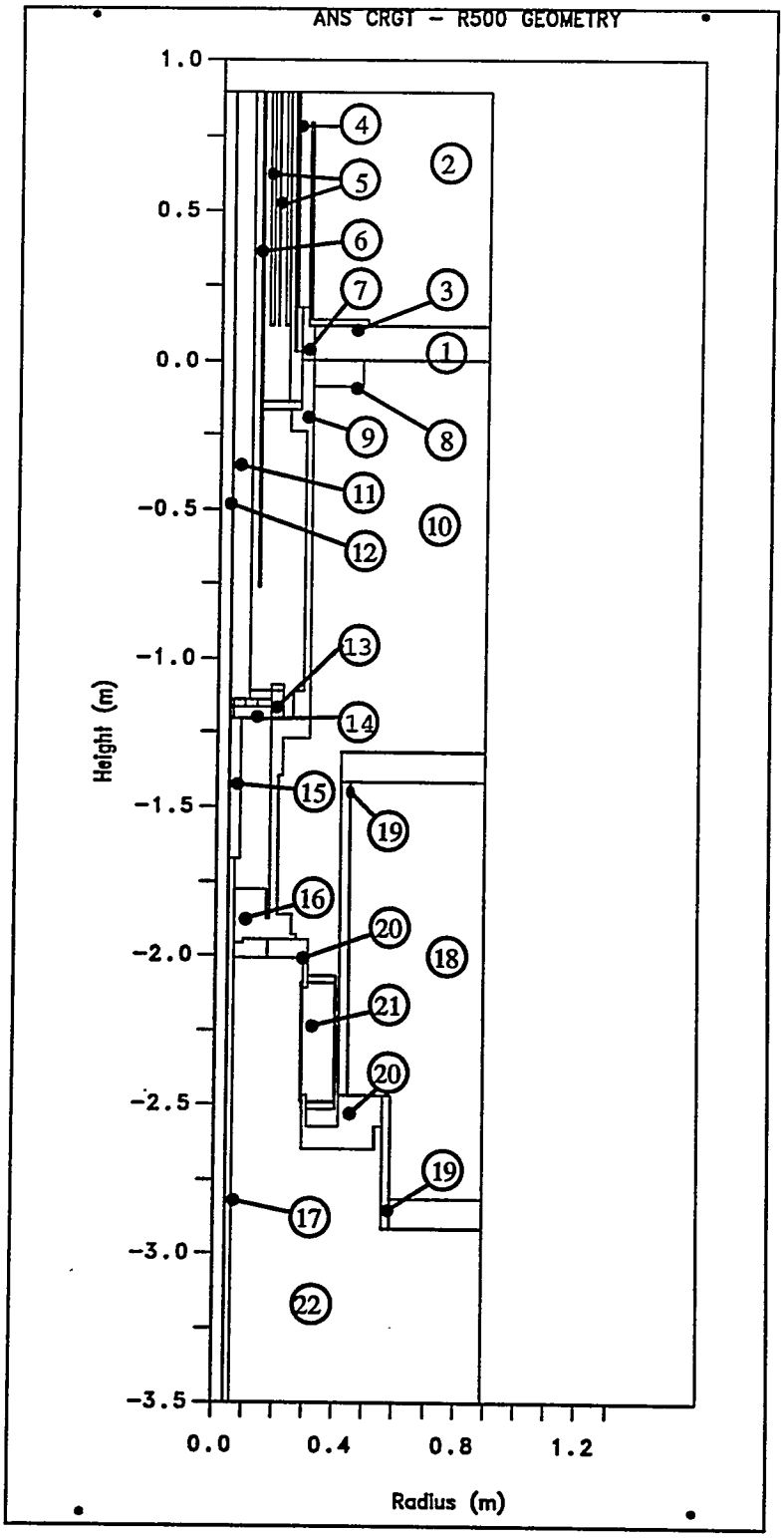

Fig. 2.2. DORT model R500. The description of the labeled zones is given in Table 2.1.

Table 2.1. Description of the zones of model R500 in Fig. 2.2

Zone	Zone description	Material
01	Bottom of the reflector vessel	Aluminum
02	Moderator	D_2O
03	L-shaped shield	Boral/hafnium
04	Double-walled CPBT	Aluminum
05	Core support structure	Aluminum
06	Streaming plates	Aluminum
07	PCSA	Steel SS-316NG
08	Flange	Steel SS-316NG
09	CRGT	Steel SS-316NG
10	Light water pool	H_2O
11	Control rod follower	Aluminum
12	Interior of CR follower and bar	Void
13	Bolt ring	Steel SS-316NG
14	CRGT base	Inconel
15	Control rod drive structure	Aluminum
16	Control rod motors	Steel SS-316NG
17	Control rod drive bar	Steel SS-316NG
18	Concrete floor	Barytes concrete
19	Floor liner	Steel SS-316NG
20	Holding structure for CRGT and Seal	Steel SS-316NG
21	Bellows seal	Steel SS-316NG
22	Subpile room	Void

- Furthermore, the PCSTs connected to the CRGT below the reflector vessel are not considered in the model. As the source of radiation is coming through the limited cross-sectional area of the CPBT, the PCSTs filled with D_2O would provide paths for the neutrons to stream away from the critical regions and therefore lower the number of neutrons finding their way to the subpile room. However, an additional amount of D_2O provides an additional source for photoneutrons produced by high-energy gammas in (n,γ) reactions. It is therefore difficult to quantify this shortcoming of the 2-D models.

- The three central control rods are modeled by centerline cylindrical tubes, the dimensions of which reflect the material volumes of all three control rods. Because the control rod structures in the region below the reflector vessel do not contain any strong absorbing materials (mainly aluminum), this has little effect neutronically.

In the 2-D DORT model, this geometry is discretized into 111 radial and 222 axial meshes, the boundaries of which are given in Tables 2.2 and 2.3, respectively, and are presented graphically in Figs. 2.3 and 2.4. In the overlay mode, zones are defined with radial and axial boundaries. As each defined zone is overlayed on all the preceding zones, it is easy to set up complicated geometries and it is simple to change the dimensions of zones or to add new zones. This fact facilitated work in an iterative way with design engineers and material specialists as the shield design evolved during discussions.

Figure 2.2 shows model R500, for which results are presented in detail in this report. The different zones are indicated with numbers, for which brief descriptions are given in Table 2.1.

The models being investigated in this study differ only in the shield design (with additional minor changes in the arrangement in the region of the reflector vessel). An evolving picture of this upper part of the geometry is presented in chronological order for each model studied, with a short description of the changes as follows.

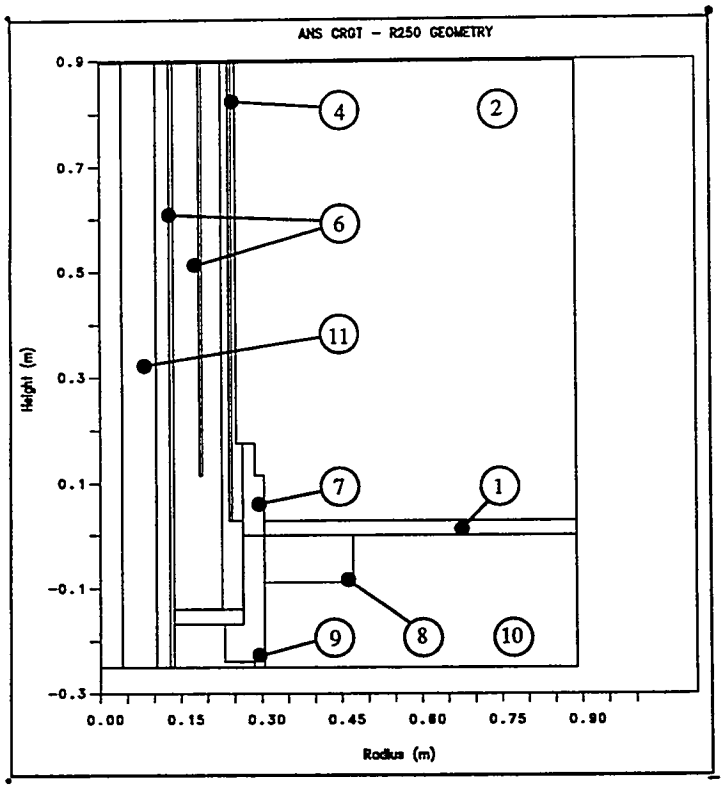

Case R250:
At the beginning of the calculations, the bottom of the reflector vessel (1) was assumed to be 25 mm thick. A shield was not yet inserted. The numbers in brackets in the text refer to the numbers in the figures and the zone description of Table 2.1.

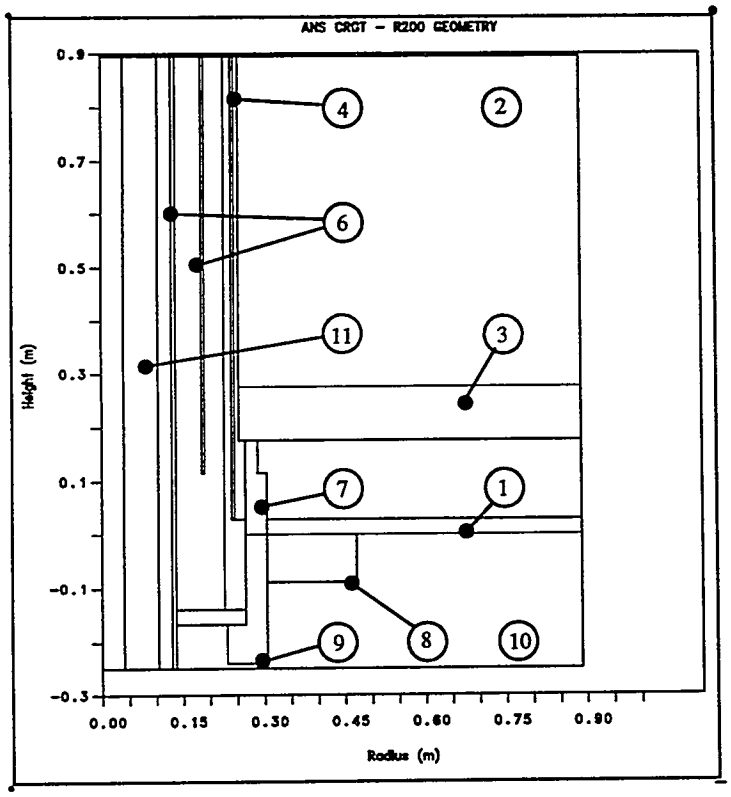

Case R200:
A 100-mm-thick horizontal shield of ideal absorber (3) was placed at the tip of the PCSA (7) extended to the bottom of the reflector vessel outside the CPBT (4).

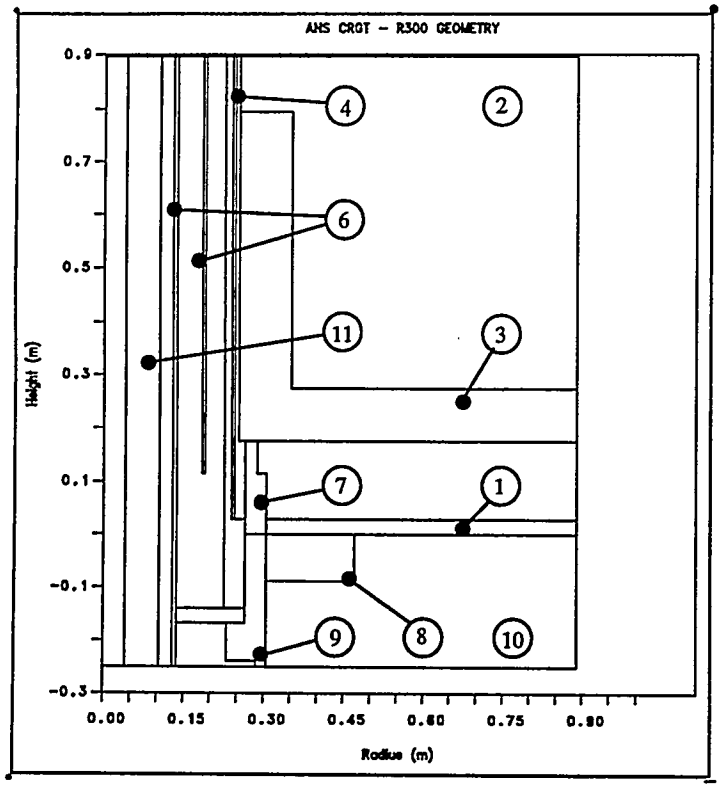

Case R300:
A vertical shield (3) was added, extending as a 100-mm-thick cylindrical sleeve from the horizontal shield upward outside the CPBT (4).

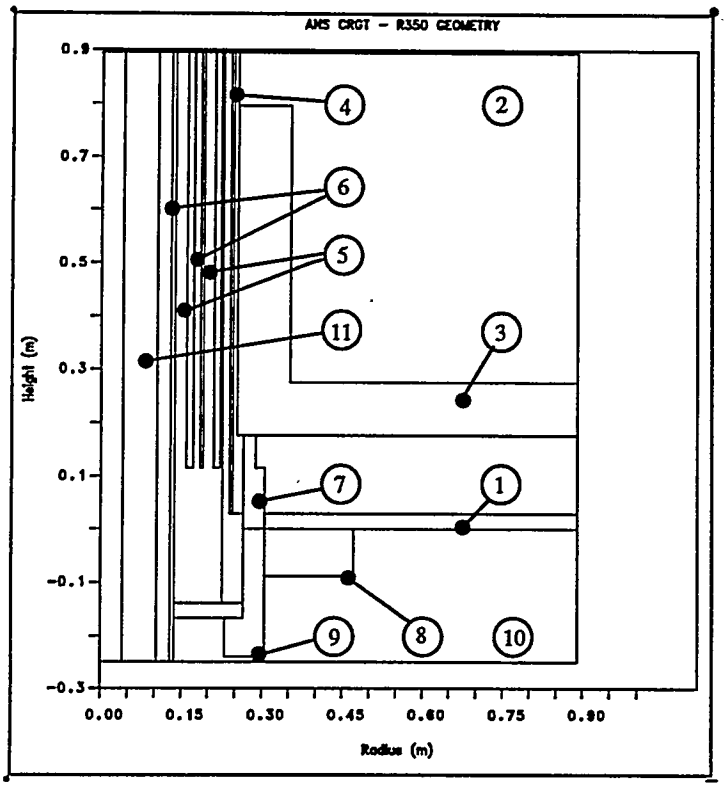

Case R350:
Two cylindrical tubes were included inside the CPBT (4) accounting for the core support structure (5) with a total cross-sectional area of 0.040 m^2.

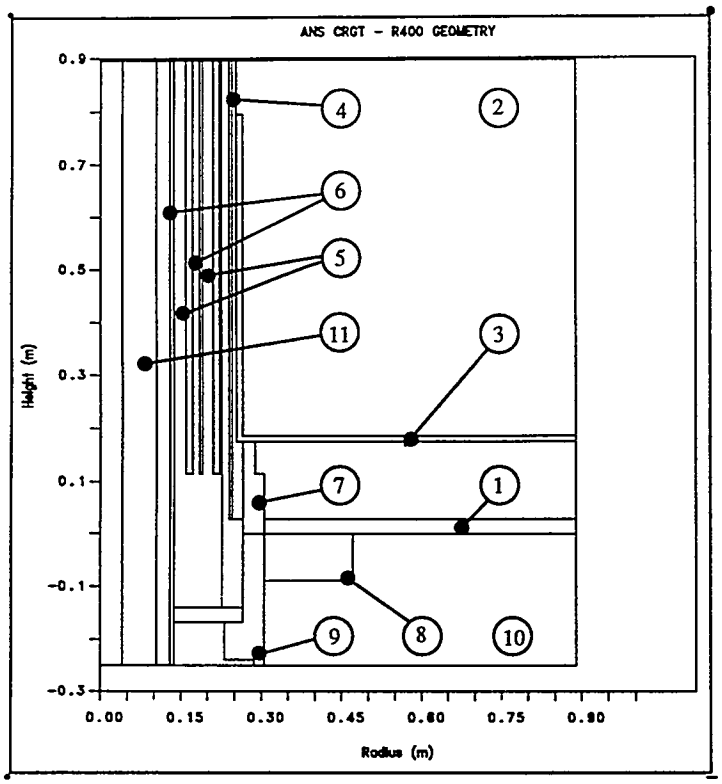

Case R400:
The ideal shield was replaced by a boral shield (3) with a thickness of 13 to 14 mm. The location of the shield was kept unchanged (i.e., horizontally extending to the bottom of the reflector vessel and vertically reaching up to z=0.79 m). A new cross section library has been used in this calculation, which includes the impurity of 0.2 mole % H_2O in D_2O.

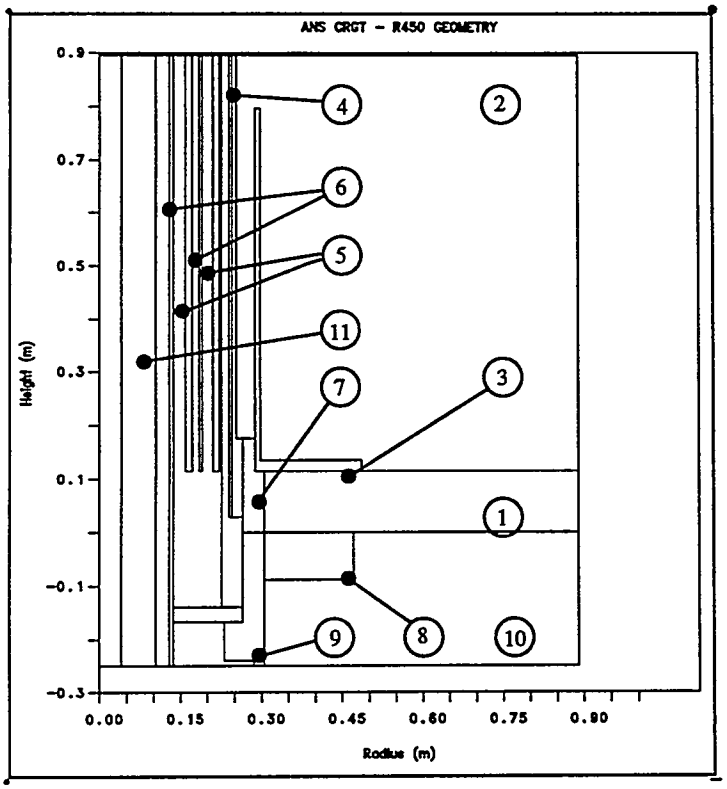

Case R450:
The thickness of the reflector vessel bottom (1) was increased to more realistic 110 mm. To be able to remove the entire shield (3) as a whole piece through the top of the reflector vessel during maintenance operations, the horizontal part of the shield was restricted to a radius of 485 mm. To prevent neutrons streaming around the outer radial tip, the shield was placed flush against the bottom of the reflector vessel.

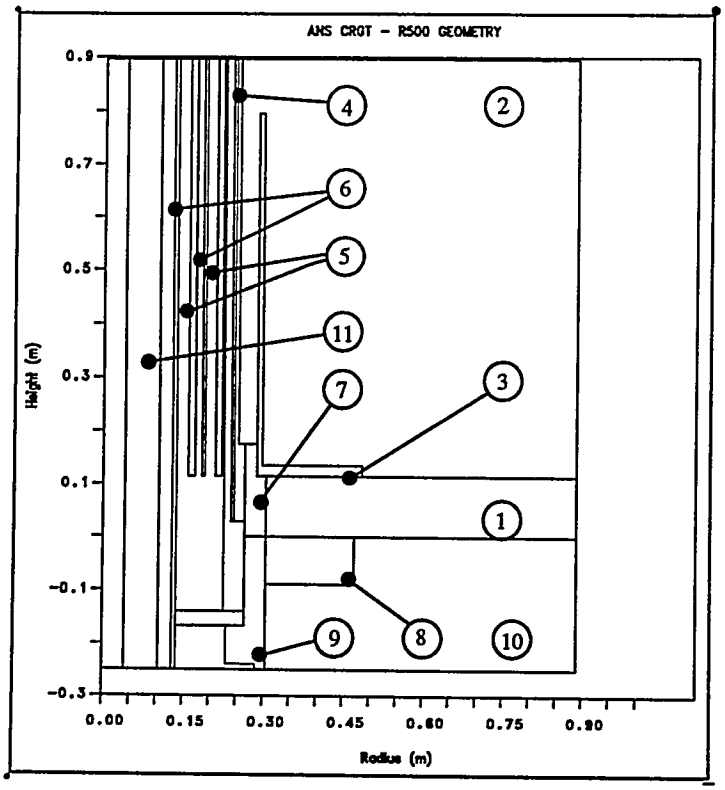

Case R500:
The shielding material was changed to hafnium with the hope of reducing the heat load produced by radiation and because hafnium seems to be less susceptible to radiation damage (compared to a boral shield).

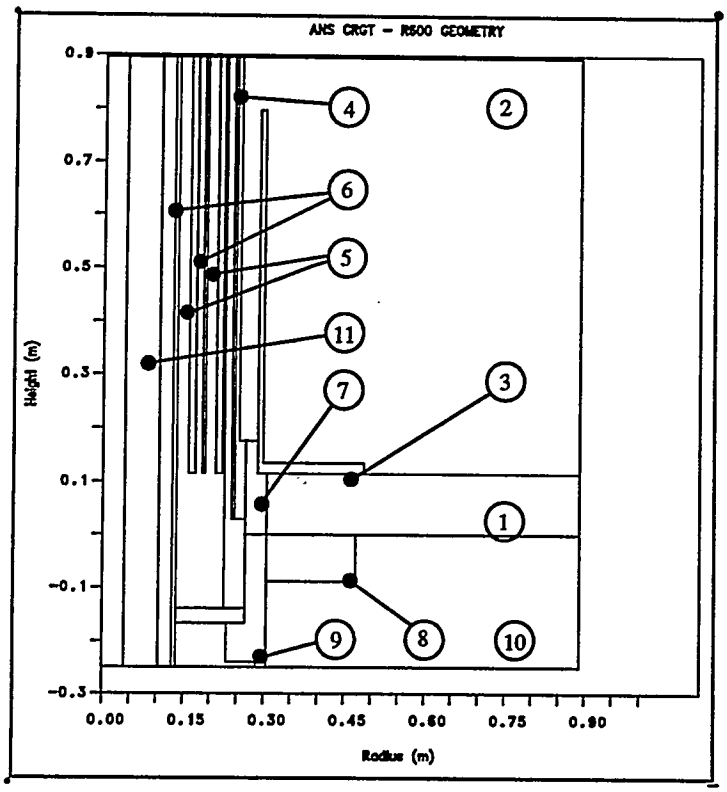

Case R600:
The geometry of R600 is similar to geometry R500; however, the density of hafnium in this calculation was reduced to a half to simulate a hafnium shield (3) with half the prior thickness.

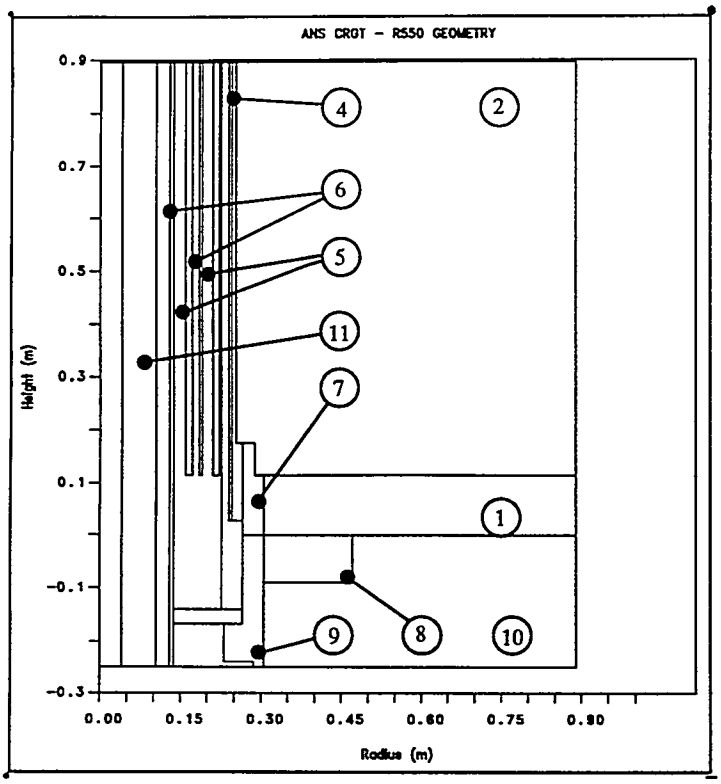

Case R550:
To complete the cycle of calculations, a model including all refinements but without the shield was investigated.

Table 2.2. Radial mesh boundaries (mm)

Radial interval	Rmin	Rmax	Radial interval	Rmin	Rmax	Radial interval	Rmin	Rmax
1	·00	3·25	38	124·40	129·50	75	351·00	360·00
2	3·25	6·50	39	129·50	136·50	76	360·00	369·00
3	6·50	7·00	40	136·50	143·88	77	369·00	378·00
4	7·00	9·50	41	143·88	151·25	78	378·00	387·00
5	9·50	12·00	42	151·25	158·62	79	387·00	396·00
6	12·00	15·00	43	158·62	166·00	80	396·00	399·00
7	15·00	18·00	44	166·00	171·00	81	399·00	405·00
8	18·00	21·00	45	171·00	176·00	82	405·00	411·00
9	21·00	24·00	46	176·00	180·50	83	411·00	418·75
10	24·00	25·00	47	180·50	185·00	84	418·75	426·50
11	25·00	28·00	48	185·00	190·00	85	426·50	434·25
12	28·00	32·00	49	190·00	196·50	86	434·25	442·00
13	32·00	35·00	50	196·50	203·00	87	442·00	449·00
14	35·00	37·50	51	203·00	210·00	88	449·00	456·00
15	37·50	40·00	52	210·00	217·00	89	456·00	463·00
16	40·00	43·06	53	217·00	221·50	90	463·00	470·00
17	43·06	46·13	54	221·50	226·00	91	470·00	485·25
18	46·13	48·36	55	226·00	231·00	92	485·25	500·50
19	48·36	50·60	56	231·00	235·00	93	500·50	515·75
20	50·60	51·59	57	235·00	240·00	94	515·75	531·00
21	51·59	52·00	58	240·00	245·00	95	531·00	544·00
22	52·00	52·40	59	245·00	250·00	96	544·00	557·00
23	52·40	53·37	60	250·00	253·00	97	557·00	570·00
24	53·37	55·32	61	253·00	259·00	98	570·00	583·00
25	55·32	57·27	62	259·00	265·00	99	583·00	596·75
26	57·27	60·00	63	265·00	275·00	100	596·75	610·50
27	60·00	66·00	64	275·00	285·00	101	610·50	624·25
28	66·00	72·00	65	285·00	288·00	102	624·25	638·00
29	72·00	78·00	66	288·00	291·00	103	638·00	663·00
30	78·00	84·00	67	291·00	298·00	104	663·00	688·00
31	84·00	90·00	68	298·00	305·00	105	688·00	713·00
32	90·00	97·00	69	305·00	310·00	106	713·00	738·00
33	97·00	104·00	70	310·00	315·00	107	738·00	768·00
34	104·00	109·10	71	315·00	324·00	108	768·00	798·00
35	109·10	114·20	72	324·00	333·00	109	798·00	828·00
36	114·20	119·30	73	333·00	342·00	110	828·00	858·00
37	119·30	124·40	74	342·00	351·00	111	858·00	888·00

Table 2.3. Axial mesh boundaries (mm)

jz[a]	Zmin	Zmax	jz[a]	Zmin	Zmax	jz[a]	Zmin	Zmax	jz[a]	Zmin	Zmax
1	−3527·00	−3476·00	57	−2070·00	−2050·00	113	−1057·00	−1038·50	168	−127·25	−114·50
2	−3476·00	−3425·00	58	−2050·00	−2030·00	114	−1038·50	−1020·00	169	−114·50	−101·75
3	−3425·00	−3374·00	59	−2030·00	−2010·00	115	−1020·00	−1001·50	170	−101·75	−89·00
4	−3374·00	−3323·00	60	−2010·00	−1985·00	116	−1001·50	−983·00	171	−89·00	−71·20
5	−3323·00	−3272·00	61	−1985·00	−1960·00	117	−983·00	−970·00	172	−71·20	−53·40
6	−3272·00	−3221·00	62	−1960·00	−1948·00	118	−970·00	−957·00	173	−53·40	−35·60
7	−3221·00	−3170·00	63	−1948·00	−1939·00	119	−957·00	−937·00	174	−35·60	−17·80
8	−3170·00	−3119·00	64	−1939·00	−1930·00	120	−937·00	−917·00	175	−17·80	0·00
9	−3119·00	−3068·00	65	−1930·00	−1916·50	121	−917·00	−897·00	176	0·00	14·00
10	−3068·00	−3017·00	66	−1916·50	−1903·00	122	−897·00	−877·00	177	14·00	28·00
11	−3017·00	−2992·00	67	−1903·00	−1889·50	123	−877·00	−857·00	178	28·00	49·50
12	−2992·00	−2967·00	68	−1889·50	−1876·00	124	−857·00	−837·00	179	49·50	71·00
13	−2967·00	−2942·00	69	−1876·00	−1864·00	125	−837·00	−818·00	180	71·00	92·50
14	−2942·00	−2917·00	70	−1864·00	−1850·00	126	−818·00	−799·00	181	92·50	114·00
15	−2917·00	−2897·00	71	−1850·00	−1836·00	127	−799·00	−780·00	182	114·00	134·33
16	−2897·00	−2877·00	72	−1836·00	−1822·00	128	−780·00	−762·00	183	134·33	154·67
17	−2877·00	−2857·00	73	−1822·00	−1808·00	129	−762·00	−739·40	184	154·67	175·00
18	−2857·00	−2837·00	74	−1808·00	−1794·00	130	−739·40	−716·80	185	175·00	180·00
19	−2837·00	−2817·00	75	−1794·00	−1780·00	131	−716·80	−694·20	186	180·00	185·00
20	−2817·00	−2796·13	76	−1780·00	−1754·25	132	−694·20	−671·60	187	185·00	190·00
21	−2796·13	−2775·25	77	−1754·25	−1728·50	133	−671·60	−649·00	188	190·00	195·00
22	−2775·25	−2754·38	78	−1728·50	−1702·75	134	−649·00	−626·40	189	195·00	200·00
23	−2754·38	−2733·50	79	−1702·75	−1677·00	135	−626·40	−603·80	190	200·00	205·00
24	−2733·50	−2712·62	80	−1677·00	−1657·00	136	−603·80	−581·20	191	205·00	210·00
25	−2712·62	−2691·75	81	−1657·00	−1637·00	137	−581·20	−558·60	192	210·00	215·00
26	−2691·75	−2670·88	82	−1637·00	−1617·00	138	−558·60	−536·00	193	215·00	220·00
27	−2670·88	−2650·00	83	−1617·00	−1598·50	139	−536·00	−513·40	194	220·00	225·00
28	−2650·00	−2631·00	84	−1598·50	−1580·00	140	−513·40	−490·80	195	225·00	230·00
29	−2631·00	−2612·00	85	−1580·00	−1552·00	141	−490·80	−468·20	196	230·00	235·00
30	−2612·00	−2593·00	86	−1552·00	−1524·00	142	−468·20	−445·60	197	235·00	240·00
31	−2593·00	−2574·00	87	−1524·00	−1496·00	143	−445·60	−423·00	198	240·00	245·00
32	−2574·00	−2554·33	88	−1496·00	−1468·00	144	−423·00	−400·40	199	245·00	250·00
33	−2554·33	−2534·67	89	−1468·00	−1440·00	145	−400·40	−377·80	200	250·00	255·00
34	−2534·67	−2515·00	90	−1440·00	−1428·50	146	−377·80	−355·20	201	255·00	260·00
35	−2515·00	−2504·00	91	−1428·50	−1417·00	147	−355·20	−332·60	202	260·00	265·00
36	−2504·00	−2493·00	92	−1417·00	−1397·00	148	−332·60	−310·00	203	265·00	270·00
37	−2493·00	−2490·00	93	−1397·00	−1377·00	149	−310·00	−299·00	204	270·00	275·00
38	−2490·00	−2480·00	94	−1377·00	−1357·00	150	−299·00	−288·00	205	275·00	315·00
39	−2480·00	−2470·00	95	−1357·00	−1337·00	151	−288·00	−280·25	206	315·00	355·00
40	−2470·00	−2440·00	96	−1337·00	−1317·00	152	−280·25	−272·50	207	355·00	395·00
41	−2440·00	−2410·00	97	−1317·00	−1301·33	153	−272·50	−264·75	208	395·00	435·00
42	−2410·00	−2380·00	98	−1301·33	−1285·67	154	−264·75	−257·00	209	435·00	475·00
43	−2380·00	−2350·00	99	−1285·67	−1270·00	155	−257·00	−248·50	210	475·00	515·00
44	−2350·00	−2320·00	100	−1270·00	−1253·75	156	−248·50	−240·00	211	515·00	555·00
45	−2320·00	−2290·00	101	−1253·75	−1237·50	157	−240·00	−228·00	212	555·00	595·00
46	−2290·00	−2260·00	102	−1237·50	−1221·25	158	−228·00	−216·00	213	595·00	635·00
47	−2260·00	−2230·00	103	−1221·25	−1205·00	159	−216·00	−204·00	214	635·00	675·00
48	−2230·00	−2200·00	104	−1205·00	−1185·00	160	−204·00	−192·00	215	675·00	715·00
49	−2200·00	−2170·00	105	−1185·00	−1165·00	161	−192·00	−180·00	216	715·00	755·00
50	−2170·00	−2140·00	106	−1165·00	−1152·50	162	−180·00	−168·00	217	755·00	795·00
51	−2140·00	−2110·00	107	−1152·50	−1140·00	163	−168·00	−160·50	218	795·00	835·00
52	−2110·00	−2102·50	108	−1140·00	−1125·00	164	−160·50	−153·00	219	835·00	850·25
53	−2102·50	−2095·00	109	−1125·00	−1110·00	165	−153·00	−146·50	220	850·25	865·50
54	−2095·00	−2092·00	110	−1110·00	−1090·00	166	−146·50	−140·00	221	865·50	880·75
55	−2092·00	−2081·00	111	−1090·00	−1073·50	167	−140·00	−127·25	222	880·75	896·00
56	−2081·00	−2070·00	112	−1073·50	−1057·00						

[a] Axial interval.

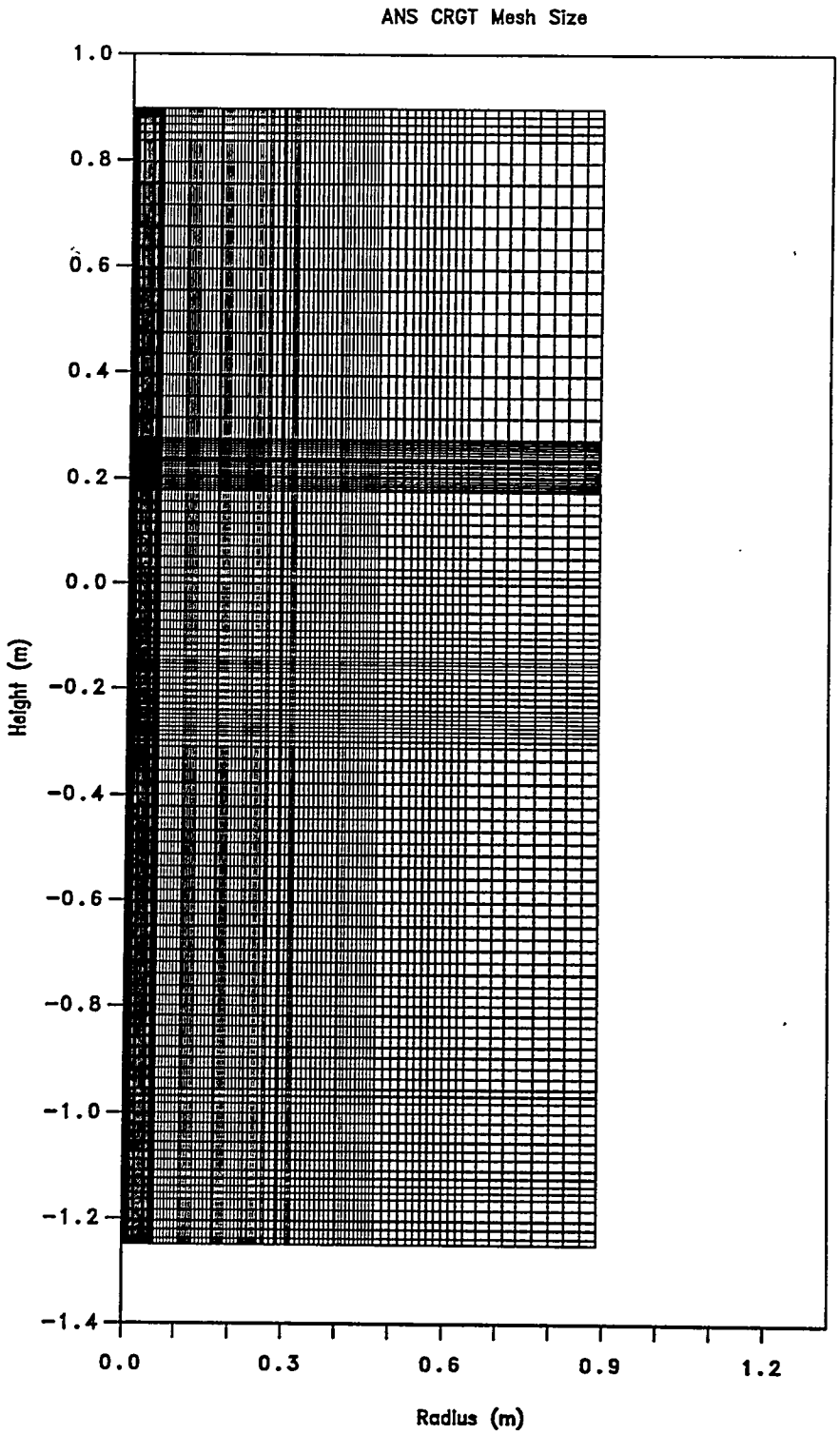

Fig. 2.3. The fine mesh configuration of the upper part of the DORT model. The mesh boundaries are listed in Tables 2.1 and 2.2.

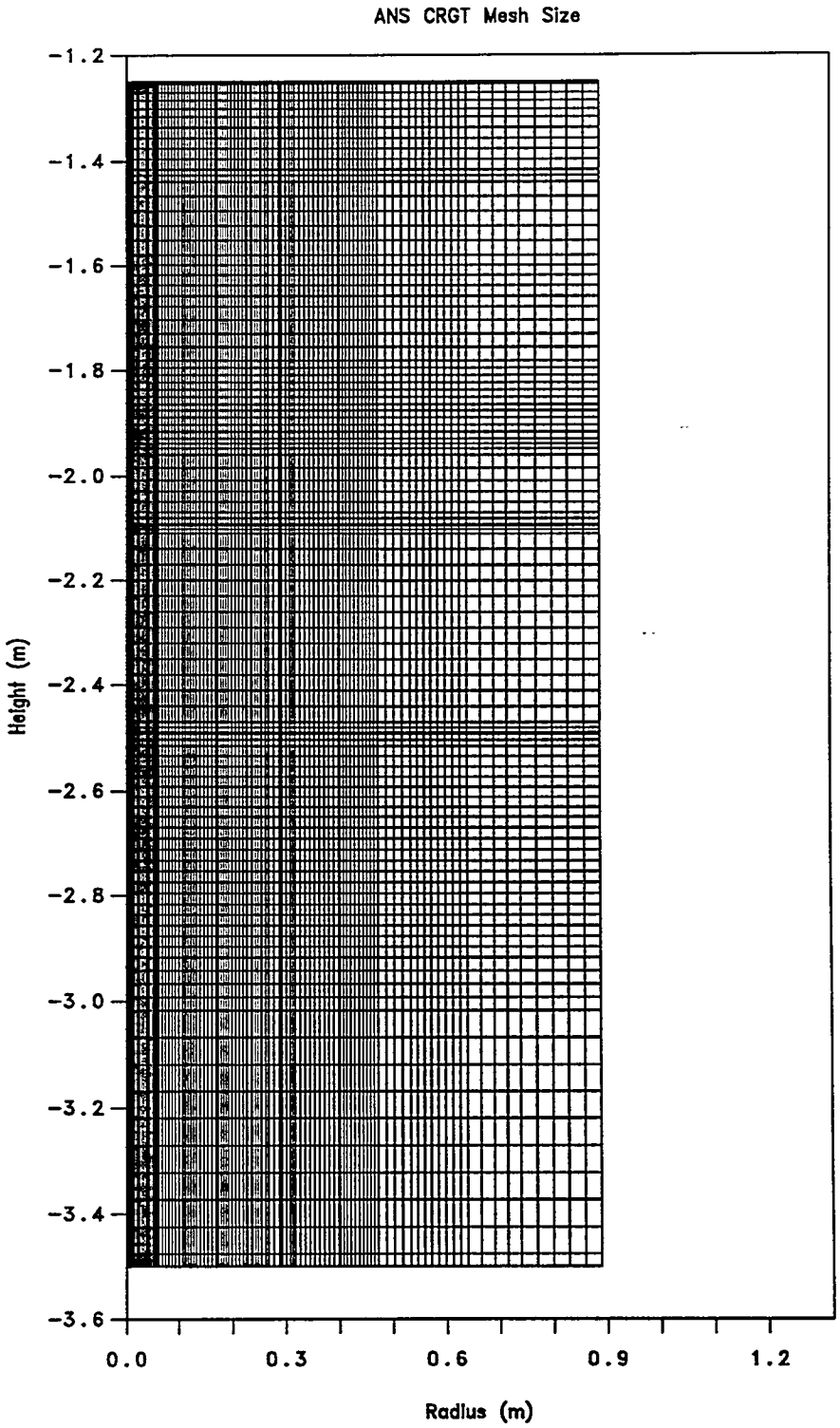

Fig. 2.4. The fine mesh configuration of the lower part of the DORT model. The mesh boundaries are listed in Tables 2.1 and 2.2.

3. DATA SETS

3.1 NEUTRON AND PHOTON CROSS SECTION

The DORT-ready cross section data used in the present work were based on the ANSL-V cross section library described in technical report ORNL-6618.[3] The 39 neutron groups and 44 gamma groups are listed in Table 3.1.

To do the shielding calculations with the DORT code, the cross sections had to be post-processed to

- add the delayed fission product gamma production terms for the ^{238}U and ^{235}U,
- convert the cross sections to the GIP-format[4] DORT is able to read,
- set the value of $\nu\Sigma_f$ in all data sets to a negligible small value that allows DORT to accelerate the convergence of the calculations by turning it into an eigenvalue problem, and
- add the photoneutron production capability.

These steps are described in detail in Sect. 4 of the report *Initial Global 2-D Shielding Analysis for the ANS Core and Reflector*[5] and are sketched briefly in Fig. 3.1. The list of macroscopic cross sections that were used in this study is given in Table 3.2 along with their material specifications.

3.2 QUADRATURE SET

Streaming through the D_2O-filled CRGT and streaming around the shields are important effects to be described properly in the DORT calculations. Therefore, a fully symmetric S_{10} quadrature set with 70 discrete angular directions was used rather than the S_8 set with 48 directions used in the report *Initial Global 2-D Shielding Analysis for the ANS Core and Reflector*.[5] The cosines of the discrete directions and their quadrature weights are listed in Table 3.3.

3.3 EXTERNAL BOUNDARY SOURCES

The CRGT and subpile room are coupled neutronically to the CPBT and the reflector vessel. For this reason, the upper surface of the present models was located 888 mm above the bottom of the reflector vessel.

The calculation of the neutron and gamma fluxes in the reflector vessel was the subject of the report *Initial Global 2-D Shielding Analysis for the ANS Core and Reflector*.[5] The fluxes obtained in that calculation served as boundary source for the present calculations.

Table 3.1. Energy group boundaries of the 39 neutron and 44 gamma groups of the ANSL-V library

Group number	Neutron groups Emax – Emin (eV) – (eV)	Gamma groups Emax – Emin (eV) – (eV)
1	2·00E + 07 – 6·43E + 06	2·00E + 07 – 1·40E + 07
2	6·43E + 06 – 3·00E + 06	1·40E + 07 – 1·20E + 07
3	3·00E + 06 – 1·85E + 06	1·20E + 07 – 1·00E + 07
4	1·85E + 06 – 1·40E + 06	1·00E + 07 – 8·00E + 06
5	1·40E + 06 – 9·00E + 05	8·00E + 06 – 7·50E + 06
6	9·00E + 05 – 4·00E + 05	7·50E + 06 – 7·00E + 06
7	4·00E + 05 – 1·00E + 05	7·00E + 06 – 6·50E + 06
8	1·00E + 05 – 1·70E + 04	6·50E + 06 – 6·00E + 06
9	1·70E + 04 – 3·00E + 03	6·00E + 06 – 5·50E + 06
10	3·00E + 03 – 5·50E + 02	5·50E + 06 – 5·00E + 06
11	5·50E + 02 – 1·00E + 02	5·00E + 06 – 4·50E + 06
12	1·00E + 02 – 3·00E + 01	4·50E + 06 – 4·00E + 06
13	3·00E + 01 – 1·00E + 01	4·00E + 06 – 3·50E + 06
14	1·00E + 01 – 3·00E + 00	3·50E + 06 – 3·00E + 06
15	3·00E + 00 – 1·77E + 00	3·00E + 06 – 2·50E + 06
16	1·77E + 00 – 1·30E + 00	2·50E + 06 – 2·35E + 06
17	1·30E + 00 – 1·00E + 00	2·35E + 06 – 2·15E + 06
18	1·00E + 00 – 7·65E − 01	2·15E + 06 – 2·00E + 06
19	7·65E − 01 – 5·88E − 01	2·00E + 06 – 1·80E + 06
20	5·88E − 01 – 4·79E − 01	1·80E + 06 – 1·66E + 06
21	4·79E − 01 – 3·97E − 01	1·66E + 06 – 1·57E + 06
22	3·97E − 01 – 3·30E − 01	1·57E + 06 – 1·50E + 06
23	3·30E − 01 – 2·70E − 01	1·50E + 06 – 1·44E + 06
24	2·70E − 01 – 2·15E − 01	1·44E + 06 – 1·33E + 06
25	2·15E − 01 – 1·62E − 01	1·33E + 06 – 1·20E + 06
26	1·62E − 01 – 1·04E − 01	1·20E + 06 – 1·00E + 06
27	1·04E − 01 – 5·00E − 02	1·00E + 06 – 8·00E + 05
28	5·00E − 02 – 3·00E − 02	8·00E + 05 – 7·00E + 05
29	3·00E − 02 – 1·00E − 02	7·00E + 05 – 6·00E + 05
30	1·00E − 02 – 4·45E − 03	6·00E + 05 – 5·12E + 05
31	4·45E − 03 – 3·25E − 03	5·12E + 05 – 5·10E + 05
32	3·25E − 03 – 2·60E − 03	5·10E + 05 – 4·50E + 05
33	2·60E − 03 – 2·15E − 03	4·50E + 05 – 4·00E + 05
34	2·15E − 03 – 1·80E − 03	4·00E + 05 – 3·00E + 05
35	1·80E − 03 – 1·45E − 03	3·00E + 05 – 2·00E + 05
36	1·45E − 03 – 1·13E − 03	2·00E + 05 – 1·50E + 05
37	1·13E − 03 – 8·50E − 04	1·50E + 05 – 1·00E + 05
38	8·50E − 04 – 5·50E − 05	1·00E + 05 – 7·50E + 04
39	5·50E − 05 – 1·00E − 05	7·50E + 04 – 7·00E + 04
40	–	7·00E + 04 – 6·00E + 04
41	–	6·00E + 04 – 4·50E + 04
42	–	4·50E + 04 – 3·00E + 04
43	–	3·00E + 04 – 2·00E + 04
44	–	2·00E + 04 – 1·00E + 04

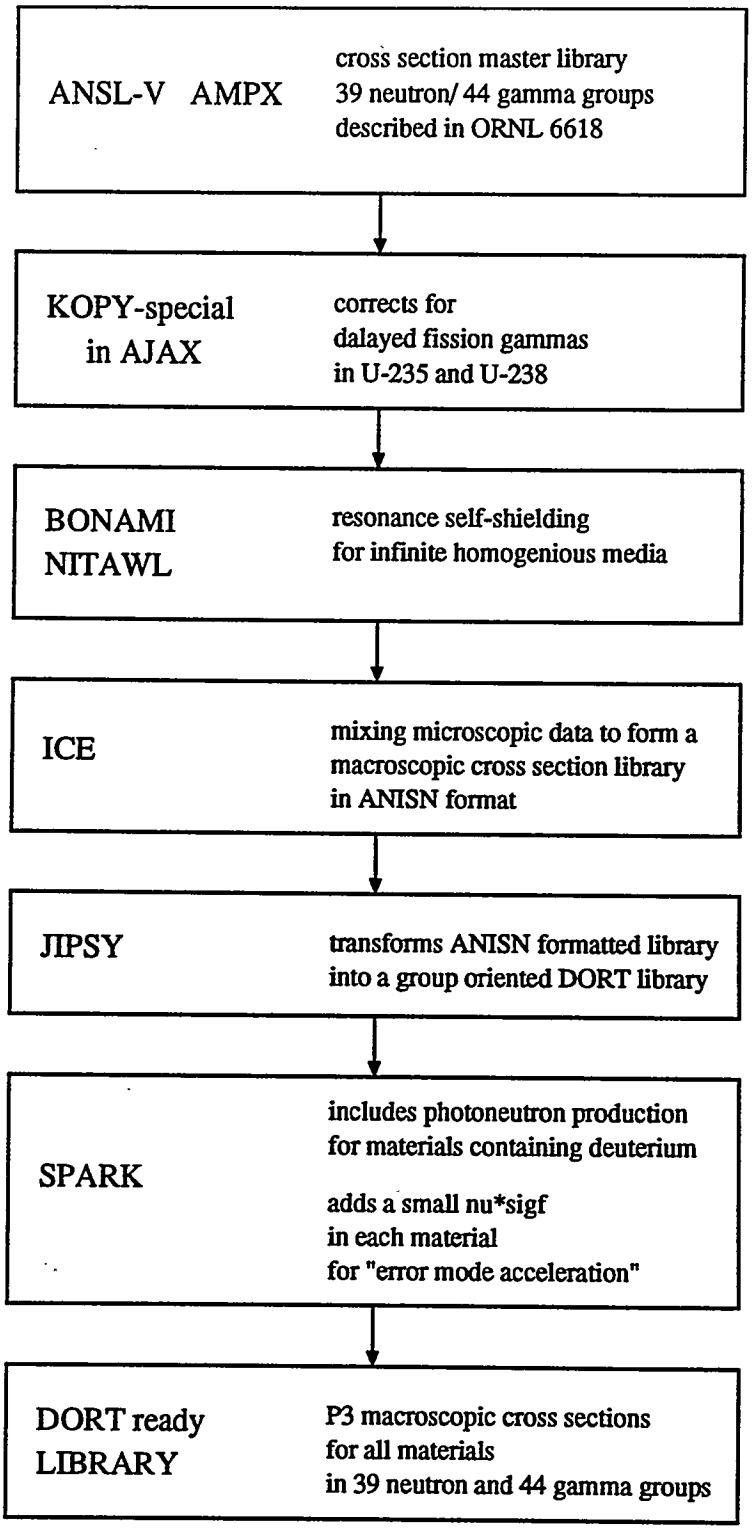

Fig. 3.1. Post-processing of the ANSL-V cross section data into DORT-ready cross sections for the shielding task.

Table 3.2. Nuclide number densities [atom/(barn cm)] for the materials used in the DORT calculations

Heavy water D_2O with temperature T=322.15 K	
D	5.9561E–02
O	2.9781E–02

D_2O in reflector with 0.2 mole % H_2O with temperature T=318.0 K	
D	6.5906E–02
H	1.3242E–04
O	3.3019E–02

Regular water H_2O with temperature T=322.15 K	
H	6.6111E–02
O	3.3055E–02

Aluminum 6061 with temperature T=339.15 K	
Mg	6.6871E–04
Al	5.8219E–02
Si	3.4722E–04
Ti	5.0919E–05
Cr	6.2517E–05
Mn	4.4377E–05
Fe	2.0373E–04
Cu	7.6072E–05
Zn	6.2149E–05

Table 3.2 (continued)

Steel SS-316NG with temperature T=323 K	
Cr	1.5620E–02
Fe	5.5440E–02
Ni	1.0170E–02
Mn	1.7390E–03
Mo	1.2450E–03
Si	2.0410E–03

Inconel-718 with temperature T=323 K	
Cr	1.7100E–02
Fe	1.6840E–02
Ni	4.4710E–02
Mn	1.7130E–04
Mo	1.6310E–03
Si	1.5870E–04
Ti	9.8220E–04

Ideal neutron absorber $\sigma_t = 100000$ barn	
–	1.0000E–02

Natural hafnium for control rod (13.31 g/cc) with temperature T=322.15 K	
Hf	4.4773E–02

Boral ($\rho = 2.64$ g/cc, 35 weight % B_4C) with temperature T=323 K	
Al	3.8300E–02
B-10	7.9620E–03
B-11	3.2323E–02
C	1.0071E–02

Table 3.2 (continued)

Barytes concrete with temperature T=323 K	
H	1.6810E–02
B-10	3.3780E–04
B-11	1.3680E–03
O	4.1950E–02
Na	3.1930E–04
Mg	1.5490E–04
Al	7.5340E–04
Si	1.2600E–03
S	5.4010E–03
Ca	3.2730E–03
Ti	1.3360E–04
Mn	1.7130E–04
Fe	6.8750E–04
Ba-134	1.3037E–04
Ba-135	3.5557E–04
Ba-136	4.2364E–04
Ba-137	6.0575E–04
Ba-138	3.8787E–03

Void	
O	1.0000E–25

Table 3.3. The fully symmetric S_{10} quadrature set with 70 discrete directions as used in the DORT calculations

M	Weight	μ^a	τ^b	M	Weight	μ^a	τ^b
1	0·0000E+00	−2·7217E−01	−9·6225E−01	36	0·0000E+00	−2·7217E−01	9·6225E−01
2	2·3001E−02	−1·9245E−01	−9·6225E−01	37	2·3001E−02	−1·9245E−01	9·6225E−01
3	2·3001E−02	1·9245E−01	−9·6225E−01	38	2·3001E−02	1·9245E−01	9·6225E−01
4	0·0000E+00	−5·4433E−01	−8·3887E−01	39	0·0000E+00	−5·4433E−01	8·3887E−01
5	1·7468E−02	−5·0918E−01	−8·3887E−01	40	1·7468E−02	−5·0918E−01	8·3887E−01
6	1·7468E−02	−1·9245E−01	−8·3887E−01	41	1·7468E−02	−1·9245E−01	8·3887E−01
7	1·7468E−02	1·9245E−01	−8·3887E−01	42	1·7468E−02	1·9245E−01	8·3887E−01
8	1·7468E−02	5·0918E−01	−8·3887E−01	43	1·7468E−02	5·0918E−01	8·3887E−01
9	0·0000E+00	−7·2008E−01	−6·9389E−01	44	0·0000E+00	−7·2008E−01	6·9389E−01
10	1·2346E−02	−6·9389E−01	−6·9389E−01	45	1·2346E−02	−6·9389E−01	6·9389E−01
11	1·3051E−02	−5·0918E−01	−6·9389E−01	46	1·3051E−02	−5·0918E−01	6·9389E−01
12	1·2346E−02	−1·9245E−01	−6·9389E−01	47	1·2346E−02	−1·9245E−01	6·9389E−01
13	1·2346E−02	1·9245E−01	−6·9389E−01	48	1·2346E−02	1·9245E−01	6·9389E−01
14	1·3051E−02	5·0918E−01	−6·9389E−01	49	1·3051E−02	5·0918E−01	6·9389E−01
15	1·2346E−02	6·9389E−01	−6·9389E−01	50	1·2346E−02	6·9389E−01	6·9389E−01
16	0·0000E+00	−8·6066E−01	−5·0918E−01	51	0·0000E+00	−8·6066E−01	5·0918E−01
17	1·7468E−02	−8·3887E−01	−5·0918E−01	52	1·7468E−02	−8·3887E−01	5·0918E−01
18	1·3051E−02	−6·9389E−01	−5·0918E−01	53	1·3051E−02	−6·9389E−01	5·0918E−01
19	1·3051E−02	−5·0918E−01	−5·0918E−01	54	1·3051E−02	−5·0918E−01	5·0918E−01
20	1·7468E−02	−1·9245E−01	−5·0918E−01	55	1·7468E−02	−1·9245E−01	5·0918E−01
21	1·7468E−02	1·9245E−01	−5·0918E−01	56	1·7468E−02	1·9245E−01	5·0918E−01
22	1·3051E−02	5·0918E−01	−5·0918E−01	57	1·3051E−02	5·0918E−01	5·0918E−01
23	1·3051E−02	6·9389E−01	−5·0918E−01	58	1·3051E−02	6·9389E−01	5·0918E−01
24	1·7468E−02	8·3887E−01	−5·0918E−01	59	1·7468E−02	8·3887E−01	5·0918E−01
25	0·0000E+00	−9·8131E−01	−1·9245E−01	60	0·0000E+00	−9·8131E−01	1·9245E−01
26	2·3001E−02	−9·6225E−01	−1·9245E−01	61	2·3001E−02	−9·6225E−01	1·9245E−01
27	1·7468E−02	−8·3887E−01	−1·9245E−01	62	1·7468E−02	−8·3887E−01	1·9245E−01
28	1·2346E−02	−6·9389E−01	−1·9245E−01	63	1·2346E−02	−6·9389E−01	1·9245E−01
29	1·7468E−02	−5·0918E−01	−1·9245E−01	64	1·7468E−02	−5·0918E−01	1·9245E−01
30	2·3001E−02	−1·9245E−01	−1·9245E−01	65	2·3001E−02	−1·9245E−01	1·9245E−01
31	2·3001E−02	1·9245E−01	−1·9245E−01	66	2·3001E−02	1·9245E−01	1·9245E−01
32	1·7468E−02	5·0918E−01	−1·9245E−01	67	1·7468E−02	5·0918E−01	1·9245E−01
33	1·2346E−02	6·9389E−01	−1·9245E−01	68	1·2346E−02	6·9389E−01	1·9245E−01
34	1·7468E−02	8·3887E−01	−1·9245E−01	69	1·7468E−02	8·3887E−01	1·9245E−01
35	2·3001E−02	9·6225E−01	−1·9245E−01	70	2·3001E−02	9·6225E−01	1·9245E−01

[a]Cosine of the discrete direction vector at a point with respect to the +R direction.

[b]Cosine of the discrete direction vector at a point with respect to the +Z axis.

In those cases where the horizontal shield extended over the whole bottom of the reflector vessel, the neutrons and gammas from the outer radial surface are blocked and do not influence the flux levels in the CRGT and subpile room. In these cases, an external radial boundary source at the top of the geometry (Z=0.89 m) was used. However, in the cases with the reduced horizontal shield, neutrons and gammas coming from the D_2O at the outer radial side can stream around the outer radial edge of the shield and contribute to radiation damage and the dose rates. They were included as an external axial boundary source at the outer radius (R=0.89 m) of the geometry.

The radial boundary source along the top surface of the present model (1184 mm below the core midplane) and the axial boundary source along the side of the present model (at R=890 mm) were therefore taken from the DORT results for the *Initial Global 2-D Shielding Analysis for the ANS Core and Reflector.*[5] Because the mesh specification and the quadrature set of the *Initial Global Shielding Analysis* were different from those used in the present study, the boundary source files were first processed by the BSPRP2 code[6] to make the necessary adjustments.

3.4 KERMA FACTORS

Multigroup neutron and gamma kerma factors were produced for the materials aluminum, iron, boral, and hafnium. They were used to convert the scalar flux results of the DORT calculations into heating rates that were necessary to estimate the heat generation in the shielding materials caused by radiation.

The gamma kerma factors were taken directly from the ANSL-V cross section library and are based on calculations by the SMUG module of the AMPX cross section processing code system[7] using theoretical expressions. The neutron kerma factors were extracted from the KAOS-V kerma factor library[8] and collapsed to the 39 neutron group structure by the RETRIEVE module supplied with the KAOS-V library accounting for prompt and delayed energy release including the β and α energies.

As there was no easy way to account correctly for the gammas originating from decay (this would need to be treated by a separate transport calculation), all decay energy was assumed to be deposited locally. This may result in small overestimates of some heating rates.

Plots and values of the neutron and gamma kerma factors for boral and hafnium are shown in Figs. 3.2 and 3.3 and the Tables 3.4 and 3.5, respectively. Kerma factors for aluminum and iron are described in Sect. 5 and in Appendix D1 of the *Initial Global 2-D Shielding Analysis for the ANS Core and Reflector.*[5]

3.5 FLUX-TO-DOSE CONVERSION FACTORS

The neutron and gamma flux-to-dose conversion factors for the energy group structure of the ANSL-V library were generated by the ANSIDOSE.F program described in Ref. 5 and were computed according to American National Standards Institute (ANSI) standard ANSI/ANS-6.1.1-1977.[9] The conversion factors are listed in Table 3.6. The newer standard ANSI/ANS-6.1.1-1991[10] has been released; however, the applicability of this standard is still a matter of debate among the technical community and was therefore not used in this work.

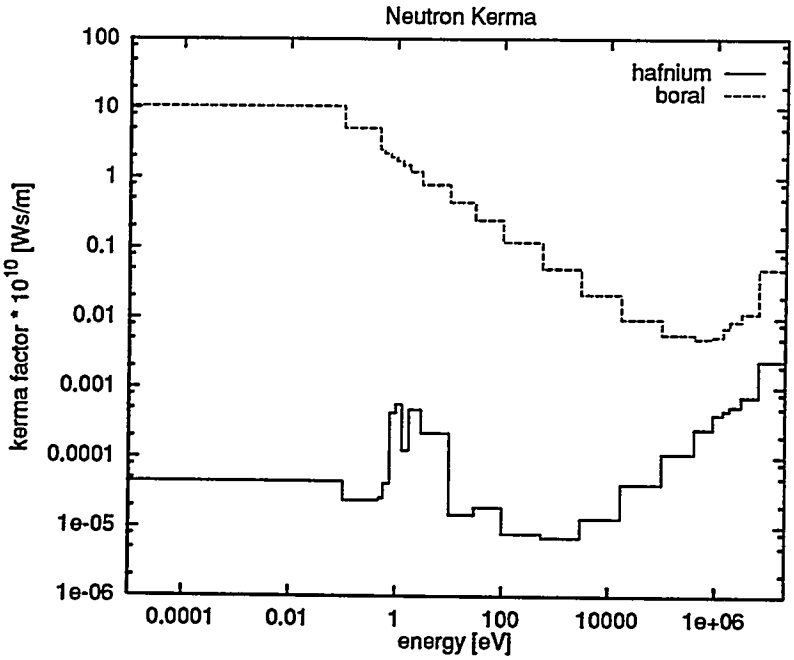

Fig. 3.2. Plot of the neutron kerma factors for boral and hafnium.

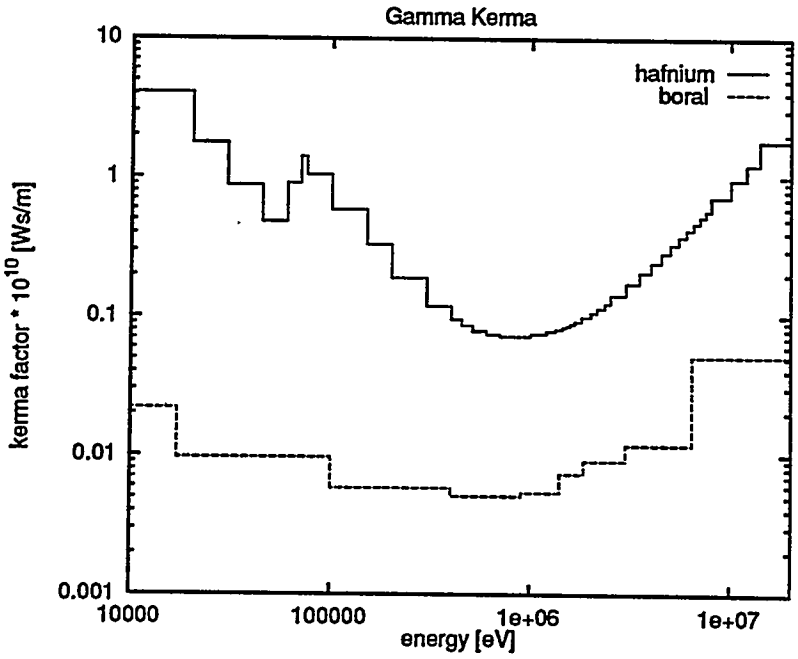

Fig. 3.3. Plot of the gamma kerma factors for boral and hafnium.

Table 3.4. Neutron kerma factors for boral and hafnium

Energy boundaries (eV)		Kerma factors (Ws/m)	
Group number	Emin – Emax	Hafnium	Boral
1	2.00E+07 – 6.43E+06	2.4346E–13	5.1186E–12
2	6.43E+06 – 3.00E+06	7.4030E–14	1.1809E–12
3	3.00E+06 – 1.85E+06	5.3942E–14	9.0512E–13
4	1.85E+06 – 1.40E+06	4.7585E–14	7.3638E–13
5	1.40E+06 – 9.00E+05	4.1094E–14	5.3993E–13
6	9.00E+05 – 4.00E+05	2.5492E–14	5.0953E–13
7	4.00E+05 – 1.00E+05	1.1253E–14	5.8249E–13
8	1.00E+05 – 1.70E+04	4.1023E–15	9.6174E–13
9	1.70E+04 – 3.00E+03	1.3237E–15	2.1733E–12
10	3.00E+03 – 5.50E+02	7.0079E–16	5.1697E–12
11	5.50E+02 – 1.00E+02	7.9805E–16	1.2167E–11
12	1.00E+02 – 3.00E+01	1.9169E–15	2.4948E–11
13	3.00E+01 – 1.00E+01	1.4978E–15	4.4467E–11
14	1.00E+01 – 3.00E+00	2.2319E–14	7.9073E–11
15	3.00E+00 – 1.77E+00	4.8283E–14	1.2095E–10
16	1.77E+00 – 1.30E+00	1.2558E–14	1.4933E–10
17	1.30E+00 – 1.00E+00	5.6548E–14	1.7175E–10
18	1.00E+00 – 7.65E–01	4.2968E–14	1.9596E–10
19	7.65E–01 – 5.88E–01	4.2381E–15	2.2374E–10
20	5.88E–01 – 4.79E–01	2.6166E–15	2.5190E–10
21	4.79E–01 – 3.97E–01	2.4305E–15	5.1131E–10
22	3.97E–01 – 3.30E–01	2.4305E–15	5.1144E–10
23	3.30E–01 – 2.70E–01	2.4305E–15	5.1144E–10
24	2.70E–01 – 2.15E–01	2.4305E–15	5.1144E–10
25	2.15E–01 – 1.62E–01	2.4305E–15	5.1144E–10
26	1.62E–01 – 1.04E–01	2.4305E–15	5.1144E–10
27	1.04E–01 – 5.00E–02	4.5046E–15	1.0588E–09
28	5.00E–02 – 3.00E–02	4.5103E–15	1.0603E–09
29	3.00E–02 – 1.00E–02	4.5103E–15	1.0603E–09
30	1.00E–02 – 4.45E–03	4.5103E–15	1.0603E–09
31	4.45E–03 – 3.25E–03	4.5103E–15	1.0603E–09
32	3.25E–03 – 2.60E–03	4.5103E–15	1.0603E–09
33	2.60E–03 – 2.15E–03	4.5103E–15	1.0603E–09
34	2.15E–03 – 1.80E–03	4.5103E–15	1.0603E–09
35	1.80E–03 – 1.45E–03	4.5103E–15	1.0603E–09
36	1.45E–03 – 1.13E–03	4.5103E–15	1.0603E–09
37	1.13E–03 – 8.50E–04	4.5103E–15	1.0603E–09
38	8.50E–04 – 5.50E–05	4.5103E–15	1.0603E–09
39	5.50E–05 – 1.00E–05	4.5103E–15	1.0603E–09

Table 3.5. Gamma kerma factors for boral and hafnium

Energy boundaries (eV)		Kerma factors (Ws/m)	
Group number	Emin – Emax	Hafnium	Boral
1	2.00E+07 – 1.40E+07	1.8060E–10	1.1476E–11
2	1.40E+07 – 1.20E+07	1.2225E–10	8.7036E–12
3	1.20E+07 – 1.00E+07	9.5918E–11	7.4037E–12
4	1.00E+07 – 8.00E+06	7.1689E–11	6.1478E–12
5	8.00E+06 – 7.50E+06	5.7545E–11	5.3766E–12
6	7.50E+06 – 7.00E+06	5.2148E–11	5.0696E–12
7	7.00E+06 – 6.50E+06	4.7014E–11	4.7698E–12
8	6.50E+06 – 6.00E+06	4.2143E–11	4.4764E–12
9	6.00E+06 – 5.50E+06	3.7426E–11	4.1823E–12
10	5.50E+06 – 5.00E+06	3.2905E–11	3.8885E–12
11	5.00E+06 – 4.50E+06	2.8597E–11	3.5956E–12
12	4.50E+06 – 4.00E+06	2.4554E–11	3.3035E–12
13	4.00E+06 – 3.50E+06	2.0762E–11	3.0086E–12
14	3.50E+06 – 3.00E+06	1.7305E–11	2.7106E–12
15	3.00E+06 – 2.50E+06	1.4159E–11	2.4034E–12
16	2.50E+06 – 2.35E+06	1.2322E–11	2.1979E–12
17	2.35E+06 – 2.15E+06	1.1467E–11	2.0853E–12
18	2.15E+06 – 2.00E+06	1.0676E–11	1.9701E–12
19	2.00E+06 – 1.80E+06	9.8867E–12	1.8493E–12
20	1.80E+06 – 1.66E+06	9.2005E–12	1.7283E–12
21	1.66E+06 – 1.57E+06	8.7986E–12	1.6442E–12
22	1.57E+06 – 1.50E+06	8.5420E–12	1.5843E–12
23	1.50E+06 – 1.44E+06	8.2994E–12	1.5338E–12
24	1.44E+06 – 1.33E+06	8.0528E–12	1.4665E–12
25	1.33E+06 – 1.20E+06	7.7915E–12	1.3689E–12
26	1.20E+06 – 1.00E+06	7.4650E–12	1.2263E–12
27	1.00E+06 – 8.00E+05	7.1871E–12	1.0387E–12
28	8.00E+05 – 7.00E+05	7.1775E–12	8.8629E–13
29	7.00E+05 – 6.00E+05	7.3834E–12	7.7771E–13
30	6.00E+05 – 5.12E+05	7.8548E–12	6.7055E–13
31	5.12E+05 – 5.10E+05	8.2261E–12	6.1761E–13
32	5.10E+05 – 4.50E+05	8.6120E–12	5.8024E–13
33	4.50E+05 – 4.00E+05	9.5337E–12	5.1276E–13
34	4.00E+05 – 3.00E+05	1.1840E–11	4.1803E–13
35	3.00E+05 – 2.00E+05	1.8998E–11	2.8937E–13
36	2.00E+05 – 1.50E+05	3.2932E–11	1.9606E–13
37	1.50E+05 – 1.00E+05	5.8634E–11	1.4718E–13
38	1.00E+05 – 7.50E+04	1.0451E–10	1.3780E–13
39	7.50E+04 – 7.00E+04	1.4005E–10	1.5438E–13
40	7.00E+04 – 6.00E+04	9.0822E–11	1.7558E–13
41	6.00E+04 – 4.50E+04	4.8102E–11	2.4728E–13
42	4.50E+04 – 3.00E+04	8.8232E–11	4.8198E–13
43	3.00E+04 – 2.00E+04	1.7689E–10	1.1206E–12
44	2.00E+04 – 1.00E+04	4.0863E–10	3.5060E–12

Table 3.6. Neutron and gamma flux-to-dose-rate conversion factors in the 39 neutron group and 44 gamma group structure of the ANSL-V library

	Neutron dose [(s· m^2) · mrem/h]		Gamma dose [(s· m^2) · mrem/h]	
Group number	Emin – Emax	n-dose	Emin – Emax	γ-dose
1	2.00E+07 – 6.43E+06	1.4916E–05	2.00E+07 – 1.40E+07	1.4880E–06
2	6.43E+06 – 3.00E+06	1.4464E–05	1.40E+07 – 1.20E+07	1.1776E–06
3	3.00E+06 – 1.85E+06	1.2701E–05	1.20E+07 – 1.00E+07	1.0264E–06
4	1.85E+06 – 1.40E+06	1.2811E–05	1.00E+07 – 8.00E+06	8.7716E–07
5	1.40E+06 – 9.00E+05	1.2977E–05	8.00E+06 – 7.50E+06	7.8468E–07
6	9.00E+05 – 4.00E+05	1.0281E–05	7.50E+06 – 7.00E+06	7.4783E–07
7	4.00E+05 – 1.00E+05	5.1183E–06	7.00E+06 – 6.50E+06	7.1104E–07
8	1.00E+05 – 1.70E+04	1.2319E–06	6.50E+06 – 6.00E+06	6.7426E–07
9	1.70E+04 – 3.00E+03	3.8365E–07	6.00E+06 – 5.50E+06	6.3749E–07
10	3.00E+03 – 5.50E+02	3.7247E–07	5.50E+06 – 5.00E+06	6.0069E–07
11	5.50E+02 – 1.00E+02	4.0150E–07	5.00E+06 – 4.50E+06	5.6001E–07
12	1.00E+02 – 3.00E+01	4.2926E–07	4.50E+06 – 4.00E+06	5.2272E–07
13	3.00E+01 – 1.00E+01	4.4744E–07	4.00E+06 – 3.50E+06	4.8324E–07
14	1.00E+01 – 3.00E+00	4.5677E–07	3.50E+06 – 3.00E+06	4.4117E–07
15	3.00E+00 – 1.77E+00	4.5576E–07	3.00E+06 – 2.50E+06	3.9596E–07
16	1.77E+00 – 1.30E+00	4.5185E–07	2.50E+06 – 2.35E+06	3.6472E–07
17	1.30E+00 – 1.00E+00	4.4779E–07	2.35E+06 – 2.15E+06	3.4703E–07
18	1.00E+00 – 7.65E–01	4.4299E–07	2.15E+06 – 2.00E+06	3.2876E–07
19	7.65E–01 – 5.88E–01	4.3793E–07	2.00E+06 – 1.80E+06	3.0979E–07
20	5.88E–01 – 4.79E–01	4.3207E–07	1.80E+06 – 1.66E+06	2.9067E–07
21	4.79E–01 – 3.97E–01	4.2569E–07	1.66E+06 – 1.57E+06	2.7730E–07
22	3.97E–01 – 3.30E–01	4.1988E–07	1.57E+06 – 1.50E+06	2.6775E–07
23	3.30E–01 – 2.70E–01	4.1336E–07	1.50E+06 – 1.44E+06	2.5985E–07
24	2.70E–01 – 2.15E–01	4.0551E–07	1.44E+06 – 1.33E+06	2.4928E–07
25	2.15E–01 – 1.62E–01	3.9534E–07	1.33E+06 – 1.20E+06	2.3392E–07
26	1.62E–01 – 1.04E–01	3.7835E–07	1.20E+06 – 1.00E+06	2.1180E–07
27	1.04E–01 – 5.00E–02	3.6750E–07	1.00E+06 – 8.00E+05	1.8326E–07
28	5.00E–02 – 3.00E–02	3.6748E–07	8.00E+05 – 7.00E+05	1.6038E–07
29	3.00E–02 – 1.00E–02	3.6748E–07	7.00E+05 – 6.00E+05	1.4417E–07
30	1.00E–02 – 4.45E–03	3.6748E–07	6.00E+05 – 5.12E+05	1.2815E–07
31	4.45E–03 – 3.25E–03	3.6748E–07	5.12E+05 – 5.10E+05	1.2019E–07
32	3.25E–03 – 2.60E–03	3.6748E–07	5.10E+05 – 4.50E+05	1.1281E–07
33	2.60E–03 – 2.15E–03	3.6748E–07	4.50E+05 – 4.00E+05	1.0321E–07
34	2.15E–03 – 1.80E–03	3.6748E–07	4.00E+05 – 3.00E+05	8.7594E–08
35	1.80E–03 – 1.45E–03	3.6748E–07	3.00E+05 – 2.00E+05	6.3060E–08
36	1.45E–03 – 1.13E–03	3.6748E–07	2.00E+05 – 1.50E+05	4.3908E–08
37	1.13E–03 – 8.50E–04	3.6748E–07	1.50E+05 – 1.00E+05	3.2767E–08
38	8.50E–04 – 5.50E–05	3.6748E–07	1.00E+05 – 7.50E+04	2.6816E–08
39	5.50E–05 – 1.00E–05	3.6748E–07	7.50E+04 – 7.00E+04	2.5783E–08
40	–		7.00E+04 – 6.00E+04	2.6006E–08
41	–		6.00E+04 – 4.50E+04	2.8439E–08
42	–		4.50E+04 – 3.00E+04	4.1154E–08
43	–		3.00E+04 – 2.00E+04	8.2669E–08
44	–		2.00E+04 – 1.00E+04	2.1439E–07

3.6 FLUX-TO-DPA CONVERSION FACTORS

For most materials, displacement damage is caused by neutron-absorbing reactions and the subsequent decay, in which fast neutrons knock on atoms or the recoil impulse of the decay particle pushes the rest nucleus and displaces atoms from their original lattice sites, as for the iron atoms in steel. In both cases, the DPA are directly proportional to the flux level and can be estimated by standard flux-to-DPA conversion factors.

In some materials, however, sequential reactions play a significant role. In nickel, which is a significant component in stainless steel 316NG, a portion of the ^{58}Ni is converted to ^{56}Fe in the reaction sequence

$$^{58}Ni \quad (n,\gamma) \quad ^{59}Ni \quad (n,\alpha)^{56}Fe, \tag{3.1}$$

where the ^{56}Fe atom and the α-particle have recoil energies of 0.340 MeV and 4.757 MeV, respectively. (Note, for comparison, that the recoil energy of a nickel atom is a factor of 10 lower because of the absorption of a typical fission neutron.)

Because the α-particle is produced by a two-step reaction, the probability of its appearance is no longer linear with the neutron flux but is time dependent and can be derived as:[11]

$$\frac{N(\alpha)}{N_o(^{58}Ni)} = \frac{\sigma_\alpha}{\sigma_T} + \frac{\sigma_\alpha e^{-\sigma_{gamma}\phi t}}{\sigma_\gamma - \sigma_T} - \frac{\sigma_\alpha \sigma_\gamma e^{-\sigma_T \phi t}}{(\sigma_\gamma - \sigma_T)\sigma_T}, \tag{3.2}$$

where

N(α)	= α particles produced,
N$_o$(^{58}Ni)	= initial number of ^{58}Ni atoms,
σ_α	= spectral averaged ^{59}Ni(n,α) cross section,
σ_T	= spectral averaged total absorption cross section of ^{59}Ni,
σ_γ	= spectral averaged ^{58}Ni(n,γ) cross section,
ϕ	= scalar flux,
t	= irradiation time.

For a thermal neutron spectrum, the nickel cross sections are approximately $\sigma_\alpha = 11.6$ barn, $\sigma_T = 92$ barn, $\sigma_\gamma = 4.6$ barn. Although the nickel content in stainless steel 316NG varies from 10 to 15%, it was assumed to be 14 wt % in the present study.

Assuming that half of the ^{56}Fe energy, and 0.13% of the α- energy, will be expended in nuclear events,[11] the creation of one α-particle is accompanied by a total damage energy of 0.176 MeV, which gives a total of 1760 displaced atoms per generated α particle. Thus, in stainless steel 316NG, the DPA contributions from iron (calculated by flux-to-DPA conversion factors) and nickel (calculated by the formula given previously) add up to a total DPA value. Depending on the fluence (ϕt), one or other contribution may dominate, as can be seen in Fig. 3.4.

It is not only the displacements that cause problems in the strength and durability of the steel but also the high level of helium (as α-particle) deposited in the damaged lattice, which is recognized to be very harmful and must be estimated. The number of helium atoms produced by a given fluence is plotted in Fig. 3.5.

As there are few experimental data available for irradiation effects of steel in a thermal neutron spectrum at low temperatures, "acceptable levels" of helium production and DPA

must eventually be more clearly defined by material scientists.

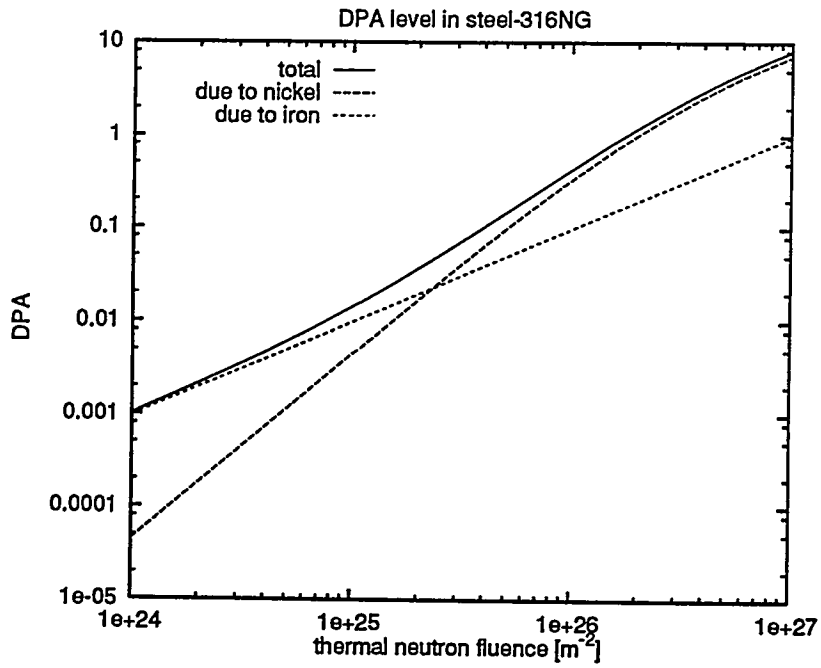

Fig. 3.4. DPA level in stainless steel 316NG vs thermal fluence (flux times exposure time).

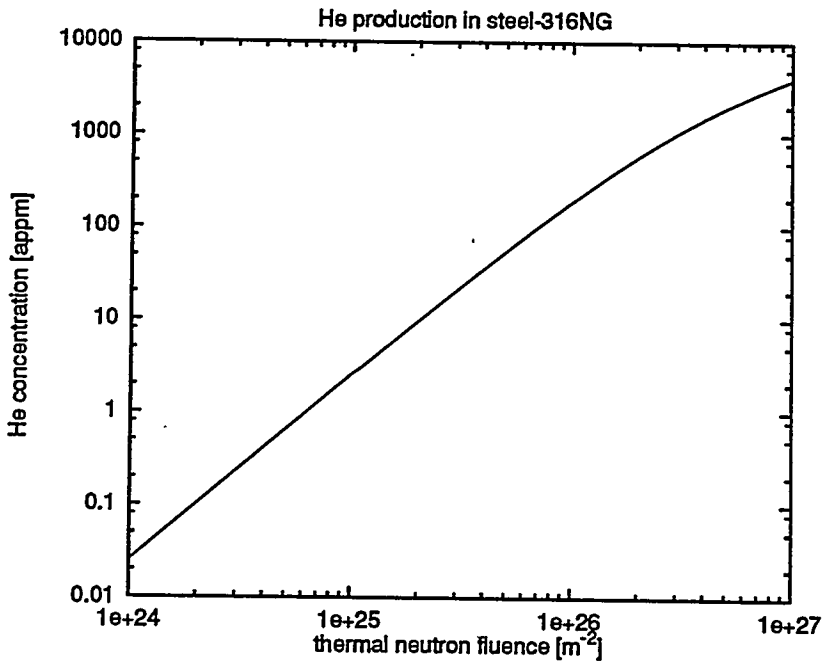

Fig. 3.5. Helium production in stainless steel 316NG vs thermal fluence (flux times exposure time).

4. THE DORT ITERATION SCHEME

Several characteristics make analysis of the CRGT and subpile room problem a very central processing unit (CPU)-time consuming one:

- The problem consists of 111 radial × 222 axial meshes. The fluxes in the meshes have to be converged spatially in so-called inner iterations.
- The number of 39 neutron groups and 44 gamma groups add up to 83 energy groups totally, which is a significantly large number for a discrete ordinates problem.
- Thermal neutron groups must be treated differently as downscattering and upscattering occur. Thus, because more than half of the neutron groups lie in the thermal energy range (25 of 39 groups), it is necessary to converge the fluxes in terms of energy in so-called outer iterations.
- Large regions of the problems consist of D_2O, a material with a very low absorption cross section and a large neutron diffusion length. Many inner iterations are needed for convergence in such regions.
- Furthermore, D_2O has a low threshold energy of 2.225 MeV for (γ,n)-reactions (photoneutron production), which is mathematically described by upscattering from gamma groups into neutron groups. So a second upscattering mechanism is present in the CRGT and subpile room problem, which needs to be treated with outer iterations.

The DORT program is discretizing the transport problem energetically and spatially and solving for the flux profile by converging energetically in so-called outer iterations and spatially in so-called inner iterations. The program starts the outer iterations with the group of the highest neutron energy, performs a number of inner iterations for spatial convergence, calculates downscattering and upscattering losses, and continues with the next neutron group. As long as no upscattering is present, one outer iteration is sufficient as downscattering is regarded in the following neutron groups having lower energy. After finishing the neutron groups, the calculation continues in the same way with the gamma groups in the order from high gamma energies to low energies. Upscattering does not occur in the gamma intern transport, which allows restricting the number of outer iterations to one. However, the photoneutron production phenomena is described mathematically as upscattering from gamma groups to neutron groups.

The nature of the problem makes it necessary to apply a three-step calculation to make the problem converge in a reasonable time:

Step 1 converges the fast and epithermal neutron fluxes in the groups 1 to 15, applying 1 outer iteration and 30 inner iterations.

Step 2 converges the thermal neutrons fluxes in the groups 16 to 39, using 50 outer iterations and 2 inner iterations for each outer using error-mode extrapolation.

Step 3 converges the gamma fluxes in the groups 40 to 83, using 1 outer iteration and 30 inner iterations.

To account for the photoneutrons the whole scheme has to be repeated, which means that essentially only one photoneutron iteration is performed. Note, however, that for solving the different cases the final flux file of the previous case is used as a starting guess, which is already a good approximation of the solution as long as the changes in between the cases are small

and the first calculation is fully converged. It therefore seemed sufficient to have only one photoneutron iteration. A more elaborate strategy for cases without a good starting guess for the flux is described in *Initial Global 2-D Shielding Analysis for the ANS Core and Reflector.*[5]

To proof the convergence, several checks were done. The output of all step 2 calculations was rearranged by the program CHKCON,[5] which lists tables of key fluxes (i.e., fluxes in specified meshes) in every energy group vs outer iteration number, which makes changes easily recognized visually. Fifty outer iterations were sufficient in all cases for thermal neutron flux convergence.

In one case, a calculation was performed by repeating the three-step scheme twice. No significant change of the broad group flux plots of the cases with one- and two-time application of the three-step scheme could be seen.

In one case, 50 additional outer iterations with two inner iterations each were done covering the energy groups 1 to 56 to check the convergence of the photoneutron production. The fluxes changed only in the percent range in some positions in the first few iterations, and the broad flux plots of ingoing and outgoing flux files showed only minor differences.

Finally, in a double check for the fluxes at the bottom of the reflector vessel, the calculation R550 without shield was compared against the results of Ref. 5 and showed good agreement.

5. FLUX RESULTS AND DOSE RATES

Showing detailed results for all the shielding cases investigated would certainly not be practical or desirable. To present as much information as possible, the fine group fluxes were processed to broad group fluxes and plotted as contour lines. The broad group fluxes are defined as follows.

Broad group name	Energy range	Fine groups
Fast neutron flux	0.1–14 MeV	1–7
Epithermal neutron flux 1	100 eV–0.1 MeV	8–11
Epithermal neutron flux 2	0.625–100 eV	12–19
Thermal neutron flux	0–0.625 eV	20–39
High-energy gamma flux	> 2 MeV	40–57
Low-energy gamma flux	< 2 MeV	58–83

Detailed flux information can be found in Figs. A.1–A.24 in Appendix A for three technical relevant cases: for case R550 without any shield around the base of the CPBT, for case R400 with the radially extended boral shield, and for case R500 with the radially restricted hafnium shield. Plots of neutron and gamma dose rates are also included in Appendix A.

The neutron dose rates are dominated by the fast neutron fluxes. High- and low-energy fluxes contribute equally to the gamma dose rate. Although the high-energy gamma flux is a factor of 10 lower than the low-energy flux, its contribution to the gamma dose rate is balanced by higher flux-to-dose-rate conversion factors. Comparing the case R550 without any shield against the cases R450 and R500 with shield, it becomes obvious that the shield has no influence at all on the fluxes and dose rates in the subpile room. Case R400 for the radially extended boral shield shows about a factor of 10 lower neutron and gamma dose rates in the subpile room compared against the corresponding dose rates in cases R500 and R550. Note, however, that the sources from the outer radial boundary are missing in this case, which makes a great difference especially, for the deep-penetrating, high-energy gamma fluxes. This affects both the gamma and neutron dose rates because it originates in the fact that the fast neutron flux is built up mainly by photoneutrons produced by the high-energy gamma fluxes because the threshold for photoneutron production in deuterium is 2.225 MeV.

Changes in the shield design were motivated mainly by the need to reduce the thermal neutron flux in the PCSA and its flange (both fabricated of steel). For documentation of the ongoing work and the lessons learned, the thermal neutron fluxes in the upper part of the geometry are plotted for all cases investigated. The description of the geometric zones overlayed on the flux contour plots is in Sect. 2. In the following text associated with each figure, the numbers in parentheses refer to components shown in Fig. 2.2 and described in Table 2.1. All fluxes are given in units ($m^{-2} \cdot s^{-1}$).

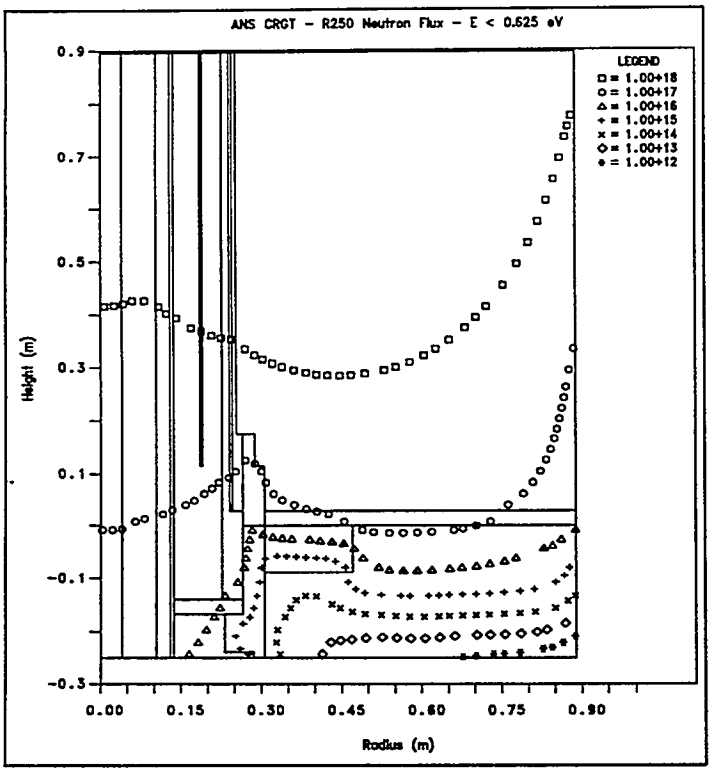

Case R250:
The neutron fluxes are given in units $[m^{-2} \cdot s^{-1}]$. Without any shield, the tip of the PCSA (7) reaches into the thermal neutron flux level of $2 \cdot 10^{17}$ $m^{-2} \cdot s^{-1}$ and the parts of the flange (8) near the reflector vessel are exposed to a flux of almost $1 \cdot 10^{17}$ $m^{-2} \cdot s^{-1}$. The rapid drop of the fluxes at the outer radial boundary is artificial and is caused by lack of the radial boundary source.

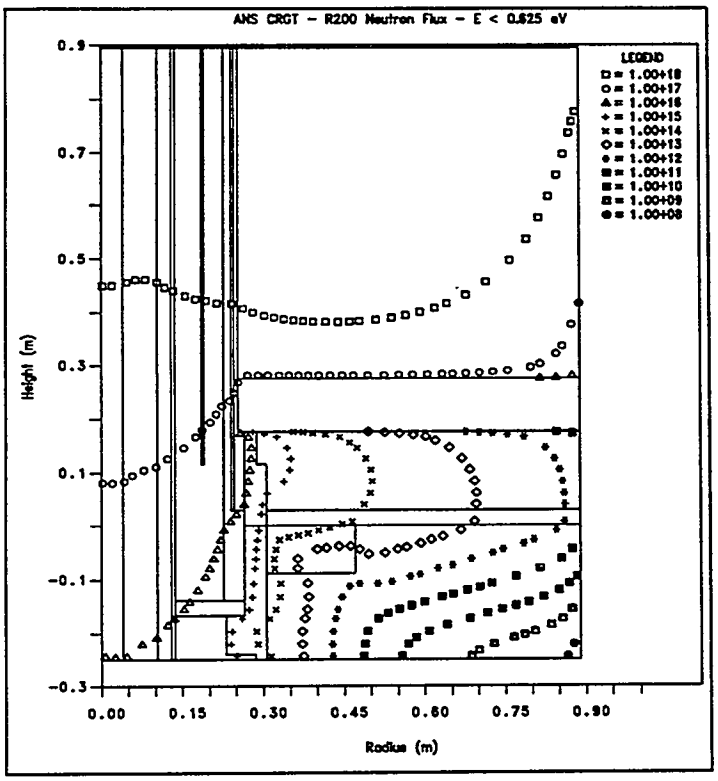

Case R200:
The horizontal shield (3) of an ideal absorber lowers the thermal neutron flux at the tip of the PCSA (7) by about a factor of 10 to about $2 \cdot 10^{16}$ $m^{-2} \cdot s^{-1}$ and reduces the maximal flux in the flange (8) by more than a factor of 100, to values below $1 \cdot 10^{15}$ $m^{-2} \cdot s^{-1}$. The shield blocks neutrons coming from the reflector vessel; however, the D_2O-filled CPBT allows neutrons to stream down and into the 150-mm-wide layer between the shield and the bottom of the reflector vessel.

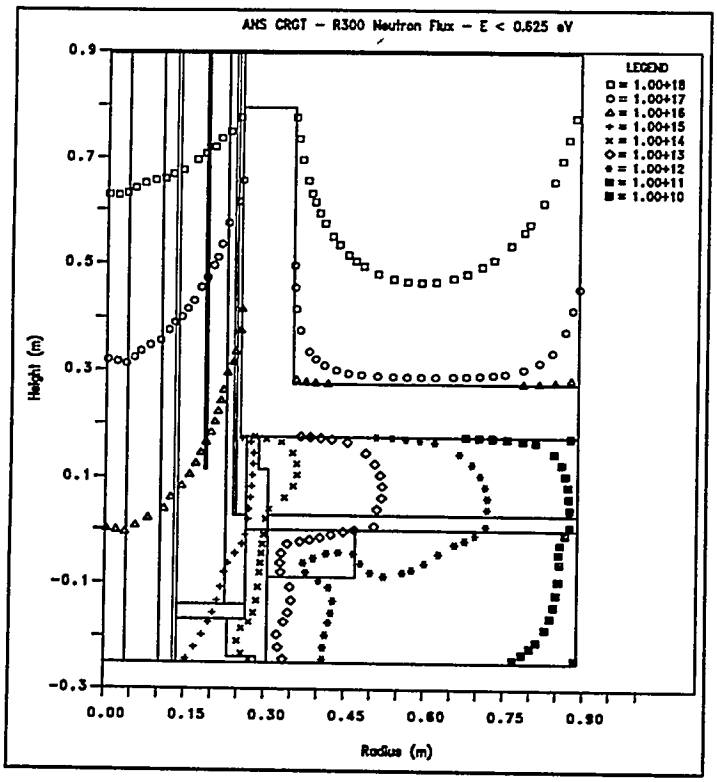

Case R300:
Extending the ideal shield material vertically outward from the CPBT (4) to a height of 0.79 m reduces the thermal neutron flux at the tip of the PCSA (7) about a factor of 100, compared with the unshielded case R250, to $2 \cdot 10^{15}$ $m^{-2} \cdot s^{-1}$. Also, the flux at the flange (8) is now reduced by about a factor of 1000, to below $1 \cdot 10^{14}$ $m^{-2} \cdot s^{-1}$.

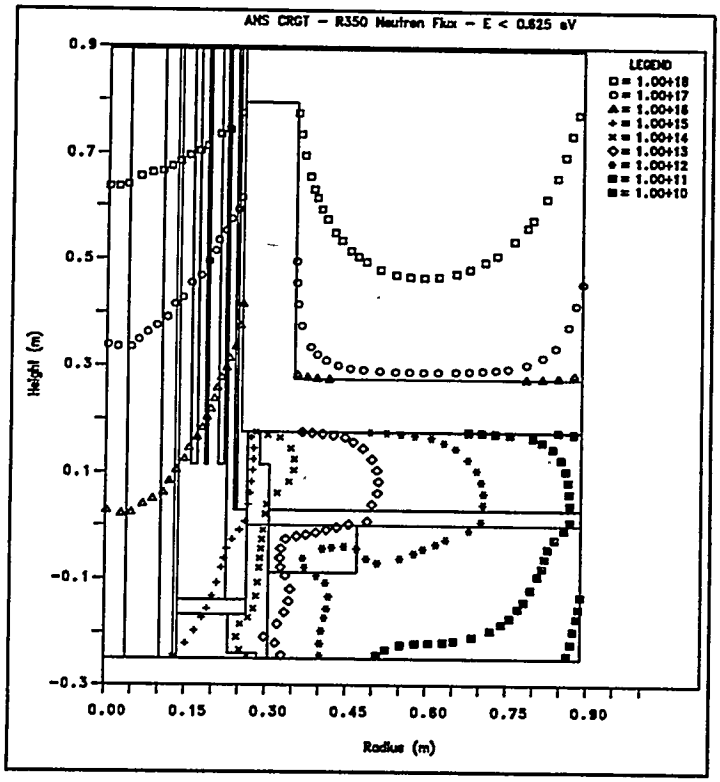

Case R350:
Including the core support structure (5) into the D_2O of the CPBT (4), which is a significant volume of aluminum, has little effect neutronically.

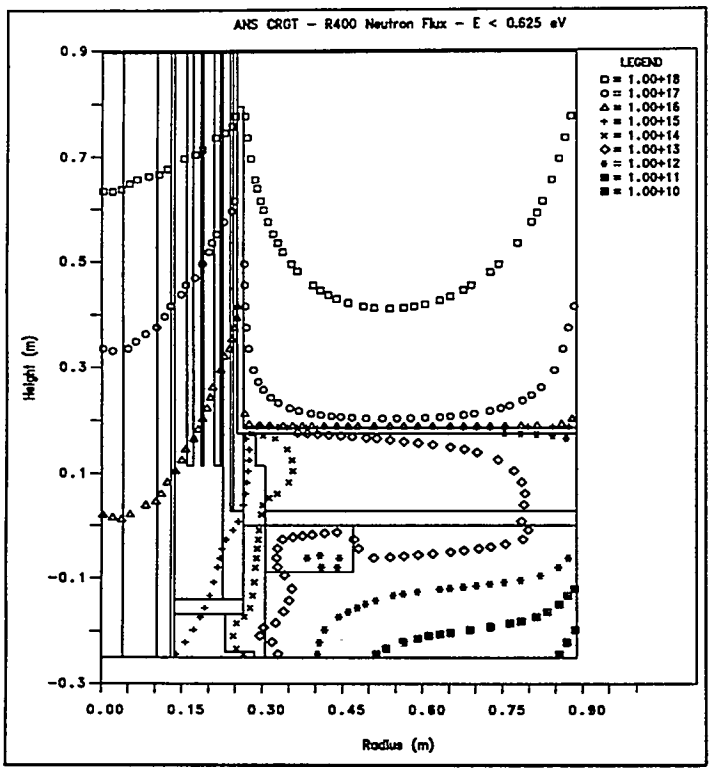

Case R400:
Replacing the 10-cm-thick ideal shield by a realistic 13 to 15-mm-thick boral shield (3) without changing the overall shield dimensions does not have influence on the fluxes in the PCSA (7) and the flange (8). This demonstrates that the shielding performance of boral is almost as good as the shielding performance of the ideal absorber.

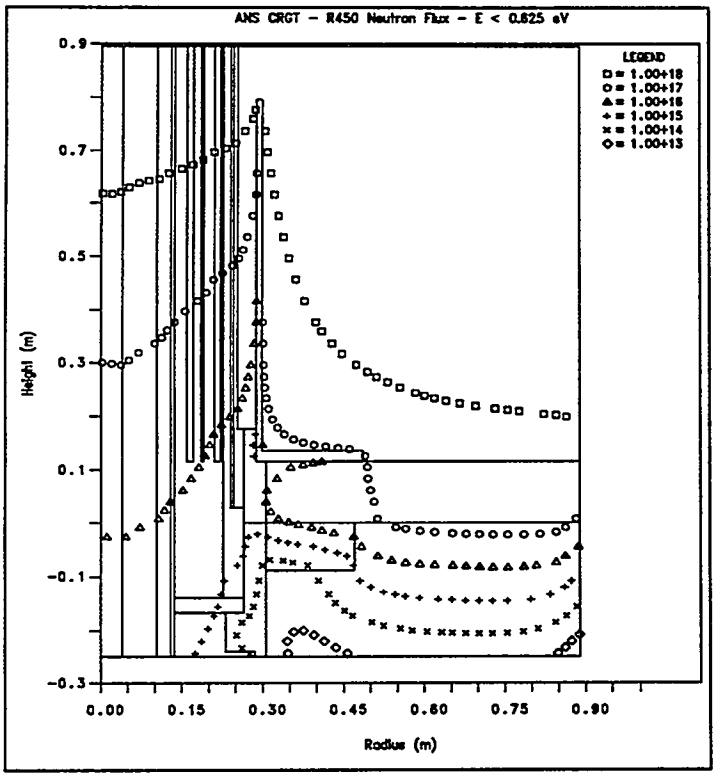

Case R450:
Restricting the horizontal shield component to the radius of 485 mm and placing it flush against the extended reflector vessel bottom (1) exposes the PCSA to the thermal neutron flux of about $8 \cdot 10^{15}$ $m^{-2} \cdot s^{-1}$ and the flange to about $2 \cdot 10^{16}$ $m^{-2} \cdot s^{-1}$. This is a reduction in thermal neutron flux of a factor of 20 for the PCSA (7) and 3 for the flange (8) compared with the unshielded case R550. Note that in this case and the following cases the radial boundary source has been taken into account.

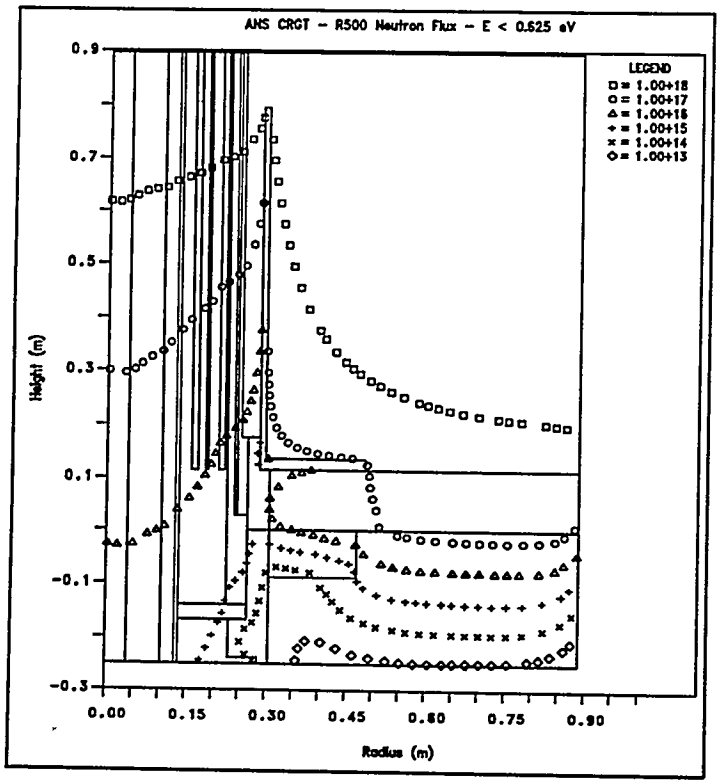

Case R500:
Using hafnium as shielding material instead of boral has no effect on the thermal neutron fluxes, although the neutron absorption in hafnium is a factor of 6 smaller than in boral. Even 10-mm-thick hafnium absorbs more than 99% of the thermal neutrons and is therefore "dark grey" in terms of neutron transmission.

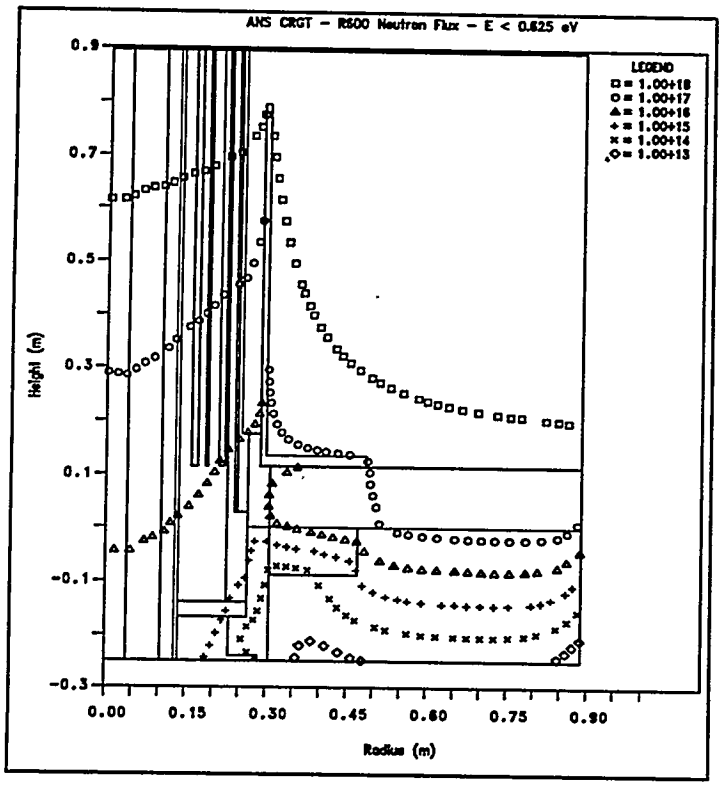

Case R600:
Also, reducing the density of hafnium by a factor of 2 shows that a shield with half the original thickness is neutronically very similar. The thermal neutron flux level in the flange (8) does not change at all, and the flux in the PCSA (7) is slightly increased to $9 \cdot 10^{15}$ $m^{-2} \cdot s^{-1}$. Obviously, streaming effects around the outer radial edge of the shield are dominating the fluxes in the PCSA (7) and the flange (8) rather than transmission effects.

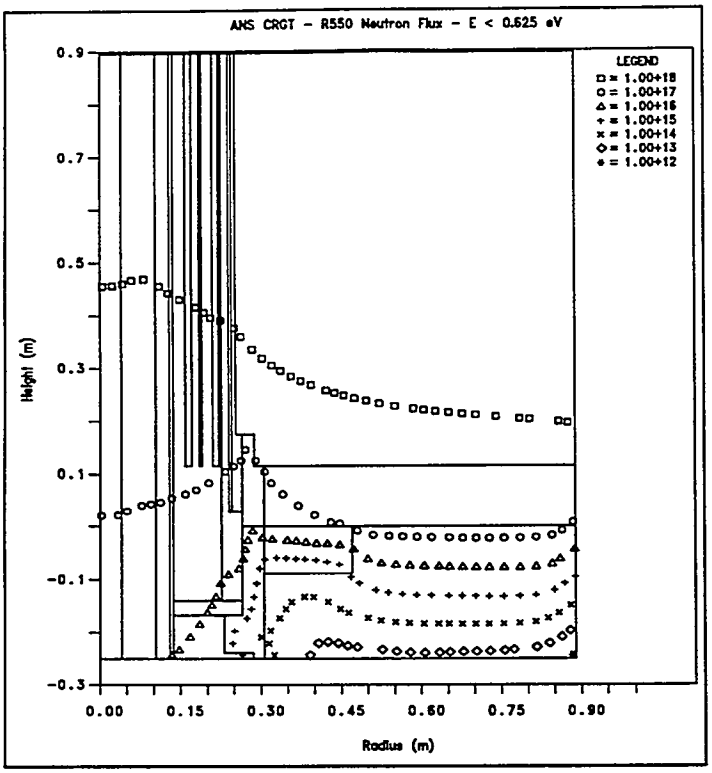

Case R550:
To verify a new cross section set and the use of the boundary source that includes the sources at the outer radial boundary, the case without any shield (R250) was repeated while taking into account all the refinements of the geometry (core support structure, 110-mm-thick reflector vessel bottom, etc.). The fluxes in the PCSA (7) and the flange (8) are similar to the first case without shielding, as expected.

6. DISPLACEMENTS PER ATOM AND HELIUM PRODUCTION IN THE STEEL COMPONENTS

Concern over radiation damage to the steel components, mainly the PCSA and its flange (see Fig. 2.2), were the major motivation for this work.

The radiation damage is usually quantified in number of DPA. As described in Sect. 3.6, the mechanism of radiation damage in austenite steel containing nickel is rather complicated. The direct contribution to DPA by knock-on of fast neutrons on lattice atoms competes with ^{59}Ni build up and the accompanied ^{59}Ni(n_{th},α)^{56}Fe reaction. The later mechanism is the origin of helium deposition, which causes swelling in steel and is an additional effect of radiation damage.

As demonstrated in Fig. 3.4, the direct knock-on mechanism dominates the DPA below a thermal neutron fluence of $2 \cdot 10^{25}$ m^{-2}, whereas above a fluence of $2 \cdot 10^{25}$ m^{-2}, the two-step absorption of nickel dominates. Critical DPA levels of 1 and higher, critical in terms of durability and mechanical strength of the steel, are reached with a thermal neutron fluence of more than $1 \cdot 10^{26}$ m^{-2}. Critical helium levels of 10 appm and higher are already reached above the thermal neutron fluence of $2 \cdot 10^{25}$ m^{-2}. Fluences of this magnitude are easily accumulated near the bottom of the reflector vessel during its 40-year lifetime.

The DPA levels and helium production in the PCSA and the flange were calculated for the cases R550 without any shield, R400 with the extended boral shield, and R500 with a radially restricted hafnium shield, assuming an exposition time of 40 years and a duty cycle factor of 0.7 because of maintenance and reloading procedures.

Figures 6.1 and 6.2 show the radially averaged DPA and helium production levels in the PCSA plotted vs the height. The DPA level of nearly 1 at the top of the PCSA in the unshielded case R550 is reduced by the restricted shield of case R500 to about $5 \cdot 10^{-3}$ and by the radially extended boral shield in case R400 to below $2 \cdot 10^{-3}$. A similar dependence is found for the helium production in the PCSA. Helium production of 500 appm at the top of the unshielded PCSA is reduced to 0.5 appm and 0.02 appm in cases R500 and R400, respectively.

In Figs. 6.3 and 6.4, the DPA and helium production levels are plotted vs the radius in the part of the flange near the bottom of the reflector vessel, again, for the unshielded case R550, case R500 with radially restricted shield, and case R400 with the radially extended shield. DPA levels of about 0.2 at the outer radial edge of the flange in case R550 are reduced 0.05 and 0.005 in cases R500 and R400, respectively. Because of streaming around the outer edge of the shield, the helium production in the flange still reaches a value of 20 appm in case R500 compared to the 90 appm in the unshielded case R550, whereas the extended shield of case R400 most effectively decreases the level to a minute $1 \cdot 10^{-4}$ appm. Unfortunately, the radially extended shield is mechanically impossible.

Detailed DPA and helium production data for all mesh intervals in the PCSA and the flange are given in Appendix B.

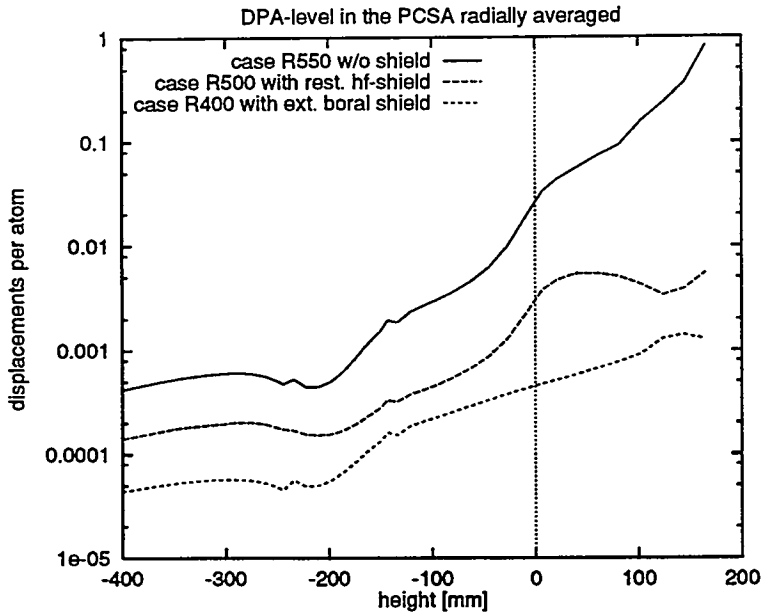

Fig. 6.1. Radially averaged DPA level in the PCSA vs height for cases R550, R500, and R400 after 40 years of reactor operation (height=0 mm corresponds to the bottom surface of the reflector vessel).

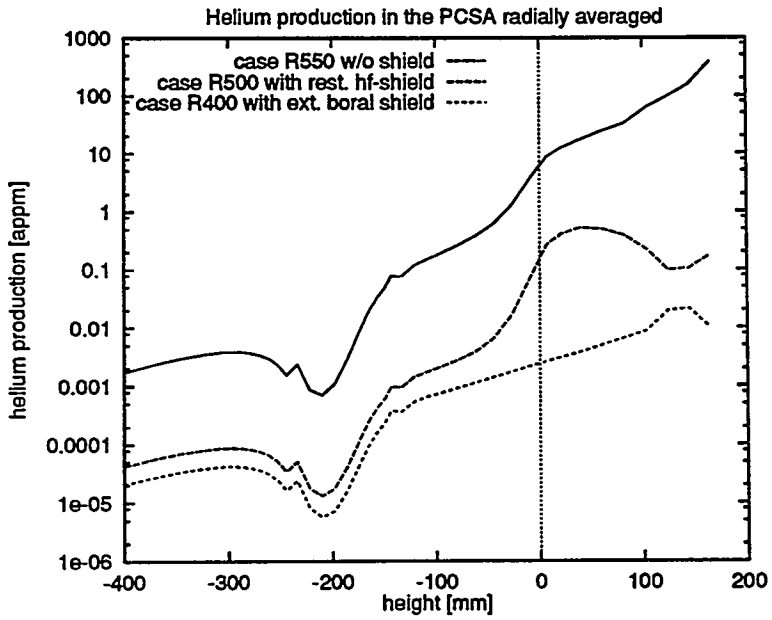

Fig. 6.2. Radially averaged helium production in the PCSA vs height for cases R550, R500, and R400 after 40 years of reactor operation (height=0 mm corresponds to the bottom surface of the reflector vessel).

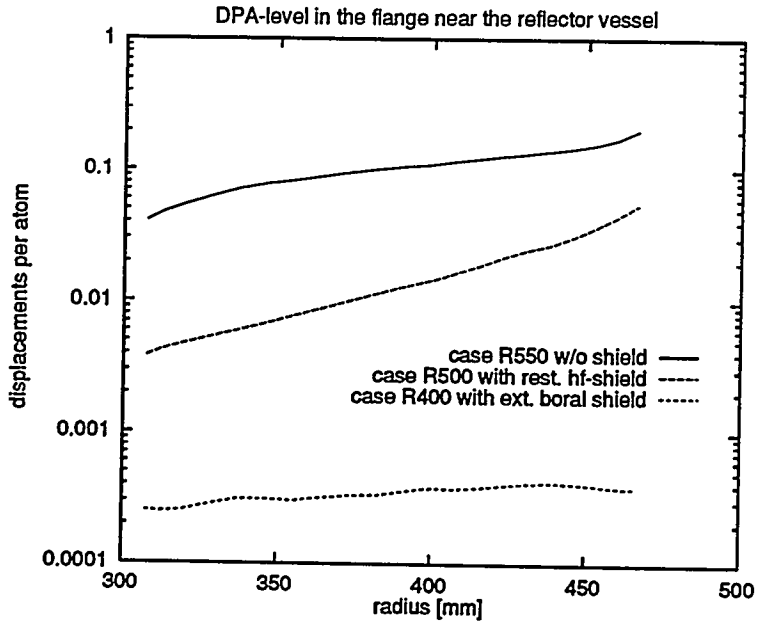

Fig. 6.3. DPA level in the flange near the reflector vessel vs radius for cases R550, R500, and R400 after 40 years of reactor operation.

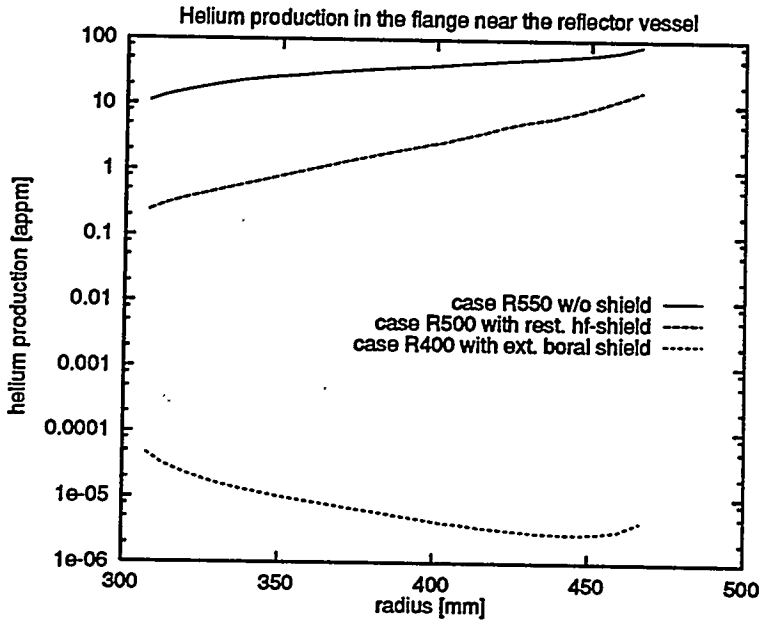

Fig. 6.4. Helium production in the flange near the reflector vessel vs radius for cases R550, R500, and R400 after 40 years of reactor operation.

7. HEATING IN THE SHIELD

Because the shield is located inside the reflector vessel, it is exposed to high neutron and gamma radiation that cause heating and activation. To calculate the heating rates for the restricted hafnium and boral shields in cases R500 and R450, the DORT fluxes were folded with the kerma factors described in Sect. 3.4.

For the case of the hafnium shield, the neutrons' contribution to heating is completely negligible (a factor of 10^5 lower compared to the γ heating, see Tables C.1 through C.3), whereas in the case with the boral shield the neutron contribution dominates the heating rate (see Tables C.4 through C.6).

In Figs. 7.1 and 7.2, the heating rates in the vertical and horizontal parts of the shield are plotted against the height and radius, respectively. Heating rates in the horizontal part of the shield go up to 3 W cm^{-3} for both the hafnium and the boral shield. The heating rates in the vertical section of the shield are reaching values up to about 60 W cm^{-3} in the upper tip of the hafnium shield and up to 70 W cm^{-3} in the boral shield. Assuming a shield thickness of 10 mm, one would have to remove a heat load of 60 – 70 W cm^{-2}, which is beyond what can be removed by free convection of D_2O.

Decreasing the length of the vertical part of the shield does not solve the heating problem because the upper part of the shield protects the lower parts from high flux levels. The only way to reduce the overall heat load is to decrease the shield thickness. Case R600 shows that a hafnium shield thickness of 5 mm would still be acceptable neutronically. In any event, cooling of the CPBT in this region will still require forced convection, which can account for the additional cooling requirements imposed by the shield.

Although the heat load is similar for both the hafnium and boral shield, boral seems to be the poorer solution for several reasons. Boral is a compound of B_4C and aluminum pressed between layers of cladding. Significant swelling can occur because neutron absorption is followed by α-decay, which produces helium. Thus, the integrity of the boral compound is not ensured. On the other hand, hafnium is a metal with rather good mechanical properties, consisting of several well-known neutron-absorbing isotopes, which cascade into other neutron-absorbing isotopes and prolong the lifetime of the shield. Overall, hafnium seems to be the preferred material for this shielding problem.

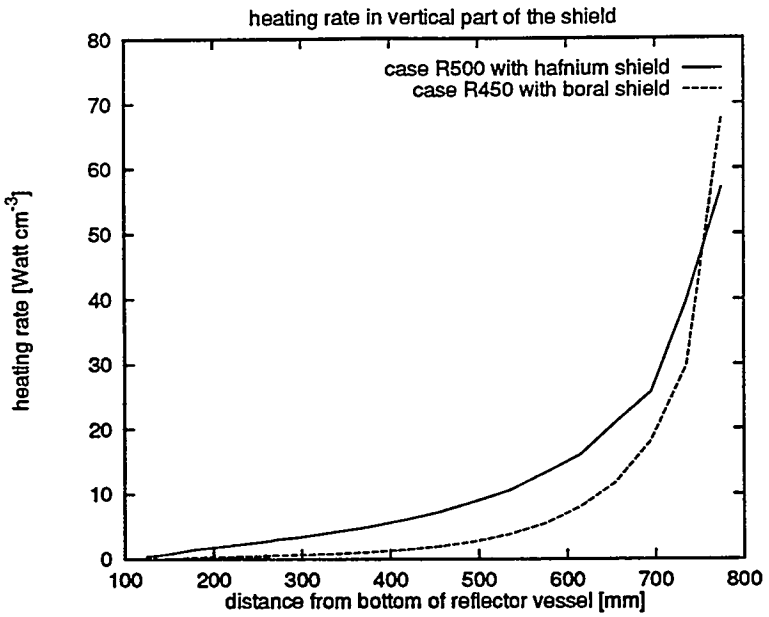

Fig. 7.1. Heating rate in the vertical part of the shield vs height for the boral shield of case R450 and for the hafnium shield of case R500.

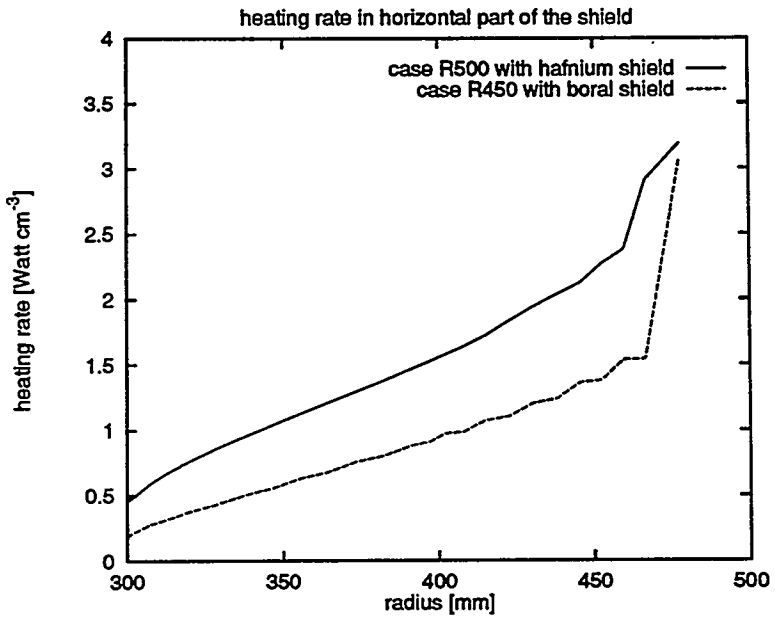

Fig. 7.2. Heating rate in the horizontal part of the shield vs radius for the boral shield of case R450 and for the hafnium shield of case R500.

8. DEPLETION AND ACTIVATION OF THE HAFNIUM SHIELD

When strong absorbers are used as shielding materials, depletion effects must be considered and shielding calculations performed under end-of-life conditions before the design can be pronounced acceptable. In addition, concerns arose that the L-shaped hafnium shield might become so activated that it might contribute significantly to the dose rate in the subpile room after shutdown. To establish the burnup profile and the activation in the shield, the cylindrical L-shaped hafnium shield was divided into six vertical zones and four horizontal zones, as shown in Fig. 8.1. Multigroup fluxes from the DORT analysis of the full-density hafnium shield of case R500 were used to determine the volume-averaged thermal flux in each of these ten zones, as well as the volume-averaged values of the "therm," "res," and "fast" parameters to be used in ORIGEN-S[12] depletion/activation analyses. A separate ORIGEN-S depletion/activation analysis was performed for each of these ten zones, assuming that the shield is irradiated for two full-power years and subsequently allowed to decay for one day. ORIGEN-S is the version of the ORIGEN code[13] applied in the SCALE system.[14] Although not essential for the depletion analyses, this decay step was included to correspond to conditions one day after shutdown of the reactor, when one might first want to gain personnel access to the subpile room below the reactor. The hafnium material used in this calculation included 3.1 wt % zirconium as well as the following impurities: 250 appm W, 40 appm Cu, 110 appm Fe, 8 appm U, 35 appm Al, and 25 appm Ti. The overall density was assumed to be 12.90 g/cc.

Table 8.1 shows the amount of each hafnium isotope initially present in the shield, as well as the final isotope concentrations present in each of the ten zones (see Fig. 8.1) at the end of two full-power years. Note that although ^{174}Hf, ^{176}Hf, and ^{177}Hf all have large thermal neutron absorption cross sections, only ^{177}Hf is present in any significant quantity. This isotope also has the largest absorption cross section and experiences the greatest depletion; after two full-power years, its concentration in zone 1 is 1.51 g cm^{-3}, or about 34% lower than its initial concentration of 2.30 g cm^{-3}. This high burnup rate is typical only for zone 1 near the top of the vertical section of the L-shaped hafnium shield. In zone 2, it is only 13% (see Table 8.1), while in all the other zones it is even less. Across the horizontal base plate, the maximum ^{177}Hf depletion occurs in zone 10, near the outer radial edge of the base plate, where it is only about 1%/year.

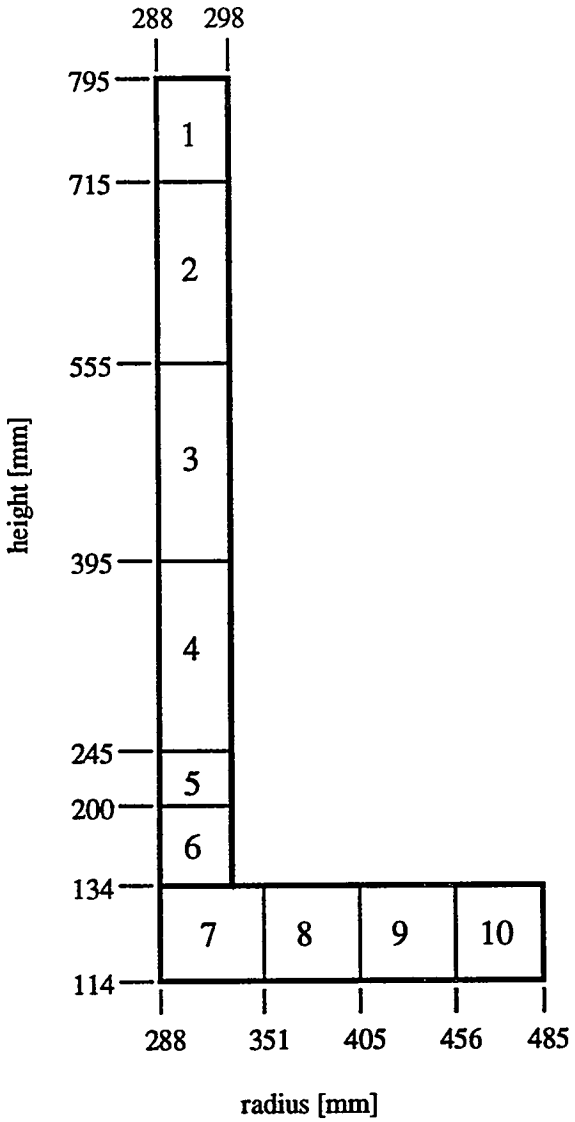

Fig. 8.1. Definition of the ten zones of the L-shaped restricted hafnium shield for the depletion/activation analyses.

Table 8.1. Hafnium isotope concentration in the ten zones of the shield at beginning of reactor operation and after two full-power years. See Fig. 8.1 for the location of each zone in the L-shaped shield

Isotope	Initial ($mg\ mm^{-3}$)	Final isotope concentration in each zone in ($mg\ mm^{-3}$)				
		Zone 1	Zone 2	Zone 3	Zone 4	Zone 5
hf174	1·95E−02	1·22E−02	1·67E−02	1·82E−02	1·88E−02	1·92E−02
hf175	0·00E+00	8·45E−04	3·71E−04	1·77E−04	8·80E−05	4·53E−05
hf176	6·41E−01	6·12E−01	6·31E−01	6·36E−01	6·38E−01	6·39E−01
hf177	2·30E+00	1·51E+00	1·99E+00	2·16E+00	2·23E+00	2·27E+00
hf178	3·38E+00	3·83E+00	3·58E+00	3·47E+00	3·42E+00	3·40E+00
hf179	1·72E+00	2·00E+00	1·81E+00	1·76E+00	1·74E+00	1·73E+00
hf180	4·43E+00	4·47E+00	4·44E+00	4·44E+00	4·44E+00	4·44E+00
hf181	0·00E+00	5·63E−03	1·90E−03	8·38E−04	4·05E−04	2·06E−04
hf182	0·00E+00	2·46E−04	2·81E−05	5·47E−06	1·28E−06	3·29E−07

Isotope	Initial ($mg\ mm^{-3}$)	Final isotope concentration in each zone in ($mg\ mm^{-3}$)				
		Zone 6	Zone 7	Zone 8	Zone 9	Zone 10
hf174	1·95E−02	1·93E−02	1·94E−02	1·93E−02	1·92E−02	1·90E−02
hf175	0·00E+00	2·15E−05	9·41E−06	2·18E−05	3·38E−05	6·70E−05
hf176	6·41E−01	6·40E−01	6·40E−01	6·40E−01	6·40E−01	6·39E−01
hf177	2·30E+00	2·29E+00	2·30E+00	2·29E+00	2·28E+00	2·25E+00
hf178	3·38E+00	3·39E+00	3·38E+00	3·39E+00	3·39E+00	3·41E+00
hf179	1·72E+00	1·73E+00	1·72E+00	1·73E+00	1·73E+00	1·74E+00
hf180	4·43E+00	4·44E+00	4·44E+00	4·44E+00	4·44E+00	4·44E+00
hf181	0·00E+00	9·70E−05	4·24E−05	9·82E−05	1·52E−04	3·06E−04
hf182	0·00E+00	7·30E−08	1·39E−08	7·50E−08	1·81E−07	7·30E−07

In Sect. 5 it is pointed out that in case R600 with the half-density hafnium shield (represents a full-density shield that is only half as thick), the thermal neutron fluxes in the region of the PCSA and the flange are almost identical compared with the case of a full-density shield. This means that the depletion after two full-power years of reactor operation has little effect on the shield performance.

With the half-density shield just mentioned, the final hafnium concentration would be 69% lower than the initial concentration. The low burnup rates in most portions of the thick shield suggest that this thinner shield may well provide adequate shielding after being depleted for two full-power years of reactor operation. The only region of possible concern in this case would be in zone 1 near the top of the shield. With time, the hafnium shield would become depleted from the top down, thus diminishing the effectiveness of the vertical section of the shield.

The gamma sources in the hafnium shield after two full-power years of irradiation and one day of decay time, shown in Table 8.2, were obtained by the ORIGEN-S depletion/activation analyses directly in the 44 gamma group structure used in the ANSL-V 39n/44g cross section

library.[3] If one had only pure hafnium metal with no impurities, there would be no decay gammas above 2 MeV. With the impurities listed in Table 8.1, however, there are a few high-energy gammas that are able to produce photoneutrons in the D_2O inside the CPBT and CRGT. Given that these high-energy gamma sources are typically five to six orders of magnitude less intense than those in the 1 to 2 MeV range, the effect of producing photoneutrons and secondary gammas originating in neutron absorption is believed to have negligible effect on the dose rate in the subpile room.

A rigorous DORT gamma-shielding analysis was performed using these gamma source terms in the 2-D model R500 without accounting for photoneutrons. With these multigroup source terms in each of the ten zones of the hafnium shield, all other sources were set to zero to evaluate the additional dose from the presence of the activated hafnium shield. The gamma dose contours of this DORT calculation are shown in Fig. 8.2. Near the top of the subpile room, the additional gamma dose rate from the activation of the hafnium shield alone was less than 0.0001 mrem/h. In reality, many more components present in this region (the reflector vessel, the CPBT and CRGT, the components inside the CPBT and CRGT, the bellows below the CRGT, the highly activated PCSA and primary coolant supply tube itself, the liner of the reactor vault, and even the unloaded fuel element and the activated beam tubes) are expected to contribute much more to the dose rate after shutdown than the hafnium shield does.

Table 8.2. Gamma sources in the ten zones of the hafnium shield from an irradiation time of two full-power years followed by a cooling time of one day after shutdown

Grp	E_{max} (eV)	Zone 1 ($s^{-1}m^{-3}$)	Zone 2 ($s^{-1}m^{-3}$)	Zone 3 ($s^{-1}m^{-3}$)	Zone 4 ($s^{-1}m^{-3}$)	Zone 5 ($s^{-1}m^{-3}$)	Zone 6 ($s^{-1}m^{-3}$)	Zone 7 ($s^{-1}m^{-3}$)	Zone 8 ($s^{-1}m^{-3}$)	Zone 9 ($s^{-1}m^{-3}$)	Zone 10 ($s^{-1}m^{-3}$)
1	2·00E+07	0·00E+00	0·00E+00	0·00E+00	0·00E+00	0·00E+00	0·00E+00	0·00E+00	0·00E+00	0·00E+00	0·00E+00
2	1·40E+07	0·00E+00	0·00E+00	0·00E+00	0·00E+00	0·00E+00	0·00E+00	0·00E+00	0·00E+00	0·00E+00	0·00E+00
3	1·20E+07	2·64E+01	3·02E+00	6·68E−01	3·15E−01	7·41E−02	1·00E−01	2·08E−01	2·16E−01	2·40E−01	1·76E−01
4	1·00E+07	5·11E+02	5·85E+01	1·30E+01	6·11E+00	1·44E+00	1·94E+00	4·03E+00	4·18E+00	4·65E+00	3·40E+00
5	8·00E+06	4·33E+02	4·96E+01	1·10E+01	5·19E+00	1·22E+00	1·64E+00	3·42E+00	3·54E+00	3·94E+00	2·89E+00
6	7·50E+06	7·47E+02	8·56E+01	1·90E+01	8·96E+00	2·10E+00	2·83E+00	5·89E+00	6·11E+00	6·80E+00	4·99E+00
7	7·00E+06	1·29E+03	1·48E+02	3·29E+01	1·55E+01	3·63E+00	4·88E+00	1·02E+01	1·05E+01	1·17E+01	8·62E+00
8	6·50E+06	2·22E+03	2·55E+02	5·68E+01	2·68E+01	6·27E+00	8·43E+00	1·75E+01	1·82E+01	2·03E+01	1·49E+01
9	6·00E+06	3·84E+03	4·41E+02	9·82E+01	4·63E+01	1·08E+01	1·46E+01	3·03E+01	3·14E+01	3·50E+01	2·57E+01
10	5·50E+06	3·07E+07	2·84E+07	1·35E+07	6·30E+06	9·70E+05	6·70E+05	6·22E+05	1·47E+06	2·45E+06	3·05E+06
11	5·00E+06	4·57E+09	4·24E+09	2·02E+09	9·39E+08	1·45E+08	9·99E+07	9·28E+07	2·19E+08	3·65E+08	4·55E+08
12	4·50E+06	6·17E+08	5·71E+08	2·72E+08	1·27E+08	1·95E+07	1·35E+07	1·25E+07	2·95E+07	4·92E+07	6·14E+07
13	4·00E+06	4·40E+09	3·94E+09	1·85E+09	8·53E+08	1·31E+08	9·03E+07	8·39E+07	1·98E+08	3·30E+08	4·13E+08
14	3·50E+06	7·13E+11	5·49E+11	2·42E+11	1·08E+11	1·63E+10	1·11E+10	1·02E+10	2·43E+10	4·08E+10	5·18E+10
15	3·00E+06	7·76E+13	6·00E+13	2·64E+13	1·18E+13	1·78E+12	1·22E+12	1·12E+12	2·66E+12	4·46E+12	5·67E+12
16	2·50E+06	1·65E+13	1·26E+13	5·52E+12	2·45E+12	3·70E+11	2·52E+11	2·32E+11	5·51E+11	9·26E+11	1·18E+12
17	2·35E+06	3·82E+13	2·65E+13	1·12E+13	4·91E+12	7·32E+11	4·95E+11	4·55E+11	1·08E+12	1·83E+12	2·34E+12
18	2·15E+06	2·47E+13	1·47E+13	5·70E+12	2·36E+12	3·39E+11	2·25E+11	2·04E+11	4·92E+11	8·39E+11	1·11E+12
19	2·00E+06	1·58E+14	9·30E+13	3·78E+13	1·62E+13	2·50E+12	1·87E+12	2·01E+12	3·72E+12	5·79E+12	6·88E+12
20	1·80E+06	3·58E+14	2·50E+14	1·08E+14	4·83E+13	7·64E+12	5·95E+12	6·66E+12	1·15E+13	1·74E+13	1·98E+13
21	1·66E+06	2·30E+15	1·72E+15	7·53E+14	3·35E+14	5·05E+13	3·44E+13	3·18E+13	7·53E+13	1·26E+14	1·61E+14
22	1·57E+06	3·56E+13	2·50E+13	1·08E+13	4·81E+12	7·59E+11	5·86E+11	6·48E+11	1·15E+12	1·74E+12	2·00E+12
23	1·50E+06	1·57E+16	6·44E+15	1·59E+15	3·90E+14	3·26E+13	1·15E+13	5·32E+12	2·49E+13	6·11E+13	1·42E+14
24	1·44E+06	2·22E+17	9·10E+16	2·24E+16	5·51E+15	4·61E+14	1·64E+14	7·68E+13	3·52E+14	8·62E+14	2·01E+15
25	1·33E+06	1·53E+19	6·24E+18	1·53E+18	3·73E+17	3·08E+16	1·06E+16	4·56E+15	2·28E+16	5·71E+16	1·35E+17
26	1·20E+06	2·06E+19	8·43E+18	2·07E+18	5·05E+17	4·16E+16	1·43E+16	6·18E+15	3·08E+16	7·72E+16	1·83E+17
27	1·00E+06	8·36E+17	3·45E+17	8·62E+16	2·17E+16	1·90E+15	7·34E+14	4·02E+14	1·59E+15	3·67E+15	8·05E+15
28	8·00E+05	1·63E+18	1·13E+18	5·00E+17	2·27E+17	3·47E+16	2·40E+16	2·25E+16	5·22E+16	8·70E+16	1·09E+17
29	7·00E+05	1·52E+19	1·04E+19	4·64E+18	2·11E+18	3·22E+17	2·22E+17	2·06E+17	4·84E+17	8·07E+17	1·01E+18
30	6·00E+05	9·92E+16	7·06E+16	3·16E+16	1·44E+16	2·20E+15	1·53E+15	1·45E+15	3·32E+15	5·50E+15	6·86E+15
31	5·12E+05	2·80E+16	1·95E+16	8·71E+15	3·96E+15	6·05E+14	4·18E+14	3·91E+14	9·11E+14	1·52E+15	1·90E+15
32	5·10E+05	4·75E+21	3·26E+21	1·45E+21	6·56E+20	1·00E+20	6·90E+19	6·42E+19	1·51E+20	2·51E+20	3·16E+20
33	4·50E+05	4·66E+15	1·52E+15	4·94E+14	1·97E+14	2·86E+13	1·96E+13	1·88E+13	4·19E+13	6·97E+13	8·97E+13
34	4·00E+05	7·58E+20	5·19E+20	2·30E+20	1·05E+20	1·60E+19	1·10E+19	1·02E+19	2·40E+19	4·01E+19	5·03E+19
35	3·00E+05	6·84E+18	3·07E+18	9·32E+17	3·13E+17	3·90E+16	2·33E+16	1·99E+16	5·07E+16	9·10E+16	1·36E+17
36	2·00E+05	9·18E+18	4·78E+18	1·70E+18	6·64E+17	9·26E+16	6·03E+16	5·43E+16	1·31E+17	2·26E+17	3·05E+17
37	1·50E+05	3·00E+21	2·05E+21	9·10E+20	4·13E+20	6·30E+19	4·34E+19	4·04E+19	9·47E+19	1·58E+20	1·99E+20
38	1·00E+05	2·25E+19	1·35E+19	5·52E+18	2·38E+18	3·53E+17	2·39E+17	2·21E+17	5·23E+17	8·80E+17	1·13E+18
39	7·50E+04	5·37E+18	3·60E+18	1·59E+18	7·19E+17	1·10E+17	7·55E+16	7·03E+16	1·65E+17	2·75E+17	3·46E+17
40	7·00E+04	4·16E+20	2·79E+20	1·22E+20	5·51E+19	8·37E+18	5·75E+18	5·35E+18	1·26E+19	2·10E+19	2·64E+19
41	6·00E+04	1·59E+21	1·09E+21	4·81E+20	2·18E+20	3·32E+19	2·29E+19	2·13E+19	5·00E+19	8·34E+19	1·05E+20
42	4·50E+04	4·62E+19	3·09E+19	1·36E+19	6·16E+18	9·39E+17	6·46E+17	6·01E+17	1·41E+18	2·36E+18	2·96E+18
43	3·00E+04	6·52E+19	4·37E+19	1·93E+19	8·74E+18	1·33E+18	9·17E+17	8·54E+17	2·00E+18	3·35E+18	4·20E+18
44	2·00E+04	1·32E+20	8·87E+19	3·92E+19	1·77E+19	2·71E+18	1·86E+18	1·73E+18	4·07E+18	6·79E+18	8·53E+18

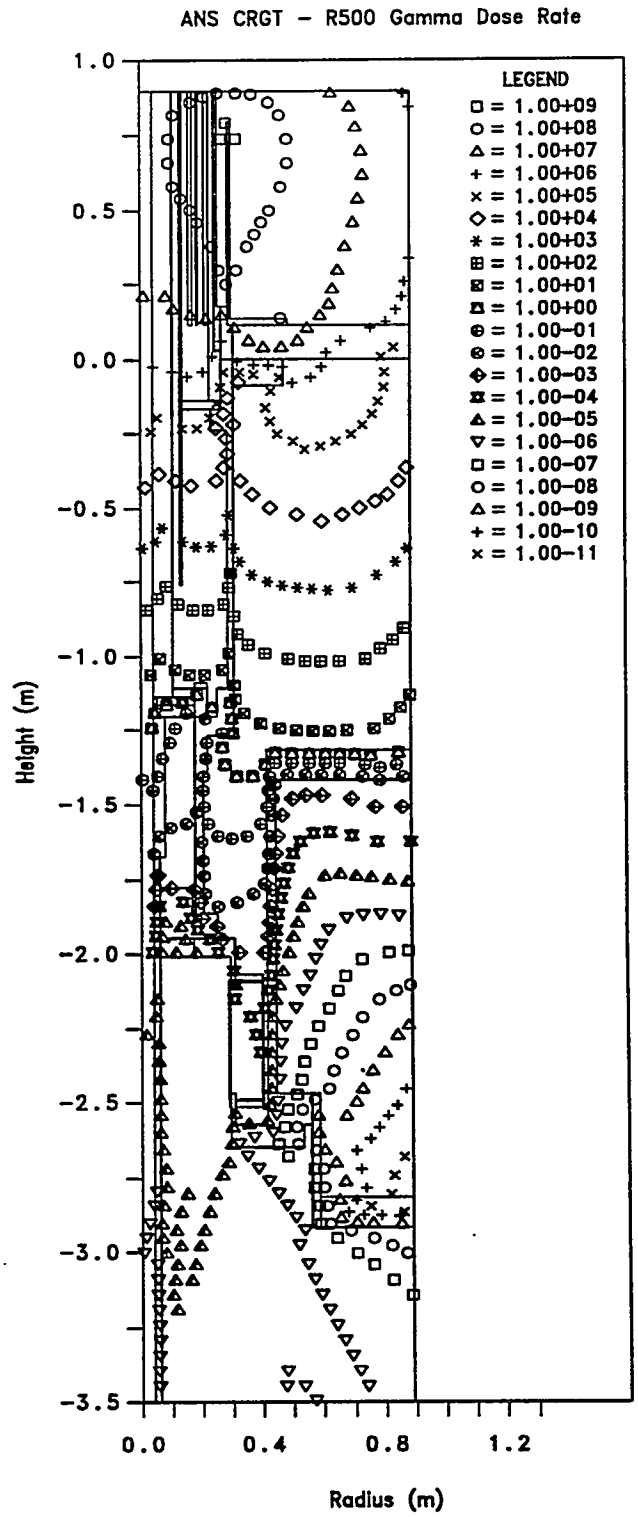

Fig. 8.2. Gamma dose rates (mrem/h) for the case R500 with the restricted hafnium shield one day after shutdown of reactor power. The gamma sources given in Table 8.2 originate in two years of irradiation of the hafnium shield.

9. CONCLUSION

The neutron and gamma dose rates in the subpile room (see Fig. 2.1) were not found to be influenced by the presence of a shield in the bottom of the reflector vessel. This shield mainly prevents neutrons from streaming down through the CRGT; however, it is not very effective in absorbing high-energy gamma rays. Those gamma rays still find their way to the subpile room and contribute directly to the gamma dose rate there. They also contribute indirectly to the neutron dose rate by producing fast neutrons in photo disintegration reactions with deuterium nuclei. Gamma and neutron dose rates of $1 \cdot 10^5$ mrem/h and $1 \cdot 10^3$ mrem/h, respectively, at the top of the subpile room do not allow manned maintenance during reactor operation.

To bring the radiation damage in the steel PCSA and its flange down to an acceptable level, two shielding designs were studied and are documented extensively: Case R400 has an L-shaped cylindrical boral shield positioned around the CPBT at the bottom of the reflector vessel with the horizontal part extended over the whole bottom; case R500 has a hafnium shield with the horizontal part of the shield restricted to a radius of 485 mm. Both shields are 10 mm and 20 mm thick in the vertical part and the horizontal part, respectively, which is enough to be regarded as "black" in terms of thermal neutron absorption. The second shielding design is motivated by the need to arrive at a shielding solution that can be removed through the top of the reflector vessel as a single piece during the changeout of the CPBT every two years.

Both shielding materials, boral and hafnium, give similar performance in terms of flux reduction in the PCSA and the flange and both yield similar heating rates in the shield itself. Heating rates of up to 70 $W \cdot cm^{-3}$ at the top of the vertical sleeve of the shield make forced convection cooling necessary.

Whereas hafnium is a metal with good mechanical properties, boral is a compound consisting of B_4C and aluminum powder pressed between two layers of aluminum cladding and is subject to embrittlement from helium production originating in the neutron absorption by ^{10}B and the subsequent α-decay. The integrity of boral, therefore, cannot be ensured, making hafnium the preferred choice.

The shielding solution for case R400 gives the absolute minimum flux and radiation damage in the PCSA and the flange that can be obtained by placing a shield across the entire bottom of the reflector vessel. The thermal neutron fluxes, which dominate the radiation damage in steels, which contain nickel, are in this case found to be $2 \cdot 10^{15}$ m^{-2} s^{-1} and $8 \cdot 10^{13}$ m^{-2} s^{-1} in the PCSA and the flange, respectively, compared against $2 \cdot 10^{17}$ m^{-2} s^{-1} and $1 \cdot 10^{17}$ m^{-2} s^{-1} in the unshielded case R550. The DPA levels in the PCSA and the flange from 40 years of reactor operation with a duty cycle of 0.7 are reduced from 1 and 0.2 in the unshielded case R550 to insignificant values of $2 \cdot 10^{-3}$ and $5 \cdot 10^{-3}$ in case R400. Also, the helium production levels are decreased in the PCSA and the flange from 500 appm and 90 appm to $2 \cdot 10^{-2}$ appm and $1 \cdot 10^{-4}$, respectively. But such a shield extending across the whole bottom of the reflector vessel is not considered very practical.

In case R500, with the restricted horizontal hafnium shield, the flux and radiation damage levels are somewhat higher. Thermal fluxes in the PCSA and the flange are $8 \cdot 10^{15}$ m^{-2} s^{-1} and $2 \cdot 10^{16}$ m^{-2} s^{-1}, respectively, which yield DPA values of $5 \cdot 10^{-3}$ and $5 \cdot 10^{-2}$ in the PCSA and the flange and which produce helium levels of 0.5 and 20 appm. These helium production levels are at the borderline of what seems to be acceptable in terms of radiation damage in steel.

A depletion/activation analysis of the hafnium shield of case R500 showed that at the top

of the vertical sleeve, the most exposed part of the shield, the naturally occuring isotope ^{177}Hf is 34% depleted at the end of two years of reactor operation. This high burnup is somewhat balanced by a subsequent buildup of ^{178}Hf, ^{179}Hf, and ^{180}Hf. In all other parts of the shield, the burnup is much smaller. Noting that case R600 with the half-density hafnium shield gives marginally inferior shielding performance compared to the full-density hafnium shield, one can certainly say that a two-year lifetime of the 10-mm hafnium shield is feasible and that the use of a thinner shield may be possible to reduce the overall heatload in the shield.

Using the decay gammas from the activation of hafnium as source for an additional transport calculation, it was shown that the activation of the hafnium shield contributes only $1 \cdot 10^{-4}$ mrem/h to the dose rate in the subpile room, one day after shutdown of the reactor.

While these studies were being performed, the reactor core design was completely changed (in response to a new DOE requirement) from a two-element design with 93% enriched uranium to a three-element design with 50% enriched uranium. The reactor fission power was fixed at 330 MW in both designs. A major effect of the design change is an increase of the CPBT radius from 250 mm to 300 mm, which increases the cross-sectional area of the CPBT about 40%. This allows 40% more neutrons to stream down into the CRGT, which will enhance the neutron and gamma dose rate in the subpile room somewhat but not more than a factor of 2. Assuming that the fluxes at the bottom of the reflector vessel stay the same in the new design and knowing that local streaming effects dominate the fluxes in those areas, the radiation damage in the PCSA and the flange are not expected to be greatly influenced by the design changes.

10. REFERENCES

1. *ANS Conceptual Design Report Summary*, ORNL/TM-12184, Martin Marietta Energy Systems, Inc., Oak Ridge National Laboratory, June 1992.

2. W. A. Rhoades and R. L. Childs, *An Updated Version of the DOT-4 One- and Two-Dimensional Neutron/Photon Transport Code*, ORNL-5851, Martin Marietta Energy Systems, Inc., Oak Ridge National Laboratory, July 1982.

3. W. E. Ford III, R.T. Primm III, J.W. Arwood, C.O. Slater, N.M. Greene, R.M. Westfall, D.L. Moses, R.Q. Wright, and L.M. Petrie, *ANSL-V: ENDF/B-V Based Multigroup Cross Section Libraries for the Advanced Neutron Source Reactor Studies*, ORNL-6618, Martin Marietta Energy Systems, Inc., Oak Ridge National Laboratory, 1990.

4. W. A. Rhoades and M. B. Emmett, *GIP: Group Organized Cross Section Input Program to be Found in DOS: The Discrete Ordinates System*, ORNL-8362, Martin Marietta Energy Systems, Inc., Oak Ridge National Laboratory, September 1982.

5. J. A. Bucholz, *Initial Global 2-D Shielding Analysis for the ANS Core and Reflector*, ORNL/TM-12672, Martin Marietta Energy Systems, Inc., Oak Ridge National Laboratory, June 1995.

6. C. O. Slater, *BSPRP2: A Computer Program to Prepare Source Input From DOT-IV "BNDRYS"—Formatted Multiple Boundary Source Data Sets*, Intra-Laboratory Correspondence sent to RSIC, Oak Ridge National Laboratory, May 1985.

7. N. M. Greene et al., *AMPX-77: A Modular Code System for Generating Coupled Multigroup Neutron-Gamma Cross-Section Libraries From ENDF/B-IV and ENDF/B-V*, ORNL/CSD/TM-238, Martin Marietta Energy Systems, Inc., Oak Ridge National Laboratory, October 1992.

8. Y. Farawila, Y. Gohar, and C. Maynard, *KAOS/LIB-V: A Library of Nuclear Response Functions Generated by KAOS-V Code From ENDF/B-V and Other Data Files*, ANL/FPP/TM-241, University of Chicago, Argonne National Laboratory, April 1989.

9. American Nuclear Society, *Neutron and Gamma-Ray Flux-to-Dose-Rate Factors*, American National Standard ANSI/ANS-6.1.1-1977, 1977.

10. American Nuclear Society, *Neutron and Gamma-Ray Flux-to-Dose-Rate Factors*, American National Standard ANSI/ANS-6.1.1-1991, 1991.

11. L. R. Greenwood, "A New Calculation of Thermal Neutron Damage and Helium Production in Nickel", *J. Nucl. Mat.* **115**, 137–142 (1983).

12. O. W. Hermann and R. M. Westfall, *ORIGEN-S: SCALE System Module to Calculate Fuel Depletion, Actinide Transmutation, Fission Product Buildup and Decay, and Associated Radiation Source Terms*, ORNL/NUREG/CSD-2, Rev. 4, Martin Marietta Energy Systems, Inc., Oak Ridge National Laboratory, February 1995.

13. M. J. Bell, *ORIGEN: The ORNL Isotope Generation and Depletion Code*, ORNL-4628, Martin Marietta Energy Systems, Inc., Oak Ridge National Laboratory, May 1973.

14. *SCALE: A Modular Code System for Performing Standardized Computer Analyses for Licensing Evaluation, Vol I, II and III*, ORNL/NUREG/CSD-2, Rev. 4, Martin Marietta Energy Systems, Inc., Oak Ridge National Laboratory, February 1995.

APPENDIX A. DETAILED FLUX AND DOSE RESULTS

Table A.1. The broad group definition for the flux plots

Broad group name	Energy range	Fine groups
Fast neutron flux	0.1–14 MeV	1–7
Epithermal neutron flux 1	100 eV–0.1 MeV	8–11
Epithermal neutron flux 2	0.625–100 eV	12–19
Thermal neutron flux	0–0.625 eV	20–39
High-energy gamma flux	> 2 MeV	40–57
Low-energy gamma flux	< 2 MeV	58–83

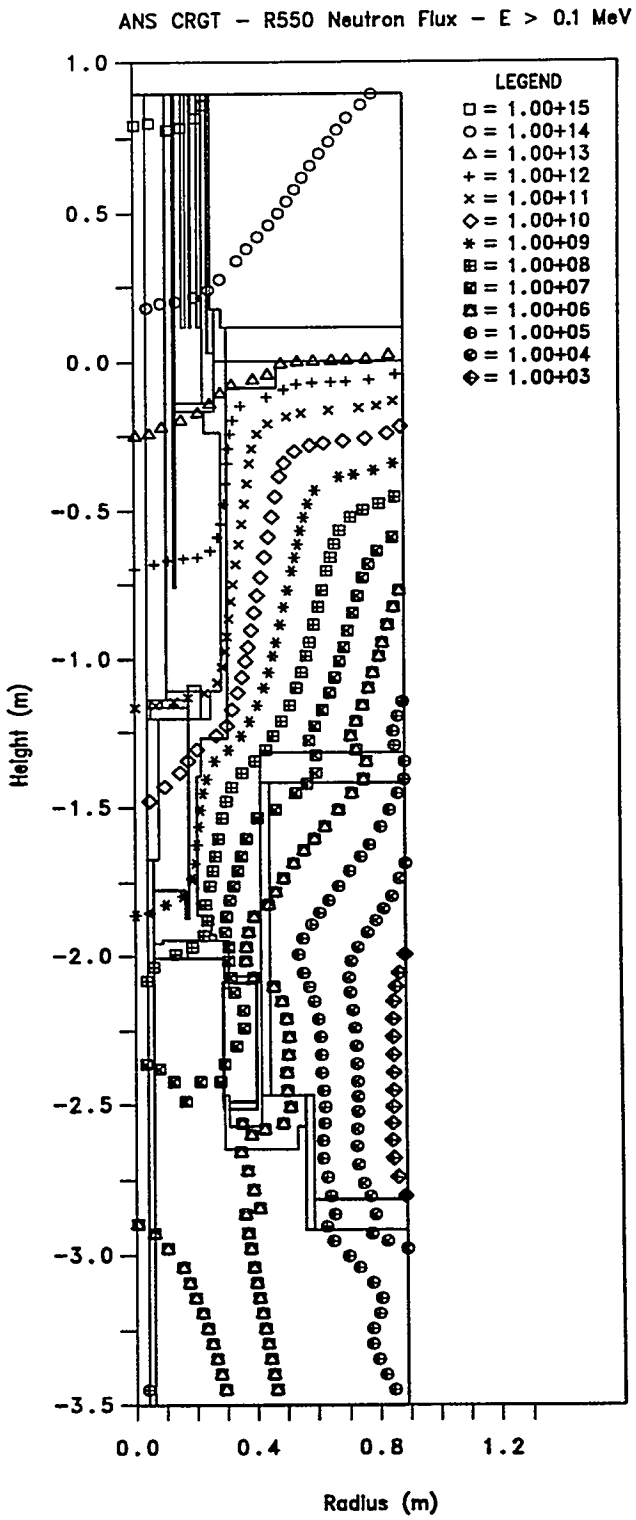

Fig. A.1. Fast neutron flux in units ($m^{-2}s^{-1}$) for case R550 without shield.

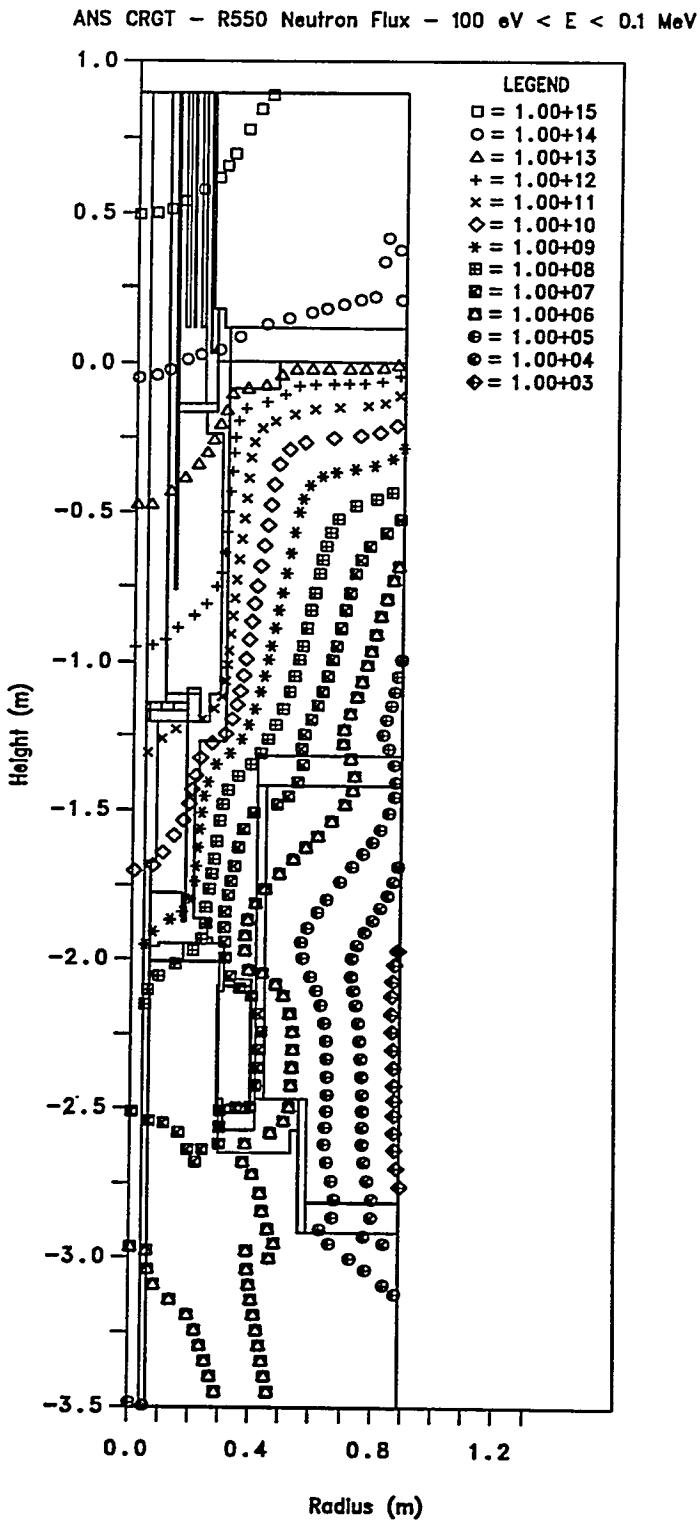

Fig. A.2. Epithermal-1 neutron flux in units ($m^{-2}s^{-1}$) for case R550 without shield.

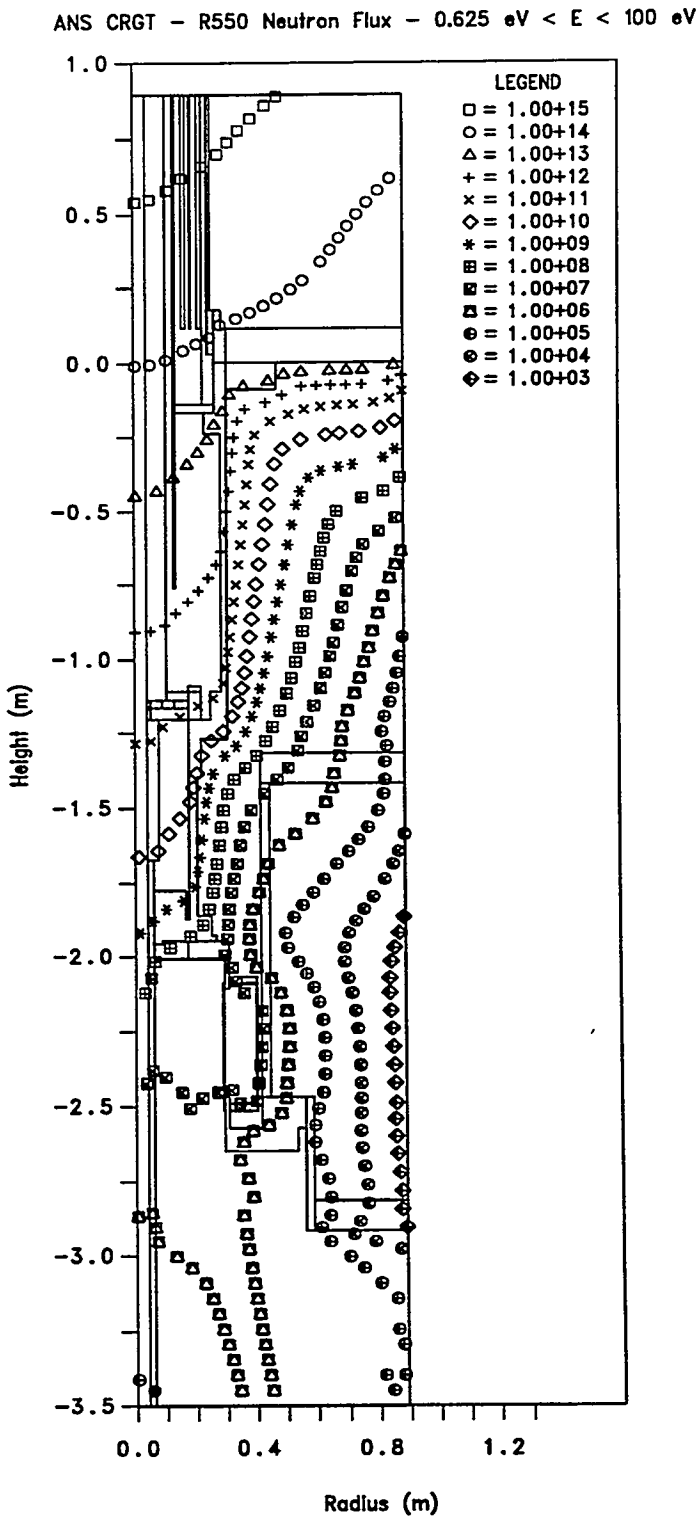

Fig. A.3. Epithermal-2 neutron flux in units ($m^{-2}s^{-1}$) for case R550 without shield.

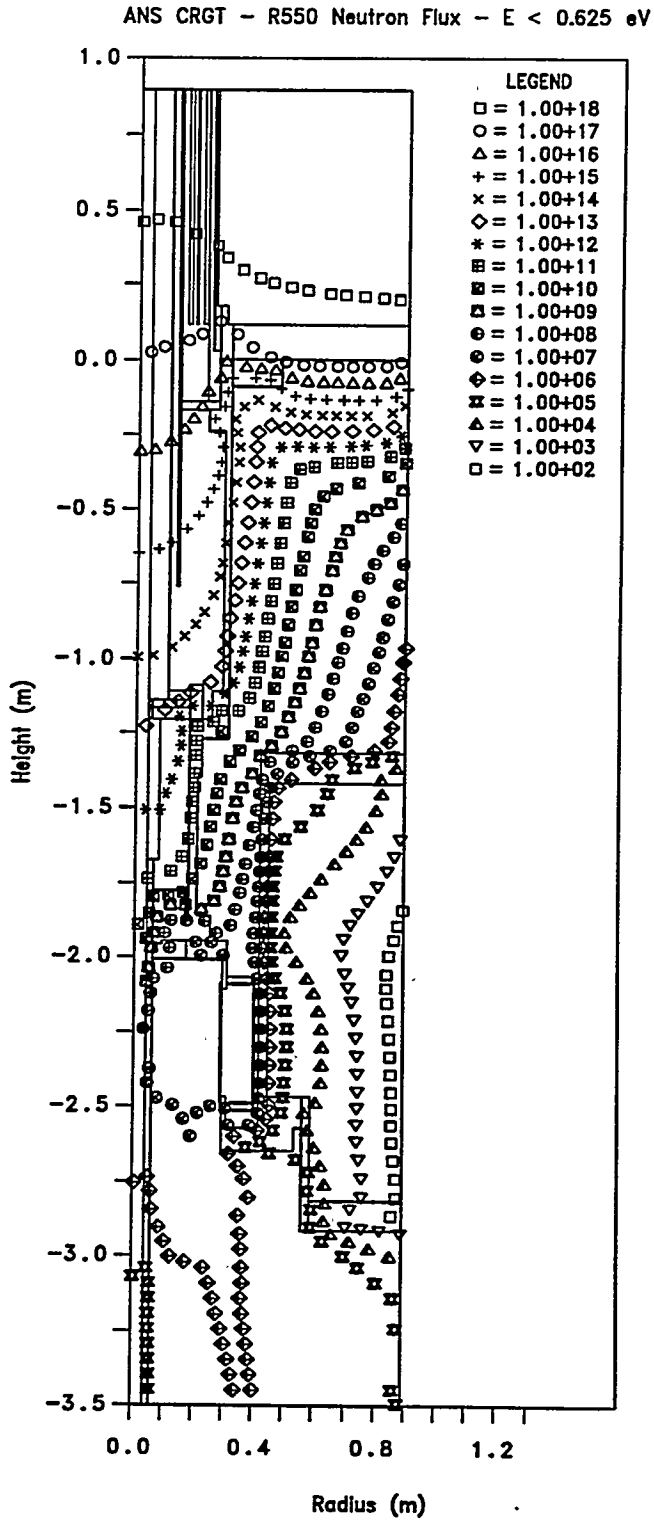

Fig. A.4. Thermal neutron flux in units ($m^{-2}s^{-1}$) for case R550 without shield.

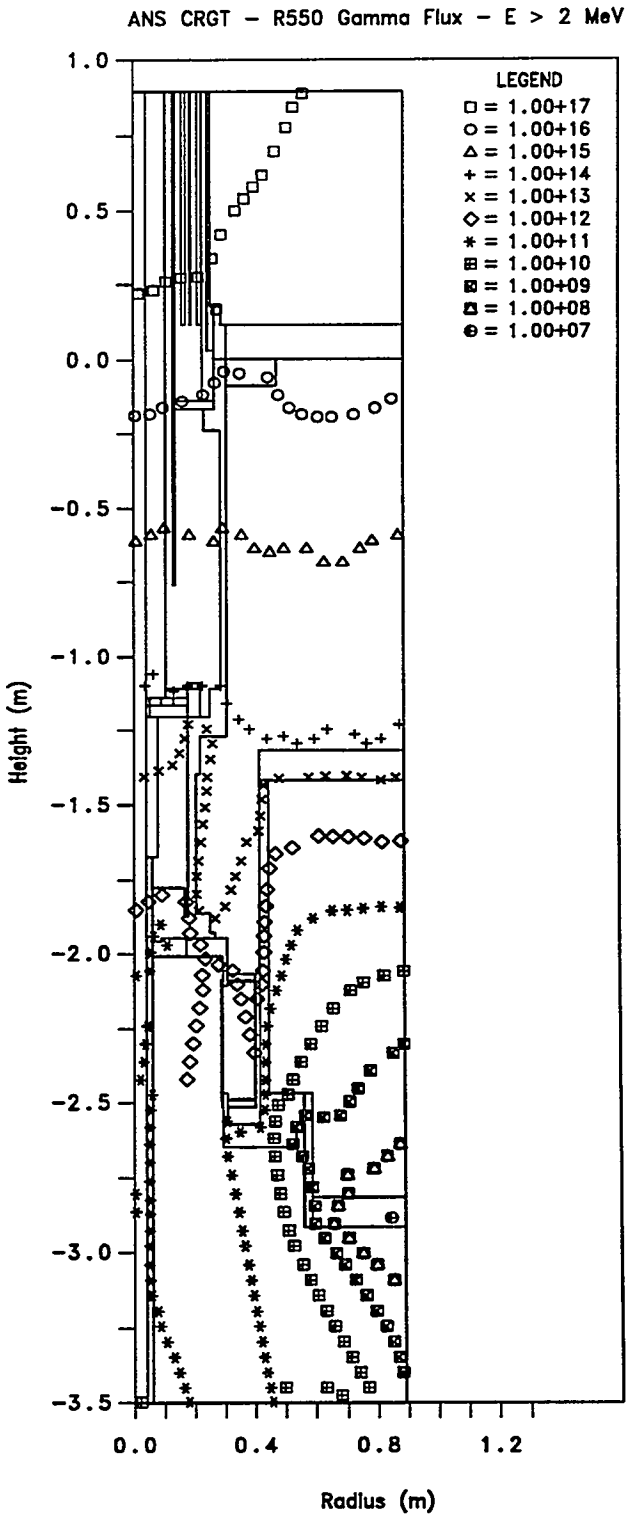

Fig. A.5. High-energy gamma flux in units ($m^{-2}s^{-1}$) for case R550 without shield.

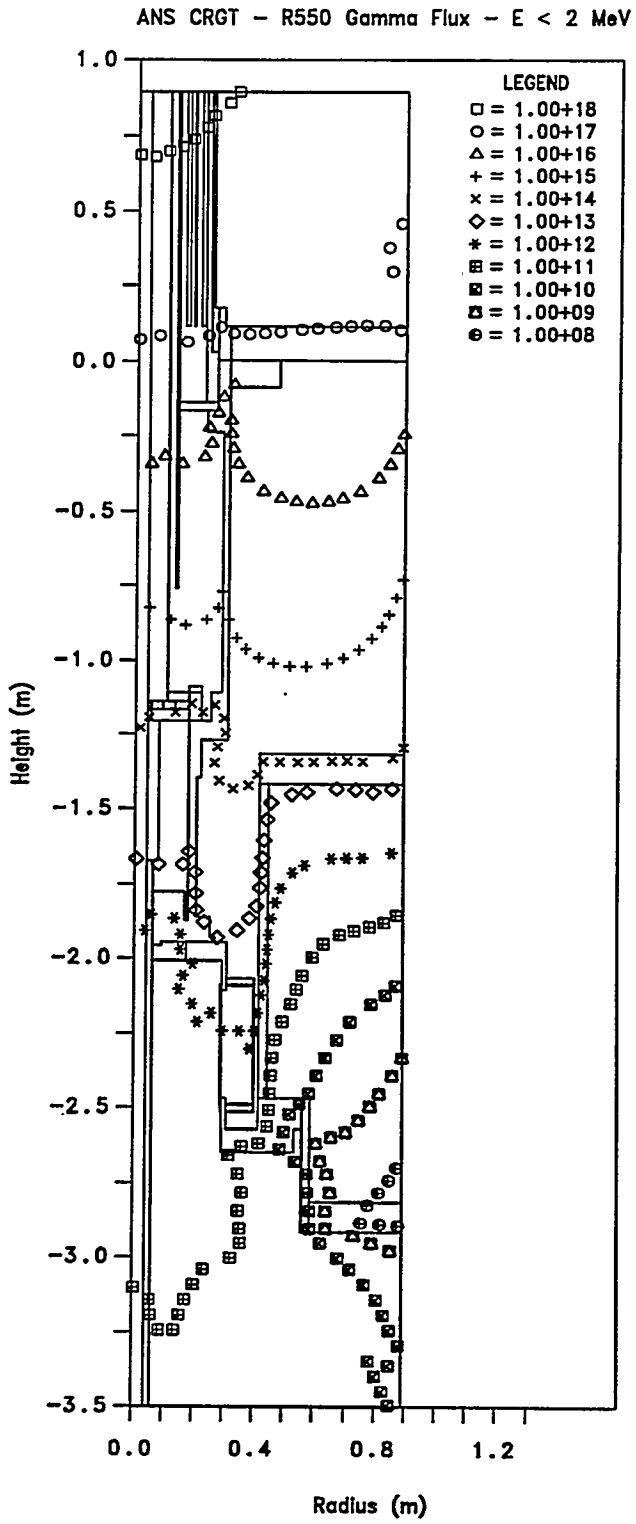

Fig. A.6. Low-energy flux in units ($m^{-2}s^{-1}$) for case R550 without shield.

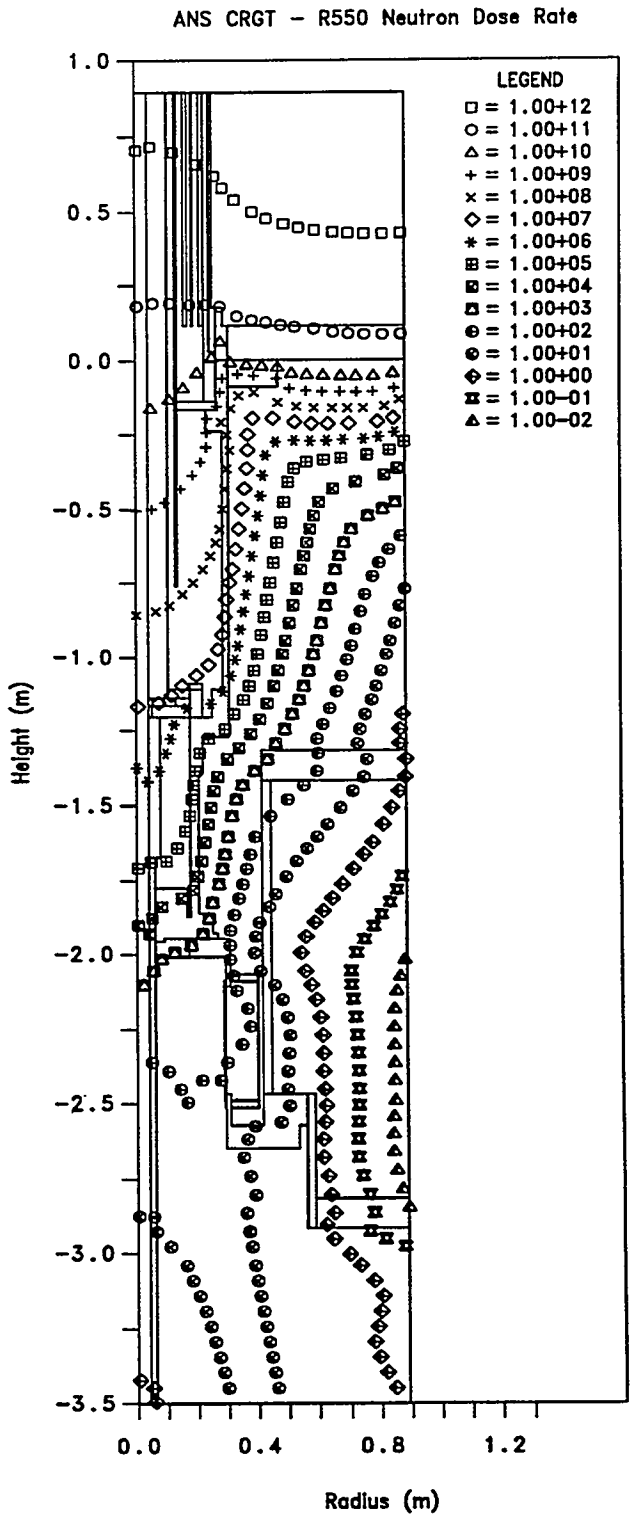

Fig. A.7. Neutron dose rate in units (mrem h^{-1}) for case R550 without shield.

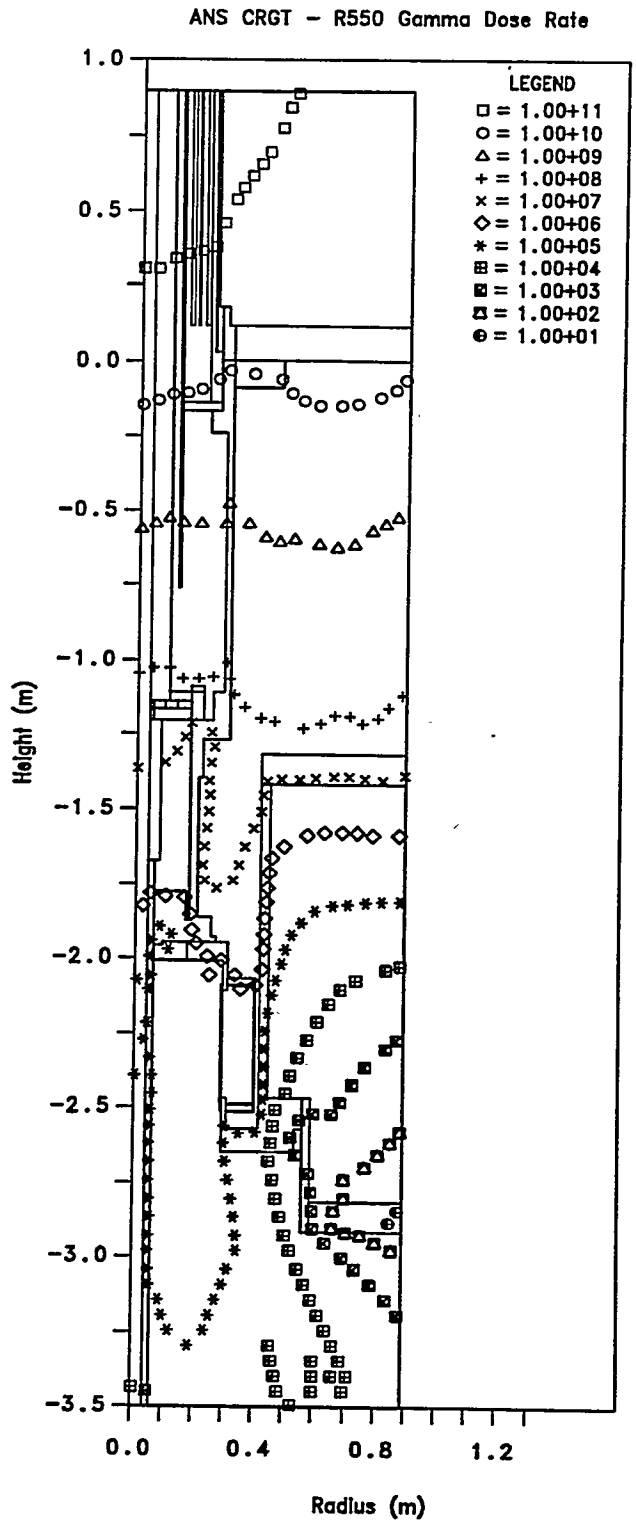

Fig. A.8. Gamma dose rate in units (mrem h^{-1}) for case R550 without shield.

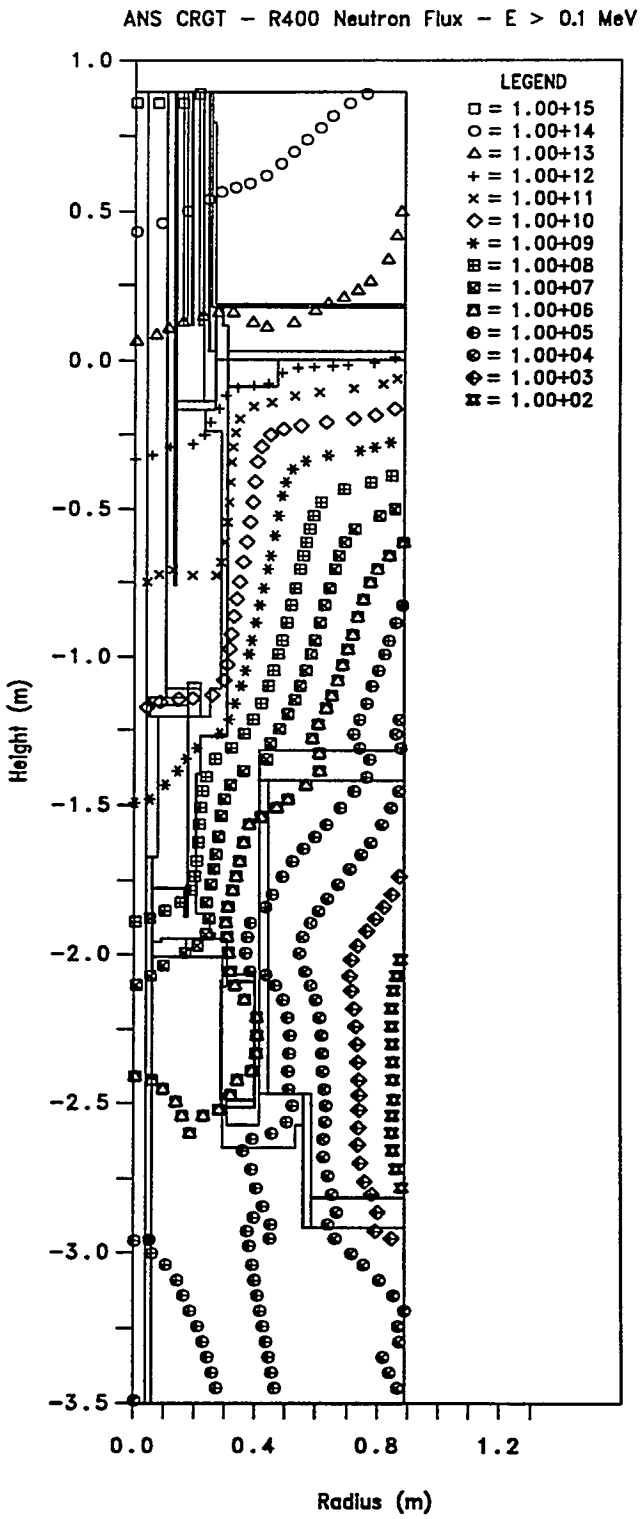

Fig. A.9. Fast neutron flux in units ($m^{-2}s^{-1}$) for case R400 with L-shaped boral shield.

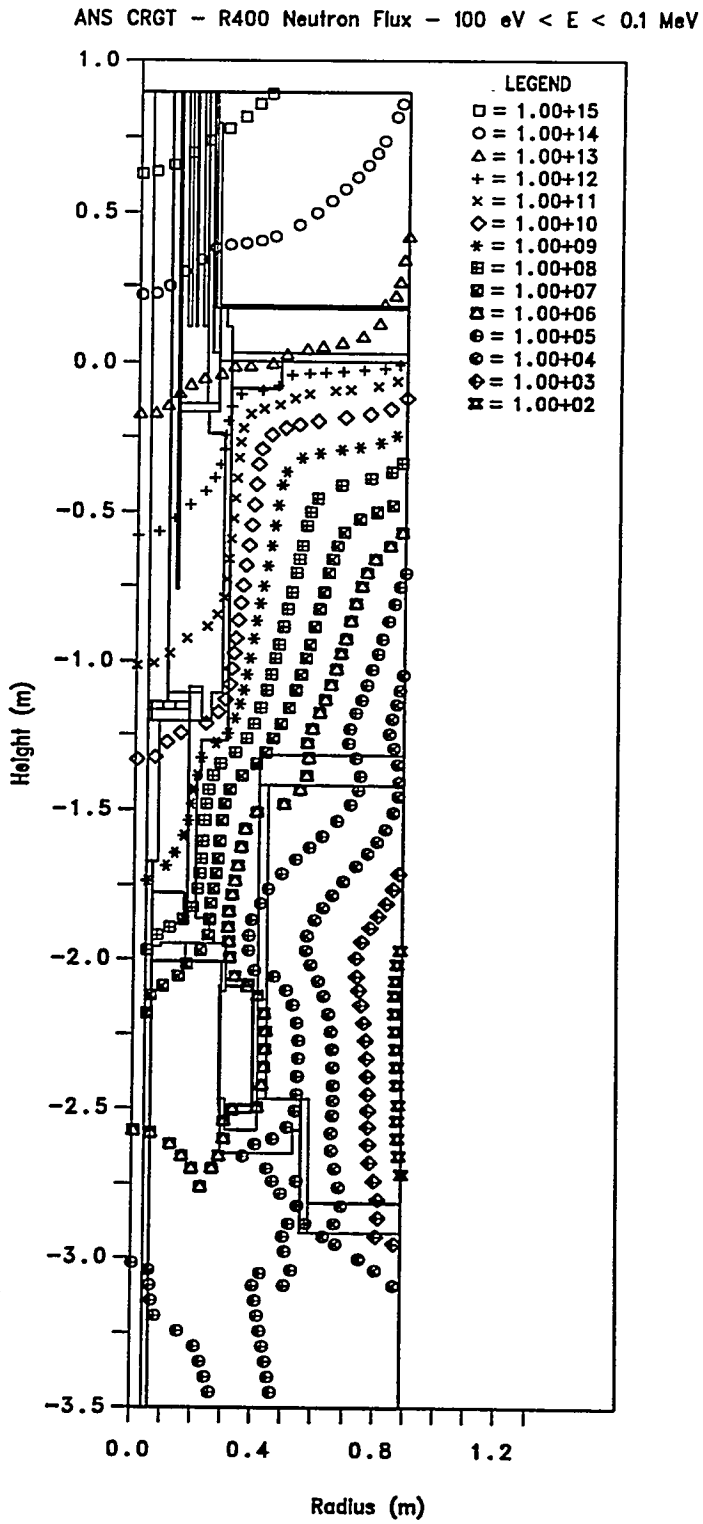

Fig. A.10. Epithermal-1 neutron flux in units ($m^{-2}s^{-1}$) for case R400 with L-shaped boral shield.

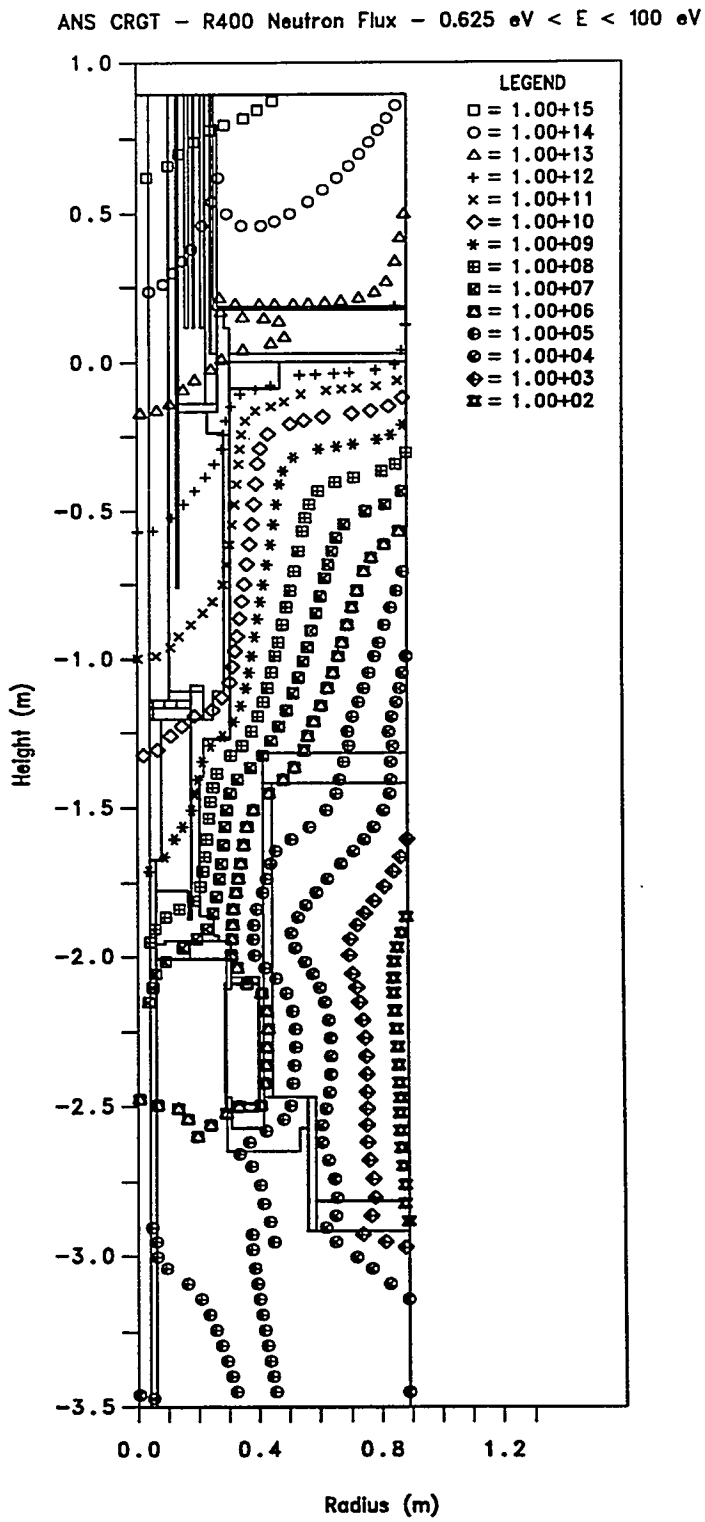

Fig. A.11. Epithermal-2 neutron flux in units ($m^{-2}s^{-1}$) for case R400 with L-shaped boral shield.

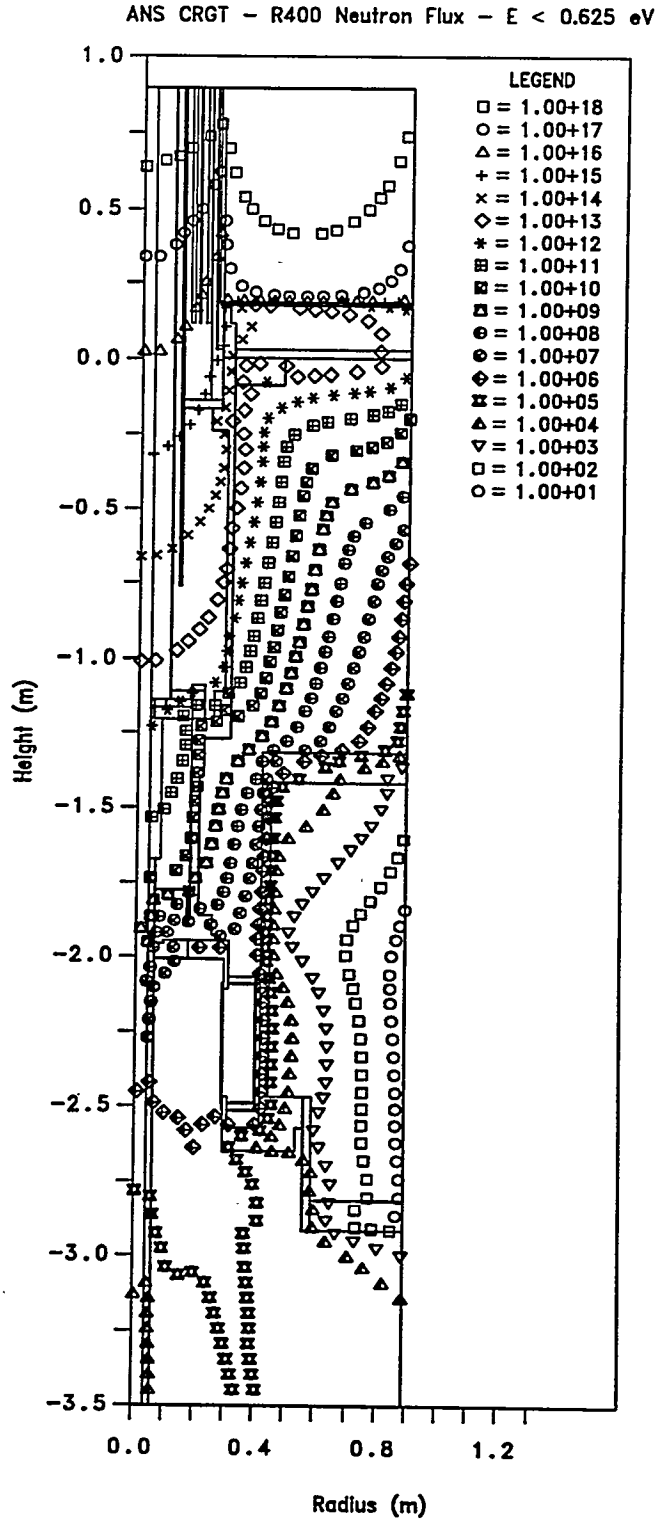

Fig. A.12. Thermal neutron flux in units ($m^{-2}s^{-1}$) for case R400 with L-shaped boral shield.

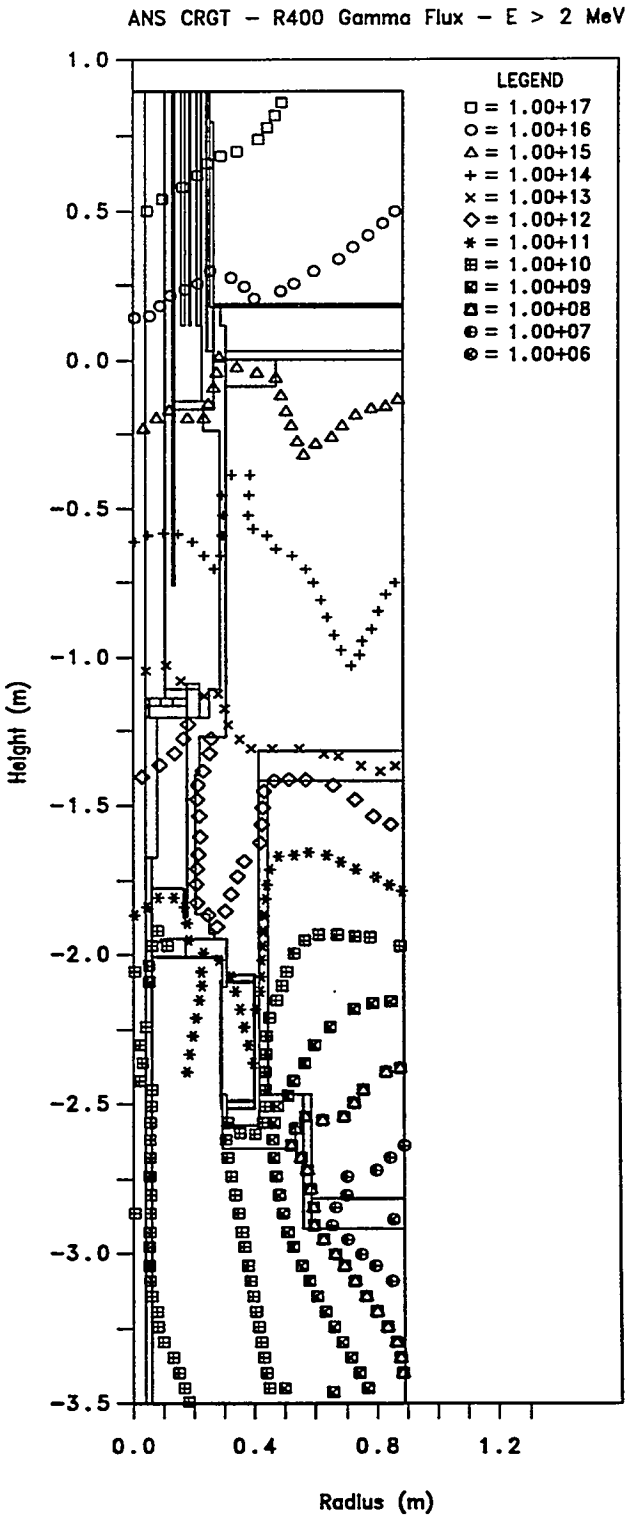

Fig. A.13. High-energy gamma flux in units ($m^{-2}s^{-1}$) for case R400 with L-shaped boral shield.

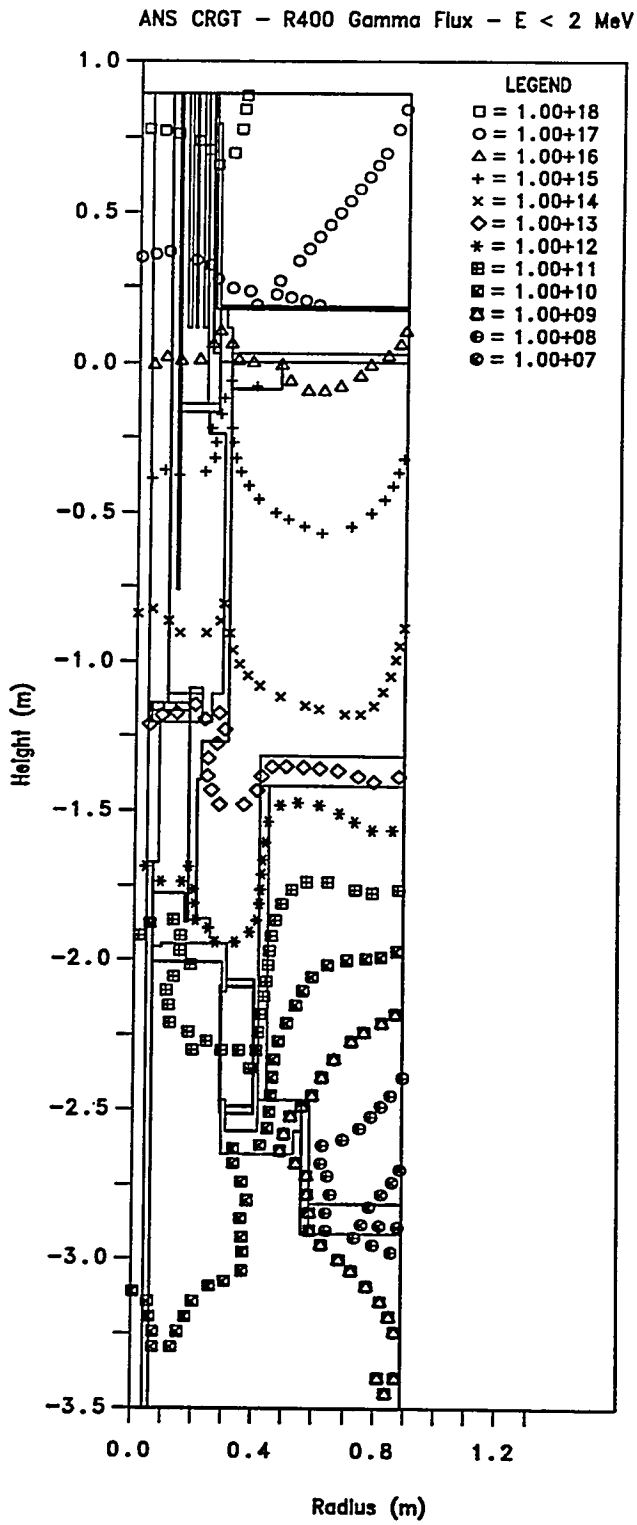

Fig. A.14. Low-energy flux in units ($m^{-2}s^{-1}$) for case R400 with L-shaped boral shield.

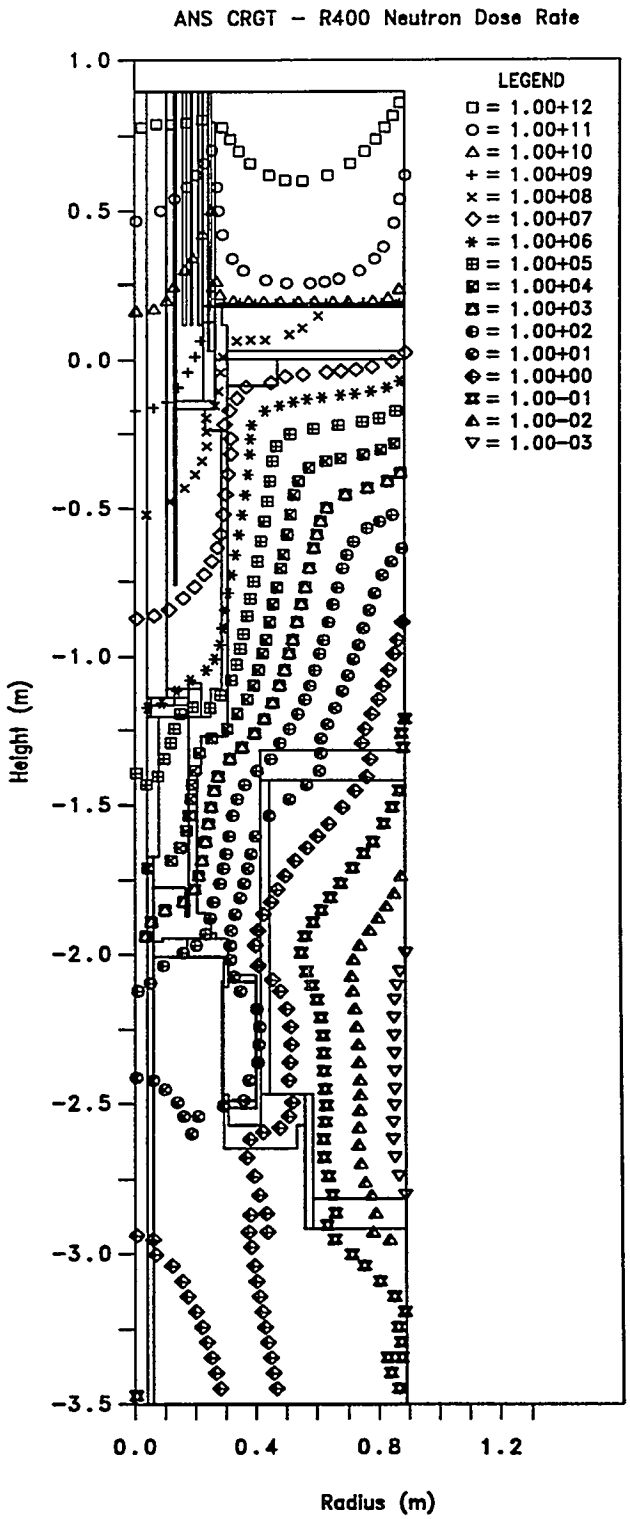

Fig. A.15. Neutron dose rate in units (mrem h^{-1}) for case R400 with L-shaped boral shield.

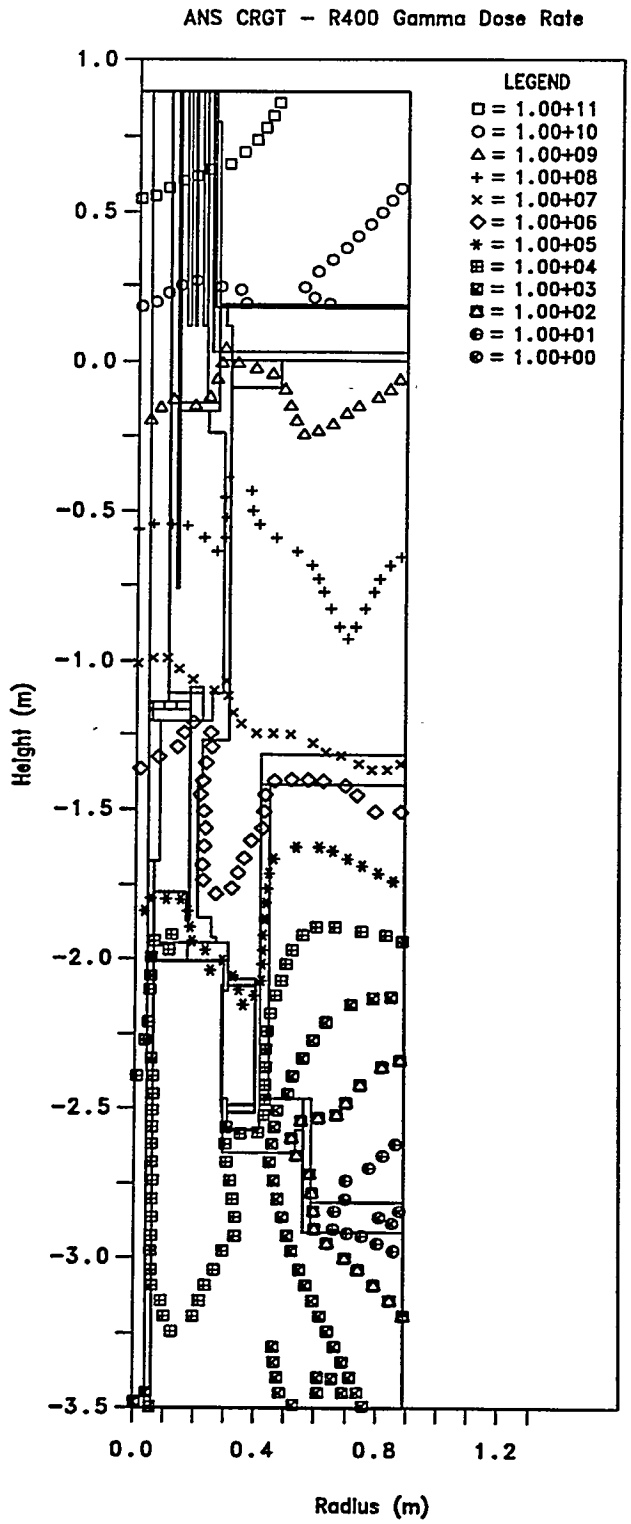

Fig. A.16. Gamma dose rate in units (mrem h^{-1}) for case R400 with L-shaped boral shield.

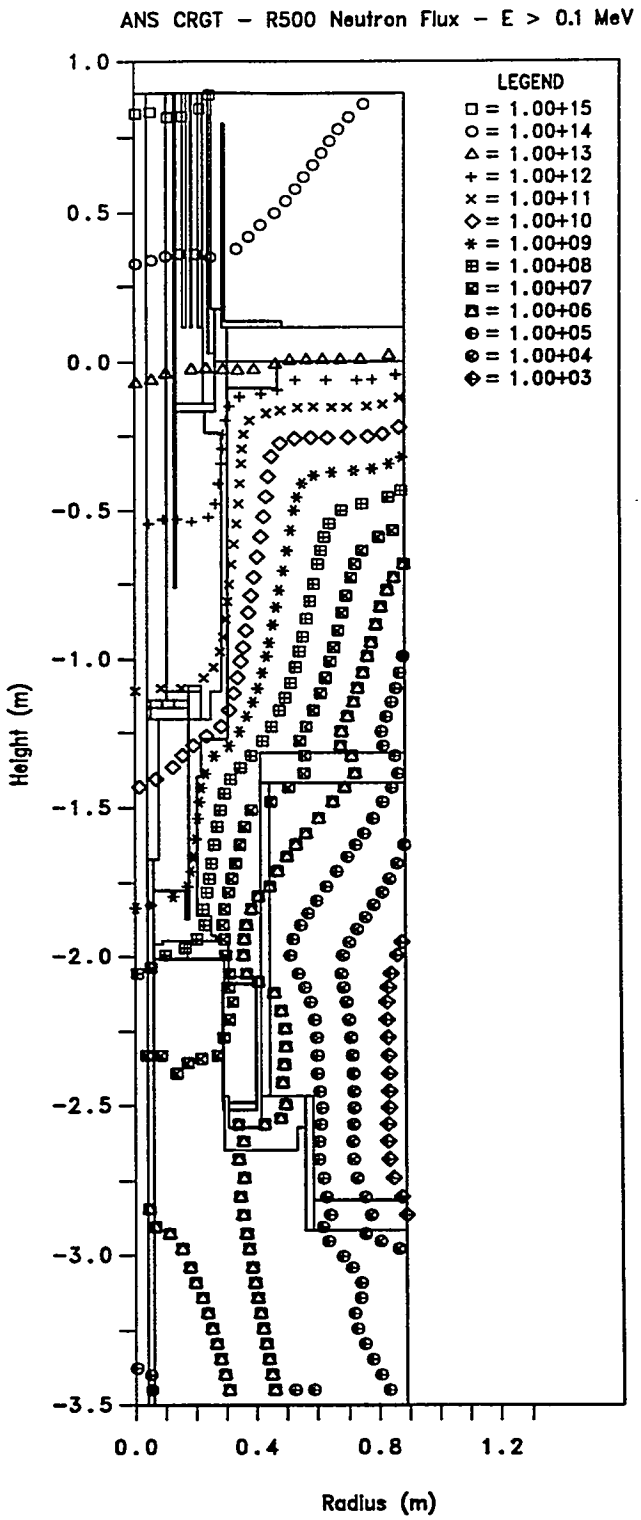

Fig. A.17. Fast neutron flux in units ($m^{-2}s^{-1}$) for case R500 with restricted hafnium shield.

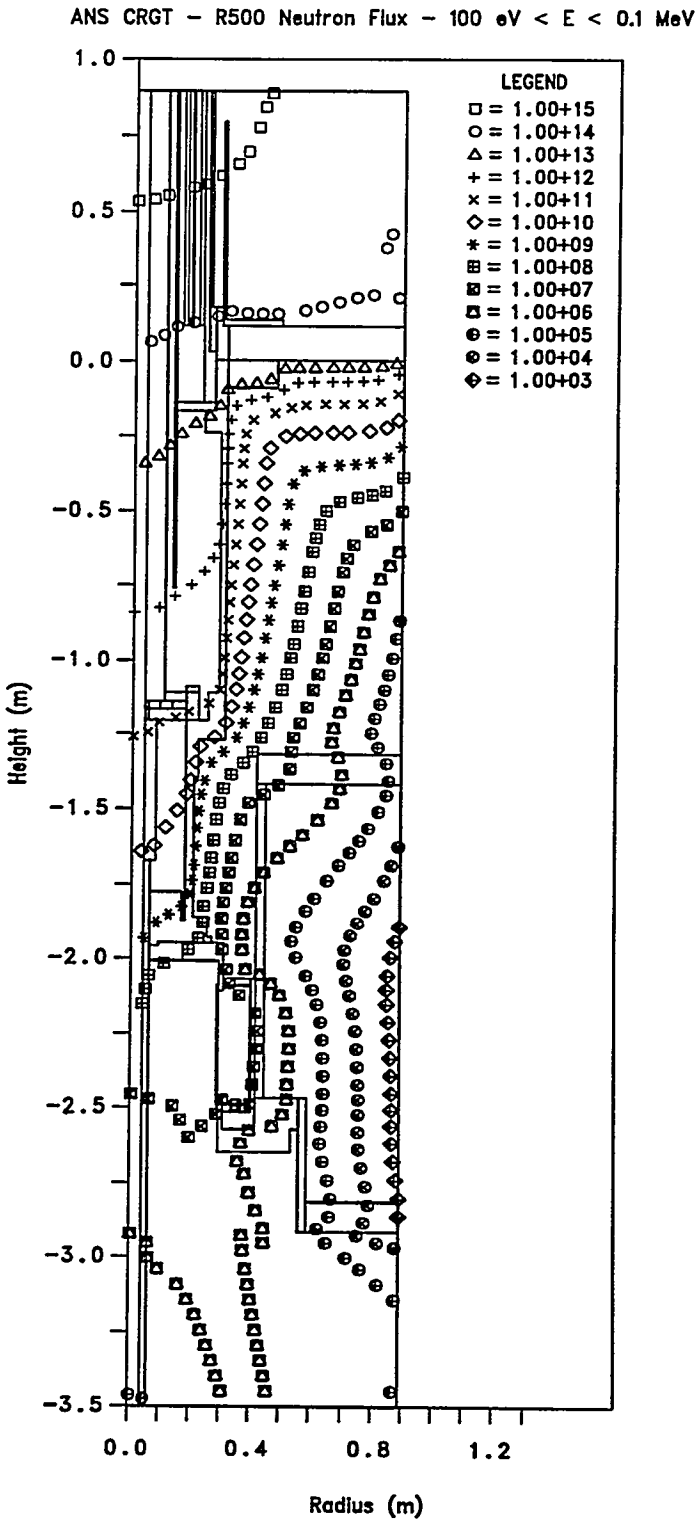

Fig. A.18. Epithermal-1 neutron flux in units ($m^{-2}s^{-1}$) for case R500 with restricted hafnium shield.

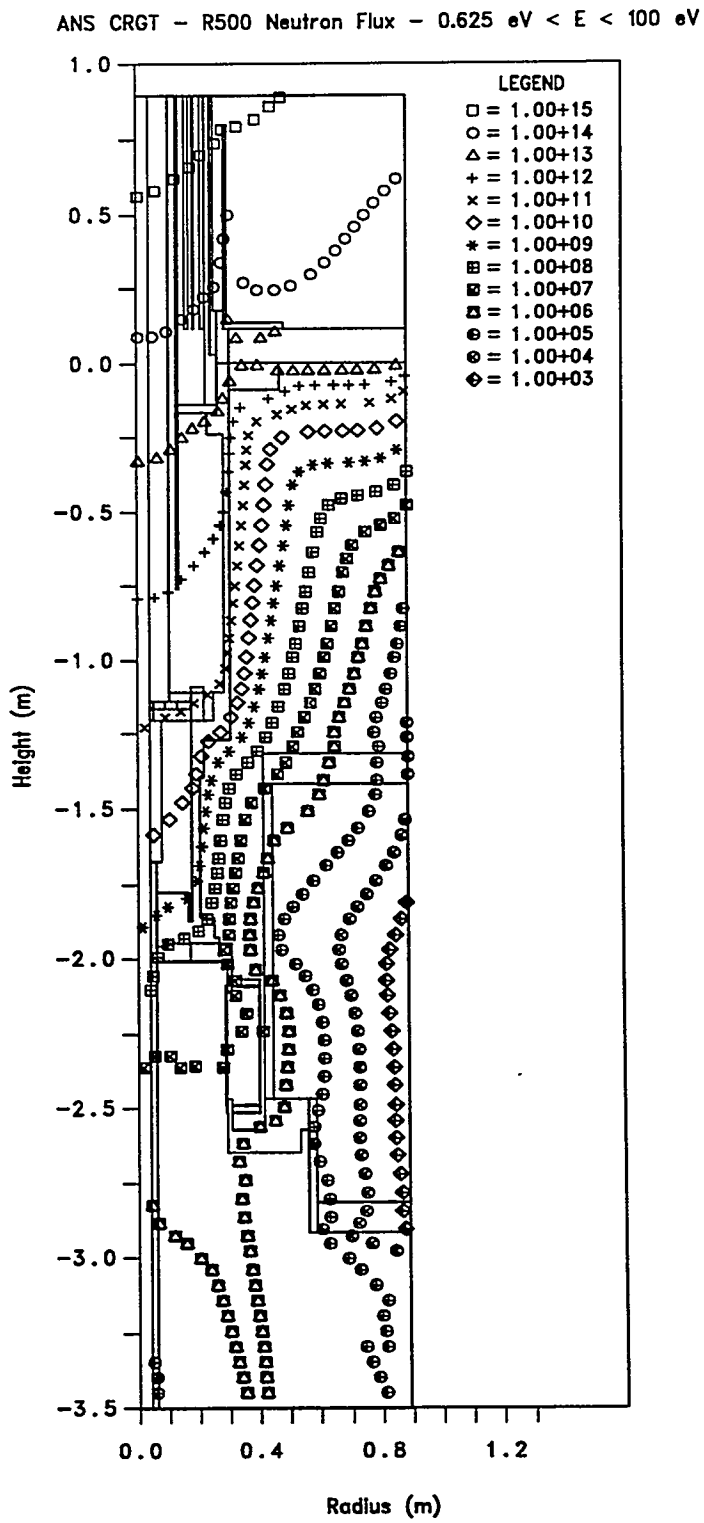

Fig. A.19. Epithermal-2 neutron flux in units ($m^{-2}s^{-1}$) for case R500 with restricted hafnium shield.

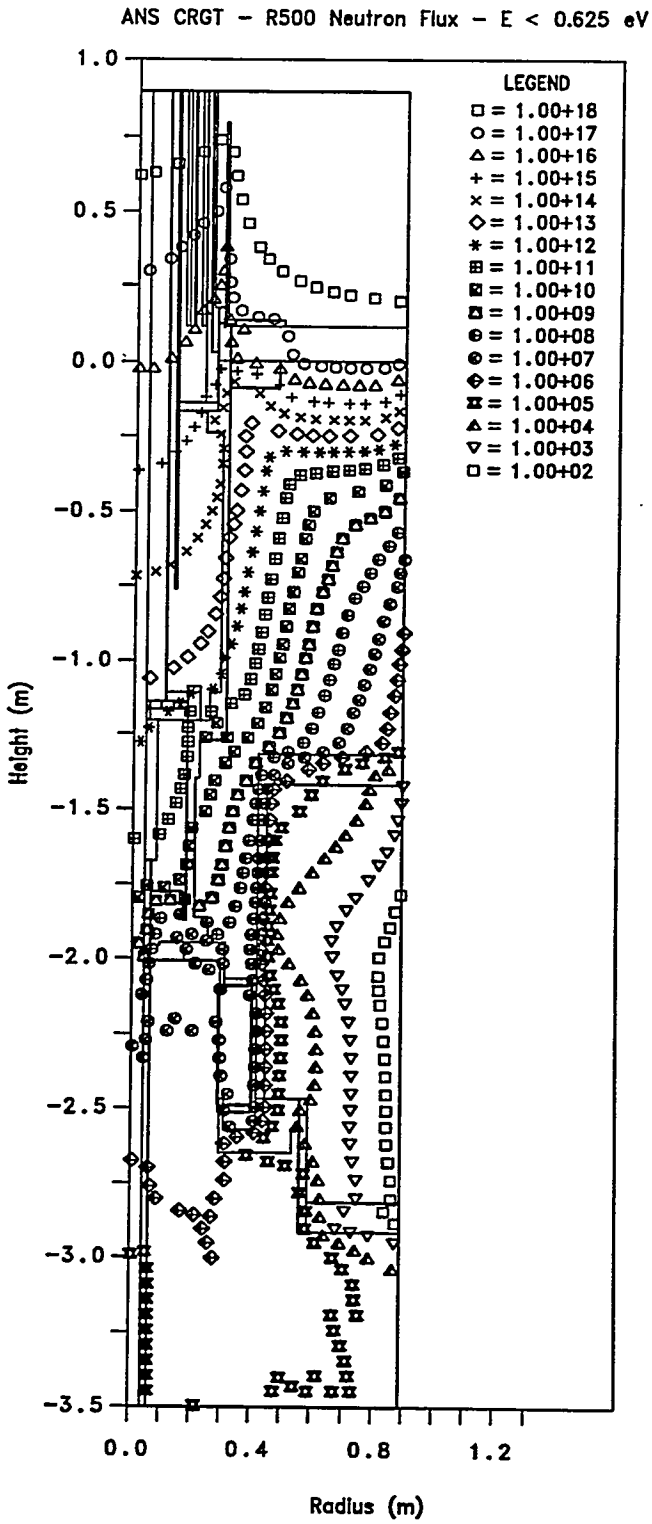

Fig. A.20. Thermal neutron flux in units ($m^{-2}s^{-1}$) for case R500 with restricted hafnium shield.

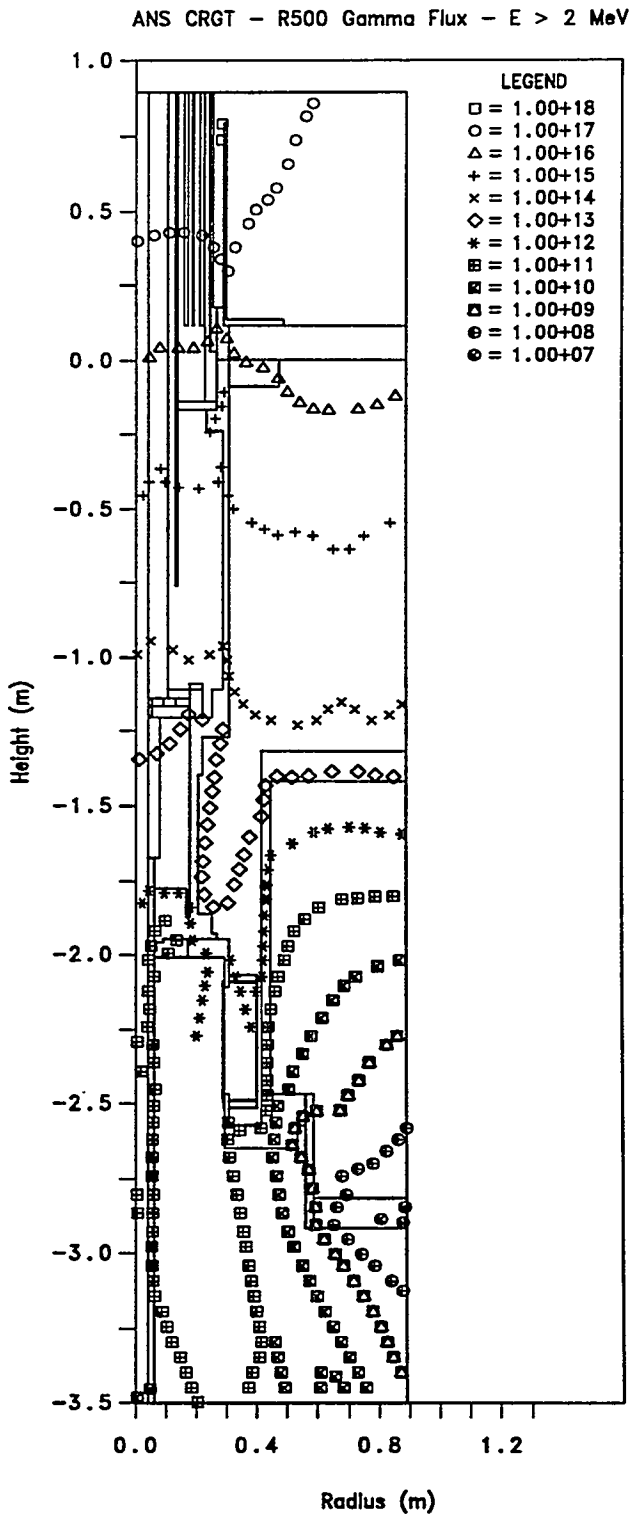

Fig. A.21. High-energy gamma flux in units ($m^{-2}s^{-1}$) for case R500 with restricted hafnium shield.

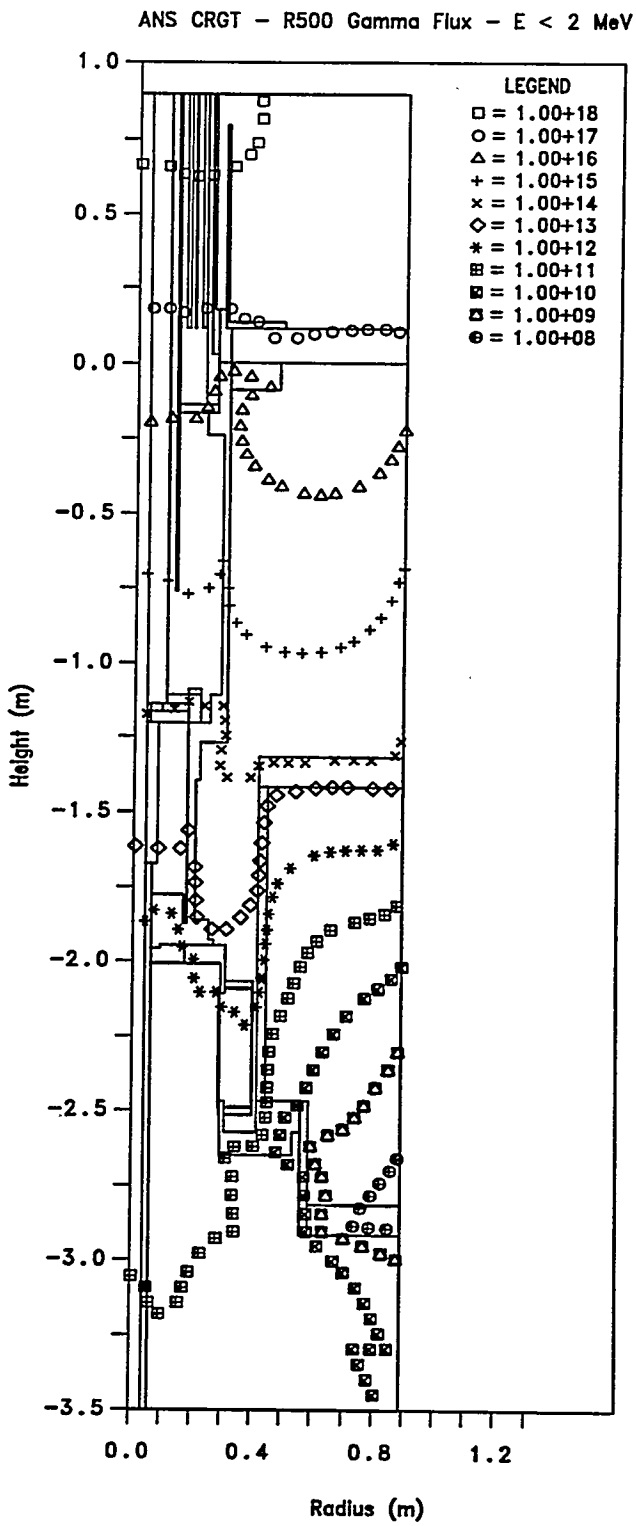

Fig. A.22. Low-energy gamma flux in units ($m^{-2}s^{-1}$) for case R500 with restricted hafnium shield.

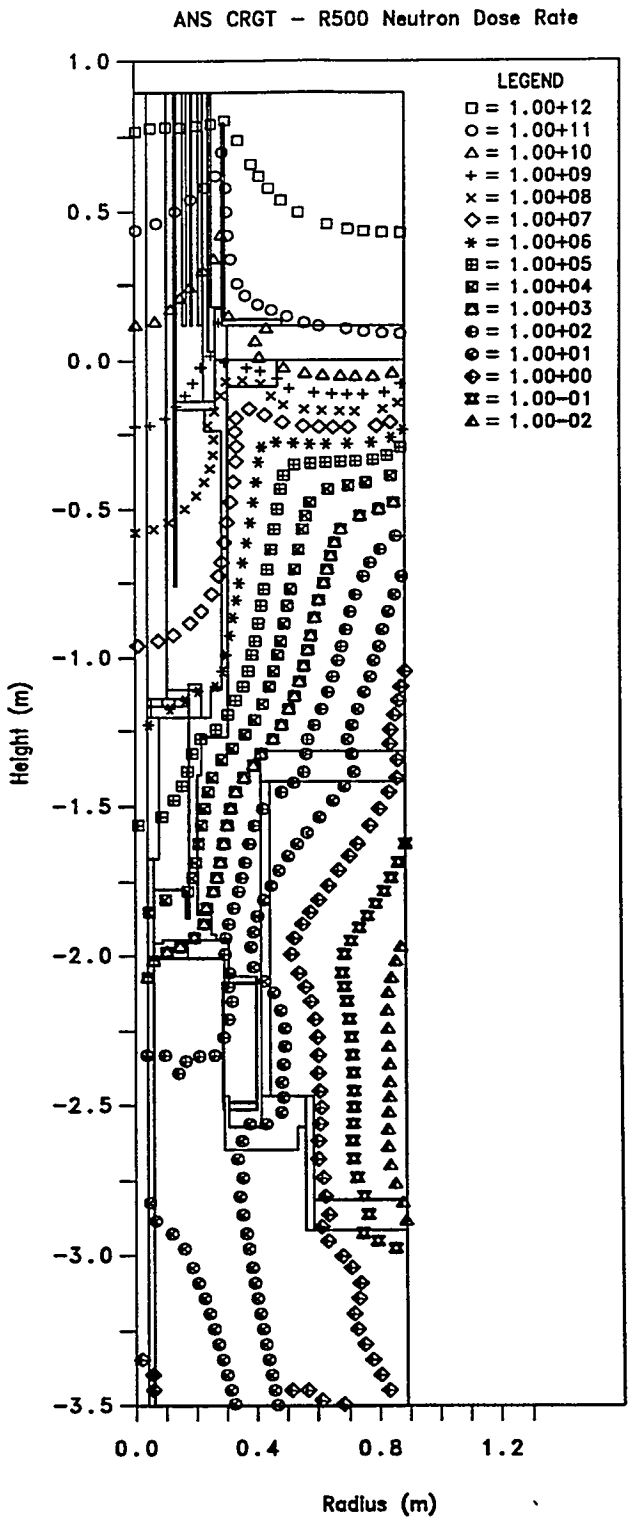

Fig. A.23. Neutron dose rate in units (mrem h^{-1}) for case R500 with restricted hafnium shield.

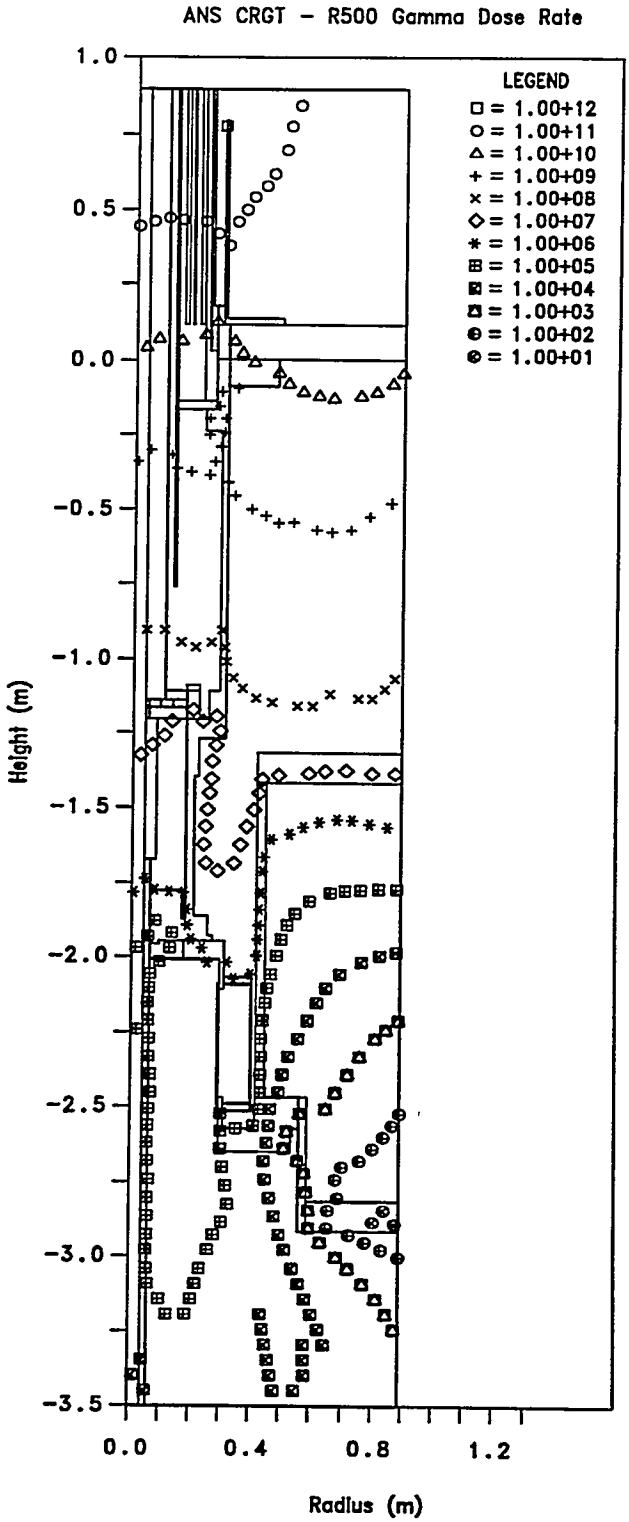

Fig. A.24. Gamma dose rate in units (mrem h^{-1}) for case R500 with restricted hafnium shield.

APPENDIX B. DISPLACEMENTS PER ATOM AND HELIUM-PRODUCTION DATA FOR CASES R400, R500, AND R550

Note that Z=0 mm in Figs. B.1, B.2, B.5, B.6, B.9, B.10 compares to the bottom of the reflector vessel as shown in Fig. 2.2.

In the tables in Appendix B, the helium production in the primary coolant supply adapter (PCSA) and its flange is listed with the displacements per atom (DPA) for cases R550 without any shield, R400 with the extended boral shield, and R500 with a radially restricted hafnium shield, assuming an exposition time of 40 years and a duty cycle factor of 0.7 for maintenance and reloading procedures. The total DPA (indicated with DPA-sum) adds up the contribution from direct (n,n') and (n,γ) reactions (indicated with DPA-fe) and the contribution from the sequential reaction $^{58}Ni \quad (n,\gamma) \quad ^{59}Ni \quad (n,\alpha)^{56}Fe$ (indicated with DPA-ni).

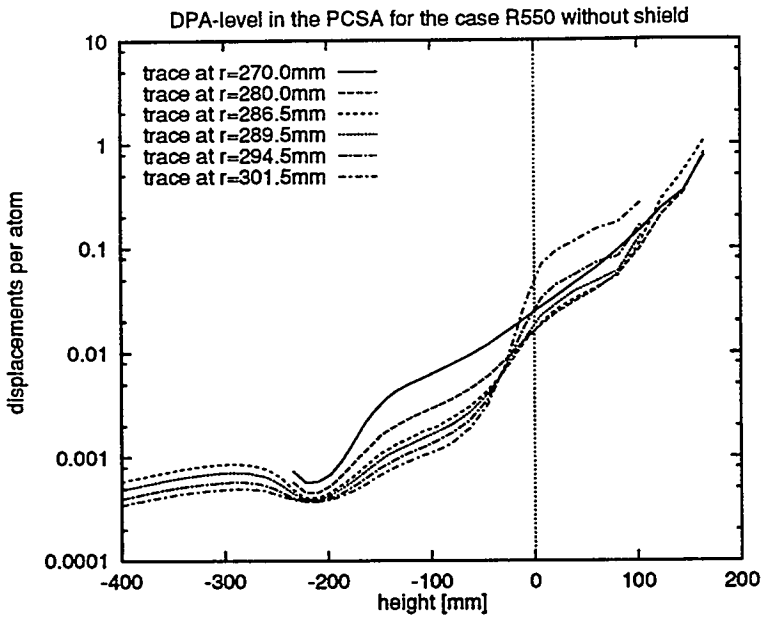

Fig. B.1. DPA level in the PCSA vs height for case R550 without shield after 40 years of reactor operation.

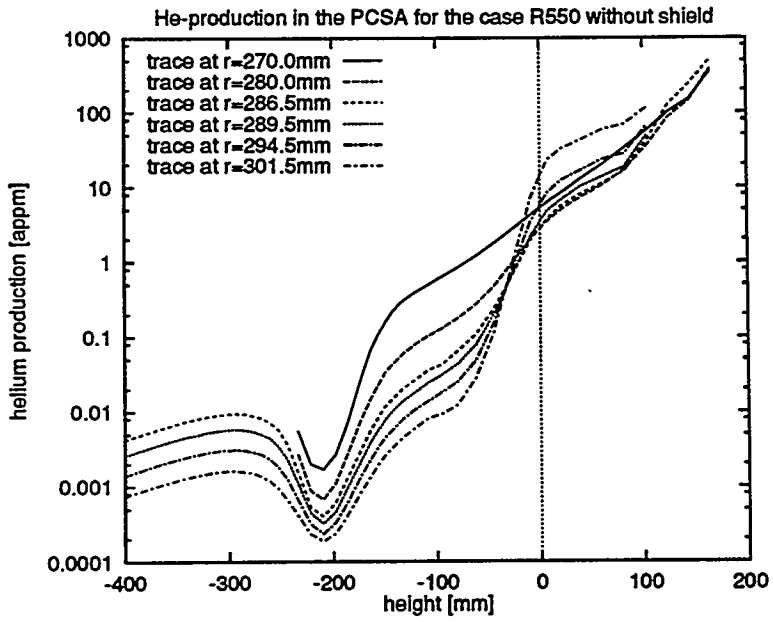

Fig. B.2. Helium production in the PCSA vs height for case R550 without shield after 40 years of reactor operation.

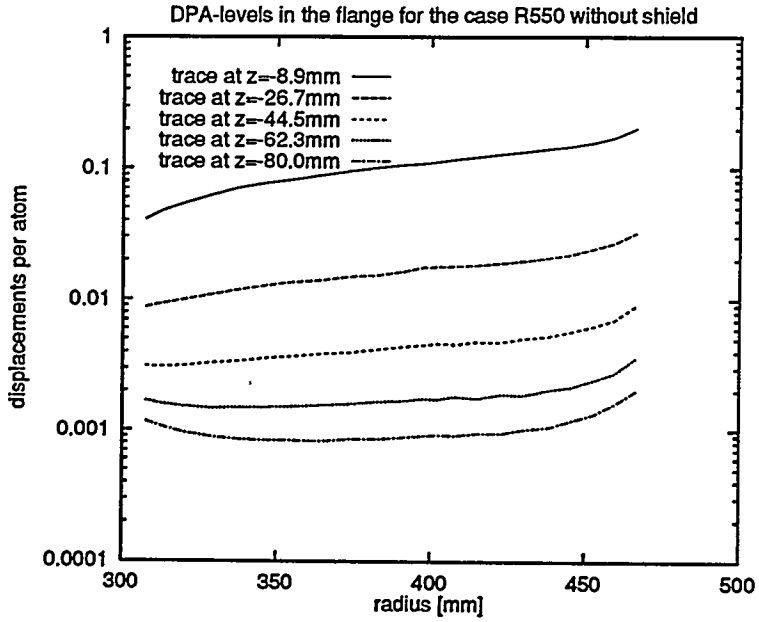

Fig. B.3. DPA level in the flange near the reflector vessel vs radius for case R550 without shield after 40 years of reactor operation.

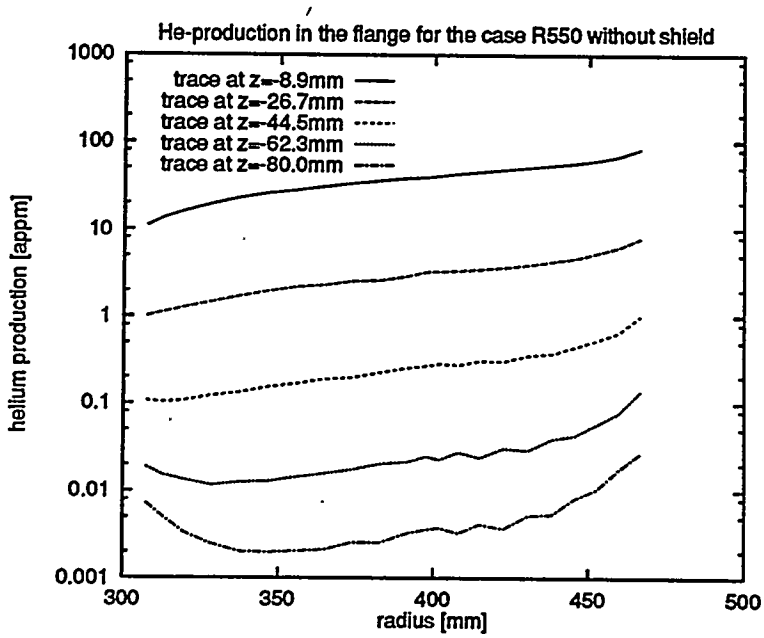

Fig. B.4. Helium production in the flange near the reflector vessel vs radius for case R550 without shield after 40 years of reactor operation.

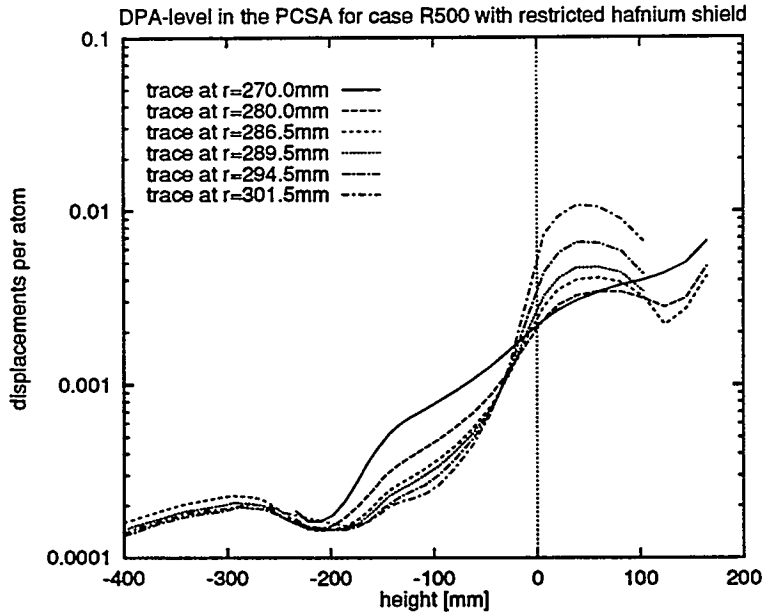

Fig. B.5. DPA level in the PCSA vs height for case R500 with radially restricted hafnium shield after 40 years of reactor operation.

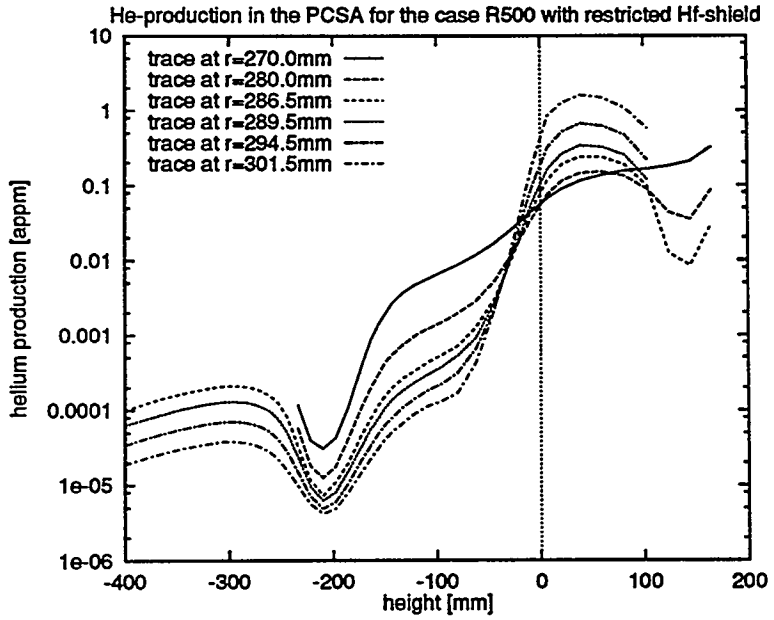

Fig. B.6. Helium production in the PCSA vs height for case R500 with radially restricted hafnium shield after 40 years of reactor operation.

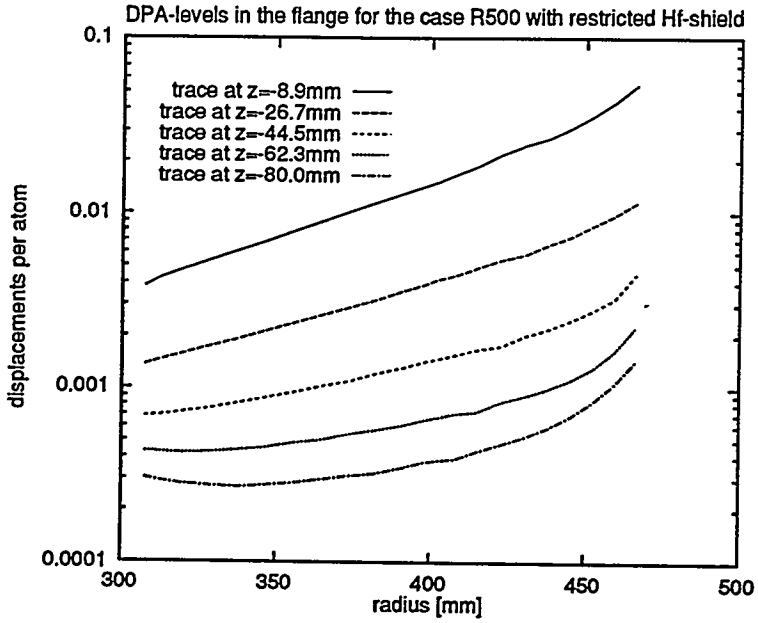

Fig. B.7. DPA level in the flange near the reflector vessel vs radius for case R500 with radially restricted hafnium shield after 40 years of reactor operation.

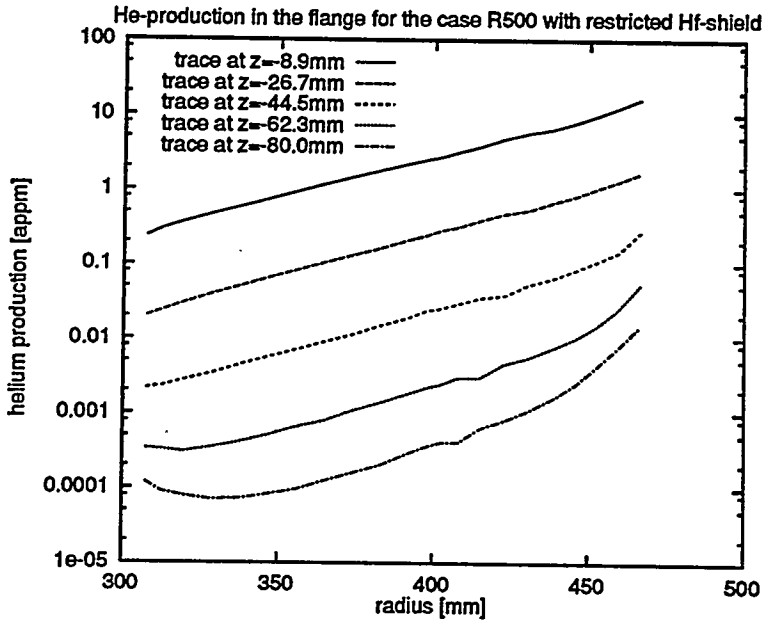

Fig. B.8. Helium production in the flange near the reflector vessel vs radius for case R500 with radially restricted hafnium shield after 40 years of reactor operation.

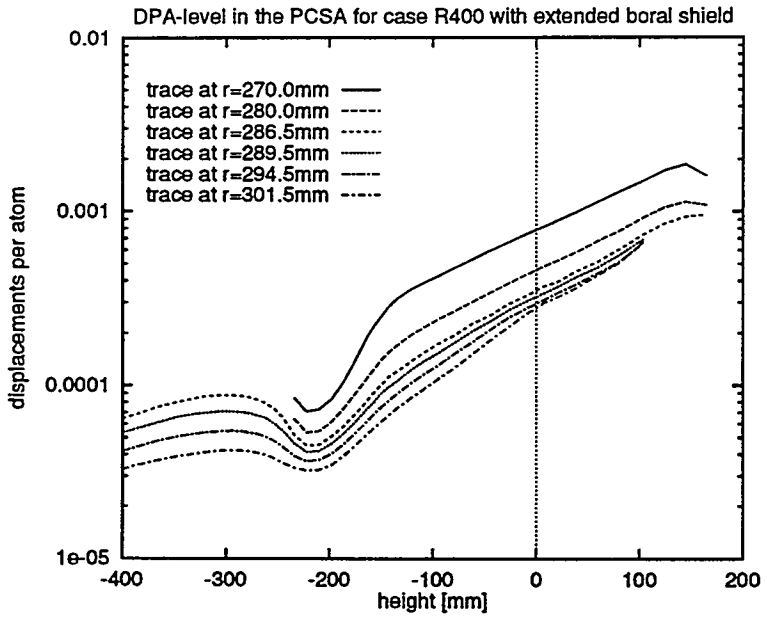

Fig. B.9. DPA level in the PCSA vs height for case R400 with radially extended boral shield after 40 years of reactor operation.

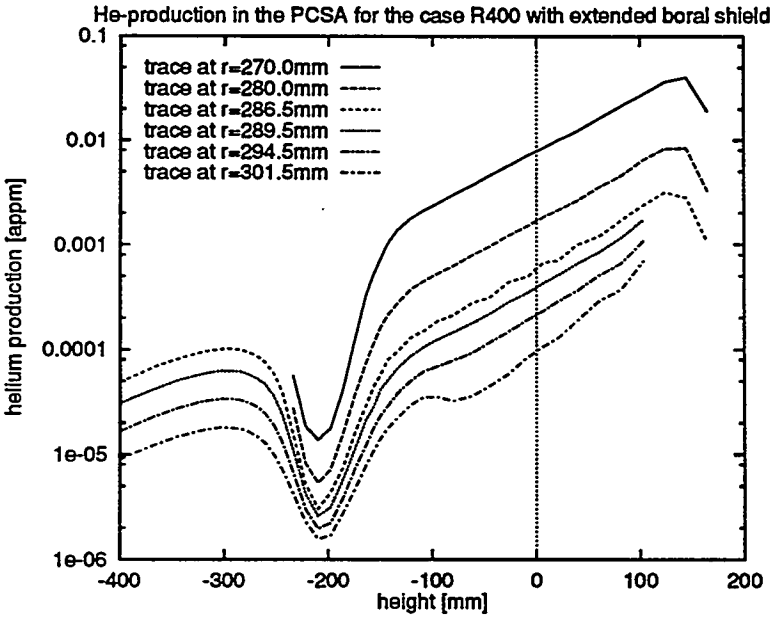

Fig. B.10. Helium production in the PCSA vs height for case R400 with radially extended boral shield after 40 years of reactor operation.

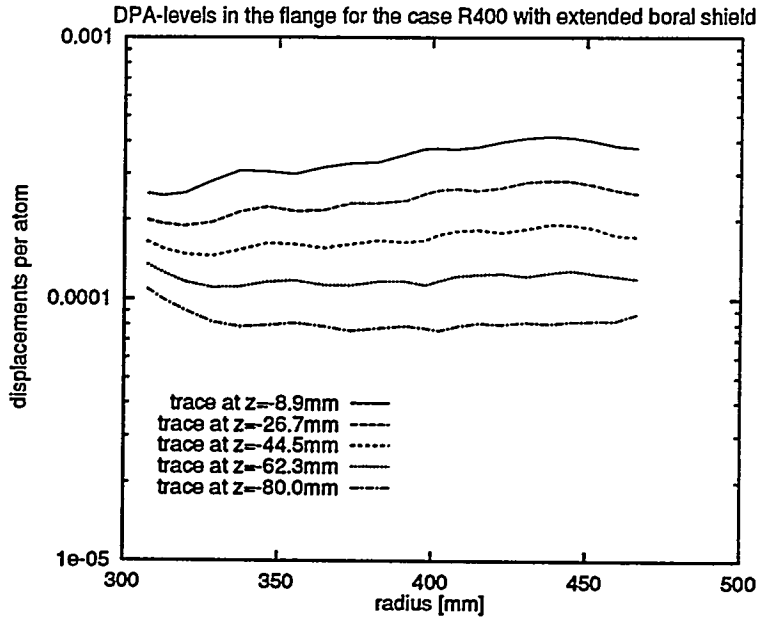

Fig. B.11. DPA level in the flange near the reflector vessel vs radius for case R400 with radially extended boral shield after 40 years of reactor operation.

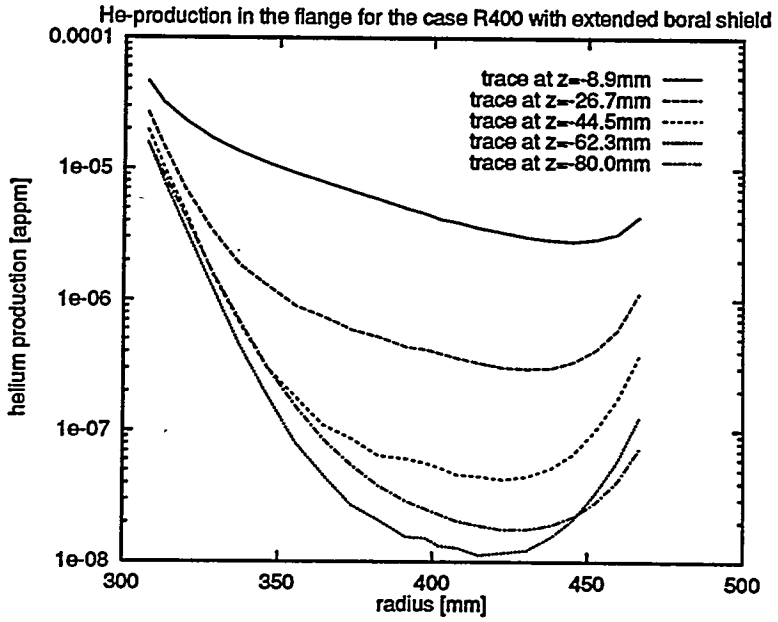

Fig. B.12. Helium production in the flange near the reflector vessel vs radius for case R400 with radially extended boral shield after 40 years of reactor operation.

Table B.1. Helium production and DPA data in the PCSA/PCST at radius 270.0 mm in case R550 without shield

Radial interval	Axial interval	Radius (mm)	Height (mm)	Volume (mm^3)	He–prod appm	DPA-ni disp/atom	DPA-fe disp/atom	DPA-sum disp/atom
63	157	270·00	−234·00	2.036E+05	5.59E–03	7.25E–04	9.85E–06	7.35E–04
63	158	270·00	−222·00	2.036E+05	2.00E–03	5.70E–04	3.53E–06	5.73E–04
63	159	270·00	−210·00	2.036E+05	1.70E–03	5.77E–04	2.99E–06	5.80E–04
63	160	270·00	−198·00	2.036E+05	2.67E–03	6.76E–04	4.70E–06	6.81E–04
63	161	270·00	−186·00	2.036E+05	7.35E–03	9.28E–04	1.29E–05	9.40E–04
63	162	270·00	−174·00	2.036E+05	2.60E–02	1.42E–03	4.59E–05	1.47E–03
63	163	270·00	−164·25	1.272E+05	6.48E–02	2.01E–03	1.14E–04	2.13E–03
63	164	270·00	−156·75	1.272E+05	1.06E–01	2.46E–03	1.87E–04	2.64E–03
63	165	270·00	−149·75	1.103E+05	1.54E–01	2.87E–03	2.71E–04	3.14E–03
63	166	270·00	−143·25	1.103E+05	2.13E–01	3.30E–03	3.76E–04	3.68E–03
63	167	270·00	−133·62	2.163E+05	2.92E–01	3.80E–03	5.15E–04	4.32E–03
63	168	270·00	−120·88	2.163E+05	3.89E–01	4.34E–03	6.86E–04	5.03E–03
63	169	270·00	−108·12	2.163E+05	4.93E–01	4.86E–03	8.68E–04	5.73E–03
63	170	270·00	−95·37	2.163E+05	6.23E–01	5.45E–03	1.10E–03	6.55E–03
63	171	270·00	−80·10	3.020E+05	8.27E–01	6.28E–03	1.46E–03	7.73E–03
63	172	270·00	−62·30	3.020E+05	1.18E+00	7.45E–03	2.07E–03	9.53E–03
63	173	270·00	−44·50	3.020E+05	1.75E+00	9.01E–03	3.08E–03	1.21E–02
63	174	270·00	−26·70	3.020E+05	2.68E+00	1.12E–02	4.71E–03	1.59E–02
63	175	270·00	−8·90	3.020E+05	4.19E+00	1.39E–02	7.38E–03	2.12E–02
63	176	270·00	7·00	2.375E+05	6.18E+00	1.67E–02	1.09E–02	2.76E–02
63	177	270·00	21·00	2.375E+05	8.40E+00	1.94E–02	1.48E–02	3.43E–02
63	178	270·00	38·75	3.647E+05	1.26E+01	2.37E–02	2.22E–02	4.59E–02
63	179	270·00	60·25	3.647E+05	1.98E+01	2.97E–02	3.49E–02	6.46E–02
63	180	270·00	81·75	3.647E+05	3.31E+01	3.85E–02	5.84E–02	9.69E–02
63	181	270·00	103·25	3.647E+05	5.66E+01	5.07E–02	9.97E–02	1.50E–01
63	182	270·00	124·17	3.449E+05	9.98E+01	6.85E–02	1.76E–01	2.44E–01
63	183	270·00	144·50	3.449E+05	1.50E+02	8.57E–02	2.63E–01	3.49E–01
63	184	270·00	164·83	3.449E+05	3.55E+02	1.41E–01	6.25E–01	7.66E–01

Table B.2. Helium production and DPA data in the PCSA/PCST at radius 280.0 mm in case R550 without shield

Radial interval	Axial interval	radius [mm]	Height [mm]	Volume [mm^3]	He–prod appm	DPA-ni disp/atom	DPA-fe disp/atom	DPA-sum disp/atom
64	157	280·00	−234·00	2.111E+05	2.71E−03	5.69E−04	4.77E−06	5.74E−04
64	158	280·00	−222·00	2.111E+05	8.82E−04	4.56E−04	1.55E−06	4.57E−04
64	159	280·00	−210·00	2.111E+05	6.78E−04	4.56E−04	1.19E−06	4.57E−04
64	160	280·00	−198·00	2.111E+05	1.11E−03	5.27E−04	1.95E−06	5.29E−04
64	161	280·00	−186·00	2.111E+05	2.83E−03	6.75E−04	4.98E−06	6.80E−04
64	162	280·00	−174·00	2.111E+05	7.49E−03	8.97E−04	1.32E−05	9.10E−04
64	163	280·00	−164·25	1.319E+05	1.46E−02	1.12E−03	2.57E−05	1.14E−03
64	164	280·00	−156·75	1.319E+05	2.26E−02	1.31E−03	3.98E−05	1.35E−03
64	165	280·00	−149·75	1.144E+05	3.33E−02	1.53E−03	5.87E−05	1.59E−03
64	166	280·00	−143·25	1.144E+05	4.21E−02	1.68E−03	7.41E−05	1.76E−03
64	167	280·00	−133·62	2.243E+05	5.71E−02	1.92E−03	1.01E−04	2.02E−03
64	168	280·00	−120·88	2.243E+05	7.91E−02	2.21E−03	1.39E−04	2.35E−03
64	169	280·00	−108·12	2.243E+05	1.02E−01	2.50E−03	1.80E−04	2.68E−03
64	170	280·00	−95·37	2.243E+05	1.29E−01	2.81E−03	2.27E−04	3.04E−03
64	171	280·00	−80·10	3.132E+05	1.75E−01	3.27E−03	3.08E−04	3.58E−03
64	172	280·00	−62·30	3.132E+05	2.68E−01	4.01E−03	4.71E−04	4.48E−03
64	173	280·00	−44·50	3.132E+05	4.70E−01	5.16E−03	8.28E−04	5.99E−03
64	174	280·00	−26·70	3.132E+05	9.55E−01	7.01E−03	1.68E−03	8.69E−03
64	175	280·00	−8·90	3.132E+05	2.02E+00	9.72E−03	3.56E−03	1.33E−02
64	176	280·00	7·00	2.463E+05	3.42E+00	1.26E−02	6.03E−03	1.86E−02
64	177	280·00	21·00	2.463E+05	4.95E+00	1.50E−02	8.71E−03	2.37E−02
64	178	280·00	38·75	3.782E+05	7.14E+00	1.79E−02	1.26E−02	3.05E−02
64	179	280·00	60·25	3.782E+05	1.05E+01	2.16E−02	1.84E−02	4.01E−02
64	180	280·00	81·75	3.782E+05	1.68E+01	2.73E−02	2.96E−02	5.69E−02
64	181	280·00	103·25	3.782E+05	3.52E+01	3.94E−02	6.21E−02	1.01E−01
64	182	280·00	124·17	3.577E+05	8.54E+01	6.26E−02	1.50E−01	2.13E−01
64	183	280·00	144·50	3.577E+05	1.42E+02	8.32E−02	2.51E−01	3.34E−01
64	184	280·00	164·83	3.577E+05	3.82E+02	1.48E−01	6.73E−01	8.20E−01

Table B.3. Helium production and DPA data in the PCSA/PCST at radius 286.5 mm in case R550 without shield

Radial interval	Axial interval	Radius [mm]	Height [mm]	Volume [mm^3]	He–prod appm	DPA-ni disp/atom	DPA-fe disp/atom	DPA-sum disp/atom
65	144	286·50	−411·70	1.220E+05	3.62E−03	5.38E−04	6.37E−06	5.44E−04
65	145	286·50	−389·10	1.220E+05	4.71E−03	6.06E−04	8.31E−06	6.15E−04
65	146	286·50	−366·50	1.220E+05	5.90E−03	6.76E−04	1.04E−05	6.86E−04
65	147	286·50	−343·90	1.220E+05	7.26E−03	7.47E−04	1.28E−05	7.60E−04
65	148	286·50	−321·30	1.220E+05	8.55E−03	8.04E−04	1.51E−05	8.19E−04
65	149	286·50	−304·50	5.940E+04	9.24E−03	8.36E−04	1.63E−05	8.52E−04
65	150	286·50	−293·50	5.940E+04	9.42E−03	8.44E−04	1.66E−05	8.61E−04
65	150	286·50	−293·50	5.940E+04	9.42E−03	8.44E−04	1.66E−05	8.61E−04
65	151	286·50	−284·12	4.185E+04	9.27E−03	8.40E−04	1.63E−05	8.57E−04
65	152	286·50	−276·38	4.185E+04	8.77E−03	8.22E−04	1.55E−05	8.38E−04
65	153	286·50	−268·62	4.185E+04	8.12E−03	7.97E−04	1.43E−05	8.12E−04
65	154	286·50	−260·88	4.185E+04	7.13E−03	7.57E−04	1.26E−05	7.69E−04
65	155	286·50	−252·75	4.590E+04	5.71E−03	6.98E−04	1.01E−05	7.08E−04
65	156	286·50	−244·25	4.590E+04	3.69E−03	6.06E−04	6.50E−06	6.12E−04
65	157	286·50	−234·00	6.480E+04	1.53E−03	4.82E−04	2.70E−06	4.85E−04
65	158	286·50	−222·00	6.480E+04	5.31E−04	4.04E−04	9.36E−07	4.05E−04
65	159	286·50	−210·00	6.480E+04	4.00E−04	4.06E−04	7.05E−07	4.06E−04
65	160	286·50	−198·00	6.480E+04	6.18E−04	4.56E−04	1.09E−06	4.57E−04
65	161	286·50	−186·00	6.480E+04	1.36E−03	5.46E−04	2.39E−06	5.48E−04
65	162	286·50	−174·00	6.480E+04	2.97E−03	6.67E−04	5.23E−06	6.72E−04
65	163	286·50	−164·25	4.050E+04	5.67E−03	8.10E−04	9.98E−06	8.20E−04
65	164	286·50	−156·75	4.050E+04	8.36E−03	9.28E−04	1.47E−05	9.43E−04
65	165	286·50	−149·75	3.510E+04	1.18E−02	1.05E−03	2.07E−05	1.07E−03
65	166	286·50	−143·25	3.510E+04	1.46E−02	1.14E−03	2.57E−05	1.17E−03
65	167	286·50	−133·62	6.885E+04	1.99E−02	1.30E−03	3.50E−05	1.33E−03
65	168	286·50	−120·88	6.885E+04	2.65E−02	1.47E−03	4.67E−05	1.52E−03
65	169	286·50	−108·12	6.885E+04	3.57E−02	1.69E−03	6.28E−05	1.75E−03
65	170	286·50	−95·37	6.885E+04	4.22E−02	1.86E−03	7.43E−05	1.94E−03
65	171	286·50	−80·10	9.613E+04	6.36E−02	2.25E−03	1.12E−04	2.36E−03
65	172	286·50	−62·30	9.613E+04	1.07E−01	2.85E−03	1.89E−04	3.04E−03
65	173	286·50	−44·50	9.613E+04	2.36E−01	3.95E−03	4.16E−04	4.37E−03
65	174	286·50	−26·70	9.613E+04	6.54E−01	5.95E−03	1.15E−03	7.11E−03
65	175	286·50	−8·90	9.613E+04	1.93E+00	9.42E−03	3.40E−03	1.28E−02
65	176	286·50	7·00	7.561E+04	3.67E+00	1.28E−02	6.46E−03	1.93E−02
65	177	286·50	21·00	7.561E+04	5.57E+00	1.57E−02	9.82E−03	2.55E−02
65	178	286·50	38·75	1.161E+05	7.88E+00	1.85E−02	1.39E−02	3.24E−02
65	179	286·50	60·25	1.161E+05	1.10E+01	2.20E−02	1.94E−02	4.14E−02
65	180	286·50	81·75	1.161E+05	1.61E+01	2.66E−02	2.83E−02	5.49E−02
65	181	286·50	103·25	1.161E+05	4.11E+01	4.23E−02	7.23E−02	1.15E−01
65	182	286·50	124·17	1.098E+05	1.25E+02	7.71E−02	2.20E−01	2.97E−01
65	183	286·50	144·50	1.098E+05	2.39E+02	1.13E−01	4.21E−01	5.34E−01
65	184	286·50	164·83	1.098E+05	5.07E+02	1.78E−01	8.93E−01	1.07E+00

Table B.4. Helium production and DPA data in the PCSA/PCST at radius 289.5 mm in case R550 without shield

Radial interval	Axial interval	Radius [mm]	Height [mm]	Volume [mm^3]	He–prod appm	DPA-ni disp/atom	DPA-fe disp/atom	DPA-sum disp/atom
66	144	289·50	−411·70	1.233E+05	2.25E–03	4.50E–04	3.96E–06	4.54E–04
66	145	289·50	−389·10	1.233E+05	2.90E–03	5.07E–04	5.10E–06	5.12E–04
66	146	289·50	−366·50	1.233E+05	3.64E–03	5.64E–04	6.41E–06	5.70E–04
66	147	289·50	−343·90	1.233E+05	4.49E–03	6.23E–04	7.92E–06	6.31E–04
66	148	289·50	−321·30	1.233E+05	5.26E–03	6.66E–04	9.27E–06	6.75E–04
66	149	289·50	−304·50	6.003E+04	5.70E–03	6.93E–04	1.00E–05	7.03E–04
66	150	289·50	−293·50	6.003E+04	5.80E–03	7.03E–04	1.02E–05	7.13E–04
66	150	289·50	−293·50	6.003E+04	5.80E–03	7.03E–04	1.02E–05	7.13E–04
66	151	289·50	−284·12	4.229E+04	5.68E–03	7.00E–04	1.00E–05	7.10E–04
66	152	289·50	−276·38	4.229E+04	5.43E–03	6.91E–04	9.57E–06	7.00E–04
66	153	289·50	−268·62	4.229E+04	4.95E–03	6.66E–04	8.72E–06	6.75E–04
66	154	289·50	−260·88	4.229E+04	4.47E–03	6.41E–04	7.87E–06	6.49E–04
66	155	289·50	−252·75	4.638E+04	3.41E–03	5.88E–04	6.01E–06	5.94E–04
66	156	289·50	−244·25	4.638E+04	2.31E–03	5.24E–04	4.07E–06	5.28E–04
66	157	289·50	−234·00	6.548E+04	1.09E–03	4.44E–04	1.91E–06	4.46E–04
66	158	289·50	−222·00	6.548E+04	4.45E–04	3.89E–04	7.84E–07	3.90E–04
66	159	289·50	−210·00	6.548E+04	3.24E–04	3.90E–04	5.70E–07	3.90E–04
66	160	289·50	−198·00	6.548E+04	4.66E–04	4.29E–04	8.21E–07	4.29E–04
66	161	289·50	−186·00	6.548E+04	1.01E–03	5.03E–04	1.77E–06	5.05E–04
66	162	289·50	−174·00	6.548E+04	2.12E–03	6.05E–04	3.74E–06	6.08E–04
66	163	289·50	−164·25	4.093E+04	3.92E–03	7.21E–04	6.90E–06	7.28E–04
66	164	289·50	−156·75	4.093E+04	5.67E–03	8.18E–04	9.99E–06	8.28E–04
66	165	289·50	−149·75	3.547E+04	7.80E–03	9.15E–04	1.37E–05	9.29E–04
66	166	289·50	−143·25	3.547E+04	1.01E–02	1.01E–03	1.78E–05	1.03E–03
66	167	289·50	−133·62	6.958E+04	1.36E–02	1.13E–03	2.40E–05	1.16E–03
66	168	289·50	−120·88	6.958E+04	1.82E–02	1.29E–03	3.21E–05	1.32E–03
66	169	289·50	−108·12	6.958E+04	2.43E–02	1.47E–03	4.28E–05	1.51E–03
66	170	289·50	−95·37	6.958E+04	3.07E–02	1.66E–03	5.41E–05	1.71E–03
66	171	289·50	−80·10	9.713E+04	4.30E–02	1.97E–03	7.57E–05	2.04E–03
66	172	289·50	−62·30	9.713E+04	7.76E–02	2.55E–03	1.37E–04	2.69E–03
66	173	289·50	−44·50	9.713E+04	2.01E–01	3.70E–03	3.54E–04	4.06E–03
66	174	289·50	−26·70	9.713E+04	6.78E–01	6.02E–03	1.19E–03	7.21E–03
66	175	289·50	−8·90	9.713E+04	2.17E+00	9.85E–03	3.82E–03	1.37E–02
66	176	289·50	7·00	7.640E+04	4.73E+00	1.43E–02	8.34E–03	2.26E–02
66	177	289·50	21·00	7.640E+04	6.73E+00	1.70E–02	1.19E–02	2.88E–02
66	178	289·50	38·75	1.173E+05	1.00E+01	2.07E–02	1.77E–02	3.83E–02
66	179	289·50	60·25	1.173E+05	1.35E+01	2.41E–02	2.39E–02	4.79E–02
66	180	289·50	81·75	1.173E+05	1.85E+01	2.84E–02	3.26E–02	6.10E–02
66	181	289·50	103·25	1.173E+05	4.90E+01	4.62E–02	8.63E–02	1.33E–01

Table B.5. Helium production and DPA data in the PCSA/PCST at radius 294.5 mm in case R550 without shield

Radial interval	Axial interval	Radius [mm]	Height [mm]	Volume [mm^3]	He–prod appm	DPA-ni disp/atom	DPA-fe disp/atom	DPA-sum disp/atom
67	144	294·50	−411·70	2.927E+05	1.22E–03	3.72E–04	2.15E–06	3.74E–04
67	145	294·50	−389·10	2.927E+05	1.56E–03	4.15E–04	2.75E–06	4.17E–04
67	146	294·50	−366·50	2.927E+05	1.99E–03	4.64E–04	3.50E–06	4.67E–04
67	147	294·50	−343·90	2.927E+05	2.42E–03	5.08E–04	4.27E–06	5.13E–04
67	148	294·50	−321·30	2.927E+05	2.85E–03	5.43E–04	5.02E–06	5.48E–04
67	149	294·50	−304·50	1.425E+05	3.07E–03	5.62E–04	5.40E–06	5.68E–04
67	150	294·50	−293·50	1.425E+05	3.11E–03	5.73E–04	5.49E–06	5.79E–04
67	150	294·50	−293·50	1.425E+05	3.11E–03	5.73E–04	5.49E–06	5.79E–04
67	151	294·50	−284·12	1.004E+05	3.06E–03	5.75E–04	5.39E–06	5.80E–04
67	152	294·50	−276·38	1.004E+05	2.87E–03	5.66E–04	5.06E–06	5.71E–04
67	153	294·50	−268·62	1.004E+05	2.68E–03	5.55E–04	4.73E–06	5.59E–04
67	154	294·50	−260·88	1.004E+05	2.32E–03	5.31E–04	4.08E–06	5.35E–04
67	155	294·50	−252·75	1.101E+05	1.82E–03	4.97E–04	3.21E–06	5.00E–04
67	156	294·50	−244·25	1.101E+05	1.25E–03	4.54E–04	2.21E–06	4.56E–04
67	157	294·50	−234·00	1.554E+05	6.58E–04	4.03E–04	1.16E–06	4.04E–04
67	158	294·50	−222·00	1.554E+05	3.18E–04	3.72E–04	5.61E–07	3.73E–04
67	159	294·50	−210·00	1.554E+05	2.36E–04	3.73E–04	4.15E–07	3.74E–04
67	160	294·50	−198·00	1.554E+05	3.35E–04	4.03E–04	5.89E–07	4.03E–04
67	161	294·50	−186·00	1.554E+05	6.34E–04	4.52E–04	1.12E–06	4.54E–04
67	162	294·50	−174·00	1.554E+05	1.35E–03	5.34E–04	2.37E–06	5.36E–04
67	163	294·50	−164·25	9.715E+04	2.29E–03	6.19E–04	4.03E–06	6.23E–04
67	164	294·50	−156·75	9.715E+04	3.34E–03	6.96E–04	5.88E–06	7.01E–04
67	165	294·50	−149·75	8.419E+04	4.58E–03	7.76E–04	8.07E–06	7.85E–04
67	167	294·50	−133·62	1.651E+05	7.75E–03	9.46E–04	1.36E–05	9.59E–04
67	167	294·50	−133·62	1.651E+05	7.75E–03	9.46E–04	1.36E–05	9.59E–04
67	168	294·50	−120·88	1.651E+05	1.08E–02	1.08E–03	1.90E–05	1.10E–03
67	169	294·50	−108·12	1.651E+05	1.39E–02	1.21E–03	2.45E–05	1.24E–03
67	170	294·50	−95·37	1.651E+05	1.81E–02	1.38E–03	3.19E–05	1.42E–03
67	171	294·50	−80·10	2.306E+05	2.49E–02	1.65E–03	4.39E–05	1.70E–03
67	172	294·50	−62·30	2.306E+05	4.77E–02	2.18E–03	8.40E–05	2.26E–03
67	173	294·50	−44·50	2.306E+05	1.55E–01	3.37E–03	2.73E–04	3.64E–03
67	174	294·50	−26·70	2.306E+05	7.81E–01	6.31E–03	1.38E–03	7.68E–03
67	175	294·50	−8·90	2.306E+05	3.43E+00	1.21E–02	6.04E–03	1.82E–02
67	176	294·50	7·00	1.813E+05	8.29E+00	1.84E–02	1.46E–02	3.31E–02
67	177	294·50	21·00	1.813E+05	1.23E+01	2.25E–02	2.17E–02	4.42E–02
67	178	294·50	38·75	2.785E+05	1.64E+01	2.60E–02	2.89E–02	5.50E–02
67	179	294·50	60·25	2.785E+05	2.33E+01	3.12E–02	4.10E–02	7.22E–02
67	180	294·50	81·75	2.785E+05	2.78E+01	3.45E–02	4.89E–02	8.35E–02
67	181	294·50	103·25	2.785E+05	6.51E+01	5.37E–02	1.15E–01	1.68E–01

Table B.6. Helium production and DPA data in the PCSA/PCST at radius 301.5 mm in case R550 without shield

Radial interval	Axial interval	Radius [mm]	Height [mm]	Volume [mm^3]	He-prod appm	DPA-ni disp/atom	DPA-fe disp/atom	DPA-sum disp/atom
68	144	301·50	−411·70	2.997E+05	6.47E−04	3.22E−04	1.14E−06	3.23E−04
68	145	301·50	−389·10	2.997E+05	8.33E−04	3.62E−04	1.47E−06	3.64E−04
68	146	301·50	−366·50	2.997E+05	1.05E−03	4.00E−04	1.84E−06	4.02E−04
68	147	301·50	−343·90	2.997E+05	1.28E−03	4.39E−04	2.26E−06	4.41E−04
68	148	301·50	−321·30	2.997E+05	1.49E−03	4.66E−04	2.63E−06	4.69E−04
68	149	301·50	−304·50	1.459E+05	1.61E−03	4.82E−04	2.83E−06	4.84E−04
68	150	301·50	−293·50	1.459E+05	1.63E−03	4.91E−04	2.87E−06	4.94E−04
68	150	301·50	−293·50	1.459E+05	1.63E−03	4.91E−04	2.87E−06	4.94E−04
68	151	301·50	−284·12	1.028E+05	1.57E−03	4.93E−04	2.76E−06	4.96E−04
68	152	301·50	−276·38	1.028E+05	1.50E−03	4.92E−04	2.64E−06	4.95E−04
68	153	301·50	−268·62	1.028E+05	1.36E−03	4.84E−04	2.39E−06	4.86E−04
68	154	301·50	−260·88	1.028E+05	1.19E−03	4.71E−04	2.10E−06	4.73E−04
68	155	301·50	−252·75	1.127E+05	9.36E−04	4.46E−04	1.65E−06	4.48E−04
68	156	301·50	−244·25	1.127E+05	6.65E−04	4.18E−04	1.17E−06	4.19E−04
68	157	301·50	−234·00	1.591E+05	4.10E−04	3.91E−04	7.22E−07	3.92E−04
68	158	301·50	−222·00	1.591E+05	2.33E−04	3.72E−04	4.10E−07	3.73E−04
68	159	301·50	−210·00	1.591E+05	1.86E−04	3.73E−04	3.28E−07	3.74E−04
68	160	301·50	−198·00	1.591E+05	2.37E−04	3.90E−04	4.18E−07	3.90E−04
68	161	301·50	−186·00	1.591E+05	4.29E−04	4.26E−04	7.56E−07	4.27E−04
68	162	301·50	−174·00	1.591E+05	8.28E−04	4.83E−04	1.46E−06	4.84E−04
68	163	301·50	−164·25	9.946E+04	1.35E−03	5.42E−04	2.38E−06	5.45E−04
68	164	301·50	−156·75	9.945E+04	1.96E−03	6.05E−04	3.45E−06	6.08E−04
68	165	301·50	−149·75	8.619E+04	2.63E−03	6.65E−04	4.64E−06	6.70E−04
68	166	301·50	−143·25	8.619E+04	3.28E−03	7.20E−04	5.78E−06	7.26E−04
68	167	301·50	−133·62	1.691E+05	4.44E−03	8.03E−04	7.82E−06	8.10E−04
68	168	301·50	−120·88	1.691E+05	6.11E−03	9.04E−04	1.08E−05	9.14E−04
68	169	301·50	−108·12	1.691E+05	8.14E−03	1.02E−03	1.43E−05	1.03E−03
68	170	301·50	−95·37	1.691E+05	9.21E−03	1.12E−03	1.62E−05	1.14E−03
68	171	301·50	−80·10	2.360E+05	1.22E−02	1.34E−03	2.16E−05	1.36E−03
68	172	301·50	−62·30	2.360E+05	2.76E−02	1.84E−03	4.87E−05	1.89E−03
68	173	301·50	−44·50	2.360E+05	1.16E−01	3.04E−03	2.05E−04	3.25E−03
68	174	301·50	−26·70	2.360E+05	9.10E−01	6.67E−03	1.60E−03	8.27E−03
68	175	301·50	−8·90	2.360E+05	7.11E+00	1.68E−02	1.25E−02	2.94E−02
68	176	301·50	7·00	1.856E+05	2.28E+01	3.00E−02	4.01E−02	7.01E−02
68	177	301·50	21·00	1.856E+05	3.24E+01	3.61E−02	5.71E−02	9.32E−02
68	178	301·50	38·75	2.851E+05	4.19E+01	4.14E−02	7.38E−02	1.15E−01
68	179	301·50	60·25	2.851E+05	5.79E+01	4.95E−02	1.02E−01	1.51E−01
68	180	301·50	81·75	2.851E+05	6.90E+01	5.48E−02	1.22E−01	1.76E−01
68	181	301·50	103·25	2.851E+05	1.14E+02	7.28E−02	2.01E−01	2.74E−01

Table B.7. Helium production and DPA data in the flange at height −8.9 mm in case R550 without shield

Radial interval	Axial interval	Radius [mm]	Height [mm]	Volume [mm^3]	He–prod appm	DPA-ni disp/atom	DPA-fe disp/atom	DPA-sum disp/atom
69	175	307·50	−8·90	1.720E+05	1.11E+01	2.09E–02	1.96E–02	4.05E–02
70	175	312·50	−8·90	1.748E+05	1.34E+01	2.29E–02	2.37E–02	4.66E–02
71	175	319·50	−8·90	3.216E+05	1.61E+01	2.51E–02	2.84E–02	5.34E–02
72	175	328·50	−8·90	3.307E+05	1.95E+01	2.76E–02	3.44E–02	6.20E–02
73	175	337·50	−8·90	3.397E+05	2.30E+01	3.00E–02	4.05E–02	7.05E–02
74	175	346·50	−8·90	3.488E+05	2.58E+01	3.18E–02	4.54E–02	7.71E–02
75	175	355·50	−8·90	3.578E+05	2.78E+01	3.30E–02	4.90E–02	8.21E–02
76	175	364·50	−8·90	3.669E+05	3.06E+01	3.47E–02	5.39E–02	8.86E–02
77	175	373·50	−8·90	3.760E+05	3.33E+01	3.63E–02	5.88E–02	9.50E–02
78	175	382·50	−8·90	3.850E+05	3.59E+01	3.77E–02	6.32E–02	1.01E–01
79	175	391·50	−8·90	3.941E+05	3.83E+01	3.90E–02	6.75E–02	1.06E–01
80	175	397·50	−8·90	1.334E+05	3.93E+01	3.95E–02	6.92E–02	1.09E–01
81	175	402·00	−8·90	2.698E+05	4.09E+01	4.03E–02	7.20E–02	1.12E–01
82	175	408·00	−8·90	2.738E+05	4.33E+01	4.15E–02	7.62E–02	1.18E–01
83	175	414·88	−8·90	3.596E+05	4.53E+01	4.25E–02	7.99E–02	1.22E–01
84	175	422·62	−8·90	3.663E+05	4.82E+01	4.39E–02	8.50E–02	1.29E–01
85	175	430·38	−8·90	3.730E+05	5.07E+01	4.51E–02	8.93E–02	1.34E–01
86	175	438·12	−8·90	3.798E+05	5.39E+01	4.65E–02	9.49E–02	1.41E–01
87	175	445·50	−8·90	3.488E+05	5.69E+01	4.79E–02	1.00E–01	1.48E–01
88	175	452·50	−8·90	3.543E+05	6.14E+01	5.00E–02	1.08E–01	1.58E–01
89	175	459·50	−8·90	3.597E+05	6.83E+01	5.30E–02	1.20E–01	1.73E–01
90	175	466·50	−8·90	3.652E+05	8.24E+01	5.95E–02	1.45E–01	2.05E–01

Table B.8. Helium production and DPA data in the flange at height −26.7 mm in case R550 without shield

Radial interval	Axial interval	Radius [mm]	Height [mm]	Volume [mm^3]	He–prod appm	DPA-ni disp/atom	DPA-fe disp/atom	DPA-sum disp/atom
69	174	307·50	−26·70	1.720E+05	1.01E+00	6.96E–03	1.77E–03	8.74E–03
70	174	312·50	−26·70	1.748E+05	1.11E+00	7.27E–03	1.96E–03	9.23E–03
71	174	319·50	−26·70	3.216E+05	1.26E+00	7.67E–03	2.22E–03	9.89E–03
72	174	328·50	−26·70	3.307E+05	1.47E+00	8.20E–03	2.60E–03	1.08E–02
73	174	337·50	−26·70	3.397E+05	1.71E+00	8.73E–03	3.02E–03	1.17E–02
74	174	346·50	−26·70	3.488E+05	1.95E+00	9.23E–03	3.44E–03	1.27E–02
75	174	355·50	−26·70	3.578E+05	2.16E+00	9.64E–03	3.81E–03	1.34E–02
76	174	364·50	−26·70	3.669E+05	2.29E+00	9.89E–03	4.03E–03	1.39E–02
77	174	373·50	−26·70	3.760E+05	2.53E+00	1.04E–02	4.45E–03	1.48E–02
78	174	382·50	−26·70	3.850E+05	2.60E+00	1.06E–02	4.58E–03	1.52E–02
79	174	391·50	−26·70	3.941E+05	2.91E+00	1.12E–02	5.12E–03	1.63E–02
80	174	397·50	−26·70	1.334E+05	3.26E+00	1.18E–02	5.74E–03	1.75E–02
81	174	402·00	−26·70	2.698E+05	3.29E+00	1.19E–02	5.80E–03	1.77E–02
82	174	408·00	−26·70	2.738E+05	3.35E+00	1.20E–02	5.91E–03	1.79E–02
83	174	414·88	−26·70	3.596E+05	3.47E+00	1.21E–02	6.12E–03	1.82E–02
84	174	422·62	−26·70	3.663E+05	3.66E+00	1.24E–02	6.45E–03	1.89E–02
85	174	430·38	−26·70	3.730E+05	3.90E+00	1.28E–02	6.87E–03	1.97E–02
86	174	438·12	−26·70	3.798E+05	4.26E+00	1.33E–02	7.50E–03	2.08E–02
87	174	445·50	−26·70	3.488E+05	4.66E+00	1.39E–02	8.21E–03	2.21E–02
88	174	452·50	−26·70	3.543E+05	5.35E+00	1.49E–02	9.42E–03	2.43E–02
89	174	459·50	−26·70	3.597E+05	6.20E+00	1.61E–02	1.09E–02	2.70E–02
90	174	466·50	−26·70	3.652E+05	7.86E+00	1.84E–02	1.39E–02	3.23E–02

Table B.9. Helium production and DPA data in the flange at height –44.5 mm in case R550 without shield

Radial interval	Axial interval	Radius [mm]	Height [mm]	Volume [mm^3]	He–prod appm	DPA-ni disp/atom	DPA-fe disp/atom	DPA-sum disp/atom
69	173	307·50	–44·50	1.720E+05	1.08E–01	2.95E–03	1.90E–04	3.14E–03
70	173	312·50	–44·50	1.748E+05	1.04E–01	2.90E–03	1.83E–04	3.09E–03
71	173	319·50	–44·50	3.216E+05	1.08E–01	2.95E–03	1.90E–04	3.14E–03
72	173	328·50	–44·50	3.307E+05	1.23E–01	3.07E–03	2.17E–04	3.29E–03
73	173	337·50	–44·50	3.397E+05	1.34E–01	3.17E–03	2.36E–04	3.40E–03
74	173	346·50	–44·50	3.488E+05	1.53E–01	3.30E–03	2.70E–04	3.57E–03
75	173	355·50	–44·50	3.578E+05	1.68E–01	3.40E–03	2.96E–04	3.70E–03
76	173	364·50	–44·50	3.669E+05	1.89E–01	3.53E–03	3.33E–04	3.87E–03
77	173	373·50	–44·50	3.760E+05	1.97E–01	3.60E–03	3.47E–04	3.94E–03
78	173	382·50	–44·50	3.850E+05	2.25E–01	3.77E–03	3.97E–04	4.17E–03
79	173	391·50	–44·50	3.941E+05	2.54E–01	3.95E–03	4.48E–04	4.40E–03
80	173	397·50	–44·50	1.334E+05	2.69E–01	4.04E–03	4.74E–04	4.51E–03
81	173	402·00	–44·50	2.698E+05	2.86E–01	4.12E–03	5.03E–04	4.63E–03
82	173	408·00	–44·50	2.738E+05	2.75E–01	4.08E–03	4.85E–04	4.57E–03
83	173	414·88	–44·50	3.596E+05	3.08E–01	4.25E–03	5.42E–04	4.79E–03
84	173	422·62	–44·50	3.663E+05	3.04E–01	4.22E–03	5.36E–04	4.76E–03
85	173	430·38	–44·50	3.730E+05	3.53E–01	4.48E–03	6.23E–04	5.10E–03
86	173	438·12	–44·50	3.798E+05	3.76E–01	4.61E–03	6.62E–04	5.27E–03
87	173	445·50	–44·50	3.488E+05	4.47E–01	4.95E–03	7.87E–04	5.74E–03
88	173	452·50	–44·50	3.543E+05	5.31E–01	5.36E–03	9.36E–04	6.29E–03
89	173	459·50	–44·50	3.597E+05	6.51E–01	5.89E–03	1.15E–03	7.04E–03
90	173	466·50	–44·50	3.652E+05	9.98E–01	7.31E–03	1.76E–03	9.07E–03

Table B.10. Helium production and DPA data in the flange at height −62.3 mm in case R550 without shield

Radial interval	Axial interval	Radius [mm]	Height [mm]	Volume [mm^3]	He-prod appm	DPA-ni disp/atom	DPA-fe disp/atom	DPA-sum disp/atom
69	172	307·50	−62·30	1.720E+05	1.88E−02	1.65E−03	3.31E−05	1.69E−03
70	172	312·50	−62·30	1.748E+05	1.53E−02	1.57E−03	2.70E−05	1.59E−03
71	172	319·50	−62·30	3.216E+05	1.34E−02	1.50E−03	2.36E−05	1.53E−03
72	172	328·50	−62·30	3.307E+05	1.16E−02	1.45E−03	2.04E−05	1.47E−03
73	172	337·50	−62·30	3.397E+05	1.25E−02	1.46E−03	2.21E−05	1.48E−03
74	172	346·50	−62·30	3.488E+05	1.28E−02	1.47E−03	2.25E−05	1.49E−03
75	172	355·50	−62·30	3.578E+05	1.42E−02	1.49E−03	2.50E−05	1.51E−03
76	172	364·50	−62·30	3.669E+05	1.56E−02	1.52E−03	2.76E−05	1.55E−03
77	172	373·50	−62·30	3.760E+05	1.73E−02	1.55E−03	3.06E−05	1.58E−03
78	172	382·50	−62·30	3.850E+05	2.02E−02	1.61E−03	3.55E−05	1.64E−03
79	172	391·50	−62·30	3.941E+05	2.13E−02	1.64E−03	3.75E−05	1.68E−03
80	172	397·50	−62·30	1.334E+05	2.45E−02	1.70E−03	4.31E−05	1.75E−03
81	172	402·00	−62·30	2.698E+05	2.27E−02	1.68E−03	3.99E−05	1.72E−03
82	172	408·00	−62·30	2.738E+05	2.76E−02	1.76E−03	4.87E−05	1.81E−03
83	172	414·88	−62·30	3.596E+05	2.37E−02	1.71E−03	4.18E−05	1.75E−03
84	172	422·62	−62·30	3.663E+05	3.07E−02	1.83E−03	5.42E−05	1.88E−03
85	172	430·38	−62·30	3.730E+05	2.89E−02	1.81E−03	5.10E−05	1.86E−03
86	172	438·12	−62·30	3.798E+05	3.88E−02	1.97E−03	6.83E−05	2.04E−03
87	172	445·50	−62·30	3.488E+05	4.26E−02	2.08E−03	7.51E−05	2.16E−03
88	172	452·50	−62·30	3.543E+05	5.74E−02	2.32E−03	1.01E−04	2.42E−03
89	172	459·50	−62·30	3.597E+05	7.70E−02	2.63E−03	1.36E−04	2.77E−03
90	172	466·50	−62·30	3.652E+05	1.37E−01	3.40E−03	2.41E−04	3.64E−03

Table B.11. Helium production and DPA data in the flange at height −80.10 mm in case R550 without shield

Radial interval	Axial interval	Radius [mm]	Height [mm]	Volume [mm^3]	He–prod appm	DPA-ni disp/atom	DPA-fe disp/atom	DPA-sum disp/atom
69	171	307·50	−80·10	1.720E+05	7.21E–03	1.16E–03	1.27E–05	1.17E–03
70	171	312·50	−80·10	1.748E+05	5.15E–03	1.06E–03	9.07E–06	1.07E–03
71	171	319·50	−80·10	3.216E+05	3.36E–03	9.60E–04	5.91E–06	9.66E–04
72	171	328·50	−80·10	3.307E+05	2.47E–03	8.85E–04	4.35E–06	8.89E–04
73	171	337·50	−80·10	3.397E+05	2.02E–03	8.45E–04	3.56E–06	8.49E–04
74	171	346·50	−80·10	3.488E+05	1.97E–03	8.28E–04	3.46E–06	8.32E–04
75	171	355·50	−80·10	3.578E+05	2.03E–03	8.27E–04	3.58E–06	8.30E–04
76	171	364·50	−80·10	3.669E+05	2.10E–03	8.17E–04	3.71E–06	8.21E–04
77	171	373·50	−80·10	3.760E+05	2.56E–03	8.45E–04	4.52E–06	8.49E–04
78	171	382·50	−80·10	3.850E+05	2.55E–03	8.44E–04	4.49E–06	8.49E–04
79	171	391·50	−80·10	3.941E+05	3.27E–03	8.75E–04	5.77E–06	8.81E–04
80	171	397·50	−80·10	1.334E+05	3.59E–03	8.94E–04	6.32E–06	9.00E–04
81	171	402·00	−80·10	2.698E+05	3.77E–03	9.08E–04	6.64E–06	9.15E–04
82	171	408·00	−80·10	2.738E+05	3.28E–03	8.97E–04	5.77E–06	9.02E–04
83	171	414·88	−80·10	3.596E+05	4.14E–03	9.34E–04	7.29E–06	9.41E–04
84	171	422·62	−80·10	3.663E+05	3.70E–03	9.34E–04	6.52E–06	9.41E–04
85	171	430·38	−80·10	3.730E+05	5.21E–03	1.01E–03	9.18E–06	1.02E–03
86	171	438·12	−80·10	3.798E+05	5.39E–03	1.04E–03	9.50E–06	1.05E–03
87	171	445·50	−80·10	3.488E+05	8.14E–03	1.18E–03	1.43E–05	1.19E–03
88	171	452·50	−80·10	3.543E+05	1.04E–02	1.30E–03	1.83E–05	1.32E–03
89	171	459·50	−80·10	3.597E+05	1.74E–02	1.56E–03	3.07E–05	1.59E–03
90	171	466·50	−80·10	3.652E+05	2.66E–02	1.97E–03	4.68E–05	2.01E–03

Table B.12. Helium production and DPA data in the PCSA/PCST at radius 270.0 mm for case R500 with restricted hafnium shield

Radial interval	Axial interval	Radius [mm]	Height [mm]	Volume [mm^3]	He-prod appm	DPA-ni disp/atom	DPA-fe disp/atom	DPA-sum disp/atom
63	157	270·00	−234·00	2.036E+05	1.18E−04	1.86E−04	2.08E−07	1.86E−04
63	158	270·00	−222·00	2.036E+05	4.00E−05	1.62E−04	7.05E−08	1.62E−04
63	159	270·00	−210·00	2.036E+05	3.10E−05	1.62E−04	5.46E−08	1.62E−04
63	160	270·00	−198·00	2.036E+05	4.24E−05	1.76E−04	7.47E−08	1.76E−04
63	161	270·00	−186·00	2.036E+05	1.05E−04	2.12E−04	1.85E−07	2.13E−04
63	162	270·00	−174·00	2.036E+05	3.43E−04	2.77E−04	6.05E−07	2.78E−04
63	163	270·00	−164·25	1.272E+05	8.29E−04	3.52E−04	1.46E−06	3.53E−04
63	164	270·00	−156·75	1.272E+05	1.35E−03	4.09E−04	2.38E−06	4.11E−04
63	165	270·00	−149·75	1.103E+05	1.92E−03	4.60E−04	3.38E−06	4.64E−04
63	166	270·00	−143·25	1.103E+05	2.66E−03	5.16E−04	4.68E−06	5.21E−04
63	167	270·00	−133·62	2.163E+05	3.59E−03	5.79E−04	6.33E−06	5.86E−04
63	168	270·00	−120·88	2.163E+05	4.69E−03	6.49E−04	8.27E−06	6.57E−04
63	169	270·00	−108·12	2.163E+05	5.69E−03	7.12E−04	1.00E−05	7.22E−04
63	170	270·00	−95·37	2.163E+05	6.89E−03	7.88E−04	1.21E−05	8.00E−04
63	171	270·00	−80·10	3.020E+05	8.64E−03	8.95E−04	1.52E−05	9.10E−04
63	172	270·00	−62·30	3.020E+05	1.17E−02	1.05E−03	2.05E−05	1.07E−03
63	173	270·00	−44·50	3.020E+05	1.68E−02	1.25E−03	2.96E−05	1.28E−03
63	174	270·00	−26·70	3.020E+05	2.64E−02	1.52E−03	4.66E−05	1.57E−03
63	175	270·00	−8·90	3.020E+05	4.40E−02	1.88E−03	7.75E−05	1.96E−03
63	176	270·00	7·00	2.375E+05	6.75E−02	2.25E−03	1.19E−04	2.37E−03
63	177	270·00	21·00	2.375E+05	8.97E−02	2.54E−03	1.58E−04	2.70E−03
63	178	270·00	38·75	3.647E+05	1.15E−01	2.86E−03	2.03E−04	3.06E−03
63	179	270·00	60·25	3.647E+05	1.38E−01	3.18E−03	2.42E−04	3.42E−03
63	180	270·00	81·75	3.647E+05	1.56E−01	3.49E−03	2.75E−04	3.76E−03
63	181	270·00	103·25	3.647E+05	1.64E−01	3.71E−03	2.89E−04	4.00E−03
63	182	270·00	124·17	3.449E+05	1.80E−01	4.07E−03	3.17E−04	4.39E−03
63	183	270·00	144·50	3.449E+05	2.08E−01	4.67E−03	3.66E−04	5.03E−03
63	184	270·00	164·83	3.449E+05	3.23E−01	6.14E−03	5.69E−04	6.71E−03

Table B.13. Helium production and DPA data in the PCSA/PCST at radius 280.0 mm for case R500 with restricted hafnium shield

Radial interval	Axial interval	Radius [mm]	Height [mm]	Volume [mm^3]	He–prod appm	DPA-ni disp/atom	DPA-fe disp/atom	DPA-sum disp/atom
64	157	280·00	−234·00	2.111E+05	5.80E–05	1.68E–04	1.02E–07	1.68E–04
64	158	280·00	−222·00	2.111E+05	1.80E–05	1.49E–04	3.18E–08	1.49E–04
64	159	280·00	−210·00	2.111E+05	1.25E–05	1.47E–04	2.21E–08	1.47E–04
64	160	280·00	−198·00	2.111E+05	1.77E–05	1.53E–04	3.11E–08	1.53E–04
64	161	280·00	−186·00	2.111E+05	4.06E–05	1.71E–04	7.16E–08	1.71E–04
64	162	280·00	−174·00	2.111E+05	1.00E–04	1.98E–04	1.77E–07	1.98E–04
64	163	280·00	−164·25	1.319E+05	1.93E–04	2.27E–04	3.41E–07	2.28E–04
64	164	280·00	−156·75	1.319E+05	2.94E–04	2.55E–04	5.18E–07	2.56E–04
64	165	280·00	−149·75	1.144E+05	4.31E–04	2.87E–04	7.59E–07	2.88E–04
64	166	280·00	−143·25	1.144E+05	5.44E–04	3.12E–04	9.58E–07	3.13E–04
64	167	280·00	−133·62	2.243E+05	7.23E–04	3.45E–04	1.27E–06	3.46E–04
64	168	280·00	−120·88	2.243E+05	9.82E–04	3.86E–04	1.73E–06	3.88E–04
64	169	280·00	−108·12	2.243E+05	1.22E–03	4.29E–04	2.16E–06	4.31E–04
64	170	280·00	−95·37	2.243E+05	1.47E–03	4.80E–04	2.59E–06	4.83E–04
64	171	280·00	−80·10	3.132E+05	1.93E–03	5.58E–04	3.40E–06	5.61E–04
64	172	280·00	−62·30	3.132E+05	2.85E–03	6.78E–04	5.02E–06	6.83E–04
64	173	280·00	−44·50	3.132E+05	5.22E–03	8.65E–04	9.19E–06	8.74E–04
64	174	280·00	−26·70	3.132E+05	1.25E–02	1.17E–03	2.21E–05	1.20E–03
64	175	280·00	−8·90	3.132E+05	3.47E–02	1.69E–03	6.11E–05	1.75E–03
64	176	280·00	7·00	2.463E+05	7.50E–02	2.26E–03	1.32E–04	2.39E–03
64	177	280·00	21·00	2.463E+05	1.14E–01	2.68E–03	2.02E–04	2.88E–03
64	178	280·00	38·75	3.782E+05	1.45E–01	3.00E–03	2.56E–04	3.26E–03
64	179	280·00	60·25	3.782E+05	1.52E–01	3.18E–03	2.67E–04	3.45E–03
64	180	280·00	81·75	3.782E+05	1.33E–01	3.21E–03	2.35E–04	3.44E–03
64	181	280·00	103·25	3.782E+05	8.88E–02	2.99E–03	1.56E–04	3.15E–03
64	182	280·00	124·17	3.577E+05	4.32E–02	2.73E–03	7.62E–05	2.81E–03
64	183	280·00	144·50	3.577E+05	3.51E–02	3.10E–03	6.18E–05	3.16E–03
64	184	280·00	164·83	3.577E+05	8.64E–02	4.65E–03	1.52E–04	4.81E–03

Table B.14. Helium production and DPA data in the PCSA/PCST at radius 286.5 mm for case R500 with restricted hafnium shield

Radial interval	Axial interval	Radius [mm]	Height [mm]	Volume [mm^3]	He–prod appm	DPA-ni disp/atom	DPA-fe disp/atom	DPA-sum disp/atom
65	144	286·50	−411·70	1.220E+05	9.01E–05	1.52E–04	1.59E–07	1.52E–04
65	145	286·50	−389·10	1.220E+05	1.11E–04	1.67E–04	1.96E–07	1.67E–04
65	146	286·50	−366·50	1.220E+05	1.40E–04	1.84E–04	2.47E–07	1.84E–04
65	147	286·50	−343·90	1.220E+05	1.67E–04	2.02E–04	2.95E–07	2.02E–04
65	148	286·50	−321·30	1.220E+05	1.94E–04	2.14E–04	3.42E–07	2.14E–04
65	149	286·50	−304·50	5.940E+04	2.08E–04	2.24E–04	3.67E–07	2.24E–04
65	150	286·50	−293·50	5.940E+04	2.10E–04	2.27E–04	3.69E–07	2.28E–04
65	150	286·50	−293·50	5.940E+04	2.10E–04	2.27E–04	3.69E–07	2.28E–04
65	151	286·50	−284·12	4.185E+04	2.06E–04	2.25E–04	3.64E–07	2.26E–04
65	152	286·50	−276·38	4.185E+04	1.95E–04	2.24E–04	3.43E–07	2.24E–04
65	153	286·50	−268·62	4.185E+04	1.79E–04	2.19E–04	3.16E–07	2.19E–04
65	154	286·50	−260·88	4.185E+04	1.57E–04	2.08E–04	2.76E–07	2.08E–04
65	155	286·50	−252·75	4.590E+04	1.24E–04	1.93E–04	2.18E–07	1.94E–04
65	156	286·50	−244·25	4.590E+04	8.16E–05	1.78E–04	1.44E–07	1.79E–04
65	157	286·50	−234·00	6.480E+04	3.28E–05	1.59E–04	5.78E–08	1.59E–04
65	158	286·50	−222·00	6.480E+04	1.17E–05	1.46E–04	2.05E–08	1.46E–04
65	159	286·50	−210·00	6.480E+04	7.23E–06	1.43E–04	1.27E–08	1.43E–04
65	160	286·50	−198·00	6.480E+04	1.09E–05	1.46E–04	1.93E–08	1.46E–04
65	161	286·50	−186·00	6.480E+04	1.93E–05	1.51E–04	3.40E–08	1.51E–04
65	162	286·50	−174·00	6.480E+04	4.37E–05	1.66E–04	7.69E–08	1.66E–04
65	163	286·50	−164·25	4.050E+04	7.61E–05	1.85E–04	1.34E–07	1.85E–04
65	164	286·50	−156·75	4.050E+04	1.15E–04	2.05E–04	2.02E–07	2.05E–04
65	165	286·50	−149·75	3.510E+04	1.56E–04	2.26E–04	2.74E–07	2.27E–04
65	166	286·50	−143·25	3.510E+04	1.98E–04	2.45E–04	3.49E–07	2.45E–04
65	167	286·50	−133·62	6.885E+04	2.60E–04	2.67E–04	4.58E–07	2.67E–04
65	168	286·50	−120·88	6.885E+04	3.39E–04	2.94E–04	5.97E–07	2.94E–04
65	169	286·50	−108·12	6.885E+04	4.32E–04	3.28E–04	7.62E–07	3.29E–04
65	170	286·50	−95·37	6.885E+04	5.39E–04	3.70E–04	9.50E–07	3.71E–04
65	171	286·50	−80·10	9.613E+04	7.14E–04	4.37E–04	1.26E–06	4.38E–04
65	172	286·50	−62·30	9.613E+04	1.26E–03	5.55E–04	2.22E–06	5.57E–04
65	173	286·50	−44·50	9.613E+04	3.01E–03	7.46E–04	5.30E–06	7.51E–04
65	174	286·50	−26·70	9.613E+04	1.10E–02	1.12E–03	1.94E–05	1.14E–03
65	175	286·50	−8·90	9.613E+04	4.47E–02	1.82E–03	7.87E–05	1.90E–03
65	176	286·50	7·00	7.561E+04	1.17E–01	2.62E–03	2.07E–04	2.83E–03
65	177	286·50	21·00	7.561E+04	1.88E–01	3.19E–03	3.32E–04	3.53E–03
65	178	286·50	38·75	1.161E+05	2.40E–01	3.59E–03	4.23E–04	4.01E–03
65	179	286·50	60·25	1.161E+05	2.36E–01	3.70E–03	4.16E–04	4.12E–03
65	180	286·50	81·75	1.161E+05	1.86E–01	3.56E–03	3.28E–04	3.89E–03
65	181	286·50	103·25	1.161E+05	9.75E–02	3.06E–03	1.72E–04	3.23E–03
65	182	286·50	124·17	1.098E+05	1.25E–02	2.19E–03	2.20E–05	2.21E–03
65	183	286·50	144·50	1.098E+05	8.42E–03	2.71E–03	1.48E–05	2.73E–03
65	184	286·50	164·83	1.098E+05	2.97E–02	4.18E–03	5.23E–05	4.23E–03

Table B.15. Helium production and DPA data in the PCSA/PCST at radius 289.5 mm for case R500 with restricted hafnium shield

Radial interval	Axial interval	Radius [mm]	Height [mm]	Volume [mm^3]	He–prod appm	DPA-ni disp/atom	DPA-fe disp/atom	DPA-sum disp/atom
66	144	289·50	−411·70	1.233E+05	5.50E–05	1.36E–04	9.68E–08	1.36E–04
66	145	289·50	−389·10	1.233E+05	7.00E–05	1.53E–04	1.23E–07	1.53E–04
66	146	289·50	−366·50	1.233E+05	8.61E–05	1.66E–04	1.52E–07	1.67E–04
66	147	289·50	−343·90	1.233E+05	1.05E–04	1.83E–04	1.84E–07	1.84E–04
66	148	289·50	−321·30	1.233E+05	1.20E–04	1.93E–04	2.11E–07	1.93E–04
66	149	289·50	−304·50	6.003E+04	1.29E–04	2.00E–04	2.27E–07	2.00E–04
66	150	289·50	−293·50	6.003E+04	1.29E–04	2.08E–04	2.28E–07	2.08E–04
66	150	289·50	−293·50	6.003E+04	1.29E–04	2.08E–04	2.28E–07	2.08E–04
66	151	289·50	−284·12	4.229E+04	1.28E–04	2.06E–04	2.25E–07	2.07E–04
66	152	289·50	−276·38	4.229E+04	1.20E–04	2.05E–04	2.11E–07	2.05E–04
66	153	289·50	−268·62	4.229E+04	1.10E–04	2.02E–04	1.94E–07	2.02E–04
66	154	289·50	−260·88	4.229E+04	9.75E–05	1.94E–04	1.72E–07	1.94E–04
66	155	289·50	−252·75	4.638E+04	7.57E–05	1.82E–04	1.33E–07	1.82E–04
66	156	289·50	−244·25	4.638E+04	5.04E–05	1.68E–04	8.87E–08	1.68E–04
66	157	289·50	−234·00	6.548E+04	2.38E–05	1.56E–04	4.20E–08	1.56E–04
66	158	289·50	−222·00	6.548E+04	9.55E–06	1.47E–04	1.68E–08	1.47E–04
66	159	289·50	−210·00	6.548E+04	6.27E–06	1.44E–04	1.11E–08	1.44E–04
66	160	289·50	−198·00	6.548E+04	8.07E–06	1.44E–04	1.42E–08	1.44E–04
66	161	289·50	−186·00	6.548E+04	1.52E–05	1.46E–04	2.68E–08	1.46E–04
66	162	289·50	−174·00	6.548E+04	3.09E–05	1.57E–04	5.45E–08	1.57E–04
66	163	289·50	−164·25	4.093E+04	5.51E–05	1.74E–04	9.70E–08	1.74E–04
66	164	289·50	−156·75	4.093E+04	7.70E–05	1.90E–04	1.36E–07	1.90E–04
66	165	289·50	−149·75	3.547E+04	1.09E–04	2.09E–04	1.91E–07	2.10E–04
66	166	289·50	−143·25	3.547E+04	1.37E–04	2.28E–04	2.42E–07	2.28E–04
66	167	289·50	−133·62	6.958E+04	1.79E–04	2.46E–04	3.16E–07	2.46E–04
66	168	289·50	−120·88	6.958E+04	2.37E–04	2.70E–04	4.17E–07	2.70E–04
66	169	289·50	−108·12	6.958E+04	3.02E–04	3.01E–04	5.31E–07	3.02E–04
66	170	289·50	−95·37	6.958E+04	3.74E–04	3.38E–04	6.60E–07	3.38E–04
66	171	289·50	−80·10	9.713E+04	5.27E–04	4.07E–04	9.28E–07	4.08E–04
66	172	289·50	−62·30	9.713E+04	9.14E–04	5.21E–04	1.61E–06	5.22E–04
66	173	289·50	−44·50	9.713E+04	2.68E–03	7.20E–04	4.72E–06	7.25E–04
66	174	289·50	−26·70	9.713E+04	1.19E–02	1.14E–03	2.09E–05	1.16E–03
66	175	289·50	−8·90	9.713E+04	5.57E–02	1.96E–03	9.82E–05	2.05E–03
66	176	289·50	7·00	7.640E+04	1.63E–01	2.96E–03	2.87E–04	3.25E–03
66	177	289·50	21·00	7.640E+04	2.61E–01	3.63E–03	4.61E–04	4.09E–03
66	178	289·50	38·75	1.173E+05	3.38E–01	4.10E–03	5.95E–04	4.70E–03
66	179	289·50	60·25	1.173E+05	3.22E–01	4.16E–03	5.68E–04	4.73E–03
66	180	289·50	81·75	1.173E+05	2.52E–01	3.98E–03	4.44E–04	4.42E–03
66	181	289·50	103·25	1.173E+05	1.19E–01	3.24E–03	2.11E–04	3.45E–03

Table B.16. Helium production and DPA data in the PCSA/PCST at radius 294.5 mm for case R500 with restricted hafnium shield

Radial interval	Axial interval	Radius [mm]	Height [mm]	Volume [mm^3]	He–prod appm	DPA-ni disp/atom	DPA-fe disp/atom	DPA-sum disp/atom
67	144	294·50	−411·70	2.927E+05	3.03E–05	1.28E–04	5.35E–08	1.28E–04
67	145	294·50	−389·10	2.927E+05	3.84E–05	1.40E–04	6.76E–08	1.40E–04
67	146	294·50	−366·50	2.927E+05	4.76E–05	1.57E–04	8.38E–08	1.57E–04
67	147	294·50	−343·90	2.927E+05	5.72E–05	1.70E–04	1.01E–07	1.70E–04
67	148	294·50	−321·30	2.927E+05	6.58E–05	1.80E–04	1.16E–07	1.80E–04
67	149	294·50	−304·50	1.425E+05	6.99E–05	1.85E–04	1.23E–07	1.85E–04
67	150	294·50	−293·50	1.425E+05	7.08E–05	1.93E–04	1.25E–07	1.93E–04
67	150	294·50	−293·50	1.425E+05	7.08E–05	1.93E–04	1.25E–07	1.93E–04
67	151	294·50	−284·12	1.004E+05	6.85E–05	1.96E–04	1.21E–07	1.96E–04
67	152	294·50	−276·38	1.004E+05	6.48E–05	1.93E–04	1.14E–07	1.93E–04
67	153	294·50	−268·62	1.004E+05	5.99E–05	1.93E–04	1.06E–07	1.93E–04
67	154	294·50	−260·88	1.004E+05	5.19E–05	1.87E–04	9.15E–08	1.88E–04
67	155	294·50	−252·75	1.101E+05	4.08E–05	1.78E–04	7.18E–08	1.78E–04
67	156	294·50	−244·25	1.101E+05	2.81E–05	1.68E–04	4.95E–08	1.68E–04
67	157	294·50	−234·00	1.554E+05	1.49E–05	1.58E–04	2.62E–08	1.58E–04
67	158	294·50	−222·00	1.554E+05	7.06E–06	1.52E–04	1.24E–08	1.52E–04
67	159	294·50	−210·00	1.554E+05	4.88E–06	1.49E–04	8.60E–09	1.49E–04
67	160	294·50	−198·00	1.554E+05	5.97E–06	1.45E–04	1.05E–08	1.45E–04
67	161	294·50	−186·00	1.554E+05	1.04E–05	1.45E–04	1.82E–08	1.45E–04
67	162	294·50	−174·00	1.554E+05	2.05E–05	1.51E–04	3.61E–08	1.51E–04
67	163	294·50	−164·25	9.715E+04	3.34E–05	1.62E–04	5.88E–08	1.62E–04
67	164	294·50	−156·75	9.715E+04	4.82E–05	1.77E–04	8.48E–08	1.77E–04
67	165	294·50	−149·75	8.419E+04	6.47E–05	1.92E–04	1.14E–07	1.93E–04
67	167	294·50	−133·62	1.651E+05	1.07E–04	2.23E–04	1.88E–07	2.23E–04
67	167	294·50	−133·62	1.651E+05	1.07E–04	2.23E–04	1.88E–07	2.23E–04
67	168	294·50	−120·88	1.651E+05	1.44E–04	2.43E–04	2.54E–07	2.43E–04
67	169	294·50	−108·12	1.651E+05	1.85E–04	2.65E–04	3.26E–07	2.65E–04
67	170	294·50	−95·37	1.651E+05	2.23E–04	3.00E–04	3.92E–07	3.01E–04
67	171	294·50	−80·10	2.306E+05	3.14E–04	3.67E–04	5.53E–07	3.68E–04
67	172	294·50	−62·30	2.306E+05	6.57E–04	4.83E–04	1.16E–06	4.84E–04
67	173	294·50	−44·50	2.306E+05	2.24E–03	6.93E–04	3.95E–06	6.97E–04
67	174	294·50	−26·70	2.306E+05	1.37E–02	1.18E–03	2.41E–05	1.21E–03
67	175	294·50	−8·90	2.306E+05	9.02E–02	2.31E–03	1.59E–04	2.47E–03
67	176	294·50	7·00	1.813E+05	3.17E–01	3.87E–03	5.58E–04	4.43E–03
67	177	294·50	21·00	1.813E+05	5.14E–01	4.79E–03	9.06E–04	5.70E–03
67	178	294·50	38·75	2.785E+05	6.66E–01	5.43E–03	1.17E–03	6.60E–03
67	179	294·50	60·25	2.785E+05	6.22E–01	5.41E–03	1.10E–03	6.51E–03
67	180	294·50	81·75	2.785E+05	4.69E–01	5.03E–03	8.27E–04	5.86E–03
67	181	294·50	103·25	2.785E+05	2.18E–01	3.94E–03	3.84E–04	4.33E–03

Table B.17. Helium production and DPA data in the PCSA/PCST at radius 301.5 mm for case R500 with restricted hafnium shield

Radial interval	Axial interval	Radius [mm]	Height [mm]	Volume [mm^3]	He-prod appm	DPA-ni disp/atom	DPA-fe disp/atom	DPA-sum disp/atom
68	144	301·50	−411·70	2.997E+05	1.68E−05	1.31E−04	2.96E−08	1.31E−04
68	145	301·50	−389·10	2.997E+05	2.11E−05	1.46E−04	3.72E−08	1.46E−04
68	146	301·50	−366·50	2.997E+05	2.60E−05	1.60E−04	4.58E−08	1.60E−04
68	147	301·50	−343·90	2.997E+05	3.12E−05	1.77E−04	5.50E−08	1.77E−04
68	148	301·50	−321·30	2.997E+05	3.56E−05	1.86E−04	6.28E−08	1.86E−04
68	149	301·50	−304·50	1.459E+05	3.82E−05	1.92E−04	6.73E−08	1.92E−04
68	150	301·50	−293·50	1.459E+05	3.81E−05	1.96E−04	6.71E−08	1.96E−04
68	150	301·50	−293·50	1.459E+05	3.81E−05	1.96E−04	6.71E−08	1.96E−04
68	151	301·50	−284·12	1.028E+05	3.71E−05	2.02E−04	6.54E−08	2.02E−04
68	152	301·50	−276·38	1.028E+05	3.50E−05	2.03E−04	6.17E−08	2.03E−04
68	153	301·50	−268·62	1.028E+05	3.18E−05	2.00E−04	5.61E−08	2.00E−04
68	154	301·50	−260·88	1.028E+05	2.78E−05	1.99E−04	4.90E−08	1.99E−04
68	155	301·50	−252·75	1.127E+05	2.20E−05	1.91E−04	3.87E−08	1.91E−04
68	156	301·50	−244·25	1.127E+05	1.58E−05	1.81E−04	2.79E−08	1.82E−04
68	157	301·50	−234·00	1.591E+05	9.81E−06	1.75E−04	1.73E−08	1.75E−04
68	158	301·50	−222·00	1.591E+05	5.60E−06	1.69E−04	9.86E−09	1.69E−04
68	159	301·50	−210·00	1.591E+05	4.21E−06	1.63E−04	7.42E−09	1.63E−04
68	160	301·50	−198·00	1.591E+05	4.85E−06	1.57E−04	8.55E−09	1.57E−04
68	161	301·50	−186·00	1.591E+05	7.94E−06	1.53E−04	1.40E−08	1.53E−04
68	162	301·50	−174·00	1.591E+05	1.40E−05	1.54E−04	2.47E−08	1.55E−04
68	163	301·50	−164·25	9.946E+04	2.22E−05	1.61E−04	3.91E−08	1.61E−04
68	164	301·50	−156·75	9.945E+04	3.11E−05	1.72E−04	5.48E−08	1.72E−04
68	165	301·50	−149·75	8.619E+04	4.15E−05	1.85E−04	7.31E−08	1.85E−04
68	166	301·50	−143·25	8.619E+04	5.14E−05	1.97E−04	9.06E−08	1.97E−04
68	167	301·50	−133·62	1.691E+05	6.65E−05	2.09E−04	1.17E−07	2.09E−04
68	168	301·50	−120·88	1.691E+05	9.13E−05	2.19E−04	1.61E−07	2.20E−04
68	169	301·50	−108·12	1.691E+05	1.14E−04	2.34E−04	2.02E−07	2.34E−04
68	170	301·50	−95·37	1.691E+05	1.31E−04	2.63E−04	2.32E−07	2.63E−04
68	171	301·50	−80·10	2.360E+05	1.69E−04	3.26E−04	2.98E−07	3.27E−04
68	172	301·50	−62·30	2.360E+05	4.26E−04	4.47E−04	7.51E−07	4.48E−04
68	173	301·50	−44·50	2.360E+05	2.14E−03	6.81E−04	3.78E−06	6.84E−04
68	174	301·50	−26·70	2.360E+05	1.64E−02	1.24E−03	2.89E−05	1.27E−03
68	175	301·50	−8·90	2.360E+05	1.63E−01	2.91E−03	2.88E−04	3.20E−03
68	176	301·50	7·00	1.856E+05	8.34E−01	5.87E−03	1.47E−03	7.34E−03
68	177	301·50	21·00	1.856E+05	1.25E+00	7.08E−03	2.20E−03	9.29E−03
68	178	301·50	38·75	2.851E+05	1.59E+00	7.98E−03	2.80E−03	1.08E−02
68	179	301·50	60·25	2.851E+05	1.48E+00	7.89E−03	2.60E−03	1.05E−02
68	180	301·50	81·75	2.851E+05	1.08E+00	7.09E−03	1.90E−03	8.99E−03
68	181	301·50	103·25	2.851E+05	5.76E−01	5.68E−03	1.01E−03	6.69E−03

Table B.18. Helium production and DPA data in the flange at height −8.9 mm for case R500 with restricted hafnium shield

Radial interval	Axial interval	Radius [mm]	Height [mm]	Volume [mm^3]	He–prod appm	DPA-ni disp/atom	DPA-fe disp/atom	DPA-sum disp/atom
69	175	307·50	−8·90	1.720E+05	2.38E–01	3.40E–03	4.18E–04	3.82E–03
70	175	312·50	−8·90	1.748E+05	2.95E–01	3.72E–03	5.20E–04	4.24E–03
71	175	319·50	−8·90	3.216E+05	3.65E–01	4.08E–03	6.42E–04	4.72E–03
72	175	328·50	−8·90	3.307E+05	4.62E–01	4.52E–03	8.13E–04	5.33E–03
73	175	337·50	−8·90	3.397E+05	5.76E–01	5.00E–03	1.01E–03	6.01E–03
74	175	346·50	−8·90	3.488E+05	7.23E–01	5.54E–03	1.27E–03	6.81E–03
75	175	355·50	−8·90	3.578E+05	9.14E–01	6.16E–03	1.61E–03	7.77E–03
76	175	364·50	−8·90	3.669E+05	1.15E+00	6.82E–03	2.02E–03	8.83E–03
77	175	373·50	−8·90	3.760E+05	1.43E+00	7.55E–03	2.52E–03	1.01E–02
78	175	382·50	−8·90	3.850E+05	1.77E+00	8.33E–03	3.12E–03	1.14E–02
79	175	391·50	−8·90	3.941E+05	2.17E+00	9.17E–03	3.82E–03	1.30E–02
80	175	397·50	−8·90	1.334E+05	2.47E+00	9.77E–03	4.35E–03	1.41E–02
81	175	402·00	−8·90	2.698E+05	2.68E+00	1.03E–02	4.72E–03	1.50E–02
82	175	408·00	−8·90	2.738E+05	3.16E+00	1.11E–02	5.57E–03	1.67E–02
83	175	414·88	−8·90	3.596E+05	3.74E+00	1.21E–02	6.59E–03	1.87E–02
84	175	422·62	−8·90	3.663E+05	4.74E+00	1.35E–02	8.36E–03	2.18E–02
85	175	430·38	−8·90	3.730E+05	5.65E+00	1.47E–02	9.96E–03	2.47E–02
86	175	438·12	−8·90	3.798E+05	6.41E+00	1.57E–02	1.13E–02	2.70E–02
87	175	445·50	−8·90	3.488E+05	7.84E+00	1.74E–02	1.38E–02	3.12E–02
88	175	452·50	−8·90	3.543E+05	9.79E+00	1.94E–02	1.73E–02	3.66E–02
89	175	459·50	−8·90	3.597E+05	1.25E+01	2.19E–02	2.21E–02	4.40E–02
90	175	466·50	−8·90	3.652E+05	1.65E+01	2.55E–02	2.91E–02	5.47E–02

Table B.19. Helium production and DPA data in the flange at height −26.7 mm for case R500 with restricted hafnium shield

Radial interval	Axial interval	Radius [mm]	Height [mm]	Volume [mm^3]	He–prod appm	DPA-ni disp/atom	DPA-fe disp/atom	DPA-sum disp/atom
69	174	307·50	−26·70	1.720E+05	2.02E–02	1.32E–03	3.55E–05	1.36E–03
70	174	312·50	−26·70	1.748E+05	2.37E–02	1.40E–03	4.17E–05	1.44E–03
71	174	319·50	−26·70	3.216E+05	2.99E–02	1.51E–03	5.26E–05	1.56E–03
72	174	328·50	−26·70	3.307E+05	3.92E–02	1.66E–03	6.91E–05	1.73E–03
73	174	337·50	−26·70	3.397E+05	5.00E–02	1.82E–03	8.80E–05	1.91E–03
74	174	346·50	−26·70	3.488E+05	6.41E–02	2.01E–03	1.13E–04	2.12E–03
75	174	355·50	−26·70	3.578E+05	8.14E–02	2.20E–03	1.43E–04	2.35E–03
76	174	364·50	−26·70	3.669E+05	1.04E–01	2.42E–03	1.83E–04	2.60E–03
77	174	373·50	−26·70	3.760E+05	1.29E–01	2.65E–03	2.27E–04	2.88E–03
78	174	382·50	−26·70	3.850E+05	1.61E–01	2.91E–03	2.84E–04	3.19E–03
79	174	391·50	−26·70	3.941E+05	2.07E–01	3.24E–03	3.65E–04	3.60E–03
80	174	397·50	−26·70	1.334E+05	2.41E–01	3.44E–03	4.25E–04	3.87E–03
81	174	402·00	−26·70	2.698E+05	2.79E–01	3.66E–03	4.92E–04	4.15E–03
82	174	408·00	−26·70	2.738E+05	3.14E–01	3.86E–03	5.53E–04	4.41E–03
83	174	414·88	−26·70	3.596E+05	3.87E–01	4.20E–03	6.81E–04	4.88E–03
84	174	422·62	−26·70	3.663E+05	4.69E–01	4.57E–03	8.26E–04	5.40E–03
85	174	430·38	−26·70	3.730E+05	5.29E–01	4.88E–03	9.31E–04	5.81E–03
86	174	438·12	−26·70	3.798E+05	6.71E–01	5.44E–03	1.18E–03	6.63E–03
87	174	445·50	−26·70	3.488E+05	8.16E–01	5.94E–03	1.44E–03	7.38E–03
88	174	452·50	−26·70	3.543E+05	1.05E+00	6.66E–03	1.84E–03	8.50E–03
89	174	459·50	−26·70	3.597E+05	1.31E+00	7.44E–03	2.30E–03	9.74E–03
90	174	466·50	−26·70	3.652E+05	1.68E+00	8.60E–03	2.96E–03	1.16E–02

Table B.20. Helium production and DPA data in the flange at height −44.5 mm for case R500 with restricted hafnium shield

Radial interval	Axial interval	Radius [mm]	Height [mm]	Volume [mm^3]	He-prod appm	DPA-ni disp/atom	DPA-fe disp/atom	DPA-sum disp/atom
69	173	307·50	−44·50	1.720E+05	2.16E−03	6.81E−04	3.80E−06	6.85E−04
70	173	312·50	−44·50	1.748E+05	2.29E−03	6.88E−04	4.04E−06	6.92E−04
71	173	319·50	−44·50	3.216E+05	2.74E−03	7.17E−04	4.83E−06	7.22E−04
72	173	328·50	−44·50	3.307E+05	3.37E−03	7.53E−04	5.94E−06	7.59E−04
73	173	337·50	−44·50	3.397E+05	4.39E−03	8.04E−04	7.73E−06	8.12E−04
74	173	346·50	−44·50	3.488E+05	5.54E−03	8.63E−04	9.76E−06	8.72E−04
75	173	355·50	−44·50	3.578E+05	7.00E−03	9.27E−04	1.23E−05	9.39E−04
76	173	364·50	−44·50	3.669E+05	8.87E−03	1.00E−03	1.56E−05	1.02E−03
77	173	373·50	−44·50	3.760E+05	1.11E−02	1.07E−03	1.96E−05	1.09E−03
78	173	382·50	−44·50	3.850E+05	1.47E−02	1.18E−03	2.58E−05	1.21E−03
79	173	391·50	−44·50	3.941E+05	1.88E−02	1.28E−03	3.31E−05	1.31E−03
80	173	397·50	−44·50	1.334E+05	2.35E−02	1.36E−03	4.14E−05	1.41E−03
81	173	402·00	−44·50	2.698E+05	2.51E−02	1.42E−03	4.43E−05	1.46E−03
82	173	408·00	−44·50	2.738E+05	2.93E−02	1.50E−03	5.17E−05	1.55E−03
83	173	414·88	−44·50	3.596E+05	3.53E−02	1.60E−03	6.22E−05	1.66E−03
84	173	422·62	−44·50	3.663E+05	3.81E−02	1.68E−03	6.71E−05	1.75E−03
85	173	430·38	−44·50	3.730E+05	5.29E−02	1.92E−03	9.32E−05	2.01E−03
86	173	438·12	−44·50	3.798E+05	6.46E−02	2.09E−03	1.14E−04	2.20E−03
87	173	445·50	−44·50	3.488E+05	8.44E−02	2.32E−03	1.49E−04	2.47E−03
88	173	452·50	−44·50	3.543E+05	1.10E−01	2.61E−03	1.94E−04	2.81E−03
89	173	459·50	−44·50	3.597E+05	1.46E−01	2.99E−03	2.58E−04	3.25E−03
90	173	466·50	−44·50	3.652E+05	2.73E−01	4.02E−03	4.80E−04	4.50E−03

Table B.21. Helium production and DPA data in the flange at height -62.3 mm for case R500 with restricted hafnium shield

Radial interval	Axial interval	Radius [mm]	Height [mm]	Volume [mm^3]	He-prod appm	DPA-ni disp/atom	DPA-fe disp/atom	DPA-sum disp/atom
69	172	307·50	−62·30	1.720E+05	3.39E−04	4.31E−04	5.97E−07	4.32E−04
70	172	312·50	−62·30	1.748E+05	3.28E−04	4.26E−04	5.78E−07	4.27E−04
71	172	319·50	−62·30	3.216E+05	3.02E−04	4.21E−04	5.32E−07	4.21E−04
72	172	328·50	−62·30	3.307E+05	3.48E−04	4.26E−04	6.14E−07	4.26E−04
73	172	337·50	−62·30	3.397E+05	4.11E−04	4.37E−04	7.23E−07	4.38E−04
74	172	346·50	−62·30	3.488E+05	5.04E−04	4.50E−04	8.87E−07	4.51E−04
75	172	355·50	−62·30	3.578E+05	6.48E−04	4.80E−04	1.14E−06	4.81E−04
76	172	364·50	−62·30	3.669E+05	7.79E−04	4.99E−04	1.37E−06	5.01E−04
77	172	373·50	−62·30	3.760E+05	1.06E−03	5.38E−04	1.86E−06	5.40E−04
78	172	382·50	−62·30	3.850E+05	1.36E−03	5.69E−04	2.39E−06	5.71E−04
79	172	391·50	−62·30	3.941E+05	1.80E−03	6.05E−04	3.18E−06	6.08E−04
80	172	397·50	−62·30	1.334E+05	2.18E−03	6.43E−04	3.85E−06	6.47E−04
81	172	402·00	−62·30	2.698E+05	2.41E−03	6.66E−04	4.24E−06	6.70E−04
82	172	408·00	−62·30	2.738E+05	2.97E−03	7.03E−04	5.24E−06	7.08E−04
83	172	414·88	−62·30	3.596E+05	2.98E−03	7.21E−04	5.25E−06	7.27E−04
84	172	422·62	−62·30	3.663E+05	4.53E−03	8.21E−04	7.99E−06	8.29E−04
85	172	430·38	−62·30	3.730E+05	5.51E−03	8.89E−04	9.72E−06	8.98E−04
86	172	438·12	−62·30	3.798E+05	7.44E−03	9.81E−04	1.31E−05	9.94E−04
87	172	445·50	−62·30	3.488E+05	1.00E−02	1.10E−03	1.77E−05	1.12E−03
88	172	452·50	−62·30	3.543E+05	1.49E−02	1.28E−03	2.63E−05	1.31E−03
89	172	459·50	−62·30	3.597E+05	2.55E−02	1.59E−03	4.49E−05	1.63E−03
90	172	466·50	−62·30	3.652E+05	5.34E−02	2.18E−03	9.41E−05	2.28E−03

Table B.22. Helium production and DPA data in the flange at height −80.10 mm for case R500 with restricted hafnium shield

Radial interval	Axial interval	Radius [mm]	Height [mm]	Volume [mm^3]	He–prod appm	DPA-ni disp/atom	DPA-fe disp/atom	DPA-sum disp/atom
69	171	307·50	−80·10	1.720E+05	1.19E–04	3.03E–04	2.09E–07	3.03E–04
70	171	312·50	−80·10	1.748E+05	8.94E–05	2.91E–04	1.58E–07	2.91E–04
71	171	319·50	−80·10	3.216E+05	7.85E–05	2.79E–04	1.38E–07	2.79E–04
72	171	328·50	−80·10	3.307E+05	6.99E–05	2.73E–04	1.23E–07	2.73E–04
73	171	337·50	−80·10	3.397E+05	7.21E–05	2.68E–04	1.27E–07	2.68E–04
74	171	346·50	−80·10	3.488E+05	8.22E–05	2.75E–04	1.45E–07	2.75E–04
75	171	355·50	−80·10	3.578E+05	9.48E–05	2.82E–04	1.67E–07	2.82E–04
76	171	364·50	−80·10	3.669E+05	1.23E–04	2.95E–04	2.16E–07	2.95E–04
77	171	373·50	−80·10	3.760E+05	1.56E–04	3.09E–04	2.76E–07	3.10E–04
78	171	382·50	−80·10	3.850E+05	1.99E–04	3.21E–04	3.51E–07	3.21E–04
79	171	391·50	−80·10	3.941E+05	2.87E–04	3.48E–04	5.05E–07	3.48E–04
80	171	397·50	−80·10	1.334E+05	3.58E–04	3.72E–04	6.31E–07	3.72E–04
81	171	402·00	−80·10	2.698E+05	4.05E–04	3.80E–04	7.14E–07	3.80E–04
82	171	408·00	−80·10	2.738E+05	4.11E–04	3.90E–04	7.25E–07	3.90E–04
83	171	414·88	−80·10	3.596E+05	6.28E–04	4.30E–04	1.11E–06	4.31E–04
84	171	422·62	−80·10	3.663E+05	7.97E–04	4.73E–04	1.40E–06	4.74E–04
85	171	430·38	−80·10	3.730E+05	1.08E–03	5.22E–04	1.91E–06	5.24E–04
86	171	438·12	−80·10	3.798E+05	1.56E–03	5.90E–04	2.76E–06	5.93E–04
87	171	445·50	−80·10	3.488E+05	2.43E–03	6.85E–04	4.28E–06	6.90E–04
88	171	452·50	−80·10	3.543E+05	4.24E–03	8.30E–04	7.47E–06	8.37E–04
89	171	459·50	−80·10	3.597E+05	7.76E–03	1.05E–03	1.37E–05	1.06E–03
90	171	466·50	−80·10	3.652E+05	1.51E–02	1.42E–03	2.66E–05	1.45E–03

Table B.23. Helium production and DPA data in the PCSA/PCST at radius 270.0 mm for case R400 with extended boral shield

Radial interval	Axial interval	Radius [mm]	Height [mm]	Volume [mm^3]	He–prod appm	DPA-ni disp/atom	DPA-fe disp/atom	DPA-sum disp/atom
63	157	270·00	−234·00	2.036E+05	5.64E–05	8.44E–05	9.94E–08	8.45E–05
63	158	270·00	−222·00	2.036E+05	1.86E–05	7.04E–05	3.27E–08	7.05E–05
63	159	270·00	−210·00	2.036E+05	1.38E–05	7.27E–05	2.43E–08	7.27E–05
63	160	270·00	−198·00	2.036E+05	1.77E–05	8.29E–05	3.13E–08	8.29E–05
63	161	270·00	−186·00	2.036E+05	4.19E–05	1.05E–04	7.39E–08	1.05E–04
63	162	270·00	−174·00	2.036E+05	1.33E–04	1.43E–04	2.35E–07	1.43E–04
63	163	270·00	−164·25	1.272E+05	3.22E–04	1.87E–04	5.68E–07	1.88E–04
63	164	270·00	−156·75	1.272E+05	5.20E–04	2.20E–04	9.17E–07	2.21E–04
63	165	270·00	−149·75	1.103E+05	7.41E–04	2.49E–04	1.31E–06	2.50E–04
63	166	270·00	−143·25	1.103E+05	1.02E–03	2.80E–04	1.80E–06	2.82E–04
63	167	270·00	−133·62	2.163E+05	1.38E–03	3.17E–04	2.44E–06	3.20E–04
63	168	270·00	−120·88	2.163E+05	1.78E–03	3.55E–04	3.14E–06	3.58E–04
63	169	270·00	−108·12	2.163E+05	2.13E–03	3.87E–04	3.76E–06	3.91E–04
63	170	270·00	−95·37	2.163E+05	2.47E–03	4.19E–04	4.36E–06	4.23E–04
63	171	270·00	−80·10	3.020E+05	3.00E–03	4.65E–04	5.28E–06	4.71E–04
63	172	270·00	−62·30	3.020E+05	3.67E–03	5.21E–04	6.47E–06	5.27E–04
63	173	270·00	−44·50	3.020E+05	4.63E–03	5.87E–04	8.16E–06	5.95E–04
63	174	270·00	−26·70	3.020E+05	5.72E–03	6.56E–04	1.01E–05	6.66E–04
63	175	270·00	−8·90	3.020E+05	7.16E–03	7.32E–04	1.26E–05	7.44E–04
63	176	270·00	7·00	2.375E+05	8.48E–03	7.99E–04	1.49E–05	8.14E–04
63	177	270·00	21·00	2.375E+05	1.00E–02	8.71E–04	1.77E–05	8.89E–04
63	178	270·00	38·75	3.647E+05	1.22E–02	9.65E–04	2.15E–05	9.87E–04
63	179	270·00	60·25	3.647E+05	1.61E–02	1.11E–03	2.84E–05	1.14E–03
63	180	270·00	81·75	3.647E+05	2.15E–02	1.27E–03	3.78E–05	1.31E–03
63	181	270·00	103·25	3.647E+05	2.78E–02	1.45E–03	4.91E–05	1.49E–03
63	182	270·00	124·17	3.449E+05	3.66E–02	1.66E–03	6.45E–05	1.72E–03
63	183	270·00	144·50	3.449E+05	4.03E–02	1.80E–03	7.10E–05	1.87E–03
63	184	270·00	164·83	3.449E+05	1.91E–02	1.57E–03	3.36E–05	1.61E–03

Table B.24. Helium production and DPA data in the PCSA/PCST at radius 280.0 mm for case R400 with extended boral shield

Radial interval	Axial interval	Radius [mm]	Height [mm]	Volume [mm^3]	He–prod appm	DPA-ni disp/atom	DPA-fe disp/atom	DPA-sum disp/atom
64	157	280·00	−234·00	2.111E+05	2.75E–05	6.40E–05	4.85E–08	6.40E–05
64	158	280·00	−222·00	2.111E+05	8.26E–06	5.34E–05	1.45E–08	5.34E–05
64	159	280·00	−210·00	2.111E+05	5.37E–06	5.44E–05	9.45E–09	5.44E–05
64	160	280·00	−198·00	2.111E+05	7.17E–06	6.15E–05	1.26E–08	6.15E–05
64	161	280·00	−186·00	2.111E+05	1.58E–05	7.38E–05	2.78E–08	7.38E–05
64	162	280·00	−174·00	2.111E+05	3.91E–05	9.15E–05	6.89E–08	9.15E–05
64	163	280·00	−164·25	1.319E+05	7.38E–05	1.09E–04	1.30E–07	1.09E–04
64	164	280·00	−156·75	1.319E+05	1.14E–04	1.24E–04	2.01E–07	1.24E–04
64	165	280·00	−149·75	1.144E+05	1.65E–04	1.40E–04	2.90E–07	1.41E–04
64	166	280·00	−143·25	1.144E+05	2.12E–04	1.54E–04	3.73E–07	1.54E–04
64	167	280·00	−133·62	2.243E+05	2.77E–04	1.72E–04	4.87E–07	1.72E–04
64	168	280·00	−120·88	2.243E+05	3.75E–04	1.95E–04	6.60E–07	1.96E–04
64	169	280·00	−108·12	2.243E+05	4.49E–04	2.16E–04	7.91E–07	2.17E–04
64	170	280·00	−95·37	2.243E+05	5.29E–04	2.39E–04	9.32E–07	2.40E–04
64	171	280·00	−80·10	3.132E+05	6.26E–04	2.65E–04	1.10E–06	2.66E–04
64	172	280·00	−62·30	3.132E+05	7.88E–04	3.01E–04	1.39E–06	3.02E–04
64	173	280·00	−44·50	3.132E+05	9.67E–04	3.41E–04	1.70E–06	3.42E–04
64	174	280·00	−26·70	3.132E+05	1.23E–03	3.84E–04	2.16E–06	3.87E–04
64	175	280·00	−8·90	3.132E+05	1.51E–03	4.32E–04	2.66E–06	4.35E–04
64	176	280·00	7·00	2.463E+05	1.84E–03	4.80E–04	3.25E–06	4.83E–04
64	177	280·00	21·00	2.463E+05	2.14E–03	5.19E–04	3.78E–06	5.23E–04
64	178	280·00	38·75	3.782E+05	2.62E–03	5.80E–04	4.61E–06	5.84E–04
64	179	280·00	60·25	3.782E+05	3.54E–03	6.74E–04	6.24E–06	6.81E–04
64	180	280·00	81·75	3.782E+05	4.57E–03	7.72E–04	8.05E–06	7.80E–04
64	181	280·00	103·25	3.782E+05	6.51E–03	9.08E–04	1.15E–05	9.20E–04
64	182	280·00	124·17	3.577E+05	8.35E–03	1.04E–03	1.47E–05	1.05E–03
64	183	280·00	144·50	3.577E+05	8.40E–03	1.12E–03	1.48E–05	1.14E–03
64	184	280·00	164·83	3.577E+05	3.26E–03	1.08E–03	5.74E–06	1.09E–03

Table B.25. Helium production and DPA data in the PCSA/PCST at radius 286.5 mm for case R400 with extended boral shield

Radial interval	Axial interval	Radius [mm]	Height [mm]	Volume [mm^3]	He-prod appm	DPA-ni disp/atom	DPA-fe disp/atom	DPA-sum disp/atom
65	144	286·50	−411·70	1.220E+05	4.42E−05	6.11E−05	7.79E−08	6.12E−05
65	145	286·50	−389·10	1.220E+05	5.45E−05	6.71E−05	9.61E−08	6.71E−05
65	146	286·50	−366·50	1.220E+05	6.88E−05	7.44E−05	1.21E−07	7.45E−05
65	147	286·50	−343·90	1.220E+05	8.18E−05	8.05E−05	1.44E−07	8.06E−05
65	148	286·50	−321·30	1.220E+05	9.48E−05	8.57E−05	1.67E−07	8.58E−05
65	149	286·50	−304·50	5.940E+04	1.01E−04	8.72E−05	1.78E−07	8.73E−05
65	150	286·50	−293·50	5.940E+04	1.02E−04	8.71E−05	1.80E−07	8.72E−05
65	150	286·50	−293·50	5.940E+04	1.02E−04	8.71E−05	1.80E−07	8.72E−05
65	151	286·50	−284·12	4.185E+04	1.00E−04	8.62E−05	1.76E−07	8.64E−05
65	152	286·50	−276·38	4.185E+04	9.43E−05	8.45E−05	1.66E−07	8.46E−05
65	153	286·50	−268·62	4.185E+04	8.67E−05	8.20E−05	1.53E−07	8.21E−05
65	154	286·50	−260·88	4.185E+04	7.54E−05	7.81E−05	1.33E−07	7.83E−05
65	155	286·50	−252·75	4.590E+04	5.97E−05	7.27E−05	1.05E−07	7.28E−05
65	156	286·50	−244·25	4.590E+04	3.90E−05	6.40E−05	6.87E−08	6.41E−05
65	157	286·50	−234·00	6.480E+04	1.54E−05	5.17E−05	2.72E−08	5.18E−05
65	158	286·50	−222·00	6.480E+04	5.24E−06	4.47E−05	9.23E−09	4.47E−05
65	159	286·50	−210·00	6.480E+04	3.04E−06	4.54E−05	5.35E−09	4.54E−05
65	160	286·50	−198·00	6.480E+04	4.35E−06	5.08E−05	7.67E−09	5.08E−05
65	161	286·50	−186·00	6.480E+04	7.45E−06	5.81E−05	1.31E−08	5.81E−05
65	162	286·50	−174·00	6.480E+04	1.68E−05	6.95E−05	2.96E−08	6.96E−05
65	163	286·50	−164·25	4.050E+04	2.90E−05	8.07E−05	5.11E−08	8.07E−05
65	164	286·50	−156·75	4.050E+04	4.41E−05	9.13E−05	7.77E−08	9.14E−05
65	165	286·50	−149·75	3.510E+04	5.82E−05	1.01E−04	1.03E−07	1.01E−04
65	166	286·50	−143·25	3.510E+04	7.97E−05	1.11E−04	1.40E−07	1.11E−04
65	167	286·50	−133·62	6.885E+04	9.56E−05	1.21E−04	1.69E−07	1.21E−04
65	168	286·50	−120·88	6.885E+04	1.30E−04	1.38E−04	2.29E−07	1.38E−04
65	169	286·50	−108·12	6.885E+04	1.52E−04	1.55E−04	2.67E−07	1.55E−04
65	170	286·50	−95·37	6.885E+04	1.86E−04	1.73E−04	3.28E−07	1.73E−04
65	171	286·50	−80·10	9.613E+04	2.12E−04	1.93E−04	3.74E−07	1.93E−04
65	172	286·50	−62·30	9.613E+04	2.77E−04	2.26E−04	4.88E−07	2.26E−04
65	173	286·50	−44·50	9.613E+04	3.16E−04	2.53E−04	5.56E−07	2.54E−04
65	174	286·50	−26·70	9.613E+04	4.40E−04	2.94E−04	7.74E−07	2.94E−04
65	175	286·50	−8·90	9.613E+04	4.95E−04	3.29E−04	8.73E−07	3.30E−04
65	176	286·50	7·00	7.561E+04	6.76E−04	3.71E−04	1.19E−06	3.72E−04
65	177	286·50	21·00	7.561E+04	7.07E−04	3.93E−04	1.25E−06	3.94E−04
65	178	286·50	38·75	1.161E+05	9.95E−04	4.53E−04	1.75E−06	4.54E−04
65	179	286·50	60·25	1.161E+05	1.20E−03	5.15E−04	2.11E−06	5.17E−04
65	180	286·50	81·75	1.161E+05	1.71E−03	6.11E−04	3.01E−06	6.14E−04
65	181	286·50	103·25	1.161E+05	2.40E−03	7.30E−04	4.22E−06	7.34E−04
65	182	286·50	124·17	1.098E+05	3.17E−03	8.46E−04	5.59E−06	8.51E−04
65	183	286·50	144·50	1.098E+05	2.81E−03	9.27E−04	4.95E−06	9.32E−04
65	184	286·50	164·83	1.098E+05	1.05E−03	9.57E−04	1.85E−06	9.59E−04

Table B.26. Helium production and DPA data in the PCSA/PCST at radius 289.5 mm for case R400 with extended boral shield

Radial interval	Axial interval	Radius [mm]	Height [mm]	Volume [mm^3]	He-prod appm	DPA-ni disp/atom	DPA-fe disp/atom	DPA-sum disp/atom
66	144	289·50	−411·70	1.233E+05	2.69E−05	5.02E−05	4.74E−08	5.02E−05
66	145	289·50	−389·10	1.233E+05	3.41E−05	5.56E−05	6.01E−08	5.57E−05
66	146	289·50	−366·50	1.233E+05	4.21E−05	6.06E−05	7.42E−08	6.07E−05
66	147	289·50	−343·90	1.233E+05	5.10E−05	6.61E−05	8.99E−08	6.62E−05
66	148	289·50	−321·30	1.233E+05	5.83E−05	6.91E−05	1.03E−07	6.92E−05
66	149	289·50	−304·50	6.003E+04	6.26E−05	7.06E−05	1.10E−07	7.07E−05
66	150	289·50	−293·50	6.003E+04	6.27E−05	7.03E−05	1.10E−07	7.05E−05
66	150	289·50	−293·50	6.003E+04	6.27E−05	7.03E−05	1.10E−07	7.05E−05
66	151	289·50	−284·12	4.229E+04	6.15E−05	7.01E−05	1.08E−07	7.02E−05
66	152	289·50	−276·38	4.229E+04	5.79E−05	6.88E−05	1.02E−07	6.89E−05
66	153	289·50	−268·62	4.229E+04	5.29E−05	6.67E−05	9.32E−08	6.68E−05
66	154	289·50	−260·88	4.229E+04	4.68E−05	6.44E−05	8.25E−08	6.45E−05
66	155	289·50	−252·75	4.638E+04	3.62E−05	5.97E−05	6.38E−08	5.97E−05
66	156	289·50	−244·25	4.638E+04	2.39E−05	5.40E−05	4.21E−08	5.40E−05
66	157	289·50	−234·00	6.548E+04	1.11E−05	4.62E−05	1.96E−08	4.63E−05
66	158	289·50	−222·00	6.548E+04	4.24E−06	4.13E−05	7.46E−09	4.13E−05
66	159	289·50	−210·00	6.548E+04	2.60E−06	4.19E−05	4.59E−09	4.19E−05
66	160	289·50	−198·00	6.548E+04	3.15E−06	4.60E−05	5.54E−09	4.60E−05
66	161	289·50	−186·00	6.548E+04	5.78E−06	5.28E−05	1.02E−08	5.28E−05
66	162	289·50	−174·00	6.548E+04	1.17E−05	6.23E−05	2.06E−08	6.23E−05
66	163	289·50	−164·25	4.093E+04	2.10E−05	7.25E−05	3.70E−08	7.26E−05
66	164	289·50	−156·75	4.093E+04	2.85E−05	8.01E−05	5.02E−08	8.01E−05
66	165	289·50	−149·75	3.547E+04	4.23E−05	9.00E−05	7.45E−08	9.01E−05
66	166	289·50	−143·25	3.547E+04	5.06E−05	9.71E−05	8.91E−08	9.72E−05
66	167	289·50	−133·62	6.958E+04	6.65E−05	1.07E−04	1.17E−07	1.07E−04
66	168	289·50	−120·88	6.958E+04	8.71E−05	1.23E−04	1.54E−07	1.23E−04
66	169	289·50	−108·12	6.958E+04	1.06E−04	1.38E−04	1.87E−07	1.38E−04
66	170	289·50	−95·37	6.958E+04	1.25E−04	1.53E−04	2.20E−07	1.53E−04
66	171	289·50	−80·10	9.713E+04	1.46E−04	1.75E−04	2.57E−07	1.75E−04
66	172	289·50	−62·30	9.713E+04	1.77E−04	2.04E−04	3.12E−07	2.04E−04
66	173	289·50	−44·50	9.713E+04	2.19E−04	2.34E−04	3.86E−07	2.34E−04
66	174	289·50	−26·70	9.713E+04	2.83E−04	2.71E−04	4.99E−07	2.71E−04
66	175	289·50	−8·90	9.713E+04	3.46E−04	3.05E−04	6.10E−07	3.06E−04
66	176	289·50	7·00	7.640E+04	4.30E−04	3.38E−04	7.58E−07	3.38E−04
66	177	289·50	21·00	7.640E+04	5.13E−04	3.69E−04	9.05E−07	3.70E−04
66	178	289·50	38·75	1.173E+05	6.55E−04	4.17E−04	1.15E−06	4.19E−04
66	179	289·50	60·25	1.173E+05	8.46E−04	4.78E−04	1.49E−06	4.79E−04
66	180	289·50	81·75	1.173E+05	1.16E−03	5.66E−04	2.04E−06	5.68E−04
66	181	289·50	103·25	1.173E+05	1.74E−03	6.89E−04	3.06E−06	6.92E−04

Table B.27. Helium production and DPA data in the PCSA/PCST at radius 294.5 mm for case R400 with extended boral shield

Radial interval	Axial interval	Radius [mm]	Height [mm]	Volume [mm^3]	He–prod appm	DPA-ni disp/atom	DPA-fe disp/atom	DPA-sum disp/atom
67	144	294·50	−411·70	2.927E+05	1.47E–05	3.97E–05	2.59E–08	3.97E–05
67	145	294·50	−389·10	2.927E+05	1.86E–05	4.35E–05	3.27E–08	4.35E–05
67	146	294·50	−366·50	2.927E+05	2.31E–05	4.77E–05	4.06E–08	4.77E–05
67	147	294·50	−343·90	2.927E+05	2.77E–05	5.09E–05	4.88E–08	5.09E–05
67	148	294·50	−321·30	2.927E+05	3.18E–05	5.32E–05	5.60E–08	5.33E–05
67	149	294·50	−304·50	1.425E+05	3.37E–05	5.42E–05	5.94E–08	5.42E–05
67	150	294·50	−293·50	1.425E+05	3.40E–05	5.45E–05	5.99E–08	5.46E–05
67	150	294·50	−293·50	1.425E+05	3.40E–05	5.45E–05	5.99E–08	5.46E–05
67	151	294·50	−284·12	1.004E+05	3.29E–05	5.41E–05	5.79E–08	5.42E–05
67	152	294·50	−276·38	1.004E+05	3.10E–05	5.32E–05	5.46E–08	5.33E–05
67	153	294·50	−268·62	1.004E+05	2.86E–05	5.21E–05	5.03E–08	5.22E–05
67	154	294·50	−260·88	1.004E+05	2.47E–05	5.02E–05	4.34E–08	5.03E–05
67	155	294·50	−252·75	1.101E+05	1.92E–05	4.75E–05	3.39E–08	4.76E–05
67	156	294·50	−244·25	1.101E+05	1.31E–05	4.38E–05	2.31E–08	4.38E–05
67	157	294·50	−234·00	1.554E+05	6.80E–06	3.92E–05	1.20E–08	3.92E–05
67	158	294·50	−222·00	1.554E+05	3.03E–06	3.65E–05	5.34E–09	3.65E–05
67	159	294·50	−210·00	1.554E+05	1.97E–06	3.72E–05	3.47E–09	3.72E–05
67	160	294·50	−198·00	1.554E+05	2.23E–06	4.03E–05	3.93E–09	4.03E–05
67	161	294·50	−186·00	1.554E+05	3.84E–06	4.58E–05	6.76E–09	4.58E–05
67	162	294·50	−174·00	1.554E+05	7.53E–06	5.37E–05	1.33E–08	5.37E–05
67	163	294·50	−164·25	9.715E+04	1.21E–05	6.13E–05	2.13E–08	6.13E–05
67	164	294·50	−156·75	9.715E+04	1.77E–05	6.85E–05	3.12E–08	6.85E–05
67	165	294·50	−149·75	8.419E+04	2.36E–05	7.50E–05	4.16E–08	7.50E–05
67	167	294·50	−133·62	1.651E+05	3.86E–05	9.01E–05	6.80E–08	9.01E–05
67	167	294·50	−133·62	1.651E+05	3.86E–05	9.01E–05	6.80E–08	9.01E–05
67	168	294·50	−120·88	1.651E+05	5.05E–05	1.03E–04	8.90E–08	1.03E–04
67	169	294·50	−108·12	1.651E+05	6.23E–05	1.16E–04	1.10E–07	1.16E–04
67	170	294·50	−95·37	1.651E+05	6.89E–05	1.30E–04	1.21E–07	1.30E–04
67	171	294·50	−80·10	2.306E+05	7.88E–05	1.51E–04	1.39E–07	1.51E–04
67	172	294·50	−62·30	2.306E+05	9.27E–05	1.77E–04	1.63E–07	1.77E–04
67	173	294·50	−44·50	2.306E+05	1.18E–04	2.09E–04	2.07E–07	2.10E–04
67	174	294·50	−26·70	2.306E+05	1.49E–04	2.45E–04	2.62E–07	2.45E–04
67	175	294·50	−8·90	2.306E+05	1.91E–04	2.79E–04	3.36E–07	2.79E–04
67	176	294·50	7·00	1.813E+05	2.33E–04	3.10E–04	4.11E–07	3.10E–04
67	177	294·50	21·00	1.813E+05	2.88E–04	3.42E–04	5.08E–07	3.42E–04
67	178	294·50	38·75	2.785E+05	3.61E–04	3.81E–04	6.36E–07	3.81E–04
67	179	294·50	60·25	2.785E+05	5.07E–04	4.42E–04	8.94E–07	4.43E–04
67	180	294·50	81·75	2.785E+05	6.63E–04	5.18E–04	1.17E–06	5.19E–04
67	181	294·50	103·25	2.785E+05	1.09E–03	6.58E–04	1.91E–06	6.59E–04

Table B.28. Helium production and DPA data in the PCSA/PCST at radius 301.5 mm for case R400 with extended boral shield

Radial interval	Axial interval	Radius [mm]	Height [mm]	Volume [mm^3]	He-prod appm	DPA-ni disp/atom	DPA-fe disp/atom	DPA-sum disp/atom
68	144	301·50	−411·70	2.997E+05	7.94E−06	3.12E−05	1.40E−08	3.12E−05
68	145	301·50	−389·10	2.997E+05	1.00E−05	3.42E−05	1.77E−08	3.43E−05
68	146	301·50	−366·50	2.997E+05	1.24E−05	3.69E−05	2.18E−08	3.69E−05
68	147	301·50	−343·90	2.997E+05	1.49E−05	3.92E−05	2.62E−08	3.92E−05
68	148	301·50	−321·30	2.997E+05	1.69E−05	4.09E−05	2.98E−08	4.09E−05
68	149	301·50	−304·50	1.459E+05	1.81E−05	4.20E−05	3.18E−08	4.20E−05
68	150	301·50	−293·50	1.459E+05	1.80E−05	4.22E−05	3.17E−08	4.22E−05
68	150	301·50	−293·50	1.459E+05	1.80E−05	4.22E−05	3.17E−08	4.22E−05
68	151	301·50	−284·12	1.028E+05	1.75E−05	4.19E−05	3.08E−08	4.20E−05
68	152	301·50	−276·38	1.028E+05	1.64E−05	4.15E−05	2.90E−08	4.16E−05
68	153	301·50	−268·62	1.028E+05	1.49E−05	4.07E−05	2.62E−08	4.07E−05
68	154	301·50	−260·88	1.028E+05	1.29E−05	3.97E−05	2.28E−08	3.97E−05
68	155	301·50	−252·75	1.127E+05	1.01E−05	3.78E−05	1.78E−08	3.78E−05
68	156	301·50	−244·25	1.127E+05	7.19E−06	3.55E−05	1.27E−08	3.56E−05
68	157	301·50	−234·00	1.591E+05	4.27E−06	3.35E−05	7.52E−09	3.35E−05
68	158	301·50	−222·00	1.591E+05	2.31E−06	3.22E−05	4.06E−09	3.23E−05
68	159	301·50	−210·00	1.591E+05	1.58E−06	3.25E−05	2.78E−09	3.25E−05
68	160	301·50	−198·00	1.591E+05	1.70E−06	3.47E−05	2.99E−09	3.48E−05
68	161	301·50	−186·00	1.591E+05	2.75E−06	3.93E−05	4.85E−09	3.93E−05
68	162	301·50	−174·00	1.591E+05	4.78E−06	4.55E−05	8.43E−09	4.55E−05
68	163	301·50	−164·25	9.946E+04	7.72E−06	5.17E−05	1.36E−08	5.17E−05
68	164	301·50	−156·75	9.945E+04	1.08E−05	5.67E−05	1.90E−08	5.67E−05
68	165	301·50	−149·75	8.619E+04	1.43E−05	6.14E−05	2.51E−08	6.15E−05
68	166	301·50	−143·25	8.619E+04	1.76E−05	6.68E−05	3.10E−08	6.69E−05
68	167	301·50	−133·62	1.691E+05	2.23E−05	7.46E−05	3.94E−08	7.46E−05
68	168	301·50	−120·88	1.691E+05	2.97E−05	8.43E−05	5.24E−08	8.44E−05
68	169	301·50	−108·12	1.691E+05	3.51E−05	9.55E−05	6.19E−08	9.56E−05
68	170	301·50	−95·37	1.691E+05	3.54E−05	1.08E−04	6.24E−08	1.08E−04
68	171	301·50	−80·10	2.360E+05	3.22E−05	1.25E−04	5.68E−08	1.25E−04
68	172	301·50	−62·30	2.360E+05	3.60E−05	1.51E−04	6.34E−08	1.51E−04
68	173	301·50	−44·50	2.360E+05	4.49E−05	1.82E−04	7.91E−08	1.82E−04
68	174	301·50	−26·70	2.360E+05	5.88E−05	2.17E−04	1.04E−07	2.17E−04
68	175	301·50	−8·90	2.360E+05	8.38E−05	2.59E−04	1.48E−07	2.60E−04
68	176	301·50	7·00	1.856E+05	1.07E−04	2.98E−04	1.89E−07	2.98E−04
68	177	301·50	21·00	1.856E+05	1.29E−04	3.23E−04	2.28E−07	3.23E−04
68	178	301·50	38·75	2.851E+05	1.86E−04	3.64E−04	3.28E−07	3.64E−04
68	179	301·50	60·25	2.851E+05	2.88E−04	4.31E−04	5.08E−07	4.31E−04
68	180	301·50	81·75	2.851E+05	3.72E−04	5.11E−04	6.56E−07	5.11E−04
68	181	301·50	103·25	2.851E+05	7.00E−04	6.68E−04	1.23E−06	6.69E−04

Table B.29. Helium production and DPA data in the flange at height −8.9 mm for case R400 with extended boral shield

Radial interval	Axial interval	Radius [mm]	Height [mm]	Volume [mm^3]	He–prod appm	DPA-ni disp/atom	DPA-fe disp/atom	DPA-sum disp/atom
69	175	307·50	−8·90	1.720E+05	4.64E–05	2.52E–04	8.18E–08	2.52E–04
70	175	312·50	−8·90	1.748E+05	3.20E–05	2.47E–04	5.64E–08	2.47E–04
71	175	319·50	−8·90	3.216E+05	2.33E–05	2.53E–04	4.11E–08	2.53E–04
72	175	328·50	−8·90	3.307E+05	1.69E–05	2.81E–04	2.97E–08	2.81E–04
73	175	337·50	−8·90	3.397E+05	1.33E–05	3.09E–04	2.35E–08	3.09E–04
74	175	346·50	−8·90	3.488E+05	1.10E–05	3.06E–04	1.93E–08	3.06E–04
75	175	355·50	−8·90	3.578E+05	9.21E–06	3.00E–04	1.62E–08	3.00E–04
76	175	364·50	−8·90	3.669E+05	7.92E–06	3.18E–04	1.39E–08	3.18E–04
77	175	373·50	−8·90	3.760E+05	6.75E–06	3.29E–04	1.19E–08	3.29E–04
78	175	382·50	−8·90	3.850E+05	5.82E–06	3.33E–04	1.03E–08	3.33E–04
79	175	391·50	−8·90	3.941E+05	4.97E–06	3.57E–04	8.76E–09	3.57E–04
80	175	397·50	−8·90	1.334E+05	4.55E–06	3.75E–04	8.01E–09	3.75E–04
81	175	402·00	−8·90	2.698E+05	4.15E–06	3.76E–04	7.31E–09	3.76E–04
82	175	408·00	−8·90	2.738E+05	3.89E–06	3.74E–04	6.85E–09	3.74E–04
83	175	414·88	−8·90	3.596E+05	3.53E–06	3.81E–04	6.22E–09	3.81E–04
84	175	422·62	−8·90	3.663E+05	3.26E–06	3.99E–04	5.75E–09	3.99E–04
85	175	430·38	−8·90	3.730E+05	3.01E–06	4.12E–04	5.30E–09	4.12E–04
86	175	438·12	−8·90	3.798E+05	2.87E–06	4.18E–04	5.05E–09	4.18E–04
87	175	445·50	−8·90	3.488E+05	2.80E–06	4.14E–04	4.93E–09	4.14E–04
88	175	452·50	−8·90	3.543E+05	2.90E–06	4.02E–04	5.10E–09	4.02E–04
89	175	459·50	−8·90	3.597E+05	3.19E–06	3.85E–04	5.61E–09	3.85E–04
90	175	466·50	−8·90	3.652E+05	4.30E–06	3.79E–04	7.58E–09	3.79E–04

Table B.30. Helium production and DPA data in the flange at height −26.7 mm for case R400 with extended boral shield

Radial interval	Axial interval	Radius [mm]	Height [mm]	Volume [mm^3]	He–prod appm	DPA-ni disp/atom	DPA-fe disp/atom	DPA-sum disp/atom
69	174	307·50	−26·70	1.720E+05	2.69E–05	2.00E–04	4.74E–08	2.00E–04
70	174	312·50	−26·70	1.748E+05	1.50E–05	1.93E–04	2.64E–08	1.93E–04
71	174	319·50	−26·70	3.216E+05	7.08E–06	1.89E–04	1.25E–08	1.89E–04
72	174	328·50	−26·70	3.307E+05	3.33E–06	1.95E–04	5.86E–09	1.95E–04
73	174	337·50	−26·70	3.397E+05	1.83E–06	2.15E–04	3.23E–09	2.15E–04
74	174	346·50	−26·70	3.488E+05	1.28E–06	2.24E–04	2.25E–09	2.24E–04
75	174	355·50	−26·70	3.578E+05	9.00E–07	2.16E–04	1.59E–09	2.16E–04
76	174	364·50	−26·70	3.669E+05	7.44E–07	2.18E–04	1.31E–09	2.18E–04
77	174	373·50	−26·70	3.760E+05	5.93E–07	2.31E–04	1.04E–09	2.31E–04
78	174	382·50	−26·70	3.850E+05	5.19E–07	2.32E–04	9.14E–10	2.32E–04
79	174	391·50	−26·70	3.941E+05	4.34E–07	2.37E–04	7.66E–10	2.37E–04
80	174	397·50	−26·70	1.334E+05	4.16E–07	2.51E–04	7.33E–10	2.51E–04
81	174	402·00	−26·70	2.698E+05	3.90E–07	2.60E–04	6.88E–10	2.60E–04
82	174	408·00	−26·70	2.738E+05	3.58E–07	2.63E–04	6.30E–10	2.63E–04
83	174	414·88	−26·70	3.596E+05	3.30E–07	2.59E–04	5.82E–10	2.59E–04
84	174	422·62	−26·70	3.663E+05	3.03E–07	2.65E–04	5.34E–10	2.65E–04
85	174	430·38	−26·70	3.730E+05	2.97E–07	2.79E–04	5.24E–10	2.79E–04
86	174	438·12	−26·70	3.798E+05	3.01E–07	2.83E–04	5.30E–10	2.83E–04
87	174	445·50	−26·70	3.488E+05	3.37E–07	2.81E–04	5.93E–10	2.81E–04
88	174	452·50	−26·70	3.543E+05	4.13E–07	2.72E–04	7.28E–10	2.72E–04
89	174	459·50	−26·70	3.597E+05	5.88E–07	2.60E–04	1.04E–09	2.60E–04
90	174	466·50	−26·70	3.652E+05	1.12E–06	2.52E–04	1.97E–09	2.52E–04

Table B.31. Helium production and DPA data in the flange at height −44.5 mm for case R400 with extended boral shield

Radial interval	Axial interval	Radius [mm]	Height [mm]	Volume [mm^3]	He–prod appm	DPA-ni disp/atom	DPA-fe disp/atom	DPA-sum disp/atom
69	173	307·50	−44·50	1.720E+05	1.97E–05	1.65E–04	3.47E–08	1.65E–04
70	173	312·50	−44·50	1.748E+05	1.04E–05	1.55E–04	1.83E–08	1.55E–04
71	173	319·50	−44·50	3.216E+05	4.72E–06	1.48E–04	8.32E–09	1.48E–04
72	173	328·50	−44·50	3.307E+05	1.58E–06	1.46E–04	2.78E–09	1.46E–04
73	173	337·50	−44·50	3.397E+05	6.54E–07	1.54E–04	1.15E–09	1.54E–04
74	173	346·50	−44·50	3.488E+05	2.97E–07	1.63E–04	5.23E–10	1.63E–04
75	173	355·50	−44·50	3.578E+05	1.80E–07	1.61E–04	3.17E–10	1.61E–04
76	173	364·50	−44·50	3.669E+05	1.10E–07	1.56E–04	1.93E–10	1.56E–04
77	173	373·50	−44·50	3.760E+05	8.69E–08	1.62E–04	1.53E–10	1.62E–04
78	173	382·50	−44·50	3.850E+05	6.43E–08	1.67E–04	1.13E–10	1.67E–04
79	173	391·50	−44·50	3.941E+05	6.09E–08	1.64E–04	1.07E–10	1.64E–04
80	173	397·50	−44·50	1.334E+05	5.64E–08	1.67E–04	9.94E–11	1.67E–04
81	173	402·00	−44·50	2.698E+05	5.21E–08	1.75E–04	9.18E–11	1.75E–04
82	173	408·00	−44·50	2.738E+05	4.59E–08	1.82E–04	8.08E–11	1.82E–04
83	173	414·88	−44·50	3.596E+05	4.47E–08	1.83E–04	7.87E–11	1.83E–04
84	173	422·62	−44·50	3.663E+05	4.23E–08	1.79E–04	7.46E–11	1.79E–04
85	173	430·38	−44·50	3.730E+05	4.46E–08	1.85E–04	7.86E–11	1.85E–04
86	173	438·12	−44·50	3.798E+05	5.15E–08	1.92E–04	9.07E–11	1.92E–04
87	173	445·50	−44·50	3.488E+05	6.65E–08	1.91E–04	1.17E–10	1.91E–04
88	173	452·50	−44·50	3.543E+05	1.01E–07	1.86E–04	1.78E–10	1.86E–04
89	173	459·50	−44·50	3.597E+05	1.72E–07	1.75E–04	3.04E–10	1.75E–04
90	173	466·50	−44·50	3.652E+05	3.71E–07	1.72E–04	6.54E–10	1.72E–04

Table B.32. Helium production and DPA data in the flange at height -62.3 mm for case R400 with extended boral shield

Radial interval	Axial interval	Radius [mm]	Height [mm]	Volume [mm^3]	He-prod appm	DPA-ni disp/atom	DPA-fe disp/atom	DPA-sum disp/atom
69	172	307·50	−62·30	1.720E+05	1.58E−05	1.35E−04	2.78E−08	1.36E−04
70	172	312·50	−62·30	1.748E+05	8.19E−06	1.26E−04	1.44E−08	1.26E−04
71	172	319·50	−62·30	3.216E+05	3.55E−06	1.17E−04	6.26E−09	1.17E−04
72	172	328·50	−62·30	3.307E+05	1.25E−06	1.11E−04	2.20E−09	1.11E−04
73	172	337·50	−62·30	3.397E+05	4.40E−07	1.12E−04	7.75E−10	1.12E−04
74	172	346·50	−62·30	3.488E+05	1.82E−07	1.16E−04	3.21E−10	1.16E−04
75	172	355·50	−62·30	3.578E+05	8.09E−08	1.18E−04	1.43E−10	1.18E−04
76	172	364·50	−62·30	3.669E+05	4.59E−08	1.14E−04	8.10E−11	1.14E−04
77	172	373·50	−62·30	3.760E+05	2.72E−08	1.13E−04	4.79E−11	1.13E−04
78	172	382·50	−62·30	3.850E+05	2.07E−08	1.17E−04	3.65E−11	1.17E−04
79	172	391·50	−62·30	3.941E+05	1.54E−08	1.17E−04	2.72E−11	1.17E−04
80	172	397·50	−62·30	1.334E+05	1.51E−08	1.13E−04	2.66E−11	1.13E−04
81	172	402·00	−62·30	2.698E+05	1.32E−08	1.17E−04	2.32E−11	1.17E−04
82	172	408·00	−62·30	2.738E+05	1.27E−08	1.23E−04	2.24E−11	1.23E−04
83	172	414·88	−62·30	3.596E+05	1.12E−08	1.24E−04	1.98E−11	1.24E−04
84	172	422·62	−62·30	3.663E+05	1.17E−08	1.25E−04	2.05E−11	1.25E−04
85	172	430·38	−62·30	3.730E+05	1.22E−08	1.22E−04	2.15E−11	1.22E−04
86	172	438·12	−62·30	3.798E+05	1.53E−08	1.26E−04	2.70E−11	1.26E−04
87	172	445·50	−62·30	3.488E+05	2.10E−08	1.29E−04	3.71E−11	1.29E−04
88	172	452·50	−62·30	3.543E+05	3.35E−08	1.25E−04	5.90E−11	1.25E−04
89	172	459·50	−62·30	3.597E+05	5.81E−08	1.23E−04	1.02E−10	1.23E−04
90	172	466·50	−62·30	3.652E+05	1.25E−07	1.20E−04	2.20E−10	1.20E−04

Table B.33. Helium production and DPA data in the flange at height −80.10 mm for case R400 with extended boral shield

Radial interval	Axial interval	Radius [mm]	Height [mm]	Volume [mm^3]	He–prod appm	DPA-ni disp/atom	DPA-fe disp/atom	DPA-sum disp/atom
69	171	307·50	−80·10	1.720E+05	1.57E–05	1.09E–04	2.77E–08	1.09E–04
70	171	312·50	−80·10	1.748E+05	9.11E–06	1.00E–04	1.60E–08	1.00E–04
71	171	319·50	−80·10	3.216E+05	4.32E–06	9.08E–05	7.61E–09	9.08E–05
72	171	328·50	−80·10	3.307E+05	1.62E–06	8.20E–05	2.86E–09	8.20E–05
73	171	337·50	−80·10	3.397E+05	6.82E–07	7.86E–05	1.20E–09	7.86E–05
74	171	346·50	−80·10	3.488E+05	3.01E–07	7.98E–05	5.31E–10	7.98E–05
75	171	355·50	−80·10	3.578E+05	1.54E–07	8.13E–05	2.71E–10	8.13E–05
76	171	364·50	−80·10	3.669E+05	8.56E–08	7.92E–05	1.51E–10	7.92E–05
77	171	373·50	−80·10	3.760E+05	5.48E–08	7.60E–05	9.65E–11	7.60E–05
78	171	382·50	−80·10	3.850E+05	3.77E–08	7.78E–05	6.64E–11	7.78E–05
79	171	391·50	−80·10	3.941E+05	2.88E–08	7.92E–05	5.08E–11	7.92E–05
80	171	397·50	−80·10	1.334E+05	2.53E–08	7.77E–05	4.46E–11	7.77E–05
81	171	402·00	−80·10	2.698E+05	2.30E–08	7.60E–05	4.05E–11	7.60E–05
82	171	408·00	−80·10	2.738E+05	2.03E–08	7.90E–05	3.58E–11	7.90E–05
83	171	414·88	−80·10	3.596E+05	1.89E–08	8.12E–05	3.32E–11	8.12E–05
84	171	422·62	−80·10	3.663E+05	1.76E–08	8.03E–05	3.09E–11	8.03E–05
85	171	430·38	−80·10	3.730E+05	1.76E–08	8.19E–05	3.11E–11	8.19E–05
86	171	438·12	−80·10	3.798E+05	1.89E–08	8.09E–05	3.33E–11	8.09E–05
87	171	445·50	−80·10	3.488E+05	2.21E–08	8.25E–05	3.89E–11	8.25E–05
88	171	452·50	−80·10	3.543E+05	2.84E–08	8.28E–05	5.00E–11	8.28E–05
89	171	459·50	−80·10	3.597E+05	4.10E–08	8.30E–05	7.22E–11	8.30E–05
90	171	466·50	−80·10	3.652E+05	7.23E–08	8.80E–05	1.27E–10	8.80E–05

APPENDIX C. DETAILED HEATING RESULTS

Table C.1. Heating rate in the horizontal part of the shield for case R500 with restricted hafnium shield

Radial interval	Axial interval	Radius (mm)	Height (mm)	Volume (mm^3)	Heating rate neutron (Watt cm^{-3})	Heating rate gamma (Watt cm^{-3})	Heating rate sum (Watt cm^{-3})
66	182	289·50	124·17	5.060E+02	2.22E—06	3.65E—01	3.65E—01
67	182	294·50	124·17	1.518E+03	2.30E—06	3.60E—01	3.60E—01
68	182	301·50	124·17	3.234E+02	5.13E—06	4.78E—01	4.78E—01
69	182	307·50	124·17	1.976E+03	6.59E—06	5.92E—01	5.92E—01
70	182	312·50	124·17	2.575E+03	7.71E—06	6.68E—01	6.68E—01
71	182	319·50	124·17	3.881E+03	8.94E—06	7.58E—01	7.58E—01
72	182	328·50	124·17	4.743E+03	1.06E—05	8.60E—01	8.60E—01
73	182	337·50	124·17	5.605E+03	1.21E—05	9.50E—01	9.50E—01
74	182	346·50	124·17	6.468E+03	1.37E—05	1.04E+00	1.04E+00
75	182	355·50	124·17	2.348E+03	1.53E—05	1.13E+00	1.13E+00
76	182	364·50	124·17	7.618E+03	1.69E—05	1.21E+00	1.21E+00
77	182	373·50	124·17	1.150E+04	1.85E—05	1.30E+00	1.30E+00
78	182	382·50	124·17	9.630E+03	2.00E—05	1.38E+00	1.38E+00
79	182	391·50	124·17	8.684E+03	2.17E—05	1.47E+00	1.47E+00
80	182	397·50	124·17	9.282E+03	2.28E—05	1.53E+00	1.53E+00
81	182	402·00	124·17	1.220E+04	2.38E—05	1.58E+00	1.58E+00
82	182	408·00	124·17	1.310E+04	2.47E—05	1.64E+00	1.64E+00
83	182	414·88	124·17	1.011E+04	2.64E—05	1.72E+00	1.72E+00
84	182	422·62	124·17	1.059E+04	2.77E—05	1.83E+00	1.83E+00
85	182	430·38	124·17	4.876E+03	2.97E—05	1.94E+00	1.94E+00
86	182	438·12	124·17	2.025E+03	3.11E—05	2.04E+00	2.04E+00
87	182	445·50	124·17	2.026E+03	3.38E—05	2.12E+00	2.12E+00
88	182	452·50	124·17	4.875E+03	3.45E—05	2.27E+00	2.27E+00
89	182	459·50	124·17	1.016E+04	3.89E—05	2.38E+00	2.38E+00
90	182	466·50	124·17	1.053E+04	3.61E—05	2.91E+00	2.91E+00
91	182	477·62	124·17	1.534E+04	7.78E—05	3.19E+00	3.19E+00

Table C.2. Heating rate in the inner vertical part of the shield for case R500 with restricted hafnium shield

Radial interval	Axial interval	Radius (mm)	Height (mm)	Volume (mm^3)	Heating rate neutron (Watt cm^{-3})	Heating rate gamma (Watt cm^{-3})	Heating rate sum (Watt cm^{-3})
66	182	289·50	124·17	3.622E+04	2.22E—06	3.65E—01	3.65E—01
66	183	289·50	144·50	3.967E+04	2.27E—06	6.46E—01	6.46E—01
66	184	289·50	164·83	4.312E+04	3.52E—06	1.10E+00	1.10E+00
66	185	289·50	177·50	4.657E+04	6.75E—06	1.40E+00	1.40E+00
66	186	289·50	182·50	5.002E+04	7.67E—06	1.49E+00	1.49E+00
66	187	289·50	187·50	6.271E+04	8.18E—06	1.57E+00	1.57E+00
66	188	289·50	192·50	6.741E+04	8.81E—06	1.65E+00	1.65E+00
66	189	289·50	197·50	5.207E+04	9.24E—06	1.72E+00	1.72E+00
66	190	289·50	202·50	5.456E+04	9.72E—06	1.79E+00	1.79E+00
66	191	289·50	207·50	5.705E+04	1.03E—05	1.86E+00	1.86E+00
66	192	289·50	212·50	5.954E+04	1.07E—05	1.93E+00	1.93E+00
66	193	289·50	217·50	6.204E+04	1.10E—05	2.01E+00	2.01E+00
66	194	289·50	222·50	8.921E+04	1.18E—05	2.09E+00	2.09E+00
66	195	289·50	227·50	9.907E+04	1.21E—05	2.17E+00	2.17E+00
66	196	289·50	232·50	1.043E+05	1.27E—05	2.24E+00	2.24E+00
66	197	289·50	237·50	1.095E+05	1.32E—05	2.32E+00	2.32E+00
66	198	289·50	242·50	1.147E+05	1.36E—05	2.40E+00	2.40E+00
66	199	289·50	247·50	8.073E+04	1.43E—05	2.49E+00	2.49E+00
66	200	289·50	252·50	8.312E+04	1.46E—05	2.55E+00	2.55E+00
66	201	289·50	257·50	7.686E+04	1.53E—05	2.66E+00	2.66E+00
66	202	289·50	262·50	7.880E+04	1.59E—05	2.71E+00	2.71E+00
66	203	289·50	267·50	8.983E+04	1.66E—05	2.87E+00	2.87E+00
66	204	289·50	272·50	1.204E+05	1.62E—05	3.00E+00	3.00E+00
66	205	289·50	295·00	1.244E+05	1.46E—05	3.27E+00	3.27E+00
66	206	289·50	335·00	1.385E+05	1.89E—05	4.07E+00	4.07E+00
66	207	289·50	375·00	1.432E+05	2.55E—05	4.91E+00	4.91E+00
66	208	289·50	415·00	9.454E+04	3.38E—05	5.98E+00	5.98E+00
66	209	289·50	455·00	9.648E+04	4.65E—05	7.18E+00	7.18E+00
66	210	289·50	495·00	1.095E+05	6.35E—05	8.77E+00	8.77E+00
66	211	289·50	535·00	8.930E+04	9.01E—05	1.05E+01	1.05E+01
66	212	289·50	575·00	1.138E+05	1.27E—04	1.32E+01	1.32E+01
66	213	289·50	615·00	1.162E+05	1.87E—04	1.60E+01	1.60E+01
66	214	289·50	655·00	1.186E+05	2.75E—04	2.11E+01	2.11E+01
66	215	289·50	695·00	7.230E+04	4.25E—04	2.57E+01	2.57E+01
66	216	289·50	735·00	1.472E+05	6.93E—04	3.97E+01	3.97E+01
66	217	289·50	775·00	1.506E+05	1.55E—03	5.72E+01	5.72E+01

Table C.3. Heating rate in the outer vertical part of the shield for case R500 with restricted hafnium shield

Radial interval	Axial interval	Radius (mm)	Height (mm)	Volume (mm^3)	Heating rate neutron (Watt cm^{-3})	Heating rate gamma (Watt cm^{-3})	Heating rate sum (Watt cm^{-3})
67	182	294·50	124·17	2.587E+05	2.30E—06	3.60E—01	3.60E—01
67	183	294·50	144·50	2.683E+05	1.40E—05	7.49E—01	7.49E—01
67	184	294·50	164·83	8.236E+04	2.46E—05	1.21E+00	1.21E+00
67	185	294·50	177·50	8.322E+04	3.05E—05	1.44E+00	1.44E+00
67	186	294·50	182·50	1.975E+05	3.28E—05	1.54E+00	1.54E+00
67	187	294·50	187·50	2.022E+05	3.53E—05	1.61E+00	1.61E+00
67	188	294·50	192·50	1.473E+05	3.77E—05	1.69E+00	1.69E+00
67	189	294·50	197·50	1.497E+05	4.00E—05	1.76E+00	1.76E+00
67	190	294·50	202·50	2.755E+05	4.28E—05	1.83E+00	1.83E+00
67	191	294·50	207·50	2.833E+05	4.49E—05	1.91E+00	1.91E+00
67	192	294·50	212·50	2.910E+05	4.75E—05	1.98E+00	1.98E+00
67	193	294·50	217·50	2.988E+05	5.00E—05	2.06E+00	2.06E+00
67	194	294·50	222·50	3.066E+05	5.21E—05	2.14E+00	2.14E+00
67	195	294·50	227·50	3.143E+05	5.50E—05	2.22E+00	2.22E+00
67	196	294·50	232·50	3.221E+05	5.68E—05	2.30E+00	2.30E+00
67	197	294·50	237·50	3.299E+05	5.96E—05	2.38E+00	2.38E+00
67	198	294·50	242·50	3.376E+05	6.18E—05	2.46E+00	2.46E+00
67	199	294·50	247·50	1.143E+05	6.47E—05	2.55E+00	2.55E+00
67	200	294·50	252·50	2.311E+05	6.64E—05	2.63E+00	2.63E+00
67	201	294·50	257·50	2.346E+05	6.96E—05	2.71E+00	2.71E+00
67	202	294·50	262·50	3.081E+05	7.14E—05	2.83E+00	2.83E+00
67	203	294·50	267·50	3.138E+05	7.50E—05	2.88E+00	2.88E+00
67	204	294·50	272·50	3.196E+05	7.57E—05	3.11E+00	3.11E+00
67	205	294·50	295·00	3.253E+05	9.09E—05	3.36E+00	3.36E+00
67	206	294·50	335·00	2.988E+05	1.11E—04	4.16E+00	4.16E+00
67	207	294·50	375·00	3.035E+05	1.36E—04	4.90E+00	4.90E+00
67	208	294·50	415·00	3.082E+05	1.59E—04	5.95E+00	5.95E+00
67	209	294·50	455·00	3.129E+05	1.90E—04	6.94E+00	6.94E+00
67	210	294·50	495·00	6.979E+05	2.20E—04	8.44E+00	8.44E+00
67	211	294·50	535·00	7.202E+05	2.62E—04	9.86E+00	9.86E+00
67	212	294·50	575·00	7.425E+05	3.05E—04	1.23E+01	1.23E+01
67	213	294·50	615·00	7.648E+05	3.70E—04	1.44E+01	1.44E+01
67	214	294·50	655·00	6.695E+05	4.42E—04	1.90E+01	1.90E+01
67	215	294·50	695·00	6.857E+05	5.67E—04	2.24E+01	2.24E+01
67	216	294·50	735·00	7.019E+05	7.36E—04	3.54E+01	3.54E+01
67	217	294·50	775·00	7.181E+05	1.39E—03	5.16E+01	5.16E+01

Table C.4. Heating rate in the horizontal part of the shield for case R450 with restricted boral shield

Radial interval	Axial interval	Radius (mm)	Height (mm)	Volume (mm^3)	Heating rate neutron (Watt cm^{-3})	Heating rate gamma (Watt cm^{-3})	Heating rate sum (Watt cm^{-3})
66	182	289·50	124·17	5.060E+02	5.71E–02	3.97E–02	9.68E–02
67	182	294·50	124·17	1.518E+03	2.55E–02	4.44E–02	6.99E–02
68	182	301·50	124·17	3.234E+02	1.60E–01	5.19E–02	2.12E–01
69	182	307·50	124·17	1.976E+03	2.24E–01	5.75E–02	2.82E–01
70	182	312·50	124·17	2.575E+03	2.56E–01	6.01E–02	3.16E–01
71	182	319·50	124·17	3.881E+03	3.10E–01	6.34E–02	3.74E–01
72	182	328·50	124·17	4.743E+03	3.63E–01	6.78E–02	4.31E–01
73	182	337·50	124·17	5.605E+03	4.30E–01	7.15E–02	5.02E–01
74	182	346·50	124·17	6.468E+03	4.80E–01	7.49E–02	5.54E–01
75	182	355·50	124·17	2.348E+03	5.50E–01	7.92E–02	6.29E–01
76	182	364·50	124·17	7.618E+03	5.95E–01	8.39E–02	6.79E–01
77	182	373·50	124·17	1.150E+04	6.68E–01	8.78E–02	7.56E–01
78	182	382·50	124·17	9.630E+03	7.13E–01	9.15E–02	8.04E–01
79	182	391·50	124·17	8.684E+03	7.87E–01	9.54E–02	8.83E–01
80	182	397·50	124·17	9.282E+03	8.15E–01	9.78E–02	9.13E–01
81	182	402·00	124·17	1.220E+04	8.73E–01	9.95E–02	9.72E–01
82	182	408·00	124·17	1.310E+04	8.84E–01	1.02E–01	9.86E–01
83	182	414·88	124·17	1.011E+04	9.66E–01	1.05E–01	1.07E+00
84	182	422·62	124·17	1.059E+04	9.94E–01	1.09E–01	1.10E+00
85	182	430·38	124·17	4.876E+03	1.09E+00	1.13E–01	1.20E+00
86	182	438·12	124·17	2.025E+03	1.12E+00	1.18E–01	1.24E+00
87	182	445·50	124·17	2.026E+03	1.24E+00	1.22E–01	1.36E+00
88	182	452·50	124·17	4.875E+03	1.25E+00	1.26E–01	1.38E+00
89	182	459·50	124·17	1.016E+04	1.40E+00	1.30E–01	1.54E+00
90	182	466·50	124·17	1.053E+04	1.40E+00	1.41E–01	1.54E+00
91	182	477·62	124·17	1.534E+04	2.93E+00	1.46E–01	3.08E+00

Table C.5. Heating rate in the inner vertical part of the shield for case R450 with restricted boral shield

Radial interval	Axial interval	Radius (mm)	Height (mm)	Volume (mm^3)	Heating rate neutron (Watt cm^{-3})	Heating rate gamma (Watt cm^{-3})	Heating rate sum (Watt cm^{-3})
66	182	289·50	124·17	3.622E+04	5.71E–02	3.97E–02	9.68E–02
66	183	289·50	144·50	3.967E+04	4.18E–02	5.19E–02	9.37E–02
66	184	289·50	164·83	4.312E+04	7.08E–02	6.86E–02	1.39E–01
66	185	289·50	177·50	4.657E+04	1.36E–01	8.15E–02	2.17E–01
66	186	289·50	182·50	5.002E+04	1.69E–01	8.49E–02	2.54E–01
66	187	289·50	187·50	6.271E+04	1.72E–01	8.82E–02	2.60E–01
66	188	289·50	192·50	6.741E+04	1.94E–01	9.14E–02	2.86E–01
66	189	289·50	197·50	5.207E+04	1.96E–01	9.39E–02	2.90E–01
66	190	289·50	202·50	5.456E+04	2.09E–01	9.56E–02	3.04E–01
66	191	289·50	207·50	5.705E+04	2.19E–01	9.72E–02	3.17E–01
66	192	289·50	212·50	5.954E+04	2.29E–01	9.93E–02	3.28E–01
66	193	289·50	217·50	6.204E+04	2.32E–01	1.02E–01	3.35E–01
66	194	289·50	222·50	8.921E+04	2.50E–01	1.05E–01	3.55E–01
66	195	289·50	227·50	9.907E+04	2.62E–01	1.07E–01	3.69E–01
66	196	289·50	232·50	1.043E+05	2.66E–01	1.09E–01	3.75E–01
66	197	289·50	237·50	1.095E+05	2.85E–01	1.12E–01	3.96E–01
66	198	289·50	242·50	1.147E+05	2.88E–01	1.14E–01	4.01E–01
66	199	289·50	247·50	8.073E+04	3.08E–01	1.16E–01	4.25E–01
66	200	289·50	252·50	8.312E+04	3.12E–01	1.19E–01	4.32E–01
66	201	289·50	257·50	7.686E+04	3.31E–01	1.23E–01	4.54E–01
66	202	289·50	262·50	7.880E+04	3.44E–01	1.25E–01	4.69E–01
66	203	289·50	267·50	8.983E+04	3.70E–01	1.32E–01	5.02E–01
66	204	289·50	272·50	1.204E+05	3.66E–01	1.38E–01	5.05E–01
66	205	289·50	295·00	1.244E+05	4.32E–01	1.49E–01	5.81E–01
66	206	289·50	335·00	1.385E+05	5.89E–01	1.79E–01	7.68E–01
66	207	289·50	375·00	1.432E+05	8.17E–01	2.12E–01	1.03E+00
66	208	289·50	415·00	9.454E+04	1.13E+00	2.54E–01	1.39E+00
66	209	289·50	455·00	9.648E+04	1.61E+00	3.10E–01	1.92E+00
66	210	289·50	495·00	1.095E+05	2.28E+00	3.76E–01	2.66E+00
66	211	289·50	535·00	8.930E+04	3.33E+00	4.58E–01	3.79E+00
66	212	289·50	575·00	1.138E+05	4.85E+00	5.65E–01	5.41E+00
66	213	289·50	615·00	1.162E+05	7.29E+00	6.91E–01	7.98E+00
66	214	289·50	655·00	1.186E+05	1.09E+01	8.66E–01	1.18E+01
66	215	289·50	695·00	7.230E+04	1.71E+01	1.07E+00	1.82E+01
66	216	289·50	735·00	1.472E+05	2.82E+01	1.45E+00	2.97E+01
66	217	289·50	775·00	1.506E+05	6.62E+01	1.86E+00	6.80E+01

Table C.6. Heating rate in the outer vertical part of the shield for case R450 with restricted boral shield

Radial interval	Axial interval	Radius (mm)	Height (mm)	Volume (mm^3)	Heating rate neutron (Watt cm^{-3})	Heating rate gamma (Watt cm^{-3})	Heating rate sum (Watt cm^{-3})
67	182	294·50	124·17	2.587E+05	2.55E–02	4.44E–02	6.99E–02
67	183	294·50	144·50	2.683E+05	4.96E–01	5.90E–02	5.55E–01
67	184	294·50	164·83	8.236E+04	8.97E–01	7.53E–02	9.72E–01
67	185	294·50	177·50	8.322E+04	1.14E+00	8.52E–02	1.22E+00
67	186	294·50	182·50	1.975E+05	1.22E+00	8.82E–02	1.31E+00
67	187	294·50	187·50	2.022E+05	1.32E+00	9.09E–02	1.41E+00
67	188	294·50	192·50	1.473E+05	1.41E+00	9.33E–02	1.50E+00
67	189	294·50	197·50	1.497E+05	1.51E+00	9.52E–02	1.60E+00
67	190	294·50	202·50	2.755E+05	1.60E+00	9.71E–02	1.69E+00
67	191	294·50	207·50	2.833E+05	1.71E+00	9.92E–02	1.81E+00
67	192	294·50	212·50	2.910E+05	1.75E+00	1.02E–01	1.85E+00
67	193	294·50	217·50	2.988E+05	1.92E+00	1.04E–01	2.02E+00
67	194	294·50	222·50	3.066E+05	1.92E+00	1.06E–01	2.02E+00
67	195	294·50	227·50	3.143E+05	2.11E+00	1.09E–01	2.22E+00
67	196	294·50	232·50	3.221E+05	2.11E+00	1.12E–01	2.22E+00
67	197	294·50	237·50	3.299E+05	2.27E+00	1.14E–01	2.39E+00
67	198	294·50	242·50	3.376E+05	2.30E+00	1.17E–01	2.42E+00
67	199	294·50	247·50	1.143E+05	2.46E+00	1.20E–01	2.58E+00
67	200	294·50	252·50	2.311E+05	2.48E+00	1.23E–01	2.61E+00
67	201	294·50	257·50	2.346E+05	2.64E+00	1.27E–01	2.77E+00
67	202	294·50	262·50	3.081E+05	2.67E+00	1.32E–01	2.80E+00
67	203	294·50	267·50	3.138E+05	2.84E+00	1.35E–01	2.97E+00
67	204	294·50	272·50	3.196E+05	2.89E+00	1.40E–01	3.03E+00
67	205	294·50	295·00	3.253E+05	3.32E+00	1.53E–01	3.48E+00
67	206	294·50	335·00	2.988E+05	4.09E+00	1.82E–01	4.27E+00
67	207	294·50	375·00	3.035E+05	4.94E+00	2.14E–01	5.15E+00
67	208	294·50	415·00	3.082E+05	5.82E+00	2.60E–01	6.08E+00
67	209	294·50	455·00	3.129E+05	6.86E+00	3.11E–01	7.17E+00
67	210	294·50	495·00	6.979E+05	7.95E+00	3.77E–01	8.33E+00
67	211	294·50	535·00	7.202E+05	9.36E+00	4.55E–01	9.81E+00
67	212	294·50	575·00	7.425E+05	1.09E+01	5.58E–01	1.14E+01
67	213	294·50	615·00	7.648E+05	1.30E+01	6.76E–01	1.37E+01
67	214	294·50	655·00	6.695E+05	1.55E+01	8.48E–01	1.63E+01
67	215	294·50	695·00	6.857E+05	1.94E+01	1.04E+00	2.05E+01
67	216	294·50	735·00	7.019E+05	2.52E+01	1.40E+00	2.66E+01
67	217	294·50	775·00	7.181E+05	4.85E+01	1.78E+00	5.03E+01

INTERNAL DISTRIBUTION

1. J. A. Bucholz
2. P. F. Cento
3–4. F. X. Gallmeier
5. D. T. Ingersoll
6. T. J. McManamy
7. J. V. Pace III
8. D. L. Selby
9. C. O. Slater
10. B. A. Worley
11. C. D. West
12. ORNL Patent Office
13–14. Central Research Library Document Reference Section
15. Y-12 Technical Library
16–17. Laboratory Records Department
18. Laboratory Records (RC)

EXTERNAL DISTRIBUTION

19. D. D. Carlson, U.S. Nuclear Regulatory Commission, T10G6, Washington, DC 20555
20. U.S. Department of Energy, Oak Ridge Operations, FEDC, MS8218, P.O. Box 2009, Oak Ridge, TN 37831-8218
21. Office of Scientific and Technical Information, P.O. Box 62, Oak Ridge, TN 37831